

## INFORMATION TO USERS

This manuscript has been reproduced from the microfilm master. UMI films the text directly from the original or copy submitted. Thus, some thesis and dissertation copies are in typewriter face, while others may be from any type of computer printer.

**The quality of this reproduction is dependent upon the quality of the copy submitted.** Broken or indistinct print, colored or poor quality illustrations and photographs, print bleedthrough, substandard margins, and improper alignment can adversely affect reproduction.

In the unlikely event that the author did not send UMI a complete manuscript and there are missing pages, these will be noted. Also, if unauthorized copyright material had to be removed, a note will indicate the deletion.

Oversize materials (e.g., maps, drawings, charts) are reproduced by sectioning the original, beginning at the upper left-hand corner and continuing from left to right in equal sections with small overlaps.

ProQuest Information and Learning  
300 North Zeeb Road, Ann Arbor, MI 48106-1346 USA  
800-521-0600

**UMI<sup>®</sup>**



**University of Alberta**

**Electrodeposition of Nanocrystalline CoFe and CoFeNi Soft Magnetic  
Thin Films from Citrate-added Baths**

**by**

**Yahui Zhang**



A thesis submitted to the Faculty of Graduate Studies and Research in partial fulfillment  
of the requirements for the degree of Doctor of Philosophy

in

Materials Engineering

Department of Chemical and Materials Engineering

Edmonton, Alberta

Spring 2005



Library and  
Archives Canada

Bibliothèque et  
Archives Canada

Published Heritage  
Branch

Direction du  
Patrimoine de l'édition

395 Wellington Street  
Ottawa ON K1A 0N4  
Canada

395, rue Wellington  
Ottawa ON K1A 0N4  
Canada

*Your file* *Votre référence*

*ISBN*

*Our file* *Notre référence*

*ISBN*

#### NOTICE:

The author has granted a non-exclusive license allowing Library and Archives Canada to reproduce, publish, archive, preserve, conserve, communicate to the public by telecommunication or on the Internet, loan, distribute and sell theses worldwide, for commercial or non-commercial purposes, in microform, paper, electronic and/or any other formats.

The author retains copyright ownership and moral rights in this thesis. Neither the thesis nor substantial extracts from it may be printed or otherwise reproduced without the author's permission.

#### AVIS:

L'auteur a accordé une licence non exclusive permettant à la Bibliothèque et Archives Canada de reproduire, publier, archiver, sauvegarder, conserver, transmettre au public par télécommunication ou par l'Internet, prêter, distribuer et vendre des thèses partout dans le monde, à des fins commerciales ou autres, sur support microforme, papier, électronique et/ou autres formats.

L'auteur conserve la propriété du droit d'auteur et des droits moraux qui protègent cette thèse. Ni la thèse ni des extraits substantiels de celle-ci ne doivent être imprimés ou autrement reproduits sans son autorisation.

---

In compliance with the Canadian Privacy Act some supporting forms may have been removed from this thesis.

Conformément à la loi canadienne sur la protection de la vie privée, quelques formulaires secondaires ont été enlevés de cette thèse.

While these forms may be included in the document page count, their removal does not represent any loss of content from the thesis.

Bien que ces formulaires aient inclus dans la pagination, il n'y aura aucun contenu manquant.

  
**Canada**

## ABSTRACT

With increasing storage density of hard-disk-drives, the need for recording heads to write on high-coercivity media has raised new requirements for the write-head core material that cannot be met by traditionally employed permalloy ( $\text{Ni}_{80}\text{Fe}_{20}$ ). Therefore, new soft magnetic materials with higher saturation flux density  $B_s$  ( $\gg 1$  Tesla) such as CoFe alloys, CoFeNi alloys, and other CoFe-based alloys have been developed during the past decades. With the advantages of simplicity, cost-effectiveness and controllable patterning, electroplating processes are being employed in the fabrication of thin-film recording heads. Conventional CoFe or CoFeNi alloy plating baths, which employ low pH levels (typically 2.0-3.0), suffer from several problems that can limit commercialization. These include poor stability, i.e., precipitation occurs in plating baths rapidly with time, low current density efficiency and voids in deposited films due to the electrodeposition of hydrogen. The voids present in deposits will degenerate film uniformity and magnetic properties. Therefore, the development of stable baths with relatively high pH levels is crucial for commercial fabrication of CoFe and CoFeNi thin films with optimal soft magnetic properties.

In this study, stable electrolytes, with the introduction of ammonium citrate as a complexing agent and bath stabilizer and relatively high pH levels (natural pH), have been developed for the electrodeposition of CoFe or CoFeNi alloys. Citrate can

effectively improve the stability of CoFe and CoFeNi plating baths. Denser and more uniform deposits can be plated out from the citrate-added baths because of the higher pH levels. CoFe and CoFeNi thin films with preferred composition, mixed fcc-bcc phases, and 10-20nm grain sizes, which are necessary for achieving optimal soft magnetic properties, have been electroplated from the citrate-added baths. So far, the saturation magnetizations of CoFe and CoFeNi films plated from citrate-added baths can exceed 2 Tesla, which is excellent, and the coercivities of the CoFe and CoFeNi films are acceptable (9 to 17 Oe). The stability diagrams of single metal and alloy plating baths, with and without citrate addition, have been calculated. Electrochemical study of the electrodeposition of Co, Fe and Ni single metals and CoFe and CoFeNi alloys, from citrate-added baths and citrate-free baths, and the corrosion properties of electroplated CoFe and CoFeNi films have been conducted. The phase formation and grain sizes in electrodeposited CoFe and CoFeNi films have been investigated using thin film x-ray diffraction (XRD) and transmission electron microscopy (TEM) methods.

**KEYWORDS** Co, Ni, Fe, citrate, electrolytes, electrodeposition, nano, crystalline materials, soft magnetic alloys, thin films.

## ACKNOWLEDGMENTS

I am earnestly grateful to Dr. D.G. Ivey for his supervision, guidance, and encouragement throughout my study at University of Alberta. I am deeply impressed by his profound knowledge and strict attitude to research and teaching, which will no doubt have a great influence to my future career.

Special appreciation is extended to Dr. J.L. Luo and Dr. Q. Liu for access to their lab equipment and helpful advice. I gratefully acknowledge Tina Barker for SEM analysis and training me to operate the SEM, and Shiraz Merali for training me to operate the XRD.

Great thanks are extended to Dr. J.A. Jung and Dr. I.Y. Isaac in the Department of Physics, University of Alberta, for their assistance in measuring magnetic properties and training me to operate the SQUID magnetometer.

I greatly appreciate Haixia Guo for her advice and cooperation in electrochemical analyses. I wish to thank everyone in our group for their cooperation and help. The assistance of Yin Huang, Anqiang He, Barbara Djurfors and Jiang Chen are especially appreciated.

Finally, the Natural Sciences and Engineering Research Council (NSERC) and the American Electroplaters and Surface Finishers Society, Inc. (AESF) are greatly acknowledged for funding this research.

# TABLE OF CONTENTS

Chapter 1 Introduction.....	1
Chapter 2 Literature Review.....	4
2.1 Introduction.....	4
2.2 Magnetic properties of Co-Fe-Ni based alloys.....	8
2.2.1 Why Co-Fe-Ni based alloys?.....	8
2.2.2 Concepts of major magnetic properties.....	12
2.3 Soft magnetic thin films developed by various processes.....	16
2.3.1 Soft magnetic thin films prepared by vacuum processes .....	16
2.3.2 Soft magnetic thin films prepared by electrodeposition.....	21
2.3.2.1 Electrodeposition of FeNi alloys.....	24
2.3.2.2 Electrodeposition of CoFe alloys.....	27
2.3.2.3 Electrodeposition of CoFeNi alloys.....	31
2.3.2.4 Electrodeposition of other soft magnetic thin-films.....	42
2.3.3 Soft magnetic thin films prepared by electroless deposition processes.....	45
2.4 Summary.....	48
Chapter 3 Experimental Methods.....	49
3.1 Experimental equipment.....	49
3.2 Bath compositions and electroplating conditions.....	51
Chapter 4 Development of Stable Citrate-added Baths and Bath Stability Study.....	54
4.1 Development of citrate-added baths for electroplating CoFe and CoFeNi alloys...55	
4.2 Stability diagrams of plating baths.....	56
4.2.1 Stability diagrams for single metal plating baths.....	56
4.2.1.1 Stability diagrams for separate Co plating baths.....	56
4.2.1.2 Stability diagrams for separate Fe plating baths.....	58

4.2.1.3 Stability diagrams for separate Ni plating baths.....	60
4.2.2 Stability diagrams for CoFe and CoFeNi alloy plating baths.....	62
4.2.2.1 Stability diagrams for CoFe alloy plating baths.....	62
4.2.2.2 Stability diagrams for CoFeNi alloy plating baths.....	65
4.3 Main complexing reactions in citrate-added plating baths.....	68
4.4 Stability of plating baths.....	71
4.5 Morphologies of CoFe and CoFeNi films electroplated from the citrate-added baths and conventional baths.....	73
4.5.1 Morphologies of CoFe films.....	74
4.5.1.1 Plan views.....	74
4.5.1.2 Cross-section views.....	76
4.5.2 Morphologies of CoFeNi films.....	78
4.5.2.1 Plan views.....	78
4.5.2.2 Cross-section views.....	81
4.6 Summary.....	81
Chapter 5 Electrodeposition of CoFe and CoFeNi thin films.....	83
5.1 Fundamentals of electrodeposition.....	83
5.1.1 Electrodeposition of single metal.....	84
5.1.1.1 Electrode reactions.....	84
5.1.1.2 The electrical double layer.....	88
5.1.1.3 Overpotential.....	90
5.1.1.4 Underpotential deposition.....	94
5.1.1.5 Electrocrystallization.....	96
5.1.1.6 Deposition rate and current efficiency.....	99
5.1.2 Electrodeposition of metal alloys.....	99
5.1.3 Pulsed current (PC) plating.....	103

5.2 Electrodeposition of CoFe and CoFeNi films from citrate-added baths.....	106
5.2.1 Electroplating of CoFe alloys.....	107
5.2.1.1 Effect of ammonium citrate.....	107
5.2.1.2 Effect of cobalt concentration.....	109
5.2.1.3 Effect of iron concentration.....	110
5.2.1.4 Effect of Co/Fe concentration ratio.....	110
5.2.1.5 Effect of current density.....	112
5.2.1.6 Effect of $t_{on}$ .....	113
5.2.1.7 Effect of agitation.....	114
5.2.1.8 Effect of plating temperature.....	115
5.2.2 Electroplating of CoFeNi alloys.....	118
5.2.2.1 Effect of ammonium citrate.....	119
5.2.2.2 Effect of cobalt concentration.....	121
5.2.2.3 Effect of iron concentration.....	121
5.2.2.4 Effect of nickel concentration.....	122
5.2.2.5 Effect of current density.....	122
5.2.2.6 Effect of $t_{on}$ .....	124
5.2.2.7 Effect of agitation.....	124
5.2.2.8 Effect of plating temperature.....	125
5.2.2.9 Anomalous phenomenon in CoFeNi alloy plating.....	127
5.3 Summary.....	129
Chapter 6 Electrochemical Study of the Electrodeposition and Corrosion Properties of CoFe and CoFeNi Films.....	131
6.1 Linear sweep voltammetry and cyclic voltammetry studies.....	132
6.1.1 Polarization curves for single metal depositions.....	132

6.1.2 Polarization curves for CoFe and CoFeNi alloy depositions.....	139
6.1.2.1 Polarization curves for the deposition of CoFe alloys with high Co content.....	139
6.1.2.2 Polarization curves for the deposition of CoFe alloys with high Fe content.....	141
6.1.2.3 Polarization curves for the deposition of CoFeNi alloys.....	143
6.2 Corrosion properties of electroplated CoFe and CoFeNi films.....	145
6.3 Summary.....	150
Chapter 7 Phase formation in electroplated CoFe and CoFeNi thin films.....	151
7.1 Thin film X-ray diffraction.....	151
7.1.1 Thin film XRD study of electrodeposited CoFe films.....	151
7.1.1.1 Effect of Fe content on phase formation in deposited CoFe films....	151
7.1.1.2 Effect of electrolyte composition on phase formation in deposited CoFe films.....	156
7.1.2 Thin film XRD study of electrodeposited CoFeNi films.....	158
7.1.2.1 Phase formation in CoFeNi films deposited from citrate-added baths...	158
7.1.2.2 Phase formation in CoFeNi films deposited from citrate-free baths....	162
7.2 TEM analysis.....	169
7.2.1 TEM analysis of electroplated CoFe films.....	169
7.2.2 TEM analysis of electroplated CoFeNi films.....	171
7.3 Summary.....	175
Chapter 8 Magnetic Properties of Electroplated CoFe and CoFeNi Thin Films.....	178
8.1 Magnetic properties of electroplated CoFe thin films.....	178
8.2 Magnetic properties of electroplated CoFeNi thin films.....	185
8.3 Summary.....	191
Chapter 9 Conclusions and Recommendations for Future Work.....	193

9.1 Main conclusions.....	193
9.2 Recommendations for future work.....	198
Appendix 1 Standard electrode potentials.....	200
Appendix 2 Construction of stability diagrams.....	203
References.....	207
Curriculum Vitae.....	220

## LIST OF TABLES

<b>Table 2-1.</b> Summary of types of magnetism.....	9
<b>Table 2-2.</b> The saturation polarization ( $I_s$ ) and Curie temperature ( $T_c$ ) of Co, Fe, Ni.....	10
<b>Table 2-3.</b> Unit conversion table for magnetism related properties.....	15
<b>Table 2-4.</b> Magnetic properties of CoFe films produced by vacuum techniques.....	20
<b>Table 2-5.</b> Main properties of some electroplated soft magnetic materials.....	23
<b>Table 2-6.</b> Composition of bath for electroplating CoFe alloys.....	28
<b>Table 2-7.</b> Composition of electrolyte for depositing CoFe alloys.....	29
<b>Table 2-8.</b> Composition of bath for electroplating CoFeNi alloys.....	32
<b>Table 2-9.</b> Bath composition for FeCoNiCu/Cu electrodeposition.....	44
<b>Table 2-10.</b> Bath composition and conditions for electroless deposition of CoNiFeB thin films.....	46
<b>Table 3-1.</b> Composition of a traditional CoFe electroplating bath.....	52
<b>Table 3-2.</b> Composition of citrate-added bath for electroplating CoFe thin films.....	52
<b>Table 3-3.</b> Composition of a traditional CoFeNi electroplating bath.....	52
<b>Table 3-4.</b> Composition of citrate-added bath for electroplating CoFeNi thin films....	53
<b>Table 4-1.</b> Stability tests for CoFe plating baths with and without the addition of ammonium citrate.....	72
<b>Table 4-2.</b> Stability tests for CoFeNi plating baths with and without the addition of ammonium citrate.....	73
<b>Table 5-1.</b> Calculated potentials of single metal electrodes at 293K for different metal ion concentrations.....	87
<b>Table 5-2.</b> Effect of Co/Fe concentration ratio in electrolyte on the Co/Fe content ratio in deposit.....	111
<b>Table 5-3.</b> CoFe films deposited from baths with the same Co/Fe concentration ratio but	

different metal concentrations.....	112
<b>Table 5-4.</b> Composition of citrate-added bath for electroplating $\text{Co}_{34}\text{Fe}_{66}$ films.....	118
<b>Table 5-5.</b> Effect of Co/Fe concentration ratio in the electrolyte on the composition of deposited CoFeNi films.....	128
<b>Table 5-6.</b> CoFeNi films deposited at the same Co/Fe concentration ratio in the plating bath but different metal concentrations (Ni concentration is fixed at 0.30M).....	128
<b>Table 6-1.</b> Compositions of baths employed in single metal depositions.....	133
<b>Table 6-2.</b> Compositions of baths employed in the deposition of CoFe alloys with high Co content.....	139
<b>Table 6-3.</b> Compositions of baths employed in the depositions of CoFe alloys with high Fe contents.....	141
<b>Table 6-4.</b> Compositions of baths employed in the deposition of CoFeNi alloys.....	143
<b>Table 7-1.</b> Composition of electrolyte for plating a $\text{Co}_{71}\text{Fe}_{29}$ thin film whose XRD spectrum is shown in Figure 7-1a.....	152
<b>Table 7-2.</b> Composition of electrolyte for plating a $\text{Co}_{71}\text{Fe}_{29}$ thin film whose XRD spectrum is shown in Figure 7-2.....	156
<b>Table 7-3.</b> Composition of electrolyte for plating $\text{Co}_{61}\text{Fe}_{28}\text{Ni}_{11}$ thin film whose XRD spectrum is shown in Figure 7-6.....	162
<b>Table 7-4.</b> Diffraction planes identified from electron diffraction pattern.....	171
<b>Table 8-1.</b> Magnetic properties of representative CoFe films plated from citrate-free baths and citrate-added baths.....	185
<b>Table 8-2.</b> Magnetic properties of representative CoFeNi films plated from traditional low pH bath and citrate-added bath.....	190

## LIST OF FIGURES

<b>Figure 2-1.</b> GMR head structure with CoFeNi film as the write head core material....	4
<b>Figure 2-2.</b> Magnetic disk storage areal density vs. year of IBM product introduction....	5
<b>Figure 2-3.</b> a. Cross-sectional SEM images of recording heads manufactured by the NEC Corporation in the years indicated. b. Schematic illustration of magnetic recording system and a cross sectional view of a magnetic recording head.....	6
<b>Figure 2-4.</b> Evolution of disk coercivity with time for IBM hard disk products.....	7
<b>Figure 2-5.</b> Soft magnetic materials with high $B_s$ and high $\rho$ , mainly developed by the Waseda group.....	7
<b>Figure 2-6.</b> Periodic table showing the magnetic behavior of each element at room temperature.....	10
<b>Figure 2-7.</b> Schematic hysteresis loops of “soft” and “hard” magnetic materials....	11
<b>Figure 2-8.</b> Composition-high saturation magnetic flux density diagram for bulk CoNiFe ternary alloys published by Bozorth.....	11
<b>Figure 2-9.</b> Schematic sketches of sputtering and evaporation processes.....	17
<b>Figure 2-10.</b> Typical setup for electrodeposition.....	22
<b>Figure 2-11.</b> Models of systems for electroplating CoFe thin films.....	29
<b>Figure 2-12.</b> Chemical structures of (a) saccharin, (b) phthalimide (PHTA) and (c) $\sigma$ TOL.....	30
<b>Figure 2-13.</b> Three-element maps showing magnetic properties of CoFeNi films.....	33
<b>Figure 2-14.</b> a) Resistivity of electrodeposited CoFeNi films as a function of DET concentration. b) Magnetic properties of electrodeposited CoFeNi films as a function of DET concentration.....	38
<b>Figure 2-15.</b> (Top) Cross section view ( $\sim 20K$ magnification) of a laminated CoFeCu/Cu film (in the middle) with four CoFeCu layers (each $0.5\mu\text{m}$ thick) and three Cu layers	

(each 10nm thick). (Bottom) Schematic showing a pulsed current waveform applied in plating.....	42
<b>Figure 3-1.</b> Schematic illustration of the electroplating setup.....	50
<b>Figure 4-1.</b> Molecular structure of ammonium citrate.....	55
<b>Figure 4-2.</b> Stability diagrams for cobalt plating baths.....	58
<b>Figure 4-3.</b> Stability diagrams for iron plating baths.....	60
<b>Figure 4-4.</b> Stability diagrams for nickel plating baths.....	62
<b>Figure 4-5.</b> Stability diagrams for CoFe alloy plating baths.....	64
<b>Figure 4-6.</b> Stability diagrams for CoFeNi alloy plating baths.....	67
<b>Figure 4-7.</b> Distribution of ion species in citric acid solution (0.30 M ) vs pH.....	68
<b>Figure 4-8.</b> Plan view SEM SE images of CoFe film plated from a bath with 0 g/L ammonium citrate and pH 2.4 at $i = 15\text{mA}/\text{cm}^2$ ; $t_{\text{on}} = 6\text{ms}$ ; $t_{\text{off}} = 4\text{ms}$ ; agitation of 600rpm.....	75
<b>Figure 4-9.</b> Plan view SEM SE images of CoFe film plated from a bath with 5 g/L ammonium citrate and pH 4.4 at $i = 15\text{mA}/\text{cm}^2$ ; $t_{\text{on}} = 6\text{ms}$ ; $t_{\text{on}} + t_{\text{off}} = 10\text{ms}$ ; agitation of 600rpm.....	76
<b>Figure 4-10.</b> Cross-section SEM SE image of CoFe film plated from a bath with 0 g/L ammonium citrate and pH 2.4 at $i = 15\text{mA}/\text{cm}^2$ ; $t_{\text{on}} = 6\text{ms}$ ; $t_{\text{on}} + t_{\text{off}} = 10\text{ms}$ ; agitation of 600rpm.....	77
<b>Figure 4-11.</b> Cross-section SEM SE image of CoFe film plated from a bath with 5 g/L ammonium citrate and pH4.4 at $i = 15\text{mA}/\text{cm}^2$ ; $t_{\text{on}} = 6\text{ms}$ ; $t_{\text{on}} + t_{\text{off}} = 10\text{ms}$ ; agitation of 600rpm.....	77
<b>Figure 4-12.</b> Plan view SEM SE images of CoFeNi film plated from a bath with 0 g/L ammonium citrate and pH 2.7 at $i = 6\text{mA}/\text{cm}^2$ ; $t_{\text{on}} = 0.3\text{ms}$ ; $t_{\text{on}} + t_{\text{off}} = 10\text{ms}$ ; agitation of 600rpm.....	79

<b>Figure 4-13.</b> Plan view SEM SE images of CoFeNi film plated from a bath with 50 g/L ammonium citrate and pH 5.3 at $i = 6\text{mA/cm}^2$ ; $t_{\text{on}} = 0.3\text{ms}$ ; $t_{\text{on}} + t_{\text{off}} = 10\text{ms}$ ; agitation of 600rpm.....	80
<b>Figure 4-14.</b> Cross-section SEM SE image of CoFeNi film plated from a bath with 0 g/L ammonium citrate and pH 2.7 at $i = 6\text{mA/cm}^2$ ; $t_{\text{on}} = 0.3\text{ms}$ ; $t_{\text{on}} + t_{\text{off}} = 10\text{ms}$ ; agitation of 600rpm.....	80
<b>Figure 4-15.</b> Cross-section SEM SE image of CoFeNi film plated from a bath with 50 g/L ammonium citrate and pH 5.3 at $i = 6\text{mA/cm}^2$ ; $t_{\text{on}} = 0.3\text{ms}$ ; $t_{\text{off}} = 9.7\text{ms}$ ; agitation of 600rpm.....	81
<b>Figure 5-1.</b> Models of the electrical double layer.....	89
<b>Figure 5-2.</b> $\log i $ versus $\eta$ Plot.....	92
<b>Figure 5-3.</b> A qualitative description of the relationship between current density and potential. Curve a is the pure activation-controlled current $i_{ac}$ and curve b is the actual current which will be measured, having a mass-transport-limited value $i_l$ .....	94
<b>Figure 5-4.</b> Underpotential deposition of lead on gold from a solution containing 0.001 M $\text{Pb}(\text{ClO}_4)_2$ and 1.0 M $\text{HClO}_4$ . Two underpotential deposition (UPD) and dissolution peaks were observed.....	95
<b>Figure 5-5.</b> Elementary reactions and steps in electrocrystallization.....	97
<b>Figure 5-6.</b> Microstructure dependence on current density.....	98
<b>Figure 5-7.</b> Current versus potential curves for deposition of three components: component 1 with the highest equilibrium potential; component 2 with lower $E_0$ and lower mass transport limited current; and component 3 with lowest $E_0$ and highest transport limited current. (Examples: Case A, $I_1 > I_2$ , $I_3 = 0$ ; Case B, $I_3 > I_1 > I_2$ ).....	100
<b>Figure 5-8.</b> Evans diagrams representing the partial currents of components A and B in anomalous codeposition of a binary alloy AB. Figures (a) and (b): both partial reactions	

are charge transfer controlled. Figures (c) and (d): one of the partial reactions is mass transport controlled.....102

**Figure 5-9.** Schematic representation and suggested nomenclature for some square-wave-modulated current systems, and definition of related parameters. (a) Pulse, (b) superimposed pulse, (c) duplex pulse, (d) pulsed pulse, (e) pulse-on-pulse, (f) pulse reverse, (g) pulse reverse (with OFF time), (h) pulsed pulse reverse and (i) Pulse-on-pulse reverse.....104

**Figure 5-10.** Concentration profiles of the two diffusion layers in PC plating at the end of a pulse.  $\delta_p$  is the thickness of the pulsating diffusion layer, and  $\delta_s$  is the thickness of the stationary diffusion layer.....105

**Figure 5-11.** Effect of ammonium citrate dosage on the composition of CoFe films plated at  $i = 15\text{mA/cm}^2$ ;  $t_{\text{on}} = 6\text{ms}$ ;  $t_{\text{off}} = 4\text{ms}$ ; agitation of 600rpm.....108

**Figure 5-12.** Effect of ammonium citrate dosage on the plating rate for depositing CoFe films at  $i = 15\text{mA/cm}^2$ ;  $t_{\text{on}} = 6\text{ms}$ ;  $t_{\text{off}} = 4\text{ms}$ ; agitation of 600rpm.....108

**Figure 5-13.** Effect of cobalt concentration on the composition of CoFe films plated at  $i = 15\text{mA/cm}^2$ ;  $t_{\text{on}} = 6\text{ms}$ ;  $t_{\text{on}} + t_{\text{off}} = 10\text{ms}$ ; agitation of 600 rpm.....109

**Figure 5-14.** EDS spectrum from a deposited film with a composition corresponding to  $\text{Co}_{65}\text{Fe}_{35}$  plated at  $i = 15\text{mA/cm}^2$ ;  $t_{\text{on}} = 6\text{ms}$ ;  $t_{\text{off}} = 4\text{ms}$ .....109

**Figure 5-15.** Effect of iron concentration on the composition of CoFe films plated at  $i = 15\text{mA/cm}^2$ ;  $t_{\text{on}} = 6\text{ms}$ ;  $t_{\text{on}} + t_{\text{off}} = 10\text{ms}$ ; agitation of 600rpm.....110

**Figure 5-16.** Effect of current density on the composition of CoFe films plated at  $t_{\text{on}} = 6\text{ms}$ ;  $t_{\text{on}} + t_{\text{off}} = 10\text{ms}$ ; agitation of 600rpm.....113

**Figure 5-17.** Effect of  $t_{\text{on}}$  on the composition of CoFe films plated at  $i = 15\text{mA/cm}^2$ ;  $t_{\text{on}} + t_{\text{off}} = 10\text{ms}$ ; agitation of 600rpm.....114

<b>Figure 5-18.</b> Effect of agitation on the composition of CoFe films plated at $i = 15\text{mA/cm}^2$ ; $t_{\text{on}} = 6\text{ms}$ ; $t_{\text{on}} + t_{\text{off}} = 10\text{ms}$ .....	115
<b>Figure 5-19.</b> Effect of plating temperature on the composition of CoFe films plated at $i = 15\text{mA/cm}^2$ ; $t_{\text{on}} = 6\text{ms}$ ; $t_{\text{on}} + t_{\text{off}} = 10\text{ms}$ ; agitation of 600rpm.....	115
<b>Figure 5-20.</b> Plan view SEM SE images of CoFe films plated at different temperatures at $i = 15\text{mA/cm}^2$ ; $t_{\text{on}} = 6\text{ms}$ ; $t_{\text{on}} + t_{\text{off}} = 10\text{ms}$ ; agitation of 600rpm.....	116
<b>Figure 5-21.</b> EDS spectra from deposited CoFe films with high iron contents.....	118
<b>Figure 5-22.</b> Effect of ammonium citrate dosage on the electroplating of CoFeNi films at $i = 6\text{mA/cm}^2$ ; $t_{\text{on}} = 0.3\text{ms}$ ; $t_{\text{off}} = 9.7\text{ms}$ ; agitation of 600rpm.....	119
<b>Figure 5-23.</b> EDS spectrum of $\text{Co}_{66}\text{Fe}_{23}\text{Ni}_{11}$ film plated from citrate-added bath.....	120
<b>Figure 5-24.</b> Effect of ammonium citrate dosage on the plating rate for depositing CoFeNi films at $i = 6\text{mA/cm}^2$ ; $t_{\text{on}} = 0.3\text{ms}$ ; $t_{\text{off}} = 9.7\text{ms}$ ; agitation of 600rpm.....	120
<b>Figure 5-25.</b> Effect of cobalt concentration on the composition of CoFeNi films plated at $i = 6\text{mA/cm}^2$ ; $t_{\text{on}} = 0.3\text{ms}$ ; $t_{\text{on}} + t_{\text{off}} = 10\text{ms}$ ; agitation of 600rpm.....	121
<b>Figure 5-26.</b> Effect of iron concentration on the composition of CoFeNi films plated at $i = 6\text{mA/cm}^2$ ; $t_{\text{on}} = 0.3\text{ms}$ ; $t_{\text{on}} + t_{\text{off}} = 10\text{ms}$ ; agitation of 600rpm.....	122
<b>Figure 5-27.</b> Effect of nickel concentration on the composition of CoFeNi films plated at $i = 6\text{mA/cm}^2$ ; $t_{\text{on}} = 0.3\text{ms}$ ; $t_{\text{on}} + t_{\text{off}} = 10\text{ms}$ ; agitation of 600rpm.....	123
<b>Figure 5-28.</b> Effect of current density on the composition of CoFeNi films plated at $t_{\text{on}} = 0.3\text{ms}$ ; $t_{\text{on}} + t_{\text{off}} = 10\text{ms}$ ; agitation of 600rpm.....	123
<b>Figure 5-29.</b> Effect of $t_{\text{on}}$ on the composition of CoFeNi films plated at $i = 6\text{mA/cm}^2$ ; $t_{\text{on}} + t_{\text{off}} = 10\text{ms}$ ; agitation of 600rpm.....	124

<b>Figure 5-30.</b> Effect of agitation on the composition of CoFeNi films plated at $i = 6\text{mA/cm}^2$ ; $t_{\text{on}} = 0.3\text{ms}$ ; $t_{\text{on}} + t_{\text{off}} = 10\text{ms}$ .....	125
<b>Figure 5-31.</b> Effect of plating temperature on the composition of CoFeNi films plated at $i = 12\text{mA/cm}^2$ ; $t_{\text{on}} = 0.3\text{ms}$ ; $t_{\text{on}} + t_{\text{off}} = 10\text{ms}$ ; agitation of 600rpm.....	125
<b>Figure 5-32.</b> Plan view SEM SE images of CoFeNi films plated at different temperatures at $i = 12\text{mA/cm}^2$ ; $t_{\text{on}} = 0.3\text{ms}$ ; $t_{\text{on}} + t_{\text{off}} = 10\text{ms}$ ; agitation of 600rpm.....	127
<b>Figure 5-33.</b> EDS spectrum of $\text{Co}_{64}\text{Fe}_{24}\text{Ni}_{11}$ film deposited from a conventional bath.....	129
<b>Figure 6-1.</b> Polarization curves for Co, Fe and Ni single metal depositions.....	135
<b>Figure 6-2.</b> Comparisons of polarization curves for Co, Fe and Ni single metal depositions.....	138
<b>Figure 6-3.</b> Polarization curves for the deposition of CoFe alloys with high Co content.....	139
<b>Figure 6-4.</b> Cyclic voltammogram for the deposition of CoFe alloy with high Co content from the citrate-added bath.....	140
<b>Figure 6-5.</b> Polarization curves for the deposition of CoFe alloys with high Fe content.....	142
<b>Figure 6-6.</b> Cyclic voltammogram for the deposition of CoFe alloy with high Fe content from the citrate-added bath.....	143
<b>Figure 6-7.</b> Polarization curves for the deposition of CoFeNi alloys from different baths.....	144
<b>Figure 6-8.</b> Cyclic voltammogram for the deposition of CoFeNi alloy from citrate-added bath.....	145
<b>Figure 6-9.</b> Anodic polarization curves for CoFe films with high Co content, plated at $i = 15\text{mA/cm}^2$ ; $t_{\text{on}} = 6\text{ms}$ ; $t_{\text{on}} + t_{\text{off}} = 10\text{ms}$ ; agitation of 600rpm.....	147

<b>Figure 6-10.</b> Schematic polarization curve for a metal or alloy that displays an active-passive transition.....	147
<b>Figure 6-11.</b> Anodic polarization curves for CoFe films with high Fe contents plated at $i = 15\text{mA/cm}^2$ ; $t_{\text{on}} = 6\text{ms}$ ; $t_{\text{on}} + t_{\text{off}} = 10\text{ms}$ ; agitation of 600rpm.....	148
<b>Figure 6-12.</b> Anodic polarization curves for CoFeNi films plated at $i = 6\text{mA/cm}^2$ ; $t_{\text{on}} = 0.3\text{ms}$ ; $t_{\text{on}} + t_{\text{off}} = 10\text{ms}$ ; agitation 600rpm.....	149
<b>Figure 7-1.</b> Thin film XRD spectra of CoFe films with different Fe contents electroplated at $i = 15\text{mA/cm}^2$ , $t_{\text{on}} = 6\text{ms}$ , $t_{\text{on}} + t_{\text{off}} = 10\text{ms}$ and agitation of 600rpm....	154
<b>Figure 7-2.</b> Phase diagram for the Co-Fe system.....	155
<b>Figure 7-3.</b> Thin film XRD spectrum of $\text{Co}_{71}\text{Fe}_{29}$ film plated at $i = 15\text{mA/cm}^2$ , $t_{\text{on}} = 6\text{ms}$ , $t_{\text{on}} + t_{\text{off}} = 10\text{ms}$ and agitation of 600rpm. Bath composition is listed in Table 7-2.....	157
<b>Figure 7-4.</b> Thin film XRD spectrum of CoFe film plated at ammonium citrate dosage of 50g/L, $i = 6\text{mA/cm}^2$ , $t_{\text{on}} = 0.3\text{ms}$ , $t_{\text{on}} + t_{\text{off}} = 10\text{ms}$ and agitation of 600rpm. Film composition is $\text{Co}_{62}\text{Fe}_{38}$ .....	157
<b>Figure 7-5.</b> Thin film XRD spectra of representative CoFeNi films plated from citrate-added baths, with ammonium citrate dosage 50g/L, at $i = 6\text{mA/cm}^2$ , $t_{\text{on}} = 0.3\text{ms}$ , $t_{\text{on}} + t_{\text{off}} = 10\text{ms}$ and agitation of 600rpm.....	161
<b>Figure 7-6.</b> Thin film XRD spectrum of CoFeNi film plated from citrate-added bath, with ammonium citrate dosage 5 g/L, at $i = 12\text{mA/cm}^2$ , $t_{\text{on}} = 9\text{ms}$ and $t_{\text{off}} = 6\text{ms}$ . Film composition is $\text{Co}_{61}\text{Fe}_{28}\text{Ni}_{11}$ .....	162
<b>Figure 7-7.</b> Thin film XRD spectra of CoFeNi films with different Fe contents electroplated from citrate-free baths under different conditions.....	164
<b>Figure 7-8.</b> a. Phase diagram for the Co-Ni system. b. Phase diagram for the Fe-Ni system.....	167

**Figure 7-9.** Ternary Co-Fe-Ni alloy diagram for phase formation as presented in reference [Osaka99-4]. Data from this work are superimposed on the diagram.....168

**Figure 7-10.** TEM bright field image and dark field image of a CoFe film plated, from a solution with ammonium citrate dosage of 5g/L, at  $i = 15 \text{ mA/cm}^2$ ,  $t_{\text{on}} = 6 \text{ ms}$ ,  $t_{\text{off}} = 4 \text{ ms}$  and agitation of 600rpm. Film composition is  $\text{Co}_{65}\text{Fe}_{35}$ .....170

**Figure 7-11.** TEM bright field image, dark field image and electron diffraction pattern of a CoFeNi film plated, from a solution with an ammonium citrate dosage of 50g/L, at  $i = 6 \text{ mA/cm}^2$ ,  $t_{\text{on}} = 0.3 \text{ ms}$ ,  $t_{\text{on}} + t_{\text{off}} = 10 \text{ ms}$  and agitation of 600rpm. Film composition is  $\text{Co}_{66}\text{Fe}_{23}\text{Ni}_{11}$ .....173

**Figure 7-12.** TEM bright field image, dark field image and electron diffraction pattern of a CoFeNi film plated, from a solution with an ammonium citrate dosage of 100g/L, at  $i = 10 \text{ mA/cm}^2$ ,  $t_{\text{on}} = 0.3 \text{ ms}$ ,  $t_{\text{on}} + t_{\text{off}} = 10 \text{ ms}$  and agitation of 600rpm. Film composition is  $\text{Co}_{72}\text{Fe}_{21}\text{Ni}_7$ .....175

**Figure 8-1.** Effect of ammonium citrate dosage on the coercivity  $H_c$  of CoFe films plated at  $i = 15 \text{ mA/cm}^2$ ;  $t_{\text{on}} = 6 \text{ ms}$ ;  $t_{\text{on}} + t_{\text{off}} = 10 \text{ ms}$ ; agitation 600 rpm.....179

**Figure 8-2.** Effect of Fe content on the coercivity  $H_c$  of CoFe films plated at  $i = 15 \text{ mA/cm}^2$ ;  $t_{\text{on}} = 6 \text{ ms}$ ;  $t_{\text{on}} + t_{\text{off}} = 10 \text{ ms}$ ; agitation 600 rpm.....180

**Figure 8-3.** Effect of plating current density on the coercivity  $H_c$  of CoFe films plated at  $t_{\text{on}} = 6 \text{ ms}$ ;  $t_{\text{on}} + t_{\text{off}} = 10 \text{ ms}$ ; agitation 600 rpm.....180

**Figure 8-4.** Effect of plating temperature on the coercivity  $H_c$  of CoFe films plated at  $i = 15 \text{ mA/cm}^2$ ;  $t_{\text{on}} = 6 \text{ ms}$ ;  $t_{\text{on}} + t_{\text{off}} = 10 \text{ ms}$ ; agitation 600 rpm.....181

**Figure 8-5.** In-plane hysteresis loop for CoFe film deposited from citrate-added bath (film composition  $\text{Co}_{65}\text{Fe}_{35}$ ) at  $i = 15 \text{ mA/cm}^2$ ;  $t_{\text{on}} = 2 \text{ ms}$ ;  $t_{\text{on}} + t_{\text{off}} = 10 \text{ ms}$ ; agitation 600 rpm.....182

**Figure 8-6.** In-plane hysteresis loop for CoFe film deposited from citrate-free bath with

natural pH (film composition $\text{Co}_{64}\text{Fe}_{36}$ ) at $i = 15\text{mA}/\text{cm}^2$ ; $t_{\text{ON}} = 2\text{ms}$ ; $t_{\text{ON}} + t_{\text{OFF}} = 10\text{ms}$ ; agitation 600 rpm.....	183
<b>Figure 8-7.</b> In-plane hysteresis loop for CoFe film deposited from citrate-added bath (film composition $\text{Co}_{34}\text{Fe}_{66}$ ) at $i = 15\text{mA}/\text{cm}^2$ ; $t_{\text{ON}} = 2\text{ms}$ ; $t_{\text{ON}} + t_{\text{OFF}} = 10\text{ms}$ ; agitation 600 rpm.....	183
<b>Figure 8-8.</b> In-plane hysteresis loop for CoFe film deposited from citrate-free bath with a pH of 2.4 (film composition $\text{Co}_{33}\text{Fe}_{67}$ ) at $i = 15\text{mA}/\text{cm}^2$ ; $t_{\text{ON}} = 2\text{ms}$ ; $t_{\text{ON}} + t_{\text{OFF}} = 10\text{ms}$ ; agitation 600 rpm.....	184
<b>Figure 8-9.</b> Effect of ammonium citrate dosage on the coercivity $H_c$ of CoFeNi films plated at $i = 6\text{mA}/\text{cm}^2$ ; $t_{\text{ON}} = 0.3\text{ms}$ ; $t_{\text{ON}} + t_{\text{OFF}} = 10\text{ms}$ ; agitation 600 rpm.....	186
<b>Figure 8-10.</b> Effect of Fe content on the coercivity $H_c$ of CoFeNi films plated at $i =$ $6\text{mA}/\text{cm}^2$ ; $t_{\text{ON}} = 0.3\text{ms}$ ; $t_{\text{ON}} + t_{\text{OFF}} = 10\text{ms}$ ; agitation 600 rpm.....	186
<b>Figure 8-11.</b> Effect of plating current density on the coercivity $H_c$ of CoFeNi films plated at $t_{\text{ON}} = 0.3\text{ms}$ ; $t_{\text{ON}} + t_{\text{OFF}} = 10\text{ms}$ ; agitation 600 rpm.....	187
<b>Figure 8-12.</b> Effect of plating temperature on the coercivity $H_c$ of CoFeNi films plated at $i = 6\text{mA}/\text{cm}^2$ ; $t_{\text{ON}} = 0.3\text{ms}$ ; $t_{\text{ON}} + t_{\text{OFF}} = 10\text{ms}$ ; agitation 600 rpm.....	188
<b>Figure 8-13.</b> In-plane hysteresis loop for CoFeNi film deposited from citrate-added bath (film composition $\text{Co}_{64}\text{Fe}_{26}\text{Ni}_{10}$ ) at $i = 6\text{mA}/\text{cm}^2$ ; $t_{\text{ON}} = 0.3\text{ms}$ ; $t_{\text{ON}} + t_{\text{OFF}} = 10\text{ms}$ ; agitation 600 rpm.....	189
<b>Figure 8-14.</b> In-plane hysteresis loop for CoFeNi film deposited from citrate-free bath with pH 2.7 (film composition $\text{Co}_{64}\text{Fe}_{24}\text{Ni}_{12}$ ) at $i = 6\text{mA}/\text{cm}^2$ ; $t_{\text{ON}} = 0.3\text{ms}$ ; $t_{\text{ON}} + t_{\text{OFF}} =$ $10\text{ms}$ ; agitation 600 rpm.....	189

## LIST OF SYMBOLS

$a$	lattice constant
$B$	magnetic flux density
$B_s$	saturation flux density
$d$	d-spacing of crystal
$D$	the average grain size
$E^\circ$	the standard electrode potential
$H$	magnetic field
$H_c$	coercivity
$H_k$	anisotropy field
$i$	current density
$i_p$	peak current density
$I$	magnetic polarization
$I_s$	saturation polarization
$m$	magnetic moment per
$M$	magnetization
$M_s$	saturation magnetization
$t$	plating time
$T$	temperature
$T_c$	Curie temperature
$t_{on}$	on-time
$t_{off}$	off-time
$\Phi$	magnetic flux
$\rho$	resistivity
$\mu$	permeability

$\mu_0$	permeability of vacuum
$\mu_r$	relative magnetic permeability
$\theta$	diffraction angle
$\lambda$	wave length
$\lambda_s$	saturation magnetostriction
$\chi$	magnetic susceptibility
$\chi_r$	relative magnetic susceptibility
$\varepsilon^0$	the standard electrode potential

## ABBREVIATIONS

ACS	the American Chemical Society
at%	atomic percent
bcc	body-centered cubic
CV	cyclic voltammetry
CNDO	complete neglect of differential overlap
DC	direct current
DET	diethylenetriamine
DMAB	dimethylamine-borane
EDA	ethylenediamine
EDS	energy dispersive x-ray spectrometer
EDX	energy-dispersive X-ray
fcc	face-centered cubic
FE-SEM	field-emission scanning electron microscopy
GMR	giant magneto-resistive
hcp	hexagonal close packed
IR	infrared
MINDO	modified intermediate neglect of differential overlap
MR	magneto-resistive
nm	nanometer
<i>o</i> TOL	<i>o</i> -toluene sulfonamide
PC	pulsed current
PHTA	phthalimide
PR	pulse-reverse
PRC	periodic reverse-current

SCA	sulfur-containing-additive
SCE	saturated calomel electrode
SE	secondary electron
SEM	scanning electron microscope
SHE	standard hydrogen electrode
SI	international system of units
SQUID	superconducting quantum interference device
STM	scanning tunneling microscopy
TEM	transmission electron microscope
THEED	transmission high energy electron diffraction
UPD	underpotential deposition
UTW	ultra thin window
UV	ultraviolet
wt%	weight percent
XPS	x-ray photoelectron spectroscopy
XRD	x-ray diffraction

## Chapter 1 Introduction

CoFe and CoFeNi alloys have been the most studied soft magnetic materials for the past decades due to their superior properties over FeNi alloys as write head core materials in hard-disk-drives. [Osaka00-1] Electrodeposited permalloy ( $\text{Ni}_{80}\text{Fe}_{20}$ ) was introduced as the core material for thin film inductive heads by IBM in 1979. [Chiu96] With increasing storage density, the need for recording heads to write on high-coercivity media at high frequencies has raised new requirements for the write-head material that cannot be met by  $\text{Ni}_{80}\text{Fe}_{20}$ . [Andricacos98] Therefore, new soft magnetic materials with higher saturation flux density  $B_s$  ( $\gg 1$  Tesla) such as CoFe alloys, CoFeNi alloys and other CoFe-based alloys have been developed.

Vacuum processes (sputtering and evaporation) and electrochemical deposition (electroless- and electro- deposition) are the major processes employed to prepare CoFe, CoFeNi and other soft magnetic thin films for fabricating recording heads. Both evaporation and sputtering processes involve complicated vacuum techniques. Sputtering processes are not suitable for fabricating thick films (more than 1 micron), and the topography of small features is difficult to control in vacuum processes. Electrodeposition processes can be applied to make films with any thickness from  $<1\mu\text{m}$  to  $>100\mu\text{m}$ . Moreover, electroplating through a mask can easily define and control small features like yokes and pole tips; and subtractive processes like etching or ion milling could be eliminated. With the advantages of simplicity, cost-effectiveness and controllable patterning, electroplating processes are being employed in the fabrication of thin-film recording heads. Electrodeposition can be well controlled by applying an external electrical potential, although the surface of the substrate must have an electrically conducting coating for deposition to occur. As an alternative, electroless deposition is suitable for depositing uniform films on substrates with fine and complex

geometries without a pre-deposited electrically conducting layer. However, so far the soft magnetic properties of electrolessly deposited materials are less ideal compared with those obtained by electrodeposition.

A stable bath is desired for commercial fabrication of metal or alloy thin films by electrodeposition. For conventional CoFe or CoFeNi alloy plating baths, low pH levels (typically 2.0-3.0) are employed to stabilize the plating bath. In these cases, acids (most often sulfuric acid  $H_2SO_4$  or hydrochloric acid HCl) act as the bath stabilizers. However, even at low pH, these plating baths still suffer from stability problems. Precipitation occurs rapidly with time [Liu03], which is a critical issue for commercial production. Furthermore, the low pH employed in conventional baths leads to significant hydrogen evolution at the cathode surface, which results in voids in deposited films and low current density efficiency. The voids included in the deposit will degenerate film uniformity and magnetic properties. Therefore, the development of stable baths with relatively high pH levels is crucial and of practical significance for commercial fabrication of CoFe and CoFeNi thin films with optimal soft magnetic properties.

In this study, stable baths with relatively high pH levels (natural pH) have been developed for CoFe or CoFeNi alloy plating by introducing ammonium citrate as a complexing agent and bath stabilizer. The electrodeposition of CoFe and CoFeNi films with soft magnetic properties from the citrate-added baths has been initially explored. CoFe and CoFeNi thin films with preferred composition, mixed fcc-bcc phases, and 10-20nm grain sizes, which are necessary for achieving ideal soft magnetic properties, have been electroplated from the citrate-added baths. The saturation magnetizations of CoFe and CoFeNi films plated from citrate-added baths can exceed 2 Tesla, which is excellent, and the coercivities of the CoFe and CoFeNi films are acceptable (8 to 17 Oe).

In order to present the work conducted in this study clearly and systematically, this thesis is written in nine chapters. Chapter 2 is a comprehensive review of the

requirements for new soft magnetic materials with high saturation flux density  $B_s$ , the magnetic properties of Co-Fe-Ni based alloys and the major processes employed to prepare CoFe, CoFeNi and other soft magnetic thin films for fabricating recording heads (including vacuum processes and electrochemical deposition).

The experimental methods, analysis techniques and equipment and the compositions of electrolytes employed in this work are introduced in Chapter 3.

Chapter 4 presents the development of citrate-added baths for electroplating CoFe and CoFeNi alloys, the calculation of stability diagrams of single metal and alloy plating baths with and without citrate addition, the main complexing reactions in citrate-added plating baths, stability tests of plating baths, and the morphologies of CoFe and CoFeNi films electroplated from the citrate-added baths and conventional baths.

The fundamentals of electrodeposition are briefly discussed, and the electrodeposition of CoFe and CoFeNi films with preferred compositions from the citrate-added baths are reported in Chapter 5.

Chapter 6 presents the electrochemical study of the electrodeposition of Co, Fe and Ni single metals and CoFe and CoFeNi alloys from citrate-added baths and citrate-free baths, and the corrosion properties of electroplated CoFe and CoFeNi films.

The study of phase formation and grain sizes in electrodeposited CoFe and CoFeNi films, using thin film XRD and TEM methods, are reported in Chapter 7.

Chapter 8 presents the study of the magnetic properties of CoFe and CoFeNi films electroplated from citrate-added baths and citrate-free baths.

In the final chapter (Chapter 9), the main conclusions and the significance of this study are summarized, and some general recommendations for future work are presented.

## Chapter 2 Literature Review

### 2.1 Introduction

Hard disk storage is presently the most important member among the storage hierarchy in modern computers, which is evidenced by the fraction of system cost devoted to it. [Thompson00] Progress in this technology is of great economic and technological interest. CoFe and CoFeNi alloys are the most studied soft magnetic materials over the past decades because of their superior properties over FeNi alloys as write head core materials in hard-disk-drives and other magnetic storage technologies. As shown in Figure 2-1, CoFeNi thin films with high saturation flux density  $B_s$  ( $\gg 1$  Tesla) have been employed to fabricate the write core in giant magneto-resistive (GMR) recording heads. [Osaka00-1] [Nonaka00] [Ohashi99]

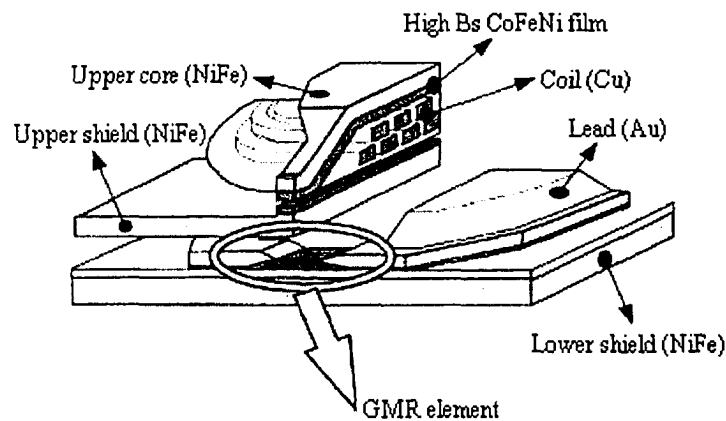


**Figure 2-1.** GMR head structure with CoFeNi film as the write head core material. [Osaka00-1]

There is an almost insatiable need for higher storage density in hard disk drives in the modern information age (Figure 2-2). By introducing GMR and MR (magneto-resistive) head technologies, the areal densities in hard disk drives have been allowed to increase at

a rate of about 60% per year. [Andricacos98] With the ever increasing storage density, the bit size on magnetic storage media and the dimension of recording heads have been decreasing (Figure 2-3). In this case, the superparamagnetic effect becomes a serious problem (refer to Figure 2-2). In order to overcome the superparamagnetic effect, the coercivity  $H_c$  of recording media has been increased to more than 3000 Oe (Figure 2-4). To write on these high coercivity media with the miniaturization of recording heads, write cores made of films with high saturation flux density  $B_s$  are required.

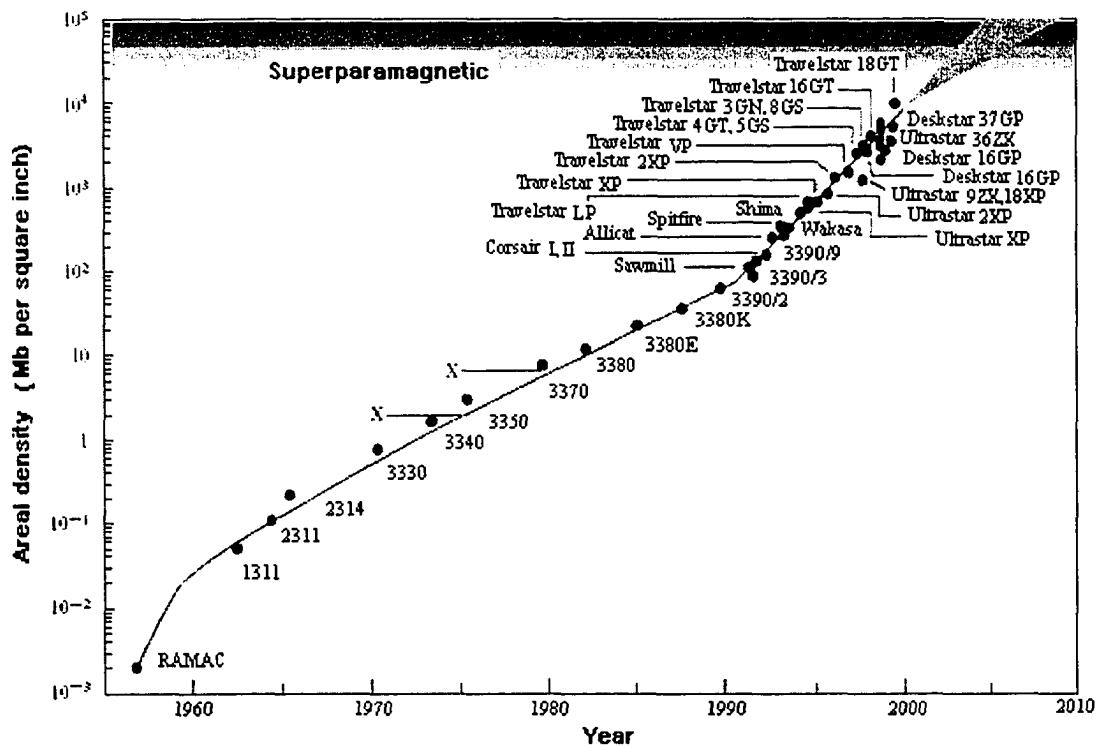


**Figure 2-2.** Magnetic disk storage areal density vs. year of IBM product introduction. [Thompson00]

Electrodeposited permalloy ( $\text{Ni}_{80}\text{Fe}_{20}$ ) was introduced as the core material of thin film inductive heads by IBM in 1979. [Chiu96] The need for recording heads to write on high-coercivity media at high frequencies has raised new requirements for the write-head material that cannot be met by  $\text{Ni}_{80}\text{Fe}_{20}$ . [Andricacos98] To meet these requirements, it is

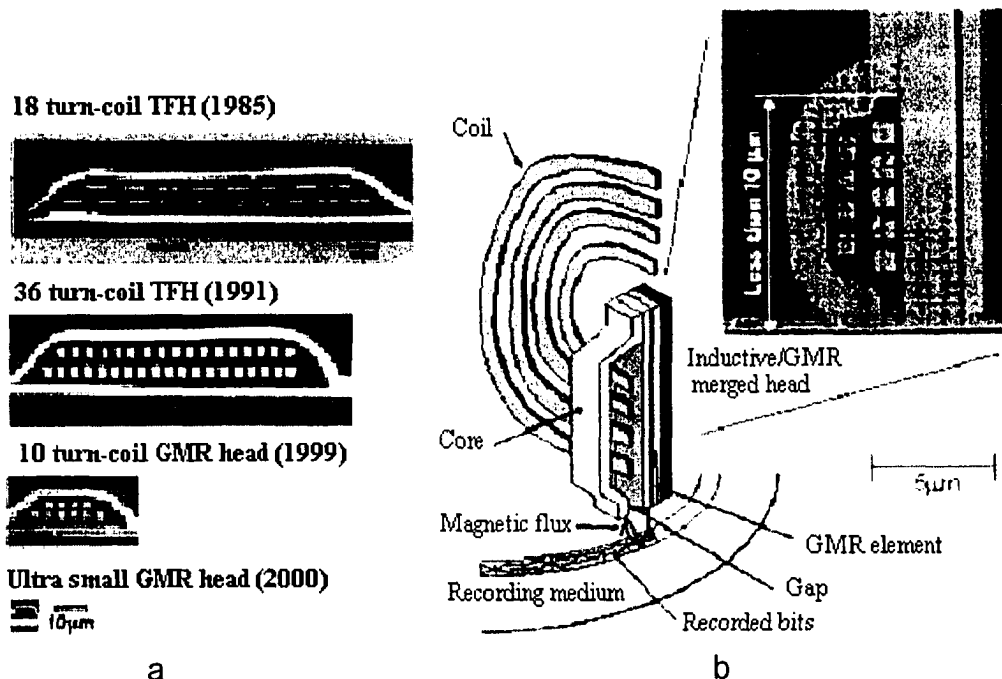


**Figure 2-3.** a. Cross-sectional SEM images of recording heads manufactured by the NEC Corporation in the years indicated. [Osaka01]  
 b. Schematic illustration of magnetic recording system and a cross sectional view of a magnetic recording head. [Waseda1]

crucial to develop materials with optimal soft magnetic properties. Andricacos and Robertson [Andricacos98] summarized the magnetic properties required for future write head core materials, which include: high saturation flux density  $B_s$  ( $\gg 1$  Tesla), low coercivity  $H_c$  (less than 2 Oe), high resistivity  $\rho$ , large permeability  $\mu$  (or low anisotropy field  $H_k$ ), and close to zero magnetostriction  $\lambda_s$ . High saturation flux density  $B_s$  can supply the necessary magnetic flux with device miniaturization. A low coercivity  $H_c$  is necessary for fast magnetization and demagnetization of the recording head. High resistivity  $\rho$  is advantageous for the suppression of eddy currents, which result in an opposite induction field and magnetic energy loss in thermal form. Eddy current is a significant factor in high frequency performance. Large permeability  $\mu$  ensures the saturation of the write head under low magnetic field, that is, low write current. Low magnetostriction  $\lambda_s$  means less strain in the soft magnetic material during the variation of

magnetic field. Only nanocrystalline soft magnetic materials may possess these properties. In addition, the corrosion resistance and ease of fabrication of materials may have the same importance as magnetic properties.

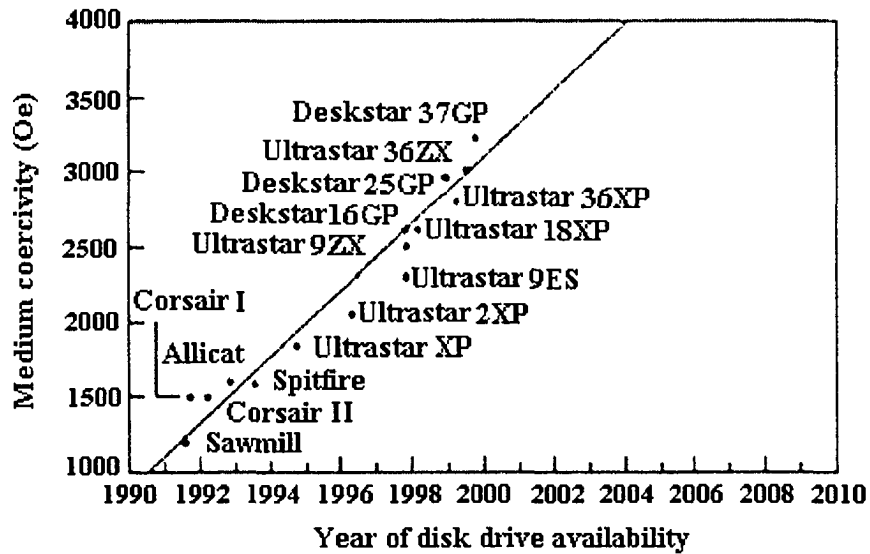


**Figure 2-4.** Evolution of disk coercivity with time for IBM hard disk products. [Thompson00]

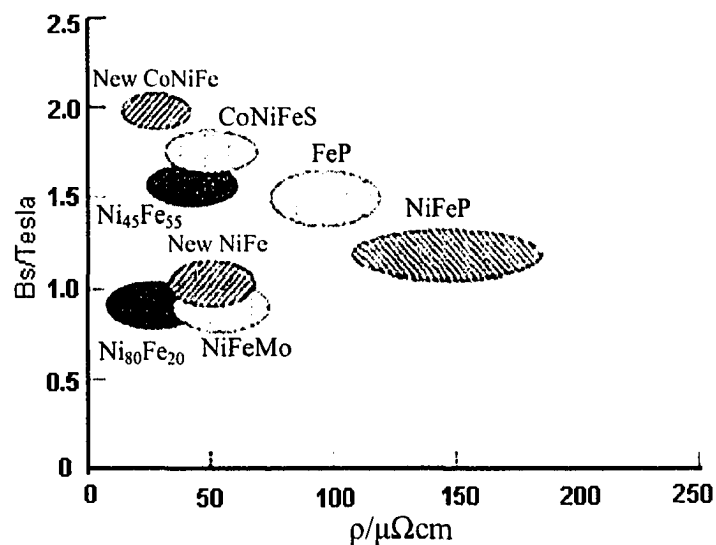


**Figure 2-5.** Soft magnetic materials with high  $B_s$  and high  $\rho$ , mainly developed by the Waseda group. [Osaka99-1]

To meet the need for high storage density, new soft magnetic materials with high saturation flux density  $B_s$  such as electroplated CoFe alloys, CoFeNi alloys, CoFeCu alloys and other CoFe-based alloys, and sputtered FeN films and other Fe-based alloys, have been developed. Figure 2-5 shows examples of soft magnetic materials with high  $B_s$  and high resistivity  $\rho$ , mainly developed by the Waseda group. [Osaka99-1]

## 2.2 Magnetic properties of Co-Fe-Ni based alloys

Bi-element and multi-element alloys containing Co, Fe, or/and Ni are the most studied soft magnetic materials. In order to find or design optimal soft magnetic materials, it is necessary to understand the origin of magnetism. Magnetism originates from the orbital and spin motions of electrons and the interaction of electrons with one another, i.e., it is determined by the electron arrangement in atoms and the crystal structure (atom arrangement).

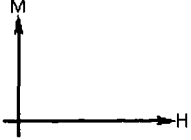
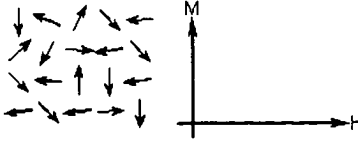
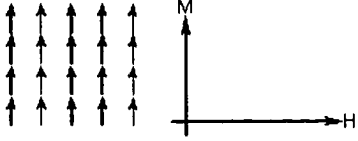
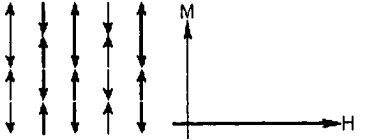
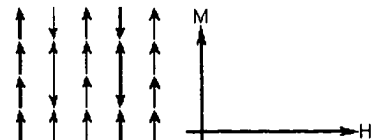
### 2.2.1 Why Co-Fe-Ni based alloys?

The magnetic behavior of materials can be classified into five types in terms of their magnetic susceptibility  $\chi$  which is the ratio of the magnetization  $M$  to the applied field  $H$ , i.e.,  $\chi = M/H$  (see Table 2-1): ferromagnetism, ferrimagnetism, antiferromagnetism, diamagnetism and paramagnetism. Ferromagnetic and ferrimagnetic materials are usually considered as “magnetic”, whereas the other three types are so weakly magnetic (the susceptibility  $\chi$  is very low) that they are usually referred to as “nonmagnetic”.

The periodic table in Figure 2-6 shows the magnetic behavior of each element. Most of the pure elements are diamagnetic or paramagnetic. Only Cr is antiferromagnetic. These elements are usually referred to as nonmagnetic. Only Fe, Co, and Ni are ferromagnetic. Table 2-2 lists the saturation polarization and Curie temperature of these three elements. Ferrimagnetism is not observed in any pure element, it can only be

obtained in compounds, such as ferrites, from which ferrimagnetism derives its name. Therefore, alloys and compounds (mainly oxides) made from Fe, Co, and Ni are the most commonly utilized magnetic materials.

**Table 2-1.** Summary of types of magnetism. [Birmingham04].

Type of Magnetism	Susceptibility	Atomic / Magnetic Behaviour	Example / Susceptibility
Diamagnetism	Small & negative	Atoms have no magnetic moment 	Au $-2.74 \times 10^{-6}$ Cu $-0.77 \times 10^{-6}$
Paramagnetism	Small & positive	Atoms have randomly oriented magnetic moments 	$\beta$ -Sn $0.19 \times 10^{-6}$ Pt $21.04 \times 10^{-6}$ Mn $66.10 \times 10^{-6}$
Ferromagnetism	Large & positive	Atoms have parallel aligned magnetic moments 	Fe $\sim 100,000$
Antiferromagnetism	Small & positive	Atoms have anti-parallel aligned magnetic moments 	Cr $3.6 \times 10^{-6}$
Ferrimagnetism	Large & positive	Atoms have mixed parallel and anti-parallel aligned magnetic moments 	Barium ferrite $\sim 3$ $\text{BaO} \cdot 6\text{Fe}_2\text{O}_3$

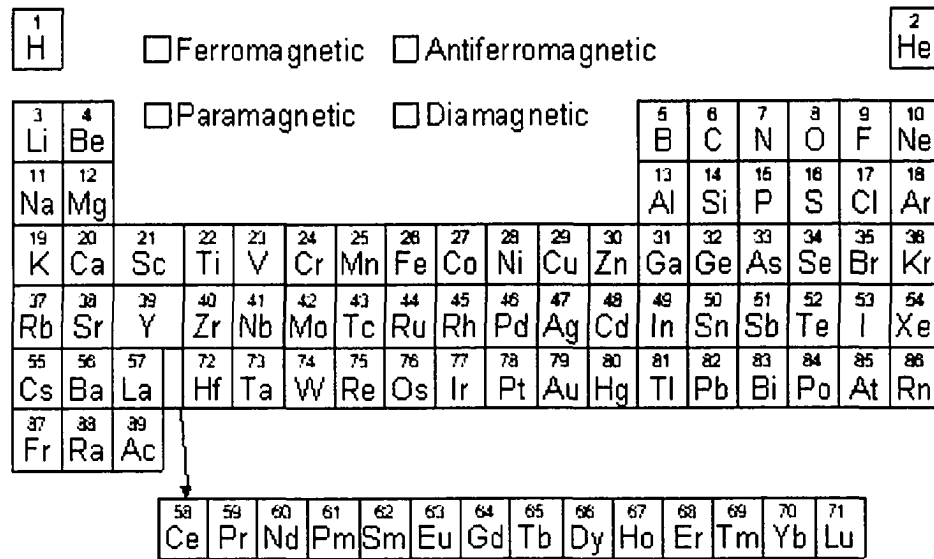


**Figure 2-6.** Periodic table showing the magnetic behavior of each element at room temperature. [Birmingham04]

**Table 2-2.** The saturation polarization ( $I_s$ ) and Curie temperature ( $T_c$ ) of Co, Fe, Ni. [Birmingham04]

Element	Magnetism	$I_s$ at 298K (Tesla)	$T_c$ (°C)
Fe	Ferro	2.15	770
Co	Ferro	1.76	1131
Ni	Ferro	0.60	358

According to the magnetic field required to demagnetize the materials (i.e., coercivity  $H_c$ ), magnetic materials are grouped into soft magnetic materials and hard magnetic materials. Soft magnetic materials have the characteristics of lower coercivity  $H_c$  and lower hysteresis loss (smaller hysteresis loop area) relative to hard magnetic materials (Figure 2-7). They are central components in micro-electro-mechanical systems (MEMS) [Myung03], especially in electromagnetic devices such as magnetic recording heads, magnetic sensors, step motors and transformers.

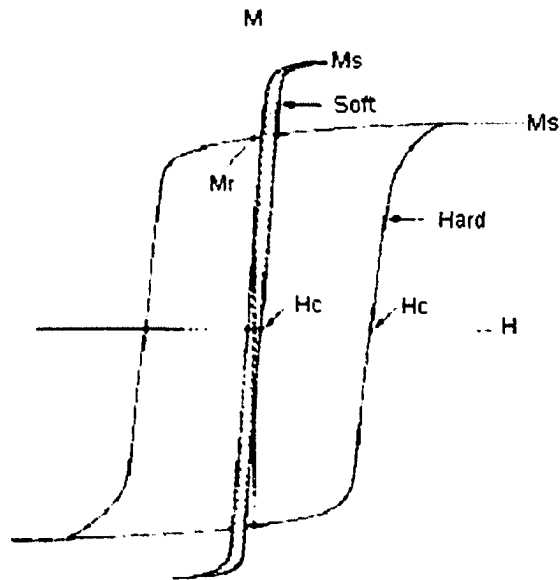


**Figure 2-7.** Schematic hysteresis loops of “soft” and “hard” magnetic materials. ( $H_c$  and  $M_s$  are coercivity and saturation magnetization, respectively.) [Howard86]

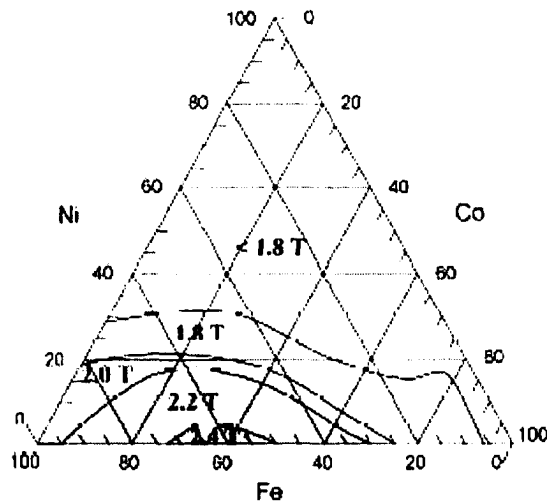


**Figure 2-8.** Composition-high saturation magnetic flux density  $B_s$  diagram for bulk CoFeNi ternary alloys published by Bozorth. [Bozorth51]

As early as 1951, Bozorth reported the composition- $B_s$  diagram of bulk CoFeNi ternary alloys (Figure 2-8). [Bozorth51] It is known that many alloys with high  $B_s$  (can

be as high as 2.4 Tesla) have compositions near Fe<sub>60</sub>Co<sub>40</sub>. However, they do not possess low coercivity  $H_c$ . Therefore, it has been a challenge to fabricate high  $B_s$  (>2 Tesla) CoFe or CoFeNi films with optimal soft magnetic properties by electroplating.

### 2.2.2 Concepts of major magnetic properties

The explanation and description of the concepts and units of magnetic properties in the literature are not uniform, and often cause confusion. Here, the concepts of some major magnetic properties are briefly introduced. [Electronic 04]

#### *Magnetic moment $m$*

The concept of magnetic moment is the starting point when discussing the behavior of magnetic materials within a magnetic field. If a bar magnet is placed in a field, it will experience a torque or moment tending to align its axis in the direction of the field. A compass needle behaves the same way.

Magnetic (dipole) moment is the torque exerted on a magnet or dipole when it is placed in a magnetic field.

#### *Magnetization $M$*

Magnetization is the magnetic moment  $m$  per unit volume of the substance:

$$M = m / V$$

#### *Magnetic flux $\Phi$*

Magnetic flux is a measure of the number of magnetic field lines that pass perpendicularly through a surface.

#### *Magnetic flux density $B$*

Magnetic flux density is simply the total flux divided by the cross sectional area of the part through which it flows -  $B = \Phi / A$

The magnetic flux density in a substance depends on both the applied field  $H$  and the magnetization  $M$  of the substance:

$$B = \mu_0 (H + M) = \mu_0 H + \mu_0 M$$

where  $\mu_0$  is the permeability of vacuum, and  $\mu_0 = 4\pi \times 10^{-7}$ .

### *Magnetic polarization I*

Magnetic polarization (also known as intensity of magnetization) is defined as:

$$I = \mu_0 M \quad (\text{units are Wb/m}^2)$$

Therefore,  $B = \mu_0 H + \mu_0 M = \mu_0 H + I$

### *Coercivity Hc*

Coercivity is the magnetic field strength needed to reduce the magnetization of a magnetic material to zero after it has reached saturation (Figure 2-7).

### *Magnetic Susceptibility $\chi$*

The magnetic susceptibility  $\chi$  is the name given to the ratio:

$$\chi = I / H$$

The relative magnetic susceptibility  $\chi_r$  is defined by

$$\chi_r = M / H = \chi / \mu_0$$

### *Permeability $\mu$*

The magnetic permeability of a particular material is defined as the ratio of magnetic flux density to field strength:

$$\mu = B / H$$

$$\mu = \mu_0 + \chi = \mu_0(1 + \chi_r)$$

The relative magnetic permeability  $\mu_r$  is defined by

$$\mu_r = \mu/\mu_0$$

The units employed in magnetic systems are very complicated and not uniform. The change over to the international system of units (SI) has been slower in the field of magnetism than in other fields. Now SI is the recommended system of units in many journals. The conversion of other unit systems to SI is listed in Table 2-3.

From Table 2-3, it can be seen that in the cgs-Gauss unit system:

$$B = H + 4\pi M$$

The unit for magnetic field strength  $H$  is Oe, and the unit for magnetic flux density  $B$  is G (Gauss), so 1Oe = 1G. Therefore, Gauss is also used as the unit of magnetic field strength  $H$  in many references.

In MKSA units,  $B = \mu_0 H + I$ .

Magnetic polarization  $I$  has the units of Wb/m<sup>2</sup>, magnetic flux density has the unit of Tesla (T), so that 1 Wb/m<sup>2</sup> = 1 T. As a result, T is also often adopted as the unit of magnetic polarization  $I$  in references.

In SI units,  $B = \mu_0 (H + M)$ .

Both magnetization  $M$  and magnetic polarization  $I$  have the same units of A/m or J/(T · m<sup>3</sup>). According to the definition of magnetic polarization  $I$ :

$$I = \mu_0 M \quad (\text{unit Wb/m}^2)$$

In SI units,  $I$  and  $M$  use the same units of A/m, so the factor  $\mu_0$  has been taken out from  $I$  in SI units. Therefore, it is not necessary to employ the concept of magnetic polarization  $I$ , or magnetization  $M$  and magnetic polarization  $I$  can be considered as identical in SI units. Magnetic susceptibility  $\chi$  and relative magnetic susceptibility  $\chi_r$  are identical in SI. Now the concept of relative magnetic susceptibility  $\chi_r$  is rarely used in references.

**Table 2-3. Unit conversion table for magnetism related properties. [Magnetics 04]**

Quantity	Symbol	cgs-Gauss units $B = H + 4\pi M$	Conversion factor to SI	MKSA units (E-H cor.) $B = \mu_0 H + I$	Conversion factor to SI	SI (E-B cor.) $B = \mu_0 (H + M)$
Magnetic flux density	$B$	G	$10^{-4}$	T, Wb/m <sup>2</sup>	1	T, Wb/m <sup>2</sup>
Magnetic flux	$\Phi$	Mx	$10^{-8}$	Wb	1	Wb
Magnetic field strength	$H$	Oe	$10^3/4\pi$	A/m	1	A/m
Magnetization	$M, I$	emu/cm <sup>3</sup>	$10^3$	Wb/m <sup>2</sup>	$1/\mu_0$	A/m, J/(T · m <sup>3</sup> )
Mass magnetization	$\sigma$	emu/g	1	(Wb · m)/kg	$1/\mu_0$	A · m <sup>2</sup> /kgJ/(T · kg)
Magnetic moment	$m$	emu	$10^{-3}$	Wb · m	$1/\mu_0$	A · m <sup>2</sup> , J/T
Susceptibility	$\chi$	—, (emu/(cm <sup>3</sup> · Oe))	$4\pi$	H/m <sup>a</sup>	$1/\mu_0$	— <sup>b</sup>
Permeability of vacuum	$\mu_0$	1	$4\pi \times 10^{-7}$	H/m	1	H/m
Permeability	$\mu$	—	$4\pi \times 10^{-7} = \mu_0$	H/m	1	H/m
Maximum energy product	$(BH)_{max}$	G · Oe	$10^{-1}/4\pi$	J/m <sup>3</sup>	1	J/m <sup>3</sup>
Energy density	$E, K$	erg/cm <sup>3</sup>	10 <sup>-1</sup>	J/m <sup>3</sup>	1	J/m <sup>3</sup>

<sup>a</sup>  $\chi = I / H$ .  $\chi_r$  is defined by  $\chi_r = \chi / \mu_0$  and is equal to  $\chi$  in SI units.

<sup>b</sup>  $\chi = M / H$  in SI units.

From  $B = \mu_0 H + \mu_0 M = \mu_0 H + I$  (paying attention to units), since  $\mu_0 H$  is a small amount ( $\mu_0 = 4\pi \times 10^{-7}$  and for magnetic materials  $M \gg$  saturation field  $H$ ), magnetic flux density  $B$ , magnetic polarization  $I$  and magnetization  $M$  all have been employed to express the strength of magnetism of magnetic materials. Usually, Tesla (T) is used as the unit. The saturation magnetization  $M_s$  measured in emu/cm<sup>3</sup> can be converted to Tesla with the factor  $\mu_0 \times 10^3$ , i.e.,  $M_s$  (in Tesla) =  $\mu_0 \times 10^3 \times M_s$  (in emu/cm<sup>3</sup>). Some references also use Gauss (G). It is recommended to employ SI units in the field of

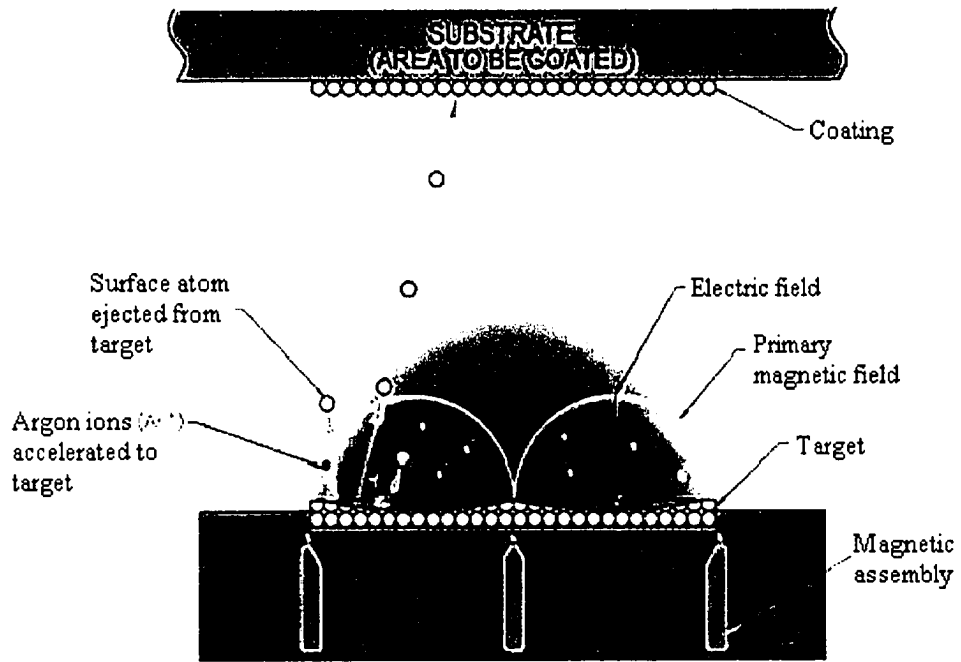
magnetism. However, due to historical reasons, the employment of units in references is mainly determined by the habits of researchers and commercial standards.

## **2.3 Soft magnetic thin films developed by various processes**

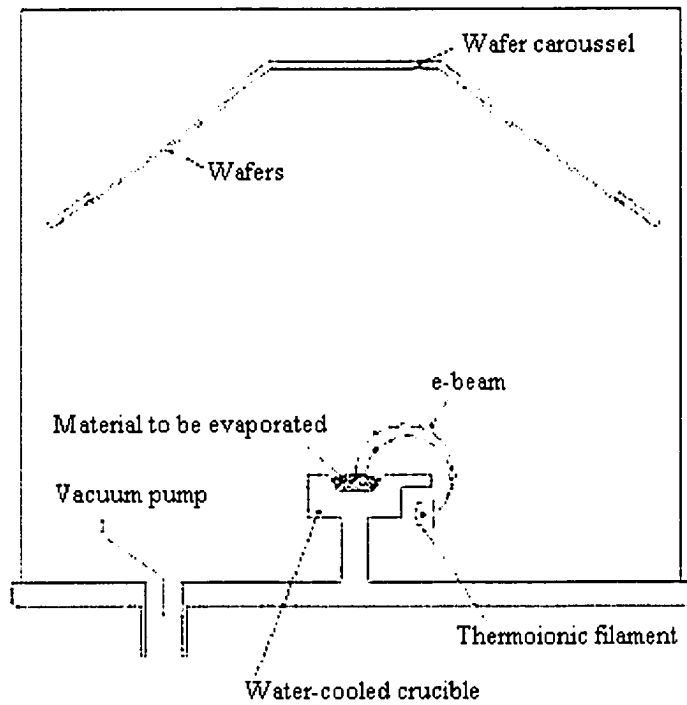
Vacuum processes (sputtering and evaporation) and electrochemical deposition (electroless- and electro- deposition) are the major processes employed to prepare CoFe, CoFeNi and other soft magnetic thin films for fabricating recording heads.

### **2.3.1 Soft magnetic thin films prepared by vacuum processes**

Sputtering and evaporation are the main vacuum processes utilized to deposit soft magnetic films. Schematic sketches of sputtering and evaporation processes are illustrated in Figures 2-9a and b, respectively. Sputtering is performed by applying a high voltage across a low-pressure gas (usually argon at about 5 millitorr ( $\approx 6.67 \times 10^{-4}$  Pascal)) to create a plasma, which consists of electrons and gas ions in a high-energy state. During sputtering, accelerated plasma ions strike a target (composed of the desired coating material), and cause atoms from that target to be ejected with enough energy to travel to, and bond with, the substrate. [Angstrom04] In evaporation, the source material is heated to boil and evaporate. A vacuum is required to allow the atoms to evaporate freely in the chamber, and they subsequently condense on all surfaces. The principle for all evaporation technologies is the same, except for the method used to heat (evaporate) the source material. There are two popular evaporation technologies: e-beam evaporation and resistive evaporation. In e-beam evaporation, an electron beam is aimed at the source causing local heating and evaporation, while in resistive evaporation, a tungsten boat, containing source material, is heated electrically to make the material evaporate. Because of its non-selective deposition, preparation of soft magnetic films using evaporation has been seldom reported.



a. Sputtering process [Angstrom04]



b. E-beam evaporation process. [MEMS04]

**Figure 2-9.** Schematic sketches of sputtering and evaporation processes.

Sputter deposited FeN and FeXN (X=Co, Ti, Ta, and Rh, etc.) films, and FeCo-based films can have saturation magnetic flux densities  $B_s$  as high as 2.45 Tesla. They are promising materials for writer pole applications. These films consist of a dominant  $\alpha$ -Fe phase with slightly expanded lattice parameters. [Chen00]

Hu et al [Hu94] built write heads with sputtered high magnetization (1.94 Tesla) polycrystalline FeN thin films, which were laminated with  $Al_2O_3$  layers. Despite the lower permeability of FeN, compared with FeNi, the heads demonstrated superior write performance on a media with 3800 Oe coercivity. Terada and coworkers [Terada84] sputtered FeN thin films with various compositions, and investigated the dependence of crystal structure and magnetic properties on sputtering conditions. Wang et al and other researchers also made similar studies on the sputtering of iron nitride thin films. [Wang90] [Wang03] [Takahashi90] [Kijima89] [Russak92]

Employing a sputtering process, Wang and coworkers [Wang00] [Sun00] [Sun02] created soft magnetic films with a sandwich structure,  $Ni_{0.81}Fe_{0.19}/(Fe_{0.7}Co_{0.3})_{1-x}N_x/Ni_{0.81}Fe_{0.19}$ , in which the FeCoN film was 100 nm thick, and the  $Ni_{0.81}Fe_{0.19}$  permalloy layer was 5 nm thick, comprising only 4.5% of the volume of the sandwich. The saturation magnetization of this new material was 2.4 Tesla. Thicker soft magnetic films with similar properties can be fabricated by laminating  $Ni_{0.81}Fe_{0.19}/(Fe_{0.7}Co_{0.3})_{1-x}N_x$  bilayers. The deposited FeCoN single layers have a strong {110} oriented bcc lattice with a high saturation magnetization of 2.45 Tesla, and a coercivity of 5 Oe. A lower coercivity of 0.6 Oe was achieved in the sandwiched material.

Wang et al [Wang99] investigated soft magnetic properties and thermal stability of FeTiN films prepared by reactive sputtering, which have compositions in the range of 8–10 at % Ti, 10.5–14 at % N, and the balance Fe. The as-deposited films exhibited good

soft magnetic properties without any post heat treatment, e.g., a low coercivity  $H_c$  of 1.5 Oe and high saturation magnetization  $M_s$  of 2.4 Tesla.

Ishiwata et al [Ishiwata91] developed high nitrogen (10.5–14.5 at % N) FeTaN films as magnetic head core material by a nitrogen reactive sputtering method followed by appropriate annealing (500–550°C). The deposited films had high saturation flux density (1.4–1.7 Tesla) and excellent soft magnetic properties: low coercivity (~0.1 Oe), high relative permeability (3000 at 20 MHz), and small saturation magnetostriction ( $< 0.5 \times 10^{-6}$ ). A fine crystal structure ( $< 10$  nm) is essential for the soft magnetism of FeTaN films. Chen [Chen99], Qiu [Qiu93] and their coworkers did similar research.

Chen et al sputtered [Chen00] FeRhN films with a high resistivity of 80–120  $\mu\Omega\text{cm}$  and saturation flux density  $B_s$  of 1.4–1.7 Tesla, using a FeRh target with about 3 at % of Rh. The films deposited under optimal sputtering conditions consisted of mixed phases of  $\alpha$ -Fe and Fe<sub>4</sub>N. It was reported that a small expansion of  $\alpha$ -Fe and Fe<sub>4</sub>N lattice is crucial for achieving soft magnetic properties. Jiang et al deposited FeRhN(~50 nm)/NiFe(~5 nm) laminated thin films by dc magnetron sputtering [Jiang02].

Yu et al [Yu02] deposited 100-nm-thick Fe<sub>35</sub>Co<sub>65</sub> films with a dc magnetron sputtering system using a Fe<sub>35</sub>Co<sub>65</sub> alloy target at 100-W target power in a 3 mtorr Ar atmosphere. Films with a saturation magnetization of 2.35 T and coercivity of over 60 Oe were obtained. It was found that, during the deposition of Fe<sub>35</sub>Co<sub>65</sub> films, an increase in oxide contamination at the grain boundaries decreased film saturation magnetization and increased coercivity.

Liao et al summarized the magnetic properties of CoFe films fabricated by evaporation and sputtering processes (Table 2-4) [Liao88]. Films with a saturation magnetization of 1.9 Tesla and coercivities around 20 Oe could be deposited by vacuum techniques.

**Table 2-4.** Magnetic properties of CoFe films produced by vacuum techniques. [Liao88]

	Vacuum evaporated	Vacuum sputtered
Film thickness	0.1-0.5 microns	0.1-0.5 microns
Operating temperature	Over 250 °C	Over 250 °C
Coercivity $H_c$	18 Oe	20 Oe
Saturation magnetization $M_s$	1.9 T	1.9 T

Tagawa et al [Tagawa01] sputtered soft magnetic FeCoAlO films using compacted targets of Fe<sub>70</sub>Co<sub>30</sub> alloy and Al<sub>2</sub>O<sub>3</sub> powders at 2 kW on water-cooled Al<sub>2</sub>O<sub>3</sub>-TiC substrates under an Ar atmosphere. The FeCo alloy concentrations in films were varied by adjusting the FeCo/Al<sub>2</sub>O<sub>3</sub> mixing ratios in the targets. Film thickness was in the range of 0.15 to 0.3 μm. The deposited FeCoAlO films were claimed to have a high saturation flux density  $B_s$  of 2.4 Tesla and a coercivity less than 1 Oe at the hard axis. Ohnuma et al [Ohnuma99] [Ohnuma02], Ikeda et al [Ikeda02] [Ikeda02-1], and Shintaku et al [Shintaku02] also reported the fabrication of soft magnetic FeCoAlO films by sputtering; similar results were obtained.

Vas'ko et al [Vas'ko02] deposited (Fe<sub>54</sub>Co<sub>46</sub>)<sub>1-x</sub>Cr<sub>x</sub> thin films (~100nm) by magnetron sputtering on Si/SiO<sub>2</sub> substrates. The films consisted of the bcc phase with (110) oriented texture. The Fe<sub>54</sub>Co<sub>46</sub> films had a saturation magnetization of 2.45 Tesla at room temperature. Doping the Fe<sub>54</sub>Co<sub>46</sub> films with 0-13 at % of Cr increased the corrosion resistance and electrical resistivity, but reduced the saturation magnetization as a function of added Cr amount. The coercivity of both doped and undoped as-deposited films decreased substantially from 80–120 Oe to 40 Oe after magnetic annealing at 220°C. Coercivity in the range 40–90 Oe makes these films feasible for a possible application in recording heads, as the field generated by a writer coil usually exceeds 200 Oe.

Hoshiand and Naoe [Hoshiand86] studied the magnetic properties of sputtered Fe-Co-M (M: Mn, V) alloy films, and found that the substitution of Mn or V is not effective in improving the soft magnetic properties of Fe-Co alloy films. The minimum coercivity  $H_c$  of films attained in their work was 16 Oe. Klemmer et al [Klemmer00] tried to sputter FeCoB thin films, while Omata [Omata90-1] fabricated NiFeCo films through evaporation; no special results were achieved.

Chapman et al [Chapman79] [Chapman81] investigated the effects of oxygen level and substrate temperature on the magnetic and structural properties of FeNi films evaporated in ultrahigh vacuum and in ordinary vacuum systems. The differences in magnetic and structural properties of FeNi films deposited were attributed to the variation of oxygen levels in the systems. When the oxygen partial pressure reached about  $10^{-10}$  Torr during deposition, the values of film coercivity increased.

Krusch [Krusch86] studied the sputter parameters of depositing permalloy for the magnetic poles of thin film heads. Argon and nitrogen mixtures were used as the sputter gas. It was found that the coercivity decreased when the nitrogen content in sputter gas was raised from 0% to more than 1%. The saturation magnetostriction  $\lambda_s$  was very sensitive to the target composition. Changing from 76.6 to 82.4 wt% Ni in target caused a  $\lambda_s$  variation from  $+5 \times 10^{-6}$  to  $-2.5 \times 10^{-6}$ . In addition,  $\lambda_s$  could be controlled by varying the nitrogen content (0-5 %) in sputter gas. Higher bias voltages resulted in more negative  $\lambda_s$  values. The sputter parameters were optimized in this research. Sputtering of permalloy for thin film heads was also explored by other researchers. [Collins81] [Yang89] [Jones95] FeNi films with similar magnetic properties were obtained.

### **2.3.2 Soft magnetic thin films prepared by electrodeposition**

Vacuum processes involve complicated and expensive vacuum operation. Sputtering processes are not suitable for fabricating thick films (more than 1 micron) needed in

some applications, where electroplating methods are preferred. Moreover, electroplating through a mask can supply easier definition and control of small features like yokes and pole tips in recording heads; and subtractive processes like etching or ion milling could be eliminated. The early development of processes for plating nickel-iron alloys enabled thin-film recording heads to be technologically and economically viable. [Chiu96] With the advantages of simplicity, cost-effectiveness and controllable patterning, electroplating processes have major significance in the fabrication of thin-film recording heads. Many researchers now have turned toward electroplating processes to satisfy new data-recording requirements.

Electrodeposition, also known as electroplating, is an electrochemical process by which metal is deposited on a conductive substrate by passing a current through the bath. In an electroplating system, there is an anode (positively charged electrode), and a cathode (negatively charged electrode) which is the substrate to be coated (Figure 2-10). Plating is done with an electrolyte which contains the metal(s), to be plated, in ionic form. As the external current is applied, positive metal ions from the solution are attracted to the negatively charged cathode and deposit on it.

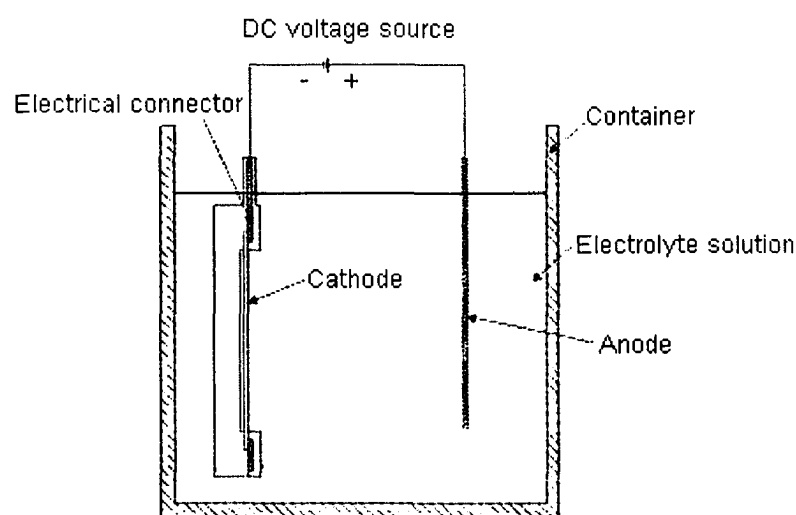


**Figure 2-10.** Typical setup for electrodeposition. [MEMS04]

Andricacos and Robertson summarized some properties of common electroplated soft magnetic materials for fabricating recording heads, as listed in Table 2-5. [Andricacos98] CoFe, CoFeNi and CoFeCu alloys have the highest possible saturation magnetization. Therefore these materials, especially CoFe and CoFeNi alloys, have attracted the most attention of researchers. In this part, the literature about electrodeposition of FeNi alloys, CoFe alloys, CoFeNi alloys and other alloys, will be reviewed sequentially.

**Table 2-5.** Main properties of some electroplated soft magnetic materials. [Andricacos98]

Material	Coercivity $H_c$ (Oe)	Anisotropy field $H_k$ (Oe)	Magnetostriction coefficient $\lambda$	Saturation magnetization relative to $Ni_{80}Fe_{20}$
$Ni_{80}Fe_{20}$	0.3	2.5	-0+*	1
$Ni_{45}Fe_{55}$	0.4	9.5	+	1.6
NiFeCo	1	6-10	-0+	0.8-2.4
NiFeCoB	0.6	14		1.5
CoNiFeS	1	20	+	1.7
CoFe	3	7-14	-0+	1.9
CoFeCr	0.3	20	-	1.7
CoFeNiCr	0.5		+	1.7
CoFeP	1	15	-0+	1-1.5
CoFeCu	1	13-18	-0+	1.7-2.2
CoB	1	40		1.2

\*  $\lambda$  can be negative, zero, or positive depending on alloy composition. For NiFe alloys,  $\lambda$  is negative below about 19 wt% Fe and positive above about 19 wt% Fe.

### 2.3.2.1 Electrodeposition of FeNi alloys

The first studied soft magnetic alloys for thin film inductive heads were FeNi alloys. Electrodeposited permalloy ( $\text{Ni}_{80}\text{Fe}_{20}$ ) was introduced as the core material of thin film inductive heads by IBM in 1979. [Chiu96] Therefore, many studies have been made on the electrodeposition of FeNi alloys. Low pH baths are usually employed in FeNi electroplating.

Electrodeposition of FeNi alloys is regarded as anomalous codeposition because the less noble metal (Fe) is deposited preferentially. In the earlier studies, the anomalous behavior was assumed to be due to the precipitation of iron hydroxide on cathode surface, which blocks nickel reduction, instead of iron reduction. [Krause97] However, this hypothesis could not explain some experimental work. Vaes et al [Vaes00] investigated the role of hydroxyl compounds during the anomalous electrodeposition of NiFe alloys. It was found that the Ni- $\text{H}_2$  and Fe- $\text{H}_2$  systems also exhibit anomalous codeposition behavior. The inhibition of Ni and H reduction in the Ni-Fe- $\text{H}_2$  system cannot be explained in terms of metal hydrolysis reactions. They concluded that metal hydrolysis does not play a determining role in anomalous NiFe codeposition.

Zech and coworkers [Zech99-1] [Zech99-2] studied the codeposition behavior of three alloy systems, FeNi, FeCo, and CoNi in acid sulfate electrolytes using rotating cylinder electrodes to control mass transport conditions. Their work confirmed that Ni deposition is inhibited by the presence of  $\text{Fe}^{2+}$  and  $\text{Co}^{2+}$  ions, while the Fe deposition rate is enhanced by the presence of  $\text{Co}^{2+}$  and  $\text{Ni}^{2+}$  ions. The anomalous codeposition of iron group metals involves both inhibiting and accelerating effects. The anomalous electrodeposition of nickel-iron was also discussed by Gangasingh and Talbot. [Gangasingh91]

Gao et al [Gao95] [Gao97] electroplated permalloy films with a composition of 81at% Ni and 19at% Fe at a voltage of  $-1.2$  V (versus the saturated calomel electrode

(SCE)) from a bath containing 0.5 M NiSO<sub>4</sub>, 0.02 M FeSO<sub>4</sub> and 0.4 M H<sub>3</sub>BO<sub>3</sub> with a pH of 3. Transmission electron microscopy analyses demonstrated that these films consisted of fcc Ni-Fe nanocrystalline grains (10–50 nm) embedded in an amorphous matrix.

Yin et al [Yin 95] studied FeNi plating bath solution chemistry by determining the Fe-Ni equilibrium concentrations at various pH levels. They found that the alloy composition was determined by solution equilibria, mass transfer of the electroactive species within the diffusion layer and by the surface coverage of organic additives on the electrode. The effects of rotation speed of the disc electrode and the presence of organic additives on the deposition of Fe-Ni alloys were observed. Boric acid increased the absolute iron deposition rate, but inhibited the rate of nickel reduction. Saccharin and ethylene diamine influenced the metal deposition rate but were not as effective as boric acid.

Venkatsetty [Venkatsetty70] plated out Ni<sub>80</sub>Fe<sub>20</sub> thin films from a citrate-complexed nickel-iron electrolyte. The magnetic properties, like the coercivity  $H_c$  and the anisotropy field  $H_k$ , were investigated as a function of current density, pH, temperature and the concentration of citrate ion. The ferromagnetic domain patterns observed as a function of thickness showed the same behavior as those observed in evaporated films. It was found that both the current density and the temperature had significant effect on film stress.

Harris et al [Harris99] found that complexing agent ethylenediamine (EDA) greatly affected the phenomenon of anomalous codeposition observed in the nickel-iron electroplating system. EDA increased the Ni/Fe ratio in the deposit when the bath was chloride-based and the pH was at least 5. Ion microprobe analysis indicated that EDA was incorporated in the deposit. They hypothesized that EDA adsorbs on the deposit surface and serves as a bridge for Ni<sup>2+</sup> deposition in preference to that for Fe<sup>2+</sup>, which

forms less stable complexes with EDA. Chloride ion in the bath is necessary for the adsorption of EDA and, thus, the relative increase in the nickel deposition rate.

Afshar et al [Afshar02] analyzed the electrodeposition of nickel, iron and nickel–iron alloys at pH 3.0 using electrochemical techniques in the presence of complexing compounds citrate and glycolic acid. Cyclic voltammetry and transient time ( $\tau$ ) measurements were employed to characterize the system. Potentiostatic  $I-t$  transients were recorded to obtain the nucleation and growth mechanism. The cyclic voltammetry results demonstrated that the electrodeposition of nickel, iron and nickel–iron alloys was a diffusion-controlled process with a typical nucleation mechanism. The redox potentials of Ni and Fe shifted to more cathodic values in electrolytes with the addition of complexing agents. The number of nucleation sites increased with increasing overpotential and nickel concentration. It was found that with the addition of glycolic acid to the sodium citrate solution, both the number of nucleation sites and the nucleation rate were increased for Ni–Fe alloy deposition. A large number of equally sized spherical grains were observed in spherical clusters. The spherical particles became finer and the surface roughness was decreased. Therefore, the microstructure of the Ni–Fe deposits was changed dramatically in the presence of glycolic acid.

Many mathematical models have been developed to simulate the electrodeposition of FeNi alloys. Yin developed a mathematical model to describe the electroplating of FeNi alloys in the presence of an organic inhibitor. [Yin97] The model includes the mass transport of participating ionic species, homogeneous chemical reactions within the diffusion layer, the metal hydroxyl ion and inhibitor adsorption, and the associated electrochemical kinetics. The model can be used to predict the iron-nickel deposition rate (iron and nickel content in the alloy) as a function of the disk rotation speed, solution pH, and the bulk concentrations of the electroactive species and the organic additive. Their model results indicated that in the presence of an organic additive (saccharin), higher

ferrous ion and nickel ion concentrations could be preserved at the interface without concentration depletion within the diffusion layer. The model also predicted that iron content in the alloy increases by increasing the concentration of organic additive and by increasing the electrolyte pH and disk rotation rate. Ramasubramanian et al [Ramasubramanian96] developed a mathematical model to describe the electrodeposition of Fe-Ni alloys and Fe-Ni-SiO<sub>2</sub> composites under potentiostatic conditions. The model predictions were found to agree well with the experimental observations for the Fe-Ni and Fe-Ni-SiO<sub>2</sub> systems. The model could predict the polarization behavior, partial current densities, and alloy composition as a function of the applied potential. Other workers have also done exploratory studies in this area. [Baker97] [Sasaki00] [Grande93-2]

In 1997, Robertson and coworkers [Robertson97] reported high magnetic moment Ni<sub>45</sub>Fe<sub>55</sub> alloy deposited by electroplating, and employed it to replace Ni<sub>80</sub>Fe<sub>20</sub> for fabricating high performance write heads. The Ni<sub>45</sub>Fe<sub>55</sub> alloy has a saturation magnetization  $M_s$  of 1.6 Tesla and resistivity  $\rho$  of 48  $\mu\cdot\Omega/\text{cm}$ . These are much higher than those of Ni<sub>80</sub>Fe<sub>20</sub>, which are only 1 Tesla and 24  $\mu\cdot\Omega/\text{cm}$ , respectively. It was stated that the recording performance of a write head built with Ni<sub>45</sub>Fe<sub>55</sub> alloy demonstrated marked improvement.

General studies on the electroplating of nickel-iron alloy films were also conducted by other researchers. [Wolf57] [Romankiw75] [Romankiw78] [Lehman80] [Bieliński79] [Bialozor84] [Lieder85] [Andricacos89] [Grande93-1] [Yin96-1] [Yin96-2] [Matlosz93] [Kieling97] [Leith99] [Sasaki95]

### 2.3.2.2 *Electrodeposition of CoFe alloys*

The electroplating of CoFe alloys has been studied by many researchers. Usually a low pH sulfate-based or chloride-based bath is utilized. Electrodeposited CoFe alloys

have much higher saturation magnetization  $M_s$  than electrodeposited FeNi alloys, but also have larger coercivity  $H_c$ .

Liao et al [Liao87] [Liao88] investigated the electrodeposition of  $C_{90}Fe_{10}$  alloys, which have a saturation flux density  $B_s$  of 1.9 Tesla and a coercivity  $H_c$  of about 9 Oe. They found that the overwrite performance of a thin film head fabricated with this alloy was superior to that of a thin film head built with permalloy. The composition of the plating bath employed by them is shown in Table 2-6. The sodium lauryl sulfate (also referred to as sodium dodecyl sulfate) acts as a surfactant to suppress pitting. Sodium saccharin is used to decrease film stress, and boric acid acts as a pH buffer for maintaining a low bath pH.

**Table 2-6.** Composition of bath for electroplating CoFe alloys. [Liao88]

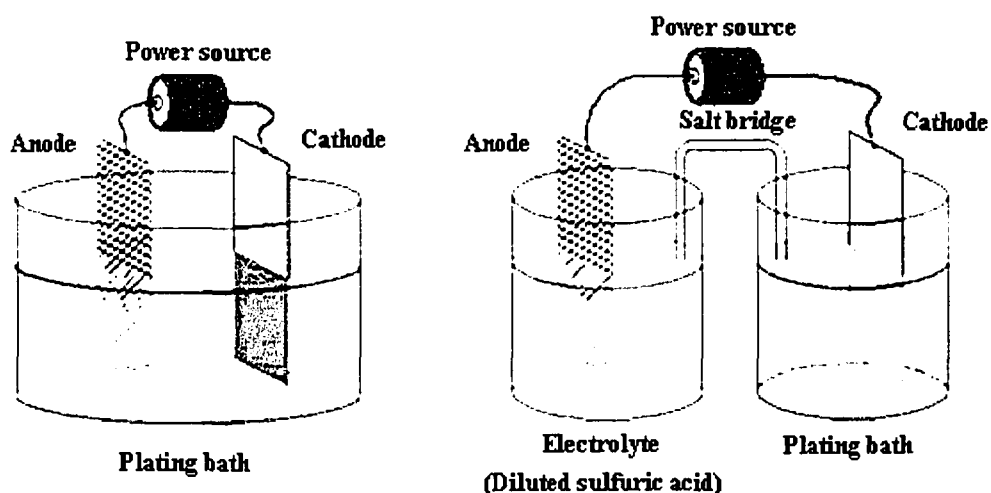
Chemical	Concentration, g/L	Chemical	Concentration, g/L
$CoSO_4 \cdot 7H_2O$	100-120	$H_3BO_3$	25-35
$FeSO_4 \cdot 7H_2O$	7-10	Sodium lauryl sulfate	0.1-0.5
Sodium saccharin	1-3	Bath pH 3.0-4.0	

Osaka and coworkers [Osaka03-1] [Imai02] reported the electrodeposition of  $Co_{35}Fe_{65}$  alloy with high saturation flux density  $B_s$  (2.4 Tesla). The electrolyte composition they employed is listed in Table 2-7. It consisted of almost the same components as the bath utilized by Liao et al, except for the introduction of  $NH_4Cl$  to improve bath conductivity, different metal salt concentrations and a lower pH. The deposition of films with a  $B_s$  of 2.4 Tesla can be realized by using a separated compartment dual cell system to reduce the oxidization of  $Fe^{2+}$  to  $Fe^{3+}$  at the anode (Figure 2-11). The coercivities of plated films are around 15 Oe, which are a little high. According to the researchers, film coercivity can be lowered to less than 10 Oe by

annealing at 350 - 400°C with the *B*s remaining at 2.4 Tesla.

**Table 2-7.** Composition of electrolyte for depositing CoFe alloys. [Osaka03-1]

Chemical	Concentration	Chemical	Concentration
CoSO <sub>4</sub> ·7H <sub>2</sub> O	0.047-0.050 M	H <sub>3</sub> BO <sub>3</sub>	0.4 M
FeSO <sub>4</sub> ·7H <sub>2</sub> O	0.050-0.053 M	Sodium lauryl sulfate	0.01 g/L
NH <sub>4</sub> Cl	0.4 M	Bath pH 2.3	



a. Conventional system

b. Separated compartment dual cell system

**Figure 2-11.** Models of systems for electroplating CoFe thin films. [Waseda2]

Bertazzoli and Pletcher [Bertazzoli93] studied the electrodeposition of FeCo alloys onto vitreous carbon from a sulfate bath at pH 4. It was found that the composition of the alloy was mainly determined by the ratio of Fe(II)/Co(II) in solution and only slightly by temperature or potential/current density. The Fe content in the deposits was always higher than the ratio of Fe(II)/Co(II) in solution, although the observation from studies of the single Fe(II) and Co(II) solutions demonstrated that the Fe(II) was more difficult to reduce than Co(II) at 200 mV. The kinetics of nucleation and early growth of the metal

lattices, as well as the kinetics of the  $M/M^{2+}$  couples, were also investigated by them. The equilibrium potentials of the alloys in the plating solutions were close to that for  $Co/Co^{2+}$  couple. However, the presence of  $Fe(II)$  in solution changed the mechanism for cobalt deposition, as well as inhibited the early stages of nucleation and growth.

Lallemand and coworkers [Lallemand04-1] [Lallemand04-2] [Lallemand02] [Ricq01] conducted comparative studies of the influence of organic additives saccharin, phthalimide (PHTA), and *o*-toluene sulfonamide (*o*TOL) on CoFe alloy electrodeposition at pH around 3. The chemical structures of these organic compounds are shown in Figure 2-12. It was noted that saccharin influenced strongly the electrode kinetics in contrast to *o*TOL and PHTA. The use of saccharin resulted in smoother, more compact and more leveled deposits as compared with PHTA or *o*TOL.

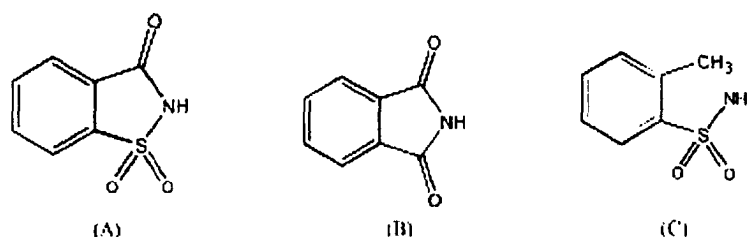


**Figure 2-12.** Chemical structures of (a) saccharin, (b) phthalimide (PHTA) and (c) *o*TOL. [Lallemand04-2]

Kim et al [Kim03] plated out iron group binary (CoFe and NiCo) and ternary (CoFeNi) alloy thin films from sulfate and chloride baths, and related film magnetic properties to their chemical composition, grain size and corresponding crystal structure. It was found that anions influenced current efficiencies, magnetic properties, and phases of electrodeposited films. Higher current efficiencies in chloride baths, relative to sulfate baths, were observed for CoFe, NiCo and CoNiFe alloy plating. The higher deposition current efficiencies in chloride baths were attributed to a catalytic effect. Anion types in CoFe and CoFeNi alloy plating baths influenced the film microstructures and resulting

magnetic properties (coercivity). CoFe deposits exhibited relatively smooth surface morphology and turned into fine crystallites with increasing  $\text{Fe}^{+2}$  concentration in the plating solution. The Fe content in CoFe deposits linearly increased with increasing  $\text{Fe}^{+2}$  concentration in plating bath for both chloride and sulfate baths.

Bai et al [Bai03] [Hu02] deposited FeCo alloy nanowires from acidic metal chloride solutions (pH 3.0) by means of cyclic voltammetry (CV) and pulse-reverse (PR) electroplating processes. The anodic dissolution process in the CV or reverse electroplating period was found to be the key factor influencing the formation of metal nanowires. They studied the morphology and crystalline phase formation of the deposits with field-emission scanning electron microscopy (FE-SEM) and X-ray diffraction (XRD).

Chang et al [Chang90] studied CoFe plating from a chloride electrolyte and observed a strong dependence of coercivity on alloy composition. A minimum coercivity of 3 Oe was obtained at about 11.5 wt% Fe. A variation of Fe content by 1% on either side of this composition caused the coercivity to double. Microstructural analysis revealed that the minimum coercivity was associated with the codeposition of fcc and bcc phases.

Yu et al [Yu00] electroplated CoFe alloys and composites from a bath with a pH of about 2.0, and systematically investigated microstructural effects, including grain size, precipitation, and structural order parameter, on the magnetic and mechanical properties of FeCo-based alloys. Other researchers also made similar studies on the electroplating of CoFe alloys. [Shinoura93] [Kakuno97] [Sasaki98] [Myung01] [Liu00-1] [Shao03]

### *2.3.2.3 Electrodeposition of CoFeNi alloys*

Studies on electroplating of CoFeNi soft magnetic materials have been extensively conducted. CoFeNi alloys can be readily plated from solutions whose compositions differ from that of a NiFe plating bath only by adding a  $\text{Co}^{2+}$  salt, usually a sulfate or chloride.

Similar to FeNi and FeCo plating solutions, low pH levels are usually employed in CoFeNi plating baths. Table 2-8 lists the composition of a typical sulfate bath for plating CoFeNi alloys, which has a low pH of 2.5-3.0. [Osaka98-1] [Osaka98-2]

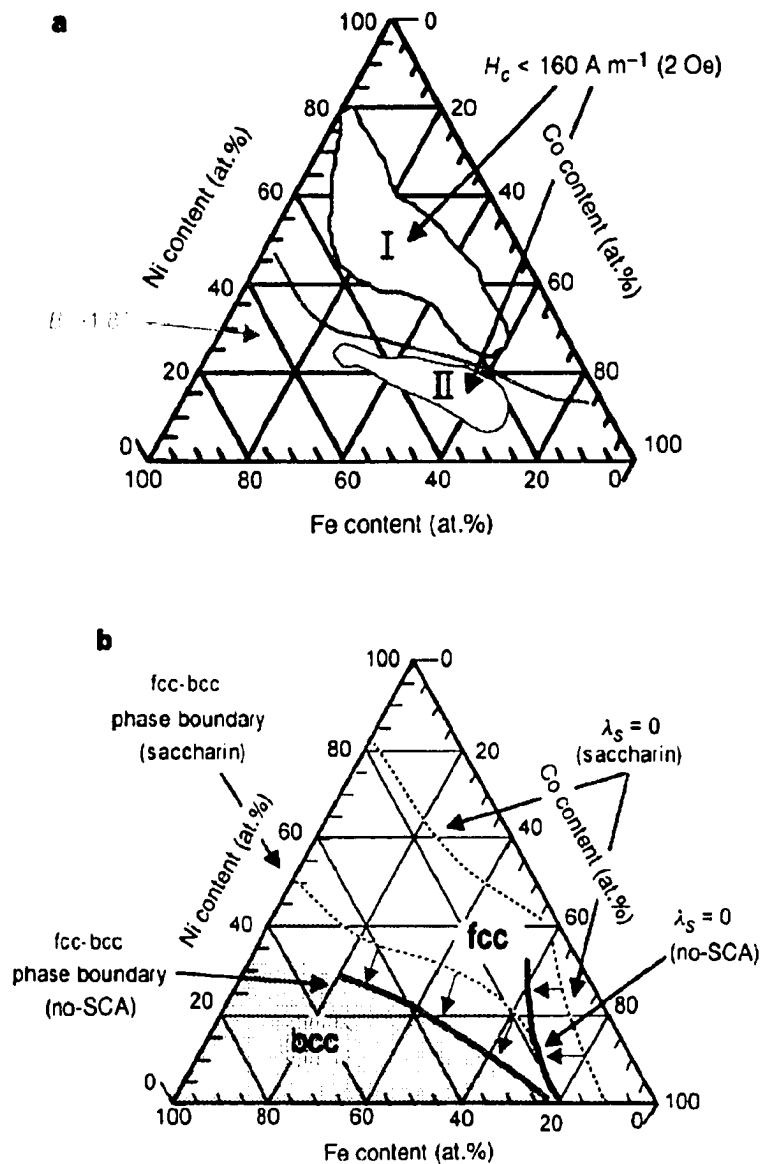
**Table 2-8.** Composition of bath for electroplating CoFeNi alloys. [Osaka98-1]

Chemical	Concentration	Chemical	Concentration
CoSO <sub>4</sub>	0.03-0.0875 M	H <sub>3</sub> BO <sub>3</sub>	0.4 M
FeSO <sub>4</sub>	0.005-0.045 M	Sodium lauryl sulfate	0.01 g/L
NiSO <sub>4</sub>	0.2 M	NH <sub>4</sub> Cl	0.28 M
Bath pH 2.5-3.0			

The optimal soft magnetic properties of CoFeNi thin films are achieved by controlling their chemical composition, phase formation, grain sizes, and the electroplating process.

Shinoura et al. [Shinoura94] electrodeposited CoFeNi alloys with compositions of 25-35 wt% Fe and 30-50 wt% Co. Soft magnetic properties were obtained in the entire range of the above compositions, but magnetostriction was positive. Annealing tests at 300°C and higher temperatures were conducted to improve the magnetic properties. It was found that a substantial decrease in observed coercivity was correlated to the coexistence of fcc and bcc crystalline phases in the deposited film.

Anderson and Chesnutt [Anderson87] investigated the electrodeposition of soft magnetic CoFeNi thin films with an emphasis on high Co content. A Co<sub>80</sub>Fe<sub>10</sub>Ni<sub>10</sub> alloy with a saturation magnetization of 1.6 Tesla, coercivity of 1.5 Oe, anisotropy field of 10 Oe, permeability of about 1000 at 1-10MHZ, and near-zero magnetostriction was electroplated from an acidic chloride bath with a pH of 2.5-3.5.



**a.** Map showing low- $H_c$  regions ( $<2Oe$ ) of CoFeNi films electroplated in solutions with saccharin (region I) and without SCA (region II). Region I is located within the low  $B_s$  ( $= 1.0\text{--}1.7$  Tesla) region. Region II is in the high- $B_s$  ( $>1.8$  Tesla) region.

**b.** Map showing fcc–bcc phase boundaries and zero  $\lambda_s$  lines. The fcc–bcc phase boundary in the film plated from the no SCA bath is shifted to the left, towards the lower Ni and the higher Fe region.

**Figure 2-13.** Three-element maps showing magnetic properties of CoFeNi films. [Osaka98-1]

Osaka and coworkers [Osaka98-1] [Osaka98-2] [Ohashi98] [Osaka99-1] [Osaka99-2]

[Osaka99-3] [Osaka99-4] [Osaka00-1] [Osaka00-2] [Osaka00-3] [Nakanishi01] [Nam01] [Osaka01] [Osaka03-2] systematically studied the soft magnetic properties of electroplated CoFeNi alloys using sulfate baths similar to the chloride baths employed by Anderson and Chesnutt [Anderson87]. The current density and bath pH they employed were varied from 3 to 20 mA/cm<sup>2</sup> and from 2.5 to 3.0, respectively. Electroplating was conducted under ambient temperature (20°C). They drew three-element diagrams illustrating the magnetic properties of CoFeNi films versus their compositions (Figure 2-13). Favorable magnetic properties ( $B_s > 1.8$  T and  $H_c < 2$  Oe) could only be achieved by using a no sulfur-containing-additive (SCA) solution (region II in Figure 2-13a) in the plating process. Analysis of film composition and microstructure indicated that sulfur (S) included in the film moved the fcc-bcc phase boundary line to the low  $B_s$  region (compare Figure 2-13a and b). The sulfur inclusion in films is due to the sodium saccharin addition. It is usually added to the plating bath as a stress reducer. Therefore, in order to move the phase boundary line to the high  $B_s$  region, the use of bath without a SCA was required. One of the films with a composition of Co<sub>65</sub>Fe<sub>23</sub>Ni<sub>12</sub> (within region II) was claimed to have the best properties: high  $B_s = 2.1$  Tesla, low  $H_c = 1.2$  Oe, low magnetostriction  $\lambda_s = 1.8 \times 10^{-6}$ , low anisotropy field  $H_k = 15$  Oe, initial permeability  $\mu_i = 600$  at 1MHz, and resistivity  $\rho = 2.1 \times 10^{-5}$  Ωcm. [Osaka98-1]

Liu and coworkers [Liu00-1] [Liu00-2] [Liu01-1] [Liu01-2] [Liu02] [Liu03] electroplated CoFeNi films from sulfate baths similar in composition to those employed by Osaka and coworkers [Osaka98-1] [Osaka98-2], and found that films with a composition of Co<sub>52</sub>Fe<sub>26</sub>Ni<sub>22</sub> exhibited optimal soft magnetic properties. These films had a saturation magnetization of 2 Tesla, coercivity around 1 Oe, resistivity of 22 μΩcm and saturation magnetostriction of about 10<sup>-6</sup>. An iron rich alloy Co<sub>19</sub>Fe<sub>52</sub>Ni<sub>29</sub> plated by them also showed similar properties. The variety of CoFeNi thin film compositions at which optimal soft magnetic properties have been achieved by different research groups

suggests that the exploration of new film compositions for ideal properties is possible.

Bai et al [Bai03-2] [Bai03-1] electroplated CoFeNi alloys from chloride baths with a pH of 2.0 by means of a cyclic voltammetry process. It was found that the anodic process in the voltammetric curves completely depressed the anomalous deposition of binary alloys while the anomaly was still obvious for ternary CoFeNi alloy deposition. From energy-dispersive X-ray (EDX) analysis, the Fe/Co ratio in the ternary CoFeNi deposits was equal to the  $\text{Fe}^{2+}/\text{Co}^{2+}$  ratio in the plating solutions when the  $\text{Ni}^{2+}$  content was continuously changed. The composition of CoFeNi deposits could be precisely predicted and controlled by adjusting the  $\text{Ni}^{2+}/(\text{Fe}^{2+}+\text{Ni}^{2+}+\text{Co}^{2+})$  concentration ratio in the plating baths.

Omata [Omata90-1] fabricated CoFeNi films through both evaporation and electroplating, and investigated variations of magnetic and structural properties with compositions. The films electroplated were Fe-rich alloys (typical composition was  $\text{Co}_{20}\text{Fe}_{45}\text{Ni}_{35}$ ), with satisfactory magnetic properties except for a highly positive magnetostriction. He and co-workers introduced Cr as a fourth element to decrease the magnetostriction, and found that small amounts of Cr could cause a substantial decrease in magnetostriction. [Omata90-2]

Zhuang and Podlaha [Zhuang00] [Zhuang03-1] investigated the kinetics of CoFeNi alloy electrodeposition and the influence of electrolyte concentration. They also developed a mathematical model to simulate the deposition process. [Zhuang03-2]

Impurity control in deposits is also very important for obtaining optimal soft magnetic properties. Generally, impurities can assist in the formation of grain boundaries, and, therefore, affect the microstructures, corrosion resistance and magnetic properties of deposited CoFeNi films. Common impurities include sulfur, carbon, hydrogen and oxygen. They are usually included into the CoFeNi films due to the addition of organic additives and specific plating conditions. Sulfur is deposited in the films with the

addition of saccharin, thiourea, or sodium lauryl sulfate to reduce film stress and improve film smoothness. Researchers found that the inclusion of sulfur will decrease the corrosion resistance, and affect the  $B_s$  and  $H_c$  of CoFeNi thin films. Most recent studies have adopted SCA-free baths.

Osaka et al [Osaka99-2] electrodeposited CoFeNi based films for write head core materials, and found that the magnetic properties, except for  $B_s$ , and corrosion properties of these films depended on very small amounts of impurities such as S and H. The increase in resistivity  $\rho$  of the high  $B_s$  CoFeNi thin film was realized by controlled inclusion of very small amount of C.

Osaka and Yokoshima [Osaka00-2] studied the influence of electroplating conditions on the microstructures of deposited CoFeNi-based films. The microstructure of thin films prepared by a wet process differed from that of films prepared by a dry process, and some of the high-performance thin films were obtained only by plating methods. A very small amount of impurities, such as H, S, and C co-deposited from the plating bath, was found to have a large effect on the microstructure of the deposited films. High-performance soft magnetic thin films were therefore achieved by controlling the microstructure with co-deposited impurities.

Sogawa et al [Sogawa00] investigated the addition of a complexing agent and/or  $\text{Na}_2\text{MoO}_4$  to a low pH plating bath to increase the resistivity of CoFeNi soft magnetic thin films. It was found that the electrical resistivity of deposited CoFeNi thin films was increased by the addition of a complexing agent such as sodium tartrate or sodium citrate. These films contained a small amount of carbon, i.e., 1 to 2 at%. The addition of  $\text{Na}_2\text{MoO}_4$  also increased the resistivity of CoFeNi thin films. A deposited film with a composition of  $\text{Co}_{59}\text{Ni}_{12}\text{Fe}_{26}\text{Mo}_1\text{C}_2$  had the following good properties:  $B_s = 1.8 \text{ T}$ ,  $H_c = 1.6 \text{ Oe}$ ,  $\rho = 129 \mu\Omega\cdot\text{cm}$ .

Takai et al [Takai97] prepared soft magnetic CoFeNiS films by electrodeposition. In their plating system, thiourea was introduced as a stress-reducing additive in the CoFeNi ternary alloy plating bath. Suitable magnetic properties were obtained at a film composition of  $(\text{Co}_{73}\text{Fe}_{15}\text{Ni}_{12})_{99.1}\text{S}_{0.9}$  (in at%). These properties include a high saturation magnetic flux density  $B_s$  of 1.7 Tesla, a high resistivity  $\rho$  of  $51 \mu\Omega\text{cm}$ , and a low saturation magnetostriction  $\lambda_s$  of  $4.4 \times 10^{-6}$ . The film consisted of crystalline grains 5 to 10 nm in diameter. The small sulfur content was believed to result in the formation of fine crystalline grains responsible for low coercivity and high resistivity.

Osaka et al [Osaka99-3] observed that two common sulfur-containing additives, saccharin and thiourea, behave differently with respect to the dependence of sulfur inclusion and coercivity of the deposited film on the additive concentration in the plating bath. Scanning tunneling microscopy (STM) studies revealed that the nature of adsorption is fundamentally different for these two additives, i.e., the adsorption of saccharin is physical and reversible, whereas thiourea undergoes irreversible chemisorption. This finding is consistent with the known behaviors of these two additives in the electroplating of nickel. Tabakovic et al [Tabakovic00] also investigated the effects of organic additives on the electrochemical preparation of soft magnetic CoFeNi films.

To increase the resistivity  $\rho$  of electrodeposited high  $B_s$  CoFeNi thin films, Osaka and coworkers [Osaka00-1] [Yokoshima99] introduced diethylenetriamine (DET) into the plating bath. The carbon content in the deposited films increased with DET concentration, which led to higher resistivity (Figure 2-14a). However, DET could also increase the film coercivity  $H_c$  and decrease saturation flux density  $B_s$  at high concentration (Figure 2-14b). The desirable soft magnetic CoFeNi thin films ( $B_s > 1.9 \text{ T}$  and  $H_c < 2.5 \text{ Oe}$ ) with resistivity  $\rho$  of 25 to  $90 \mu\Omega\cdot\text{cm}$  were plated out and depended on carbon content in the deposited films. Additionally, a CoFeNi thin film with high resistivity  $\rho = 130 \mu\Omega\cdot\text{cm}$  was obtained at  $B_s = 1.7 \text{ T}$  and  $H_c < 6 \text{ Oe}$ .

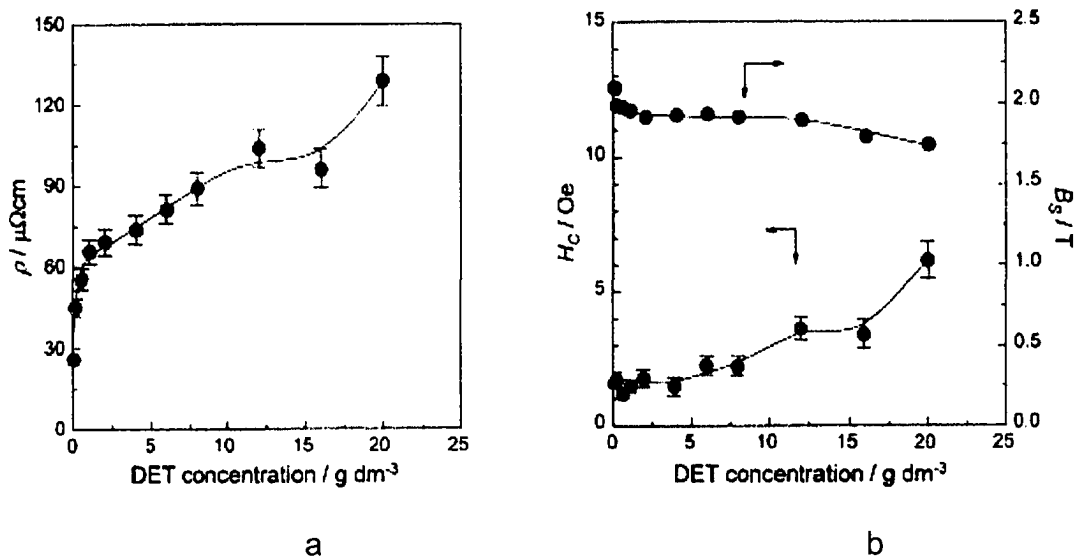


**Figure 2-14.** a) Resistivity of electrodeposited CoFeNi films as a function of DET concentration.

b) Magnetic properties of electrodeposited CoFeNi films as a function of DET concentration. [Osaka00-1]

Saito and coworkers [Saito02] also observed the effect of a small amount of sodium citrate addition (0.1g/L) on the impurity contents of electrodeposited CoFeNi films. The carbon, oxygen, and hydrogen levels in CoFeNi films increased significantly after sodium citrate addition.

To achieve ideal soft magnetic properties, grain size control is critical. Smaller grain sizes generally decrease the coercivity  $H_c$ . According to a model proposed by Herzer [Herzer90],  $H_c$  is proportional to  $D^6$ , where  $D$  is the average grain size. Hoffman [Hoffmann93] predicts that  $H_c$  changes with  $D^2$ . Both models predict that coercivity decreases with grain size. Therefore, only nano-grained alloys may achieve desirable soft magnetic properties.

Chen et al [Chen03] presented an approach to reduce grain size by incorporating a CoFeNi alloy matrix with dispersed trace metal oxides, which interrupt grain growth and enhance nucleation during electrodeposition. The oxides of Mo, W, Cr and Rh can be

deposited under certain anodic potentials during the reverse current period in a pulse-reverse plating cycle.

Osaka et al attributed the high  $B_s$  values as well as the soft magnetic properties of electroplated CoFeNi films to the fine grain sizes of 10 - 20 nm. [Osaka98-2]

Phase formation control in deposited CoFeNi films is also necessary for obtaining ideal soft magnetic properties. Optimum properties are obtained when both bcc and fcc phases coexist. [Osaka98-1] [Osaka99-1] It is believed that the competitive nucleation and growth of these two phases could lead to a smaller average grain size. [Liu00-2] [Liu01-1]

Osaka et al [Osaka98-1] found that CoFeNi films have close to zero saturation magnetostriction ( $\lambda_s = 0$ ) around the fcc and bcc phase boundary (as shown in Figure 2-13b), which ensures that they are not stressed when a changing magnetic field is applied during writing processes.

Saito and coworkers [Saito02] reported that magnetic properties, such as coercivity  $H_c$ , saturation magnetostriction  $\lambda_s$ , and saturation magnetic flux density  $B_s$ , are affected by the ratio of bcc to fcc phases. When the ratio of bcc to fcc phases was low and the grain size was small, the coercivity was less than 2 Oe. The  $\lambda_s$  and  $B_s$  values increased with an increase in bcc/fcc ratio in the film.

The electroplating conditions for depositing optimal soft magnetic CoFeNi films have been explored by researchers.

To avoid compositional gradients along the film thickness due to diffusion delay of component metal ions [Liu00-2] [Liu01-2], pulsed current (PC) plating is usually employed, which can regenerate the initial ion concentration at the cathode/solution interface.

To obtain excellent soft magnetic properties, an oriented magnetic field is often employed during the CoFeNi thin film deposition. Chesnutt [Chesnutt93] found the

application of an orthogonal switching magnetic field of 50 Oe could reduce the anisotropy field  $H_k$  of deposited films, and therefore the saturation write currents. In the works of Liu and coworkers [Liu00-1] [Liu00-2] [Liu01-1] [Liu01-2] [Liu02] [Liu03], a pre-oriented magnetic field of about 600 Oe was applied to induce an in-plane uniaxial anisotropy for ideal soft magnetic properties.

Mizutani et al [Mizutani00] investigated the thermal stability and magnetic properties of electroplated high  $B_s$  CoFeNi thin films. The plated CoFeNi films demonstrated excellent soft magnetic properties and good thermal stability with up to 350°C annealing. Annealing in a longitudinal magnetic field enabled the films to achieve an anisotropy field  $H_k$  of 35 Oe, while the  $H_k$  value could be further lowered to less than 20 Oe after annealing in a transverse magnetic field. By decreasing the core loss and anisotropy field  $H_k$ , the effective permeability of high  $B_s$  CoFeNi thin films at high frequencies was markedly improved.

Phan et al [Phan91] investigated the effects of hydrodynamic conditions, current density and bath temperature on the direct current (DC) electrodeposition of CoFeNi alloys using stationary planar and rotating cylindrical electrodes. The deposition rate of Fe showed mass transfer effects. Current efficiency of the codeposition process increased with increasing current density, while it decreased with increasing rotation rate. Higher bath temperatures and rotation rates extended the applied current density range where smooth, adherent, and metallic-looking deposits could be plated out. Higher plating temperature also decreased anomalous codeposition of Fe-Ni-Co. They [Phan94] also studied the dependence of CoFeNi alloy electrodeposition on hydrodynamics, current density and bath temperature using pulse and pulse-reverse currents. The compositions of deposits plated with pulse current (PC) were similar to those obtained with direct current (DC). The appearances of deposits obtained by PC and periodic reverse current (PRC)

were superior to those obtained by DC. Deposits were smoother and brighter at 55°C than at room temperature, and were smoother and more adherent at higher rotation rates.

The corrosion resistance of soft magnetic films is also an important property to be considered for the manufacture of magnetic devices.

Osaka and coworkers [Osaka99-4] [Osaka98-1] investigated the corrosion behavior of electroplated CoFeNi films with different crystalline structures and various sulfur contents. The corrosion properties of CoFeNi films depend highly on the sulfur content and also on the microstructure of the film. The film with a low S content (deposited from SCA-free bath) has high corrosion resistance, and the bcc film is less resistant to corrosion than the fcc and fcc-bcc films. With essentially no sulfur inclusion (<0.1 at%), even though containing more than 13 at% Fe, the CoFeNi film of mixed fcc-bcc crystal structures exhibited high corrosion resistance.

Saito et al [Saito99] found that films electroplated at a high current density (15 mA/cm<sup>2</sup>) from a bath without saccharin have a sufficient anodic pitting-corrosion potential (-65 mV). While films plated at a low current density (5 mA/cm<sup>2</sup>) from saccharin-free baths have pitting-corrosion potentials of less than -300 mV, the corrosion resistance was improved after annealing above 100°C. Films plated from baths containing saccharin also have pitting-corrosion potentials of less than -300 mV. However, their corrosion resistance did not improve after being annealed at 250°C. Saito et al believe that the degeneration of the corrosion resistance is attributed to the defects that increase the fcc (111) lattice constant. One of the most important characteristics of a highly corrosion-resistant CoNiFe film is a fine crystal structure with very few defects. Tanaka et al [Tanaka93] also conducted similar investigations on the corrosion resistance of CoFeNi alloys for thin film inductive head.

#### 2.3.2.4 Electrodeposition of other soft magnetic thin-films

Besides the common FeNi, CoFe and CoFeNi thin films, many other soft magnetic thin films have also been developed for write head core materials.

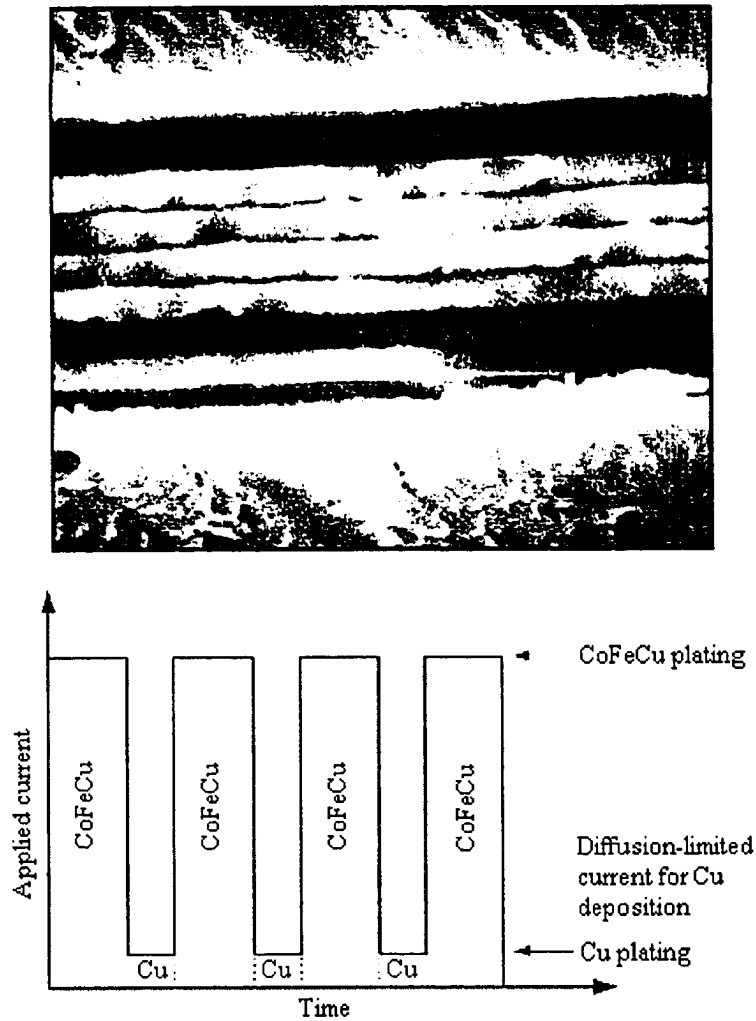


**Figure 2-15.** (Top) Cross section view (~20K magnification) of a laminated CoFeCu/Cu film (in the middle) with four CoFeCu layers (each 0.5 $\mu$ m thick) and three Cu layers (each 10nm thick). (Bottom) Schematic showing a pulsed current waveform applied in plating. [Andricacos98]

Andricacos and Robertson electroplated CoFeCu films with excellent soft magnetic properties. [Andricacos98] [Andricacos96] The saturation magnetization  $M_s$  for the

$\text{Co}_{85}\text{Fe}_{10}\text{Cu}_5$  alloy was about 2.0 Tesla. Magnetostriction was close to zero as long as the Fe content was around 10 wt%, however, it became positive at higher Fe content and negative at lower Fe content. It was found that the addition of Cu to the CoFe system leads to a decreased coercivity  $H_c$ , but increased anisotropy  $H_k$  for the CoFeCu ternary system. Microstructural studies demonstrated that Cu addition causes a decreased grain size; this may be the reason that the coercivity  $H_c$  decreases. To achieve a low coercivity, the same fraction of fcc and bcc phases is necessary. CoFeCu alloys can be deposited as laminated CoFeCu/Cu films by pulse plating, with CoFeCu as the magnetic layer and Cu as the nonmagnetic layer (Figure 2-15). The number of laminations is equal to the number of applied pulses. This process was first developed by Romankiw and Olsen in IBM for the NiFeCu/Cu lamination system. [Romankiw90]

Andricacos and Robertson fabricated recording heads with the  $\text{Co}_{85}\text{Fe}_{10}\text{Cu}_5$  alloy replacing  $\text{Ni}_{80}\text{Fe}_{20}$  as the write pole material. Comparison of the two recording heads showed that overwrite with the CoFeCu ternary alloy was obviously superior to  $\text{Ni}_{80}\text{Fe}_{20}$ , demonstrating the advantages of applying high  $M_s$  materials to improve recording performance.

Huang and coworkers [Huang02] [Huang04] explored the electrodeposition of FeCoNiCu quaternary alloys onto a rotating disk electrode from a sulphate bath with a pH of 2.5. The bath composition utilized is illustrated in Table 2-9. They developed a model describing the electrodeposition of FeCoNiCu/Cu nanometer scale multilayers to simulate both steady-state and pulsed deposition onto a ring-disk electrode. The transient model employed a two-step adsorption mechanism for the description of anomalous codeposition, convective-diffusion mass transport and a displacement mechanism for pulses to zero current. Variation in deposit composition was predicted using various pulse times as a tool for assessing interfacial compositional gradients in multilayer deposits.

**Table 2-9.** Bath composition for FeCoNiCu/Cu electrodeposition. [Huang02]

Constituent	Concentration, g/L	Concentration, mole/L
FeSO <sub>4</sub> ·7H <sub>2</sub> O	2.25	0.008
CoSO <sub>4</sub> ·7H <sub>2</sub> O	14.0	0.050
NiSO <sub>4</sub> ·6H <sub>2</sub> O	15.0	0.057
CuSO <sub>4</sub> ·5H <sub>2</sub> O	0.25	0.001
Sodium potassium tartrate (NaKC <sub>4</sub> H <sub>4</sub> O <sub>6</sub> ·4H <sub>2</sub> O)	7.5	0.0266
Sulfamic acid	1.0	0.0103
Sodium saccharin	1.0	0.0041
Triton X-100	0.6	
pH	2.5	

Chang et al [Chang92] electroplated CoFeCu alloys with a saturation magnetization  $M_s$  around 2.0 Tesla, coercivity  $H_c < 1$  Oe and a near-zero magnetostriction. They reported a ternary phase diagram for the low-coercivity and low-magnetostriction composition range (about 4-15 wt% Cu and approximately 9-13 wt% Fe). X-ray diffraction revealed that the coexistence of both fcc and bcc phases yields the optimal soft magnetic properties. The magnetic properties of CoFeCu films with mixed phases were stable after being annealed at 230°C for two hours.

Shinoura [Shinoura95] investigated the electroplating of soft magnetic Ni-Fe-Mo multilayers from a tartrate bath. Two alternative layers (100 nm Ni-Fe-4 wt% Mo/20 nm Ni-Fe-15 wt% Mo) with different molybdenum content were prepared by alternating the current density during deposition. Multilayers consisting of eight of the above bilayers had excellent magnetic properties and a resistivity of 78  $\mu\Omega\cdot\text{cm}$ .

Other soft magnetic materials have also been explored. Hironaka and Uedaira [Hironaka90] electroplated CoFeP and CoFeSnP alloys by pulsed current plating. It was found that incorporation of P caused a drastic decrease in the saturation magnetization of the alloys, and Sn incorporation (of about 7 wt%) improved their corrosion resistance. Liao [Liao92-1] tried to fabricate read/write heads using an electroplated CoFeB alloy with the B content from 0.1 to 2 wt%, and Fe content from 7 to 12 wt%. He and coworkers [Liao92-2] also electrodeposited high  $B_s$  CoFeCr thin films for high frequency recording applications.

### 2.3.3 Soft magnetic thin films prepared by electroless deposition processes

Write-head cores have currently been fabricated by electrodeposition processes. With the ever increasing areal density, the recording heads of hard disk drives have been decreasing in size. However, it may be difficult to accomplish further shrinkage of the head core structure fabricated by electrodeposition, because the non-uniform current density distribution on the structure becomes a serious problem in this situation. It could cause the non-uniform distribution of thickness and composition in the head core materials. On the other hand, electroless deposition (also called autocatalytic plating) is suitable for depositing uniform films on substrates with fine and complex geometries. Electroless deposition involves reduction reaction(s) of metal ion(s) and is autocatalytic. No external current is applied, and a reducing reagent is employed as the electron supplier:

Reducing agent  $- 2e^- \rightarrow$  oxidized components

$Co^{2+} + 2e^- \rightarrow Co$  (deposition)

$Fe^{2+} + 2e^- \rightarrow Fe$  (deposition)

$Ni^{2+} + 2e^- \rightarrow Ni$  (deposition)

Therefore, soft magnetic thin films for write core pole have been developed by many

researchers with electroless deposition processes. [Osaka03-2]

**Table 2-10.** Bath composition and conditions for electroless deposition of CoNiFeB thin films. [Yokoshima00]

Chemical	Concentration/mol·dm <sup>-3</sup>
DMAB	0.025
C <sub>3</sub> H <sub>4</sub> (OH)(COONa) <sub>3</sub>	0.05
C <sub>2</sub> H <sub>2</sub> (OH) <sub>2</sub> (COONa) <sub>2</sub>	0.20
(NH <sub>4</sub> ) <sub>2</sub> SO <sub>4</sub>	0.20
H <sub>3</sub> PO <sub>3</sub>	0.06
FeSO <sub>4</sub> ·7H <sub>2</sub> O	0.01
NiSO <sub>4</sub> ·6H <sub>2</sub> O	0 - 0.03
CoSO <sub>4</sub> ·7H <sub>2</sub> O	0.10 – 0.07
Bath temperature (°C)	70
Applied magnetic field (Oe)	200
pH	9 (adjusted with NaOH)

Osaka and coworkers [Yokoshima00] prepared soft magnetic CoNiFeB thin films with high saturation magnetic flux density  $B_s$  and good corrosion resistance by electroless deposition. The bath composition and operating conditions employed by them are listed in Table 2-10. In contrast to electroplating baths, the electroless deposition bath adopted a high pH (= 9). Dimethylamine-borane (DMAB) was utilized as a reducing agent. Electroless CoFeB thin films had high  $B_s$  but poor corrosion resistance compared with the electrodeposited NiFe (80-permalloy) film. The introduction of Ni to the CoFeB film improved corrosion resistance without sacrificing its soft magnetic properties. One of the best CoNiFeB films, with a composition of Co<sub>77</sub>Ni<sub>13</sub>Fe<sub>9</sub>B<sub>1</sub>, demonstrated excellent

magnetic and electrical properties (high  $B_s = 1.5 - 1.7$  T, low coercivity,  $H_c = 1.2$  Oe, low magnetostriction,  $\lambda_s = 2.0 \times 10^{-6}$ , and moderate resistivity,  $\rho = 40 \mu\Omega \cdot \text{cm}$ ). They also tried to increase the resistivity of electroless-deposited high- $B_s$  CoNiFeB thin films by adding a complexing agent containing  $\beta$ -alanine to the plating bath. [Sobue02]

Osaka and coworkers [Takai95] investigated the magnetic properties and structure of electroless-deposited NiFeB films compared with those of electrodeposited NiFe films. An electroless-deposited NiFeB film with 27 at% Fe had the lowest coercivity  $H_c$  of 0.5 Oe with a saturation magnetic flux density  $B_s$  of 1.0 Tesla. The crystal structure and grain size of NiFeB and NiFe films were investigated by X-ray diffraction (XRD), transmission high energy electron diffraction (THEED) and transmission electron microscopy (TEM). Both films with low  $H_c$  had an fcc structure. The grain size of the NiFeB film was smaller than 10 nm, while that of the NiFe film was larger, about 20 nm. They also reported electroless deposition of CoB, CoFeB and NiFeB alloys in the presence of an external magnetic field. [Osaka91] [Osaka92] [Osaka94] They attributed the decrease of saturation flux density  $B_s$  of  $\text{Co}_{35}\text{Fe}_{65}$  alloy to the presence of 0.3 at% of boron in films deposited from the TMAB bath. [Osaka94]

Kim et al [Kim95] developed an electroless plating solution for preparing soft magnetic Ni-Co-P thin films. In their plating process, the optimum bath composition and operating conditions were obtained by investigating the effects of these factors on deposition rate, film composition, and magnetic properties. Soft magnetic films with low coercivity ( $H_c < 1$  Oe) were prepared from this electroless Ni-Co-P plating process. The alloy films deposited from the optimum bath condition consisted of fine-grain crystallites.

In general, the soft magnetic properties of electrolessly deposited materials are less ideal compared with those of electroplated CoFe, CoFeNi and CoFeCu alloys. Other problems with electroless deposition include that the baths are usually not stable, and

there are fewer optional operation parameters to control the properties of deposit compared with electrodeposition. Operation parameters employed in electrodeposition, such as current density and  $t_{on}$ , are not available for electroless deposition.

## 2.4 Summary

Both evaporation and sputtering processes involve complicated vacuum techniques. Sputtering processes are not suitable for fabricating thick films (more than 1 micron), and the topography of small features like yokes and pole tips in recording heads is hard to control in vacuum processes.

In electrodeposition process, the films can be made in any thickness from  $<1\mu\text{m}$  to  $>100\mu\text{m}$ . Moreover, electroplating through a mask can easily define and control small features like yokes and pole tips; and subtractive processes like etching or ion milling could be eliminated. With the advantages of simplicity, cost-effectiveness and controllable patterning, electroplating processes are being employed in the fabrication of thin-film recording heads. Electrodeposition can be well controlled by applying an external electrical potential, however, it requires that the surface of the substrate must have an electrically conducting coating before deposition.

As an alternative, electroless deposition is suitable for depositing uniform films on substrates with fine and complex geometries without a pre-deposited electrically conducting layer. However, so far the soft magnetic properties of electrolessly deposited alloys are less ideal compared with those of alloys obtained by electrodeposition.

## Chapter 3 Experimental Methods

### 3.1 Experimental equipment

In this research, a pulsed current supply manufactured by Dynatronix, Inc. (Model DuPR10-1-.3) was employed to supply the plating current in electrodeposition tests. A  $50\ \Omega$  standard resistance  $R_0$  was connected in series with the plating bath to monitor the current density by monitoring the peak voltage on  $R_0$  using a Hitachi oscilloscope (Model V-212 20MHz). Agitation was introduced with a mechanical stirrer (Caframo BDC3030). A thermo-bath produced by Fisher Scientific International Inc. (Model Isotemp 202) was applied to maintain plating temperatures higher than the ambient temperature where necessary. A schematic illustration of the electroplating setup is shown in Figure 3-1. Silicon wafers coated with a Ti (25nm)/Au (250nm) blanket metallization were used as the cathode, with Au acting as a seed layer for plating. Wafers were cleaved along  $\{110\}$  planes with a diamond pen, and a plating area of 0.5 to 1.0  $\text{cm}^2$  was defined with lacquer. Platinum foil was used as the non-consumable anode. An electrolyte volume of 30 ml was used for all plating tests.

Stability diagrams (Pourbaix diagrams) were calculated with OLI Analyzer Version 1.3 software purchased from OLI systems, Inc.

The compositions and microstructures of deposited films were characterized using a Hitachi S-2700 scanning electron microscope (SEM) equipped with an ultra thin window (UTW) x-ray detector (intrinsic germanium detector). The film composition was determined using energy dispersive x-ray spectrometry (EDS) by measuring characteristic x-rays from areas approximately  $300\mu\text{m} \times 300\mu\text{m}$  in size from the upper, central, and lower part of each film. These values were then averaged. The deviation of a metal percentage in each part of the analyzed film from the average was observed to be within  $\pm 2$  at% in this study. The thickness of deposited films was measured through

freshly cleaved cross-section sample images in the SEM.

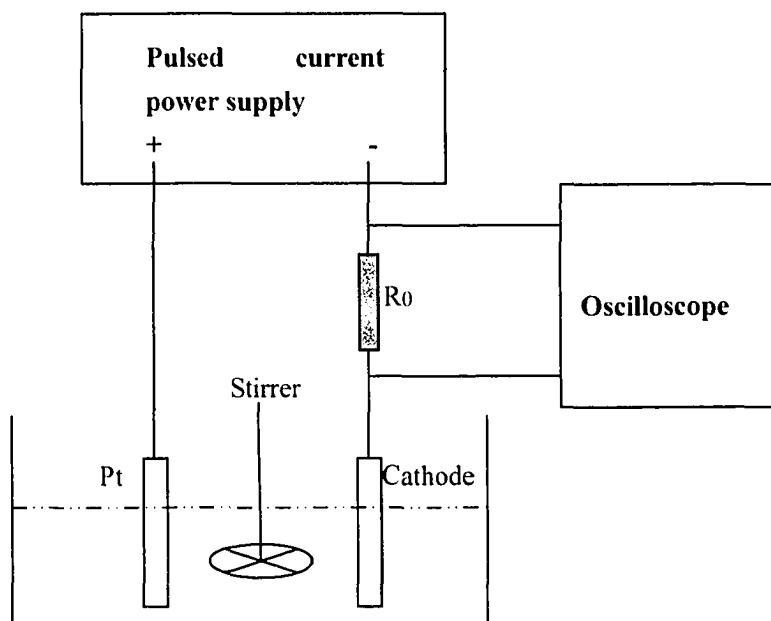


**Figure 3-1.** Schematic illustration of the electroplating setup.

A Rigaku Rotaflex XRD system, with a rotating anode and a thin film camera attachment, was employed to identify specific phases. A Cu anode operating at 40kV and 100mA was used, with an incident angle of  $2\theta = 2^\circ$  and a scan rate of  $0.5^\circ/\text{min}$ .

A JEOL 2010 transmission electron microscope (TEM), equipped with a UTW x-ray detector, and a Philips EM420 TEM were used to observe the crystallization process and grain size, and to obtain electron diffraction patterns for crystal structure analysis. The JEOL 2010 TEM was operated at 200 kV, while the Philips EM420 TEM was operated at 100 kV.

A Superconducting Quantum Interference Device (SQUID) magnetometer (Quantum Design) was applied to measure the magnetic properties of electrodeposited thin films at a temperature  $T = 300\text{K}$ .

Electrochemical analyses of plating processes and corrosion properties of

electrodeposited films were conducted using a Solartron SI1287 Electrochemical Interface System. All electrochemical experiments were conducted in a three-electrode cell without agitation. The working electrode was essentially the same as the cathode used in electrodeposition. A Pt foil was employed as the counter electrode, and a Corning saturated calomel electrode (SCE) was used as the reference electrode.

### 3.2 Bath compositions and electroplating conditions

All the electrolytes employed in this research were prepared with deionized water. All the chemicals used were of ACS (the American Chemical Society) grade. For the electrodeposition of CoFe films, the composition of the conventional low pH bath adopted was similar to that employed by Osaka and coworkers. [Osaka03-1] [Imai02] The main difference between the citrate-added bath and the traditional bath was the introduction of ammonium citrate as a bath stabilizer and a relatively high pH, which is natural without the addition of any acid or base. The compositions of these two baths are listed in Tables 3-1 and 3-2, respectively. For CoFe deposition, all plating tests were conducted using a pulsed current (PC) with a duty cycle of 10ms – 6ms of on-time ( $t_{on}$ ) and 4ms of off-time ( $t_{off}$ ), unless specified otherwise. The current density  $i$  was 15mA/cm<sup>2</sup> and the plating time was 25min, unless otherwise indicated.

For the electrodeposition of CoFeNi films, the composition of the conventional CoFeNi plating bath was based on the work of Osaka's group. [Osaka98-1] [Osaka98-2] Similar to the CoFe plating baths, the main difference between the citrate-added bath and the traditional bath was the introduction of ammonium citrate as a bath stabilizer and a relatively high pH level. The pH of the citrate-added bath was natural without the addition of any acid or base. Tables 3-3 and 3-4 list the compositions of these two baths. For CoFeNi plating, plating tests were conducted using a pulsed current (PC) with a duty cycle of 10ms – 0.3ms of  $t_{on}$  and 9.7ms of  $t_{off}$ , unless specified otherwise. The plating

time was set by the product of plating time  $t$  and current density  $i$  to about 300 minutes\* $\text{mA}/\text{cm}^2$ , unless otherwise indicated.

All plating experiments were conducted at ambient temperature and pressure, and agitation was introduced at a speed of 600 rpm, unless specified otherwise. After deposition was completed, the cathode was rinsed with deionized water, air dried and finally stored in a sample case for later composition analysis and characterization.

**Table 3-1.** Composition of a traditional CoFe electroplating bath

Chemical	Concentration	Chemical	Concentration
$\text{CoSO}_4 \cdot 7\text{H}_2\text{O}$	0.048 M	$\text{H}_3\text{BO}_3$	0.4 M
$\text{FeSO}_4 \cdot 7\text{H}_2\text{O}$	0.050 M	Sodium lauryl sulfate	0.01 g/L
$\text{NH}_4\text{Cl}$	0.4 M	Bath pH = 2.4	

**Table 3-2.** Composition of citrate-added bath for electroplating CoFe thin films

Chemical	Concentration	Chemical	Concentration
$\text{CoSO}_4 \cdot 7\text{H}_2\text{O}$	0.120 M	$\text{H}_3\text{BO}_3$	0.4 M
$\text{FeSO}_4 \cdot 7\text{H}_2\text{O}$	0.048 M	Sodium lauryl sulfate	0.01 g/L
Bath pH= 4.4 (natural)		Ammonium citrate	5 g/L (0.0206M)

**Table 3-3.** Composition of a traditional CoFeNi electroplating bath

Chemical	Concentration	Chemical	Concentration
$\text{CoSO}_4 \cdot 7\text{H}_2\text{O}$	0.03-0.0875 M	$\text{H}_3\text{BO}_3$	0.4 M
$\text{FeSO}_4 \cdot 7\text{H}_2\text{O}$	0.005-0.045 M	Sodium lauryl sulfate	0.01 g/L
$\text{NiSO}_4 \cdot 6\text{H}_2\text{O}$	0.2 M	$\text{NH}_4\text{Cl}$	0.28 M
Bath pH = 2.5-3.0			

**Table 3-4.** Composition of citrate-added bath for electroplating CoFeNi thin films

Chemical	Concentration	Chemical	Concentration
CoSO <sub>4</sub> ·7H <sub>2</sub> O	0.08 M	H <sub>3</sub> BO <sub>3</sub>	0.4 M
FeSO <sub>4</sub> ·7H <sub>2</sub> O	0.015 M	Sodium lauryl sulfate	0.01 g/L
NiSO <sub>4</sub> ·6H <sub>2</sub> O	0.3 M	Ammonium citrate	50 g/L (0.206M)
Bath pH = 5.3 (natural)			

## **Chapter 4 Development of Stable Citrate-added Baths and Bath Stability Study**

For the commercial fabrication of CoFe and CoFeNi thin films by electrodeposition, stable, long life baths are desired. Conventional CoFe and CoFeNi plating baths suffer from stability problems, that is, precipitation occurs rapidly with time [Liu03], which is undesirable for commercialization. Precipitates can affect the film properties, uniformity and smoothness, and of course, shorten the bath life. Tabakovic and coworkers [Tabakovic02] equipped their plating cell with a filtered recirculation system to compensate for bath degeneration. Furthermore, the low pH levels (typically 2.0-3.0) [Osaka03-1] [Imai02] [Osaka98-1] [Osaka98-2] [Liu03] employed in conventional baths lead to voids in deposited films, which degenerate film uniformity and magnetic properties, due to the electroplating of H<sub>2</sub>. Therefore, the development of stable baths with relatively high pH levels, which means less hydrogen evolution, is important for commercial fabrication of CoFe and CoFeNi thin films with optimal soft magnetic properties.

In this study, stable baths with the introduction of ammonium citrate as a complexing agent and bath stabilizer and relatively high pH levels (natural pH) have been developed for CoFe and CoFeNi alloy plating.

To understand the stability problems of conventional CoFe and CoFeNi plating baths, and the stabilizing mechanism of citrate, stability diagrams (also known as Pourbaix diagrams) have been calculated. Relevant bath stability tests have also been conducted. The morphologies of CoFe and CoFeNi films plated from conventional low pH baths and citrate-added baths have been investigated using SEM.

## 4.1 Development of citrate-added baths for electroplating CoFe and CoFeNi alloys

A stable bath is desired for commercial fabrication of metal or alloy thin films by electrodeposition. For CoFe, CoFeNi, CoFeCu and other Fe-based alloy plating, most researchers have employed a low pH (typically 2.0-3.0) to stabilize the plating bath. In these cases, acids (most often sulfuric acid H<sub>2</sub>SO<sub>4</sub> or hydrochloric acid HCl) are the bath stabilizers. However, even at low pH, these plating baths still suffer from stability problems. Precipitation occurs rapidly with time [Liu03], which is a critical issue for commercial production. As shown in Appendix 1, the H<sup>+</sup>/H<sub>2</sub> electrode has a more positive equilibrium potential than the Ni<sup>2+</sup>/Ni, Co<sup>2+</sup>/Co and Fe<sup>2+</sup>/Fe electrodes, which means hydrogen is more easily plated out than the metals. The low pH employed in conventional baths leads to significant hydrogen evolution on the cathode surface, which results in voids in deposited films and low current density efficiency. The voids included in the deposit will degenerate film uniformity and magnetic properties. Therefore, the development of stable baths with relatively high pH levels is crucial for commercial fabrication of CoFe and CoFeNi thin films with optimal soft magnetic properties.

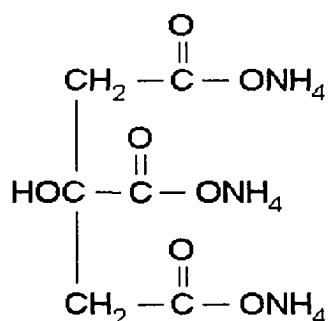


**Figure 4-1.** Molecular structure of ammonium citrate.

To stabilize a plating bath, usually one or more complexing agents are employed. In this study, stable baths with relatively high pH levels (natural pH) have been developed

for CoFe and CoFeNi alloy plating by introducing ammonium citrate as a complexing agent and bath stabilizer. The compositions of these citrate-added baths are listed in Table 3-2 and Table 3-4, respectively. The bath pHs are natural without the addition of any acid or base. Figure 4-1 illustrates the molecular structure of ammonium citrate.

## 4.2 Stability diagrams of plating baths

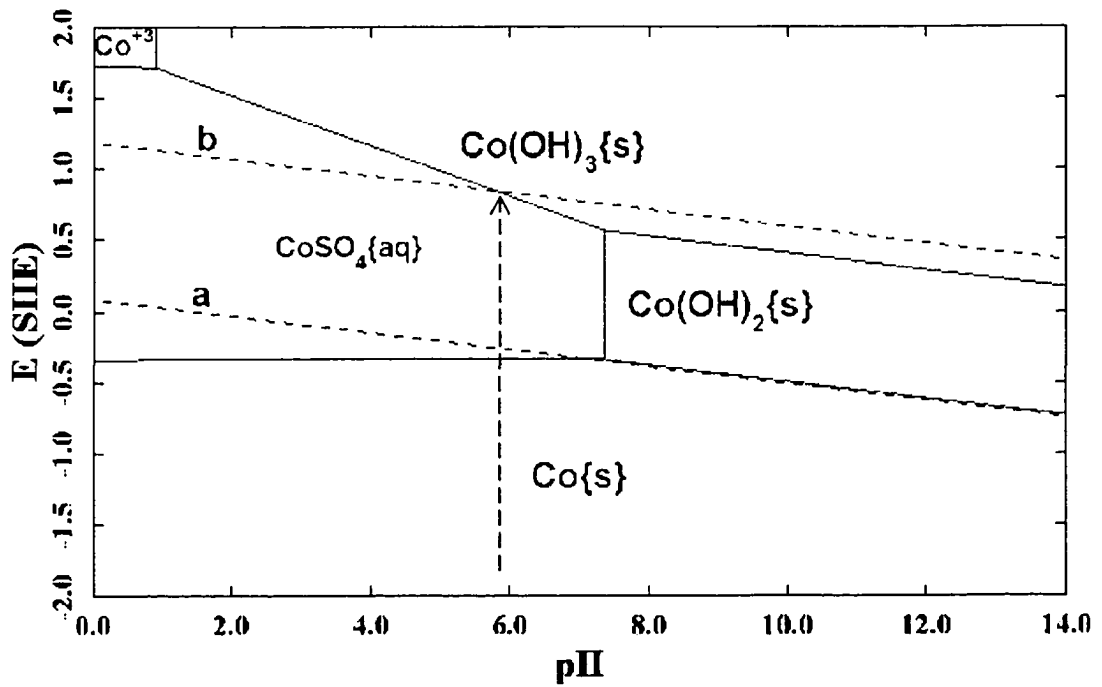
The stability of plating baths can be studied through stability diagrams. Unfortunately, no stability diagram calculations have been made in the reviewed references. In this section, the stability diagrams of single metal and alloy plating systems of interest are calculated with OLI Analyzer Software. The fundamentals of construction of stability diagrams are briefly introduced in Appendix 2.

### 4.2.1 Stability diagrams for single metal plating baths

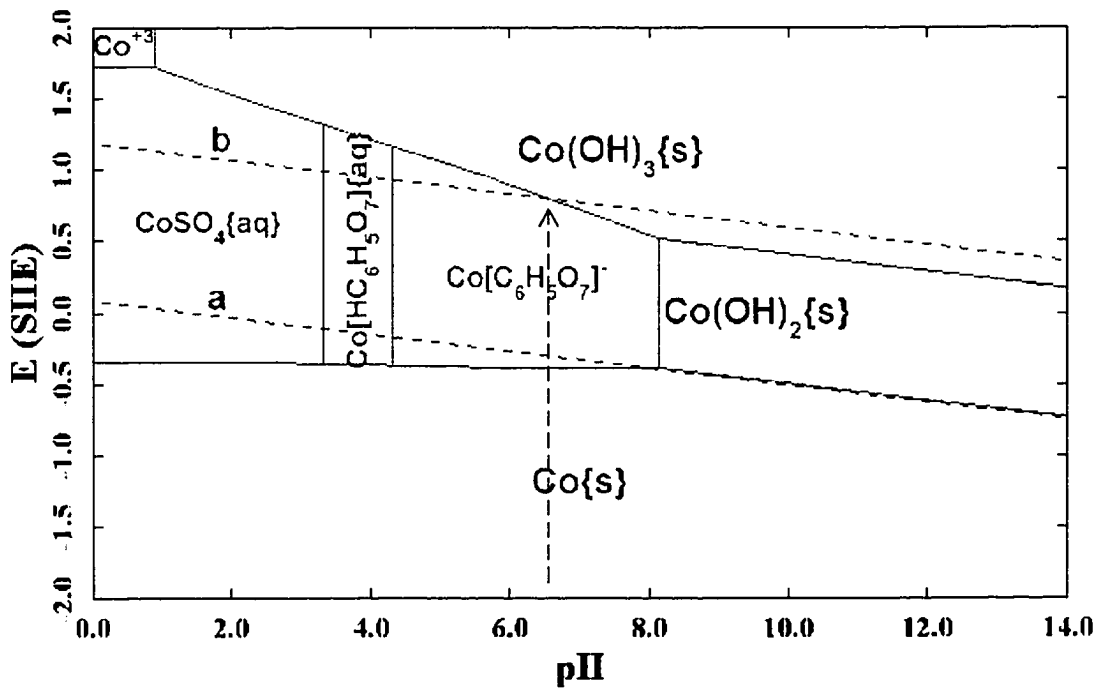
The main differences in the citrate-added CoFe and CoFeNi plating baths (Tables 3-2 and 3-4), relative to the conventional baths (Tables 3-1 and 3-3), are the introduction of a complexing agent – ammonium citrate as a bath stabilizer and relatively high pH levels (natural pH).

#### 4.2.1.1 Stability diagrams for separate Co plating baths

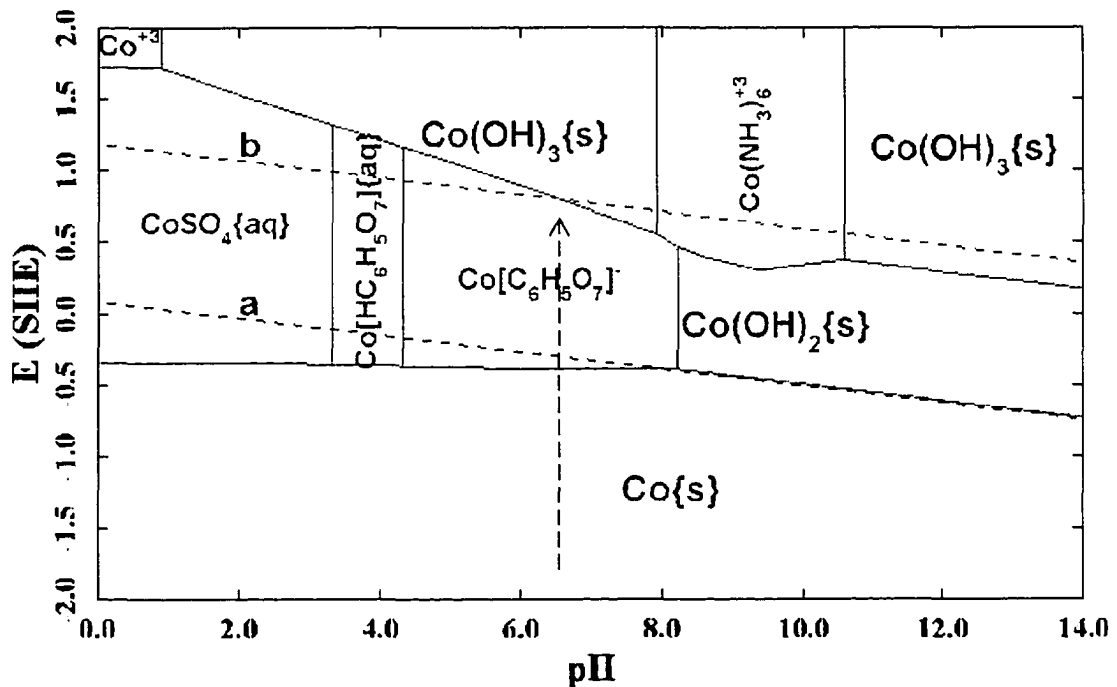
The calculated stability diagrams of single cobalt plating baths with no citrate addition, 0.08M potassium citrate ( $K_3(C_6H_5O_7)$ ) and 0.08M ammonium citrate ( $(NH_4)_3(C_6H_5O_7)$ ) are shown in Figures 4-2a, b and c, respectively. The dashed lines a and b in the diagrams refer to the equilibrium lines for  $H^+/H_2$  and  $(O_2 + H^+)/H_2O$ , respectively. The same notation is used for the other diagrams. For a cobalt plating bath open to air with no citrate addition, thermodynamically, the bath stability is controlled by the precipitation of  $Co(OH)_3$  at pH over 5.8 (Figure 4-2a). With the introduction of



a. 0.08M CoSO<sub>4</sub> bath.



b. 0.08M CoSO<sub>4</sub> and 0.08M K<sub>3</sub>(C<sub>6</sub>H<sub>5</sub>O<sub>7</sub>) bath.



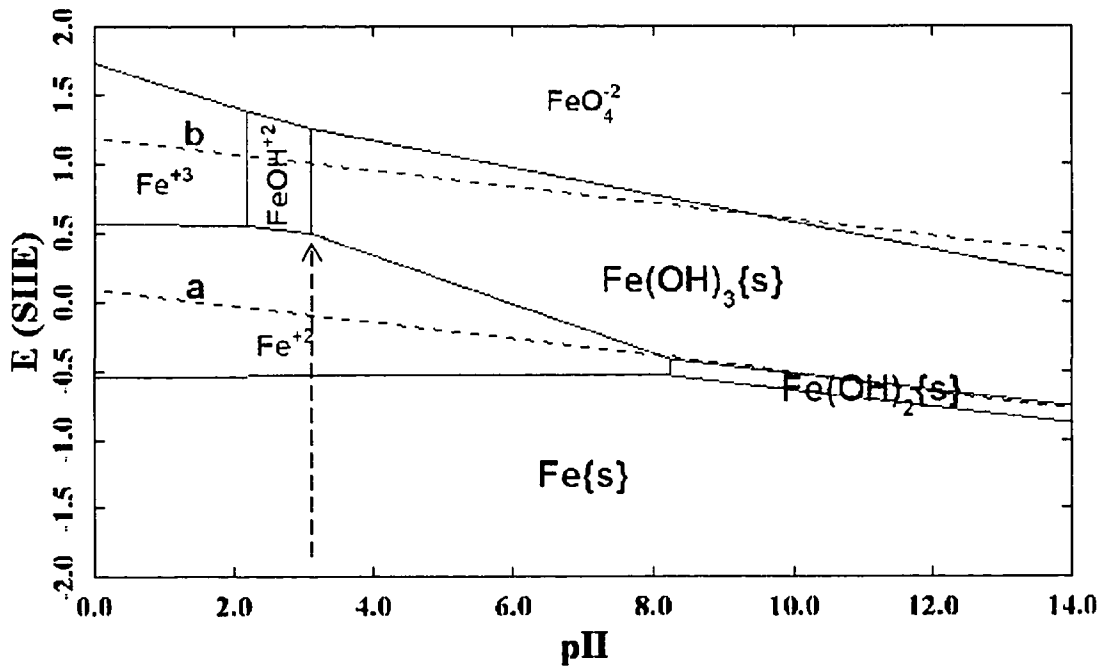
c. 0.08M  $\text{CoSO}_4$  and 0.08M  $(\text{NH}_4)_3(\text{C}_6\text{H}_5\text{O}_7)$  bath.

**Figure 4-2.** Stability diagrams for cobalt plating baths.

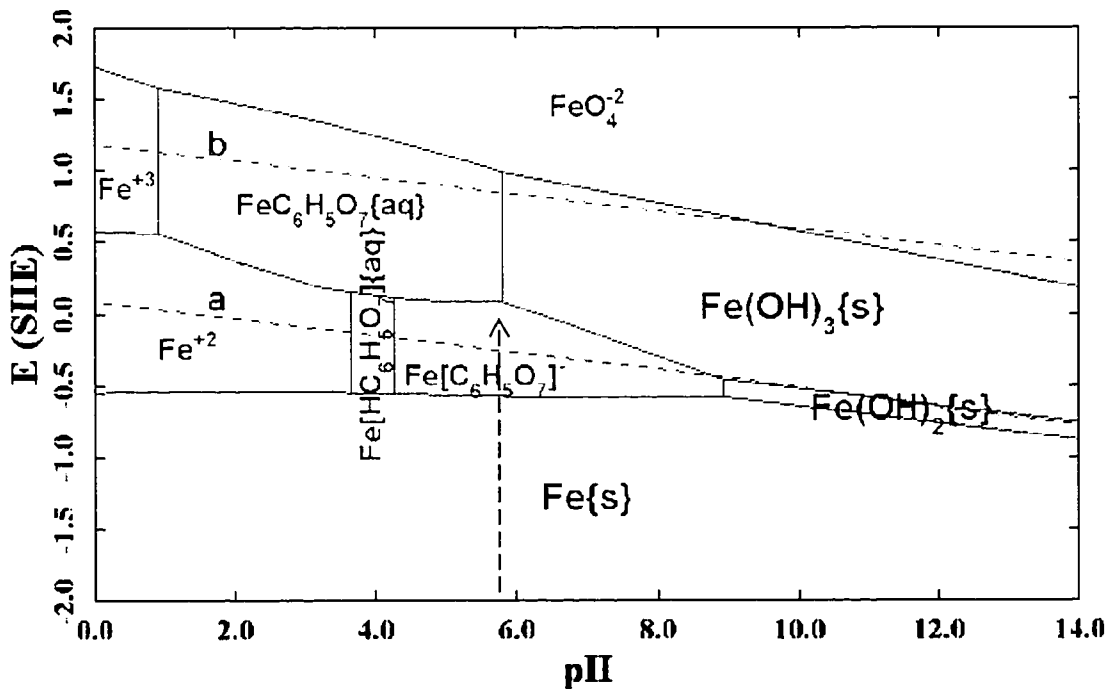
0.08M  $\text{K}_3(\text{C}_6\text{H}_5\text{O}_7)$ , the bath is stable until the precipitation of  $\text{Co}(\text{OH})_3$  at pH higher than 6.5 (Figure 4-2b). With the addition of 0.08M  $(\text{NH}_4)_3(\text{C}_6\text{H}_5\text{O}_7)$ , the bath stability is also controlled by the precipitation of  $\text{Co}(\text{OH})_3$  at pH higher than 6.5. However, the employment of ammonium citrate creates an additional stable region of  $\text{Co}(\text{NH}_3)_6^{3+}$  from pH 7.9 to 10.5, because of the complexing effect of  $\text{NH}_3$  on  $\text{Co}^{3+}$  ions (Figure 4-2c). Therefore, the introduction of citrate can improve the stability of cobalt plating baths.

#### 4.2.1.2 Stability diagrams for separate Fe plating baths

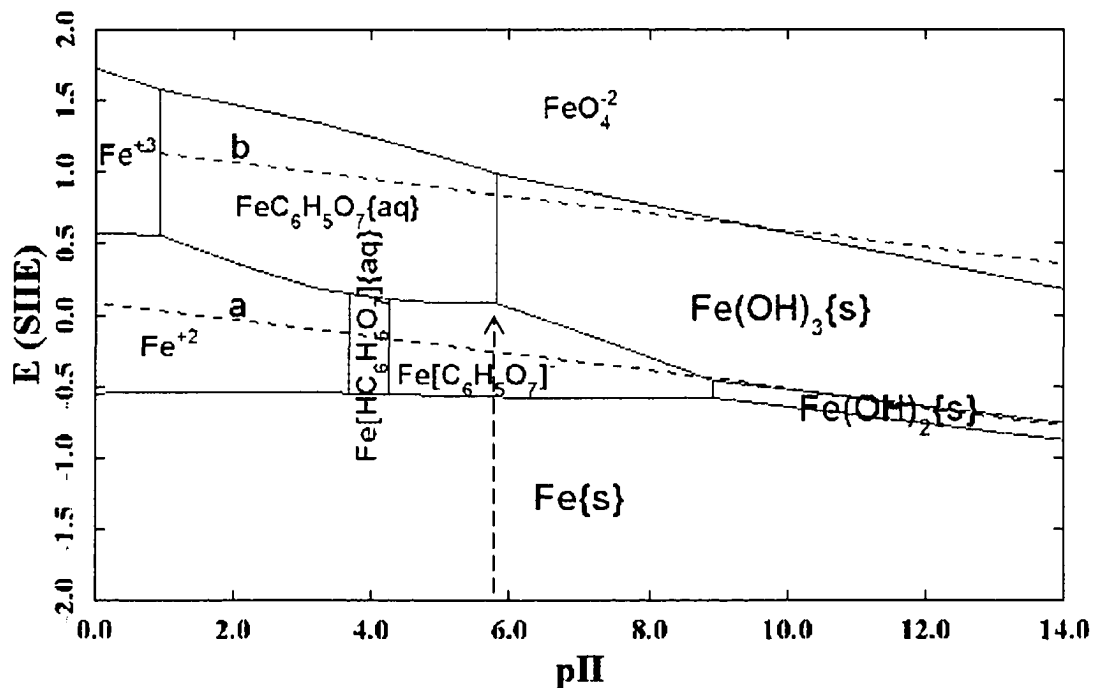
The stability diagrams for single Fe plating baths with no citrate addition, 0.015M  $\text{K}_3(\text{C}_6\text{H}_5\text{O}_7)$  and 0.015M  $(\text{NH}_4)_3(\text{C}_6\text{H}_5\text{O}_7)$  are illustrated in Figures 4-3a, b and c, respectively. For an iron plating bath open to air with no citrate addition, thermodynamically,  $\text{Fe}(\text{OH})_3$  precipitate forms at pH over 3.1 (Figure 4-3a). The addition



a. 0.015M  $FeSO_4$  bath.



b. 0.015M  $FeSO_4$  and 0.015M  $K_3(C_6H_5O_7)$  bath.



c. 0.015M FeSO<sub>4</sub> and 0.015M (NH<sub>4</sub>)<sub>3</sub>(C<sub>6</sub>H<sub>5</sub>O<sub>7</sub>) bath.

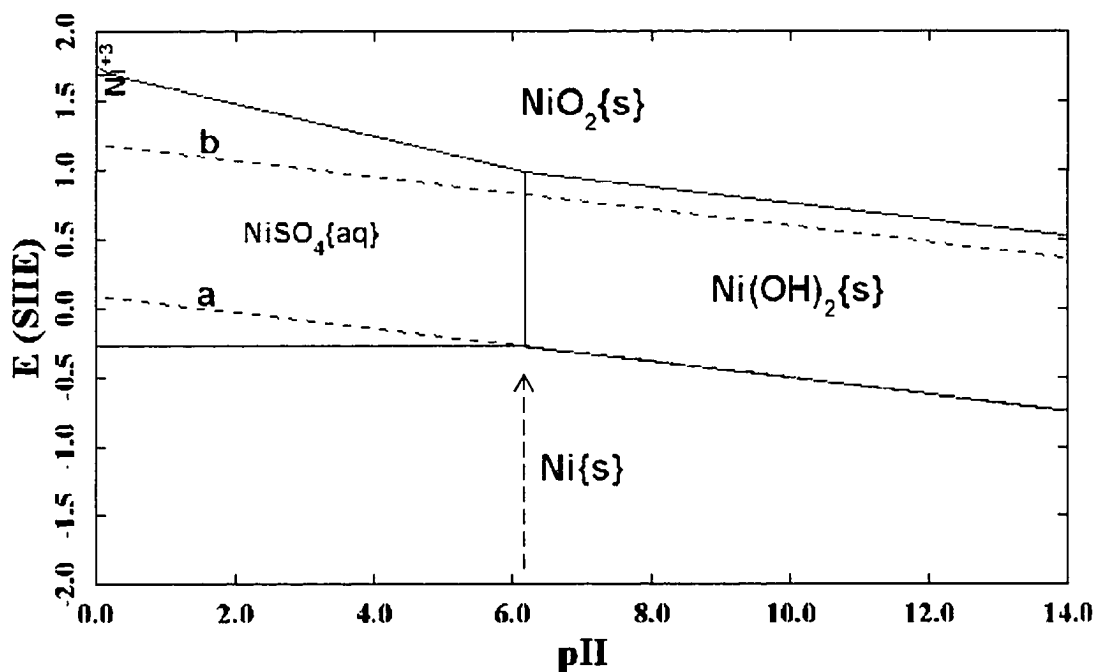
**Figure 4-3.** Stability diagrams for iron plating baths.

of citrate extends the appearance of Fe(OH)<sub>3</sub> to pH values above 5.8 (Figures 4-3b and c). Unlike the Co plating bath, the employment of ammonium citrate makes no difference relative to potassium citrate. No stable complexing ions of NH<sub>3</sub> are formed. Apparently, the introduction of citrate can effectively improve the stability of Fe plating baths.

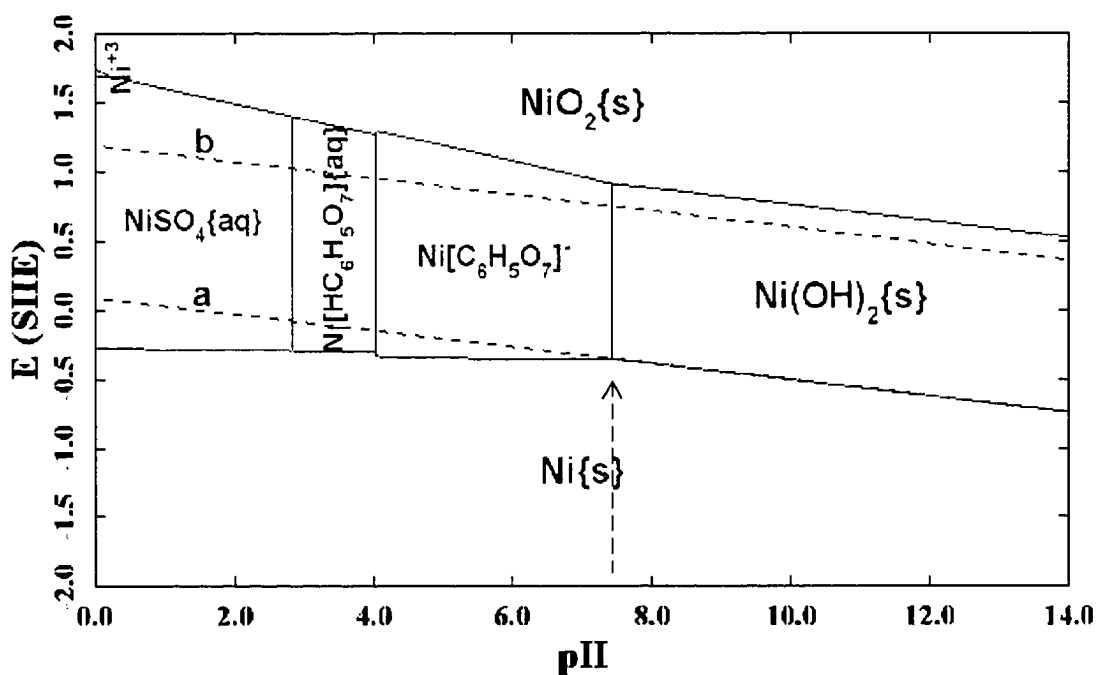
#### 4.2.1.3 Stability diagrams for separate Ni plating baths

The stability diagrams for single Ni plating baths with no citrate addition, 0.30M K<sub>3</sub>(C<sub>6</sub>H<sub>5</sub>O<sub>7</sub>) and 0.30M (NH<sub>4</sub>)<sub>3</sub>(C<sub>6</sub>H<sub>5</sub>O<sub>7</sub>) are shown in Figures 4-4a, b and c, respectively. For a Ni plating bath with no citrate addition, the bath is stable until the precipitation of Ni(OH)<sub>2</sub> at pH over 6.2 (Figure 4-4a). The introduction of citrate extends the appearance of Ni(OH)<sub>2</sub> precipitate to pH above 7.7 (Figures 4-4b and c). Similar to the Fe plating bath, the employment of ammonium citrate makes little difference relative to potassium

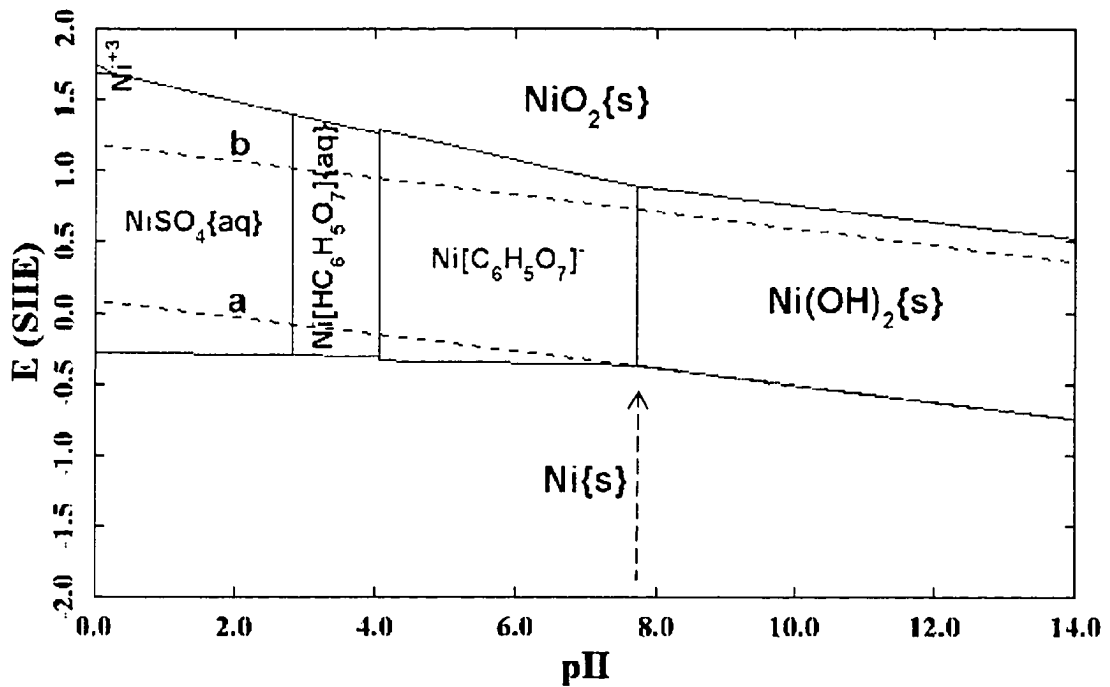
citrate. Obviously, the introduction of citrate can improve the stability of Ni plating baths.



a. 0.30M NiSO<sub>4</sub> bath.



b. 0.30M NiSO<sub>4</sub> and 0.30M K<sub>3</sub>(C<sub>6</sub>H<sub>5</sub>O<sub>7</sub>) bath.



c. 0.30M NiSO<sub>4</sub> and 0.30M (NH<sub>4</sub>)<sub>3</sub>(C<sub>6</sub>H<sub>5</sub>O<sub>7</sub>) bath.

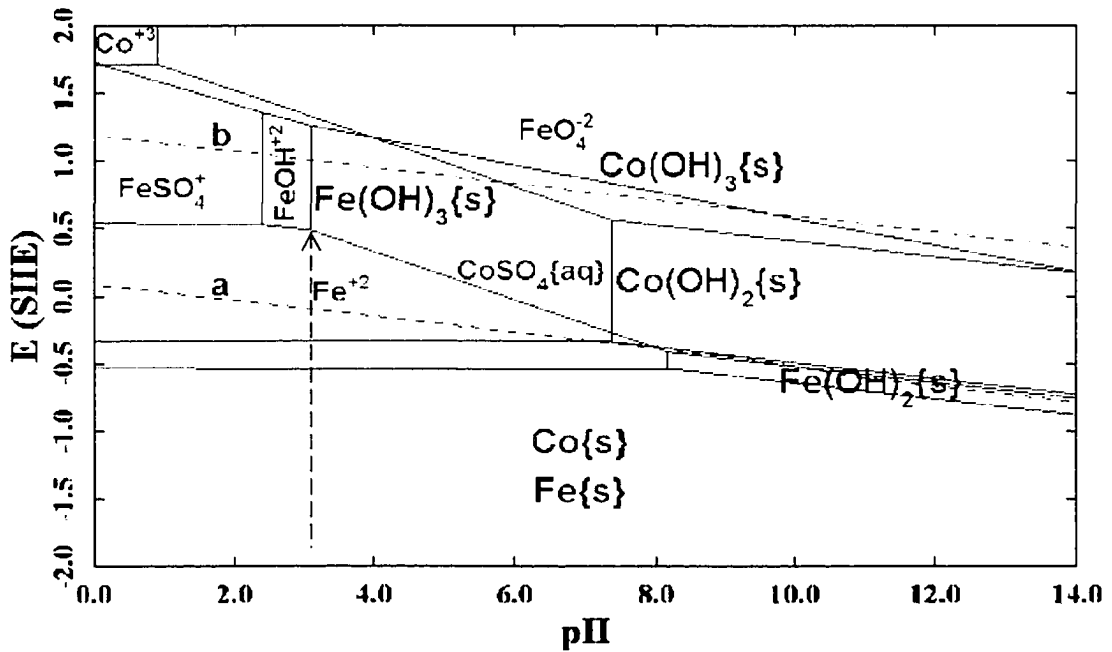
**Figure 4-4.** Stability diagrams for nickel plating baths.

#### 4.2.2 Stability diagrams for CoFe and CoFeNi alloy plating baths

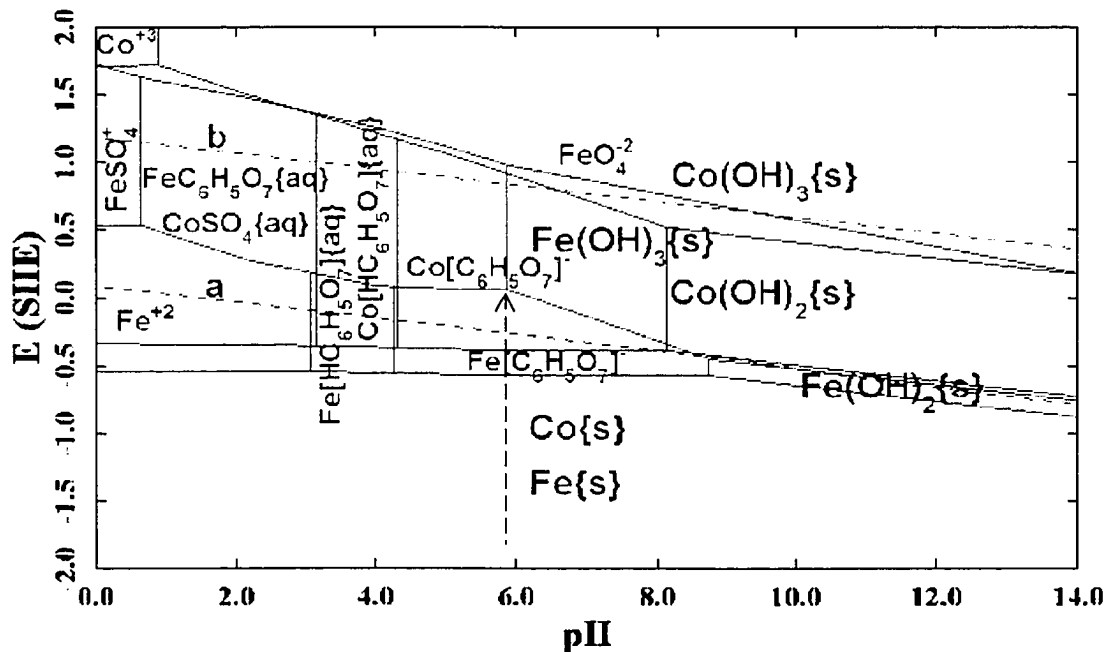
##### 4.2.2.1 Stability diagrams for CoFe alloy plating baths

The stability diagrams for CoFe plating baths with no citrate addition, 0.17M K<sub>3</sub>(C<sub>6</sub>H<sub>5</sub>O<sub>7</sub>), 0.17M (NH<sub>4</sub>)<sub>3</sub>(C<sub>6</sub>H<sub>5</sub>O<sub>7</sub>) and 0.0206M (NH<sub>4</sub>)<sub>3</sub>(C<sub>6</sub>H<sub>5</sub>O<sub>7</sub>), are illustrated in Figures 4-5a, b, c and d, respectively. The predominant areas of Co species and Fe species are defined by red and green lines, respectively. For a CoFe plating bath open to air with no citrate addition, thermodynamically, the bath stability is controlled by the precipitation of Fe(OH)<sub>3</sub> at pH over 3.1 (Figure 4-5a). The addition of 0.17M K<sub>3</sub>(C<sub>6</sub>H<sub>5</sub>O<sub>7</sub>) or (NH<sub>4</sub>)<sub>3</sub>(C<sub>6</sub>H<sub>5</sub>O<sub>7</sub>) extends the appearance of Fe(OH)<sub>3</sub> precipitate to pH above 5.8 (Figures 4-5b and c). The employment of ammonium citrate creates an additional stable region of Co(NH<sub>3</sub>)<sub>6</sub><sup>3+</sup> from pH 7.4 to 11.1, because of the complexing effect of NH<sub>3</sub> on Co<sup>3+</sup> ion (Figure 4-5c). The addition of 0.0206M (5g/L) (NH<sub>4</sub>)<sub>3</sub>(C<sub>6</sub>H<sub>5</sub>O<sub>7</sub>) extends the

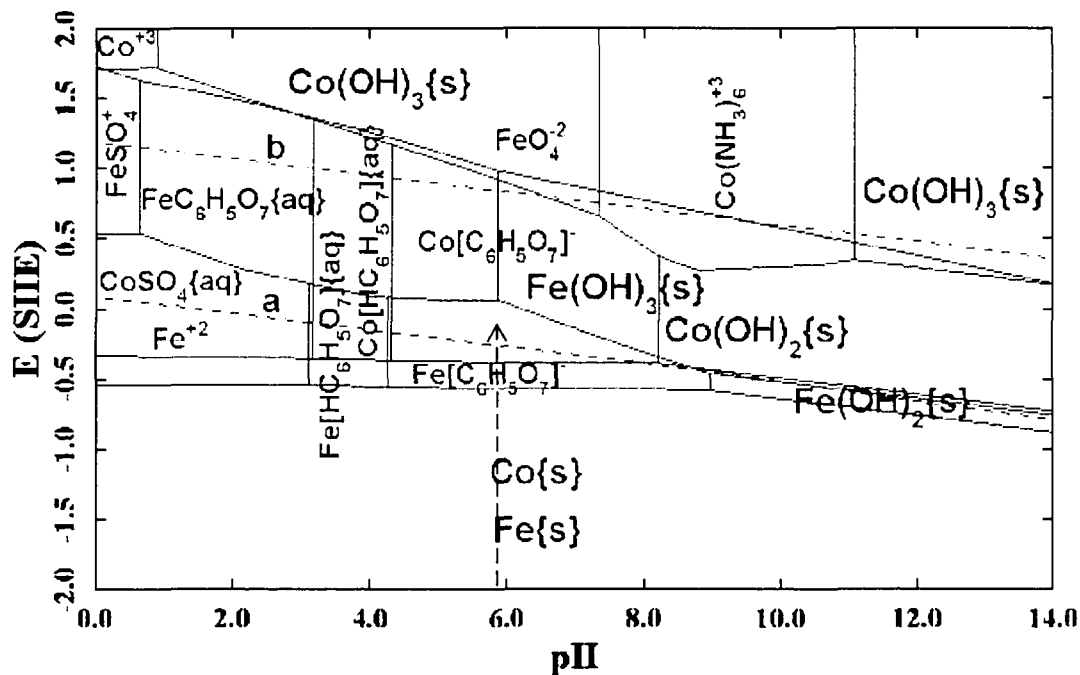
precipitation of  $\text{Fe}(\text{OH})_3$  to pH above 5.2 (Figures 4-5d). Comparing Figure 4-5d with Figure 4-5c, it is clear that the employment of a low concentration of ammonium



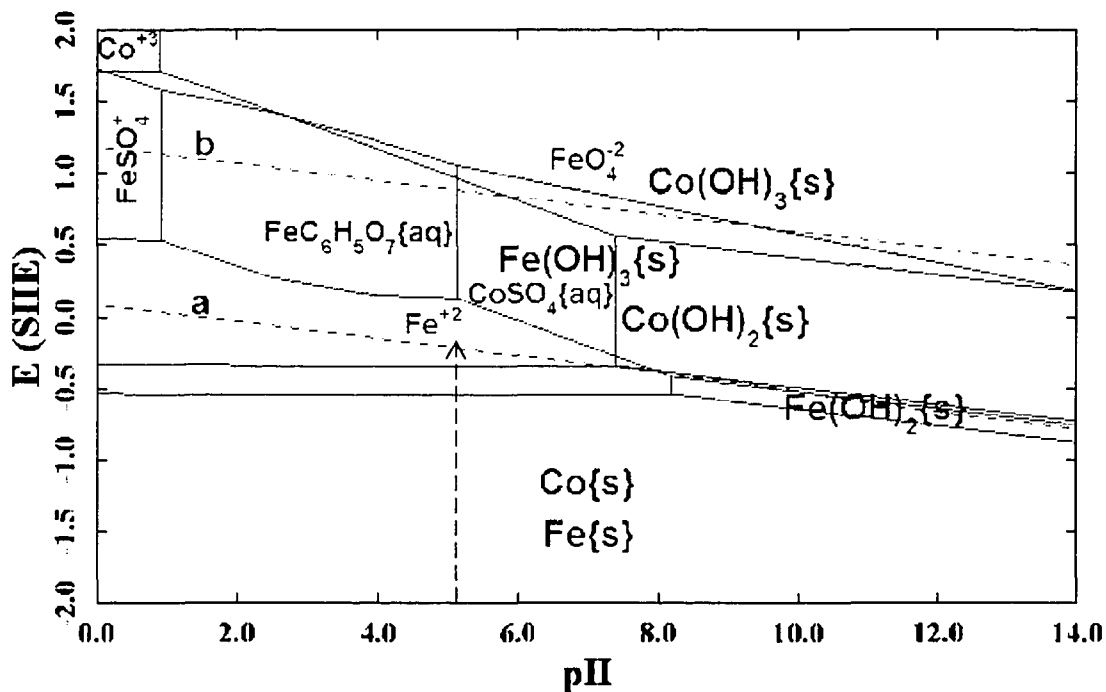
a. 0.12M  $\text{CoSO}_4$  and 0.05M  $\text{FeSO}_4$  bath.



b. 0.12M  $\text{CoSO}_4$ , 0.05M  $\text{FeSO}_4$  and 0.17M  $\text{K}_3(\text{C}_6\text{H}_5\text{O}_7)$  bath.



c. 0.12M CoSO<sub>4</sub>, 0.05M FeSO<sub>4</sub> and 0.17M (NH<sub>4</sub>)<sub>3</sub>(C<sub>6</sub>H<sub>5</sub>O<sub>7</sub>) bath.



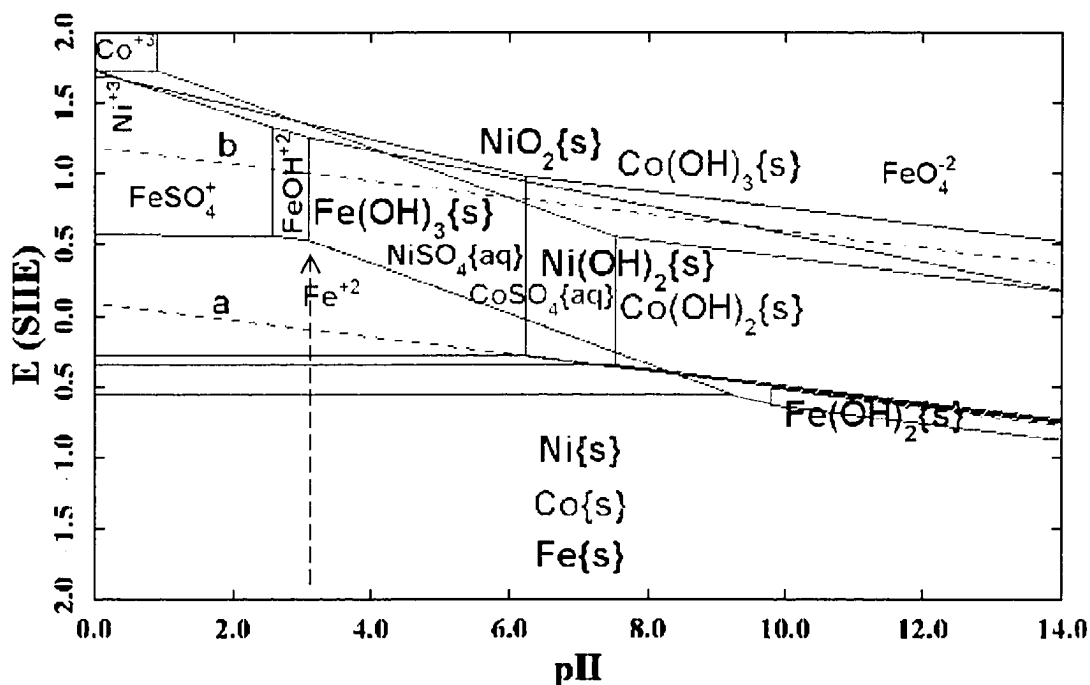
d. 0.12M CoSO<sub>4</sub>, 0.05M FeSO<sub>4</sub> and 0.0206M (i.e., 5g/L) (NH<sub>4</sub>)<sub>3</sub>(C<sub>6</sub>H<sub>5</sub>O<sub>7</sub>) bath.

Figure 4-5. Stability diagrams for CoFe alloy plating baths.

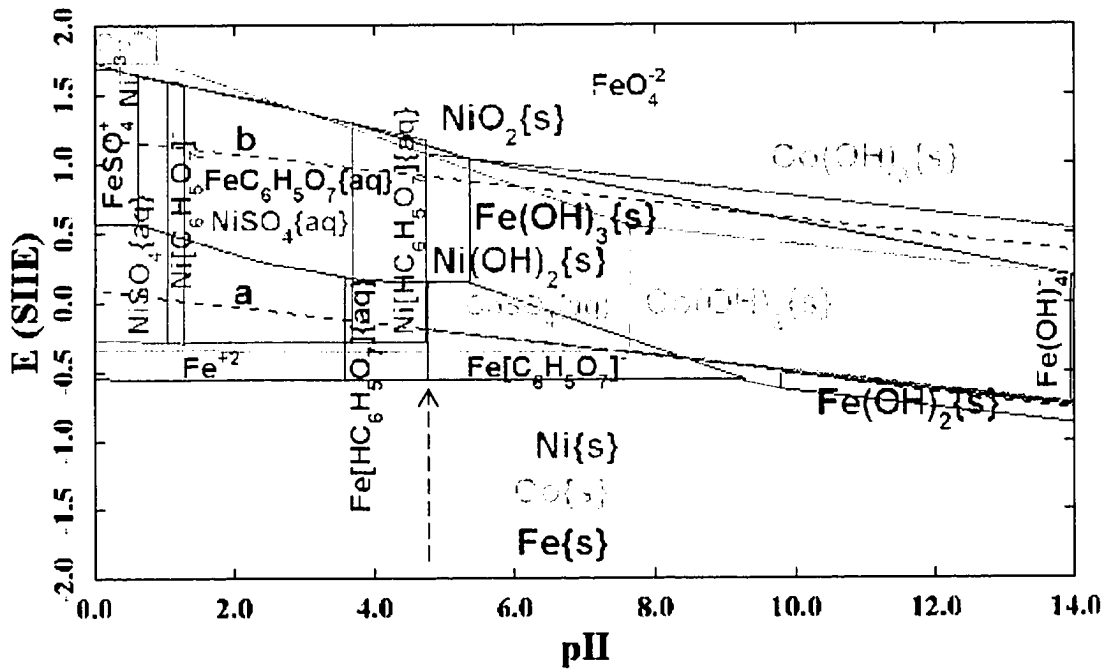
citrate will not create an additional stable region of  $\text{Co}(\text{NH}_3)_6^{3+}$  for cobalt. Generally, the introduction of citrate can effectively improve the stability of CoFe plating baths.

#### 4.2.2.2 Stability diagrams for CoFeNi alloy plating baths

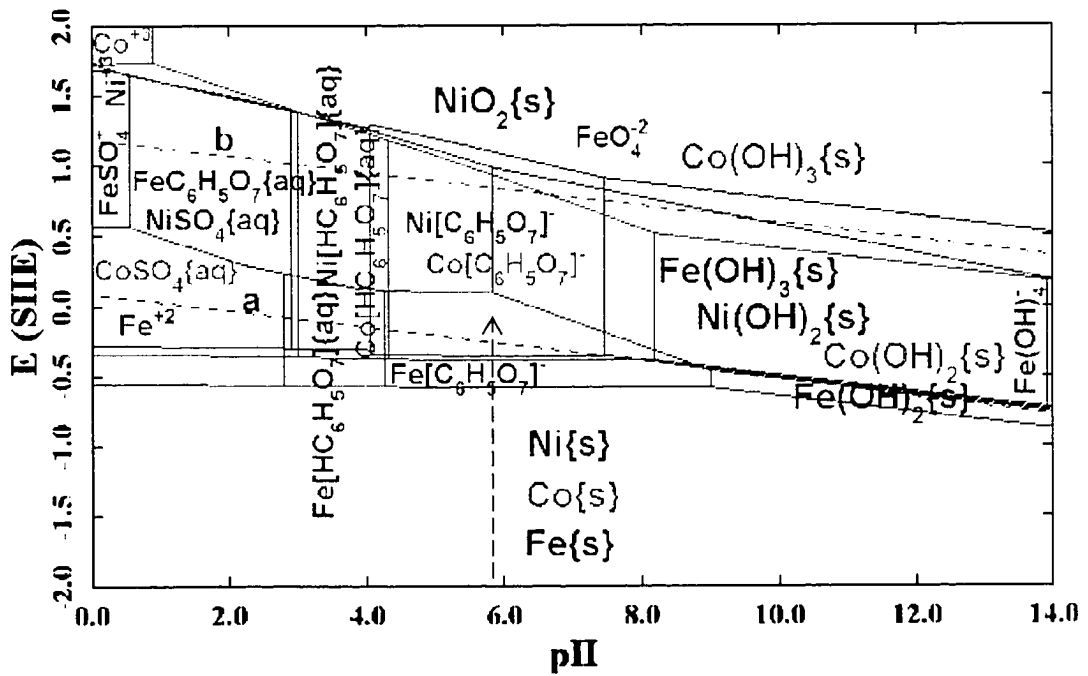
The stability diagrams for CoFeNi alloy plating baths with no citrate addition, 0.206M  $\text{K}_3(\text{C}_6\text{H}_5\text{O}_7)$ , 0.395M  $\text{K}_3(\text{C}_6\text{H}_5\text{O}_7)$  and 0.395M  $(\text{NH}_4)_3(\text{C}_6\text{H}_5\text{O}_7)$ , are illustrated in Figures 4-6a, b, c and d, respectively. The predominant areas of Co species, Fe species, and Ni species are defined by purple, green, and red lines, respectively. For a CoFeNi plating bath open to air without citrate addition, thermodynamically, the bath stability is controlled by the precipitation of  $\text{Fe}(\text{OH})_3$  at pH over 3.1 (Figure 4-6a). After the addition of 0.206M  $\text{K}_3(\text{C}_6\text{H}_5\text{O}_7)$ , the bath is thermodynamically stable until a pH~4.7 under the given concentrations of metal ions (Figure 4-6b). The addition of 0.395M  $\text{K}_3(\text{C}_6\text{H}_5\text{O}_7)$  or  $(\text{NH}_4)_3(\text{C}_6\text{H}_5\text{O}_7)$  extends the appearance of  $\text{Fe}(\text{OH})_3$  precipitate to pH values above 5.8 (Figures 4-6c and d). The employment of ammonium citrate creates an



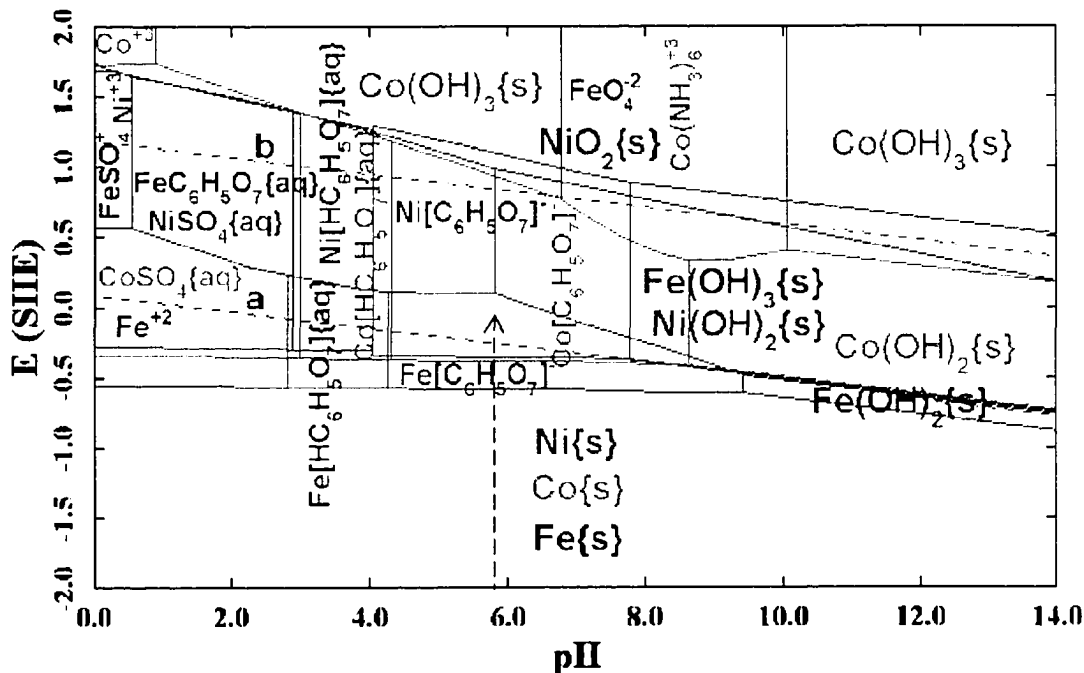
a. 0.08M  $\text{CoSO}_4$ , 0.015M  $\text{FeSO}_4$  and 0.30M  $\text{NiSO}_4$  bath.



b. 0.08M  $CoSO_4$ , 0.015M  $FeSO_4$ , 0.30M  $NiSO_4$  and 0.206M  $K_3(C_6H_5O_7)$  bath.



c. 0.08M  $CoSO_4$ , 0.015M  $FeSO_4$ , 0.30M  $NiSO_4$  and 0.395M  $K_3(C_6H_5O_7)$  bath.



d. 0.08M CoSO<sub>4</sub>, 0.015M FeSO<sub>4</sub>, 0.30M NiSO<sub>4</sub> and 0.395M (NH<sub>4</sub>)<sub>3</sub>(C<sub>6</sub>H<sub>5</sub>O<sub>7</sub>) bath.

**Figure 4-6.** Stability diagrams for CoFeNi alloy plating baths.

additional stable region of Co(NH<sub>3</sub>)<sub>6</sub><sup>3+</sup> from pH 6.8 to 10.05 because of the complexing effect of NH<sub>3</sub> on Co<sup>3+</sup> ions (Figure 4-6d). Therefore, the introduction of citrate can effectively improve the stability of CoFeNi alloy plating baths.

From Figures 4-5d, 4-6b and 4-6c, it can be seen that citrate has the strongest complexing power for Fe ions, followed by Ni<sup>2+</sup> ions, and the weakest complexing effect for Co<sup>2+</sup> ions.

The calculated stability diagrams demonstrate that, the stability of CoFe and CoFeNi plating baths open to air is dominated by the appearance of Fe(OH)<sub>3</sub> precipitate at a pH around 3.1. Therefore, it is easy to understand the selection of bath pH in the range of 2.0 to 3.0 by most researchers. [Osaka03-1] [Osaka98-1] [Osaka98-2] [Liu03] Thermodynamically, citrate additives can effectively stabilize the single metal, CoFe and

CoFeNi alloy plating baths, preventing the precipitation of metal hydroxides at higher pH levels.

### 4.3 Main complexing reactions in citrate-added plating baths

The distribution of ion species in citric acid solution at different pH values was calculated with OLI Analyzer (see Figure 4-7). At pH <3.0, citric acid ( $C_6H_8O_7$ ) is the dominant form, with some  $[H_2C_6H_5O_7]^-$  ions:

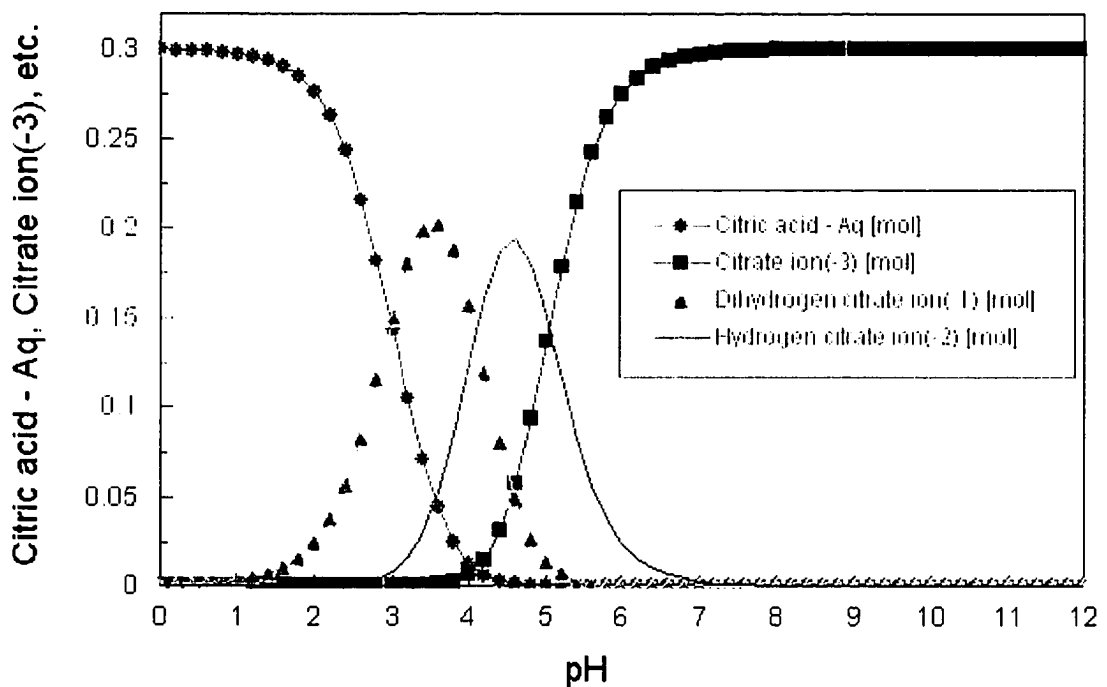
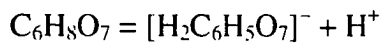
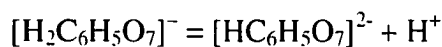
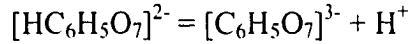


**Figure 4-7.** Distribution of ion species in citric acid solution (0.30 M) vs pH.

For  $3.0 < \text{pH} < 4.1$ ,  $[H_2C_6H_5O_7]^-$  is the dominant species, with some citric acid and  $[HC_6H_5O_7]^{2-}$  ions coexisting:

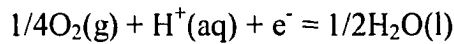


For  $4.1 < \text{pH} < 5.1$ ,  $[\text{HC}_6\text{H}_5\text{O}_7]^{2-}$  is the dominant species, with the coexistence of  $[\text{H}_2\text{C}_6\text{H}_5\text{O}_7]^-$  ions and  $[\text{C}_6\text{H}_5\text{O}_7]^{3-}$  ions:

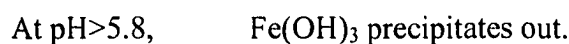
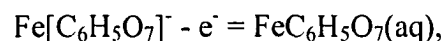
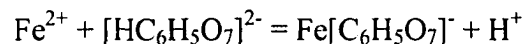
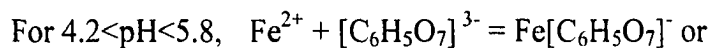
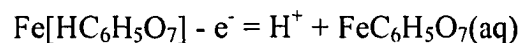
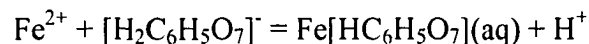
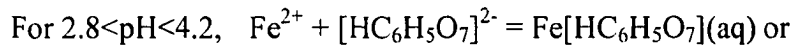


At  $\text{pH} > 5.1$ ,  $[\text{C}_6\text{H}_5\text{O}_7]^{3-}$  is the dominant species, with the coexistence of  $[\text{HC}_6\text{H}_5\text{O}_7]^{2-}$  ions. Thermodynamically, the complexing reaction between a citrate ion species and a metal ion is dominated by the complexing power of the citrate ion species to the metal ion, which can be represented by the equilibrium constant of corresponding complexing reaction.

From the above calculated stability diagrams and distribution of ion species in citric acid solution at different pHs (Figures 4-5, 4-6 and 4-7), the main chemical and electrochemical reactions involved in citrate-added baths for CoFe and CoFeNi deposition can be analyzed. Generally, according to Figures 4-5b, 4-6c and 4-7, for citrate-added baths open to air, the reduction of oxygen will occur.



For iron ions, the following reactions can occur:

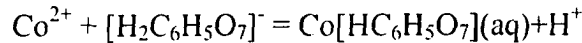


Therefore,  $\text{FeC}_6\text{H}_5\text{O}_7(\text{aq})$  contributes to stabilizing the iron species.

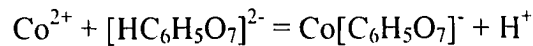
For cobalt ions, the following reactions can occur:

At pH<3.0,  $\text{Co}^{2+}$  is stable

For  $3.0 < \text{pH} < 4.3$ ,  $\text{Co}^{2+} + [\text{HC}_6\text{H}_5\text{O}_7]^{2-} = \text{Co}[\text{HC}_6\text{H}_5\text{O}_7](\text{aq})$  or



For  $4.3 < \text{pH} < 6.5$ ,  $\text{Co}^{2+} + [\text{C}_6\text{H}_5\text{O}_7]^{3-} = \text{Co}[\text{C}_6\text{H}_5\text{O}_7]^-$  or

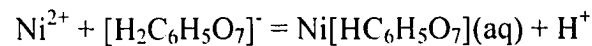


At pH>6.5,  $\text{Co}(\text{OH})_3$  precipitates out.

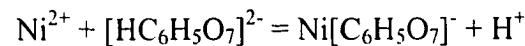
For nickel ions, the following reactions can occur:

At pH<2.9,  $\text{Ni}^{2+}$  is stable

For  $2.9 < \text{pH} < 4.0$ ,  $\text{Ni}^{2+} + [\text{HC}_6\text{H}_5\text{O}_7]^{2-} = \text{Ni}[\text{HC}_6\text{H}_5\text{O}_7](\text{aq})$  or

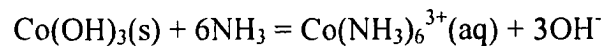
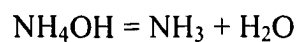


For  $4.0 < \text{pH} < 7.5$ ,  $\text{Ni}^{2+} + [\text{C}_6\text{H}_5\text{O}_7]^{3-} = \text{Ni}[\text{C}_6\text{H}_5\text{O}_7]^-$  or



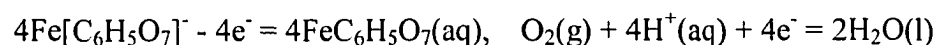
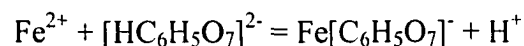
At pH>7.5,  $\text{Ni}(\text{OH})_2$  precipitates out.

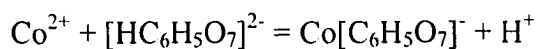
With the employment of ammonium citrate at high concentration (Figures 4-5c and 4-6d), in the pH region higher than that for the appearance of  $\text{Co}(\text{OH})_3$  precipitate, the following reactions can occur:



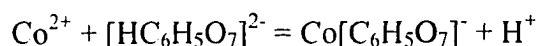
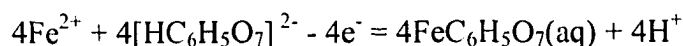
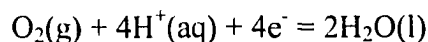
For specific plating baths, the expected reactions are described in the following paragraphs.

The main complexing reactions in CoFe alloy plating baths, with high citrate-additions at pH ~4.4 according to Figures 4-5b, 4-5c and 4-7, can be summarized as:

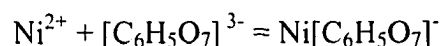
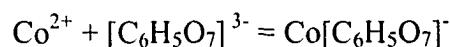
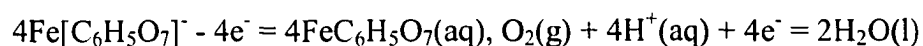
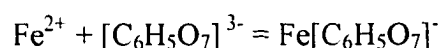




For CoFe plating baths, with low citrate dosage (0.0206M citrate) at pH ~4.4 (refer to Figures 4-5d and 4-7) the reactions will be:



The main complexing reactions in CoFeNi alloy plating baths, with high citrate-additions at pH ~5.3 according to Figures 4-6c, 4-6d and 4-7, can be summarized as:



#### 4.4 Stability of plating baths

The calculated stability diagrams demonstrate that, thermodynamically, citrate can effectively improve the stability of CoFe and CoFeNi alloy plating baths, preventing the precipitation of metal hydroxides at higher pH levels. To verify the results of stability diagram calculations, stability tests on CoFe and CoFeNi plating baths with and without the addition of ammonium citrate have been conducted. The results are summarized in Tables 4-1 and 4-2, respectively.

It can be seen that conventional CoFe and CoFeNi plating baths are not stable; their useful lifetime is less than 48 hours. Ammonium citrate can significantly improve the stability of both CoFe and CoFeNi plating baths, i.e., the citrate-added CoFe and CoFeNi plating baths are much more stable than the conventional ones. For citrate-free baths, a bath with a lower pH level is more stable.

**Table 4-1.** Stability tests for CoFe plating baths with and without the addition of ammonium citrate.

<b>Bath composition</b>	<b>pH</b>	<b>Stability</b>
0.120M CoSO <sub>4</sub> 0.050M FeSO <sub>4</sub> 0.4M H <sub>3</sub> BO <sub>3</sub> 0.01g/L sodium lauryl sulfate <i>5 g/L ammonium citrate</i>	~ 4.4 (natural)	Plated bath was transparent after more than 2 weeks. Plating results were repeatable after 2 days.
0.048M CoSO <sub>4</sub> 0.050M FeSO <sub>4</sub> 0.4M H <sub>3</sub> BO <sub>3</sub> 0.01g/L sodium lauryl sulfate 0.28M NH <sub>4</sub> Cl <i>0 g/L ammonium citrate</i>	3.8 (natural)	Precipitate appeared in plated bath within 20 hours.
0.048M CoSO <sub>4</sub> 0.050M FeSO <sub>4</sub> 0.4M H <sub>3</sub> BO <sub>3</sub> 0.01g/L sodium lauryl sulfate 0.28M NH <sub>4</sub> Cl <i>0 g/L ammonium citrate</i>	2.4 (pH adjusted with dilute H <sub>2</sub> SO <sub>4</sub> )	Precipitate appeared in plated bath after less than 24 hours.

**Table 4-2.** Stability tests for CoFeNi plating baths with and without the addition of ammonium citrate.

<b>Bath composition</b>	<b>pH</b>	<b>Stability</b>
0.08M CoSO <sub>4</sub> 0.015M FeSO <sub>4</sub> 0.3M NiSO <sub>4</sub> 0.4M H <sub>3</sub> BO <sub>3</sub> 0.01 g/L sodium lauryl sulfate <i>50 g/L ammonium citrate</i>	5.3 (natural)	Plated bath was transparent after more than one month. Plating results were repeatable after 6 days.
0.08M CoSO <sub>4</sub> 0.015M FeSO <sub>4</sub> 0.3M NiSO <sub>4</sub> 0.4M H <sub>3</sub> BO <sub>3</sub> 0.01 g/L sodium lauryl sulfate 0.28M NH <sub>4</sub> Cl <i>0 g/L ammonium citrate</i>	4.2 (natural)	Precipitate appeared in bath within 2 hours during plating.
0.08M CoSO <sub>4</sub> 0.015 M FeSO <sub>4</sub> 0.3M NiSO <sub>4</sub> , 0.4M H <sub>3</sub> BO <sub>3</sub> 0.01 g/L sodium lauryl sulfate 0.28M NH <sub>4</sub> Cl <i>0 g/L ammonium citrate</i>	2.7 (pH adjusted with dilute H <sub>2</sub> SO <sub>4</sub> )	Precipitate appeared in plated bath after less than 48 hours.

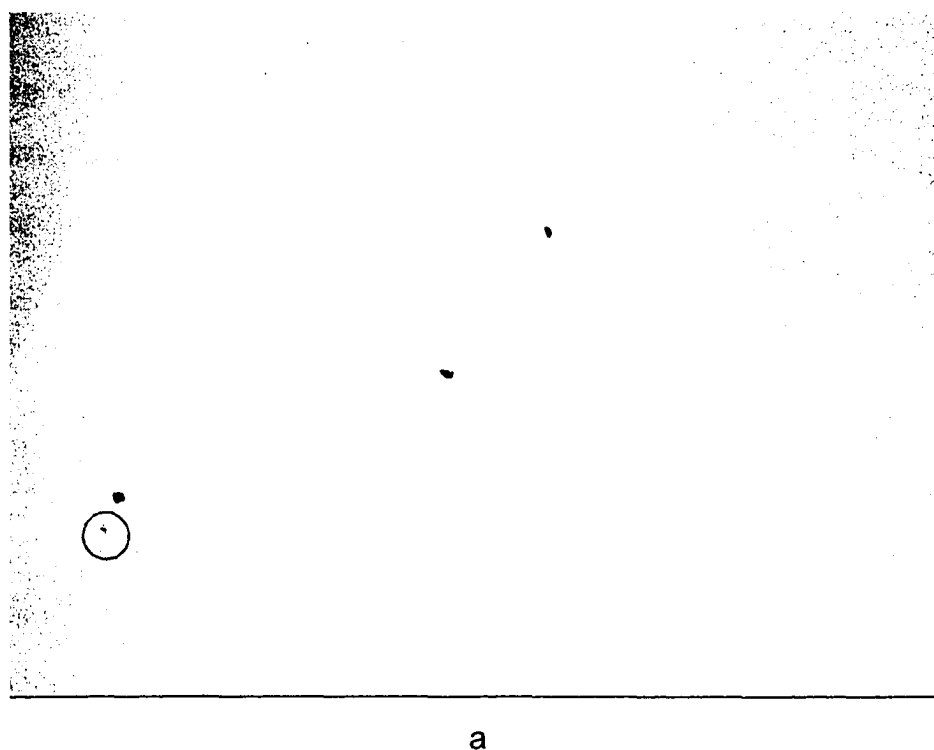
#### **4.5 Morphologies of CoFe and CoFeNi films electroplated from the citrate-added baths and conventional baths**

Besides the stability problems, conventional CoFe and CoFeNi plating baths suffer

from low current density efficiency and voids in deposited films, because of the employment of low pH levels which favor the electroplating of  $H_2$ . The voids in deposited films will degenerate film magnetic properties and uniformity. As listed in Appendix 1,  $H^+/H_2$  has a more positive equilibrium potential than the metal electrodes, which means hydrogen can be more easily reduced than the metals. The  $H^+$  concentrations in the citrate-added baths are hundreds of times lower than those in the conventional baths (pH = 2.0-3.0). [Osaka03-1] [Osaka98-1] [Osaka98-2] [Liu03] Therefore, more uniform and denser films should be plated out. The morphologies of films plated from citrate-added baths and conventional baths were investigated using SEM.

#### 4.5.1 Morphologies of CoFe films

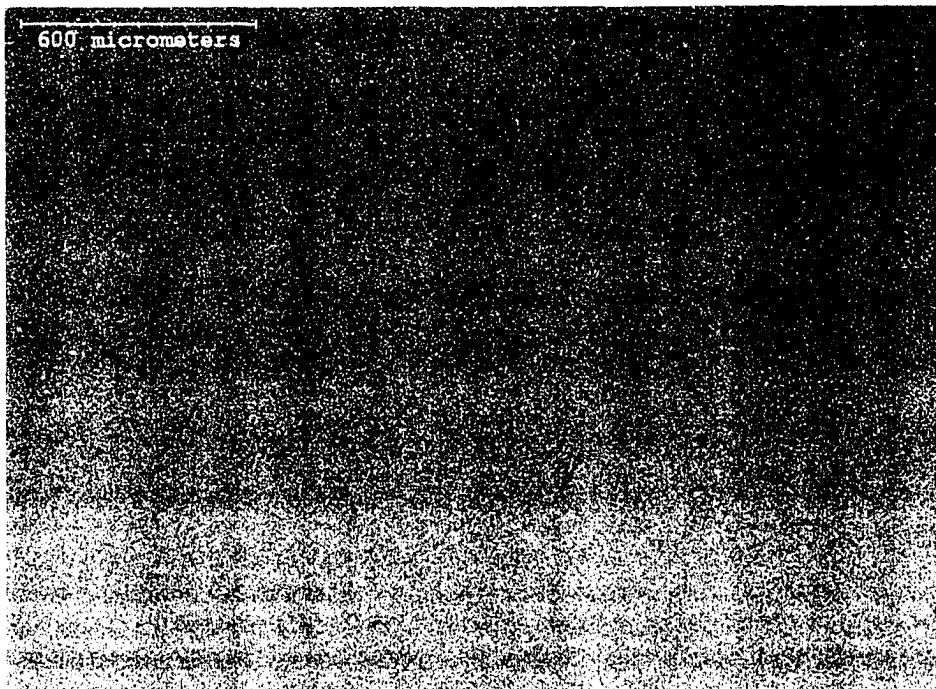
##### 4.5.1.1 Plan views



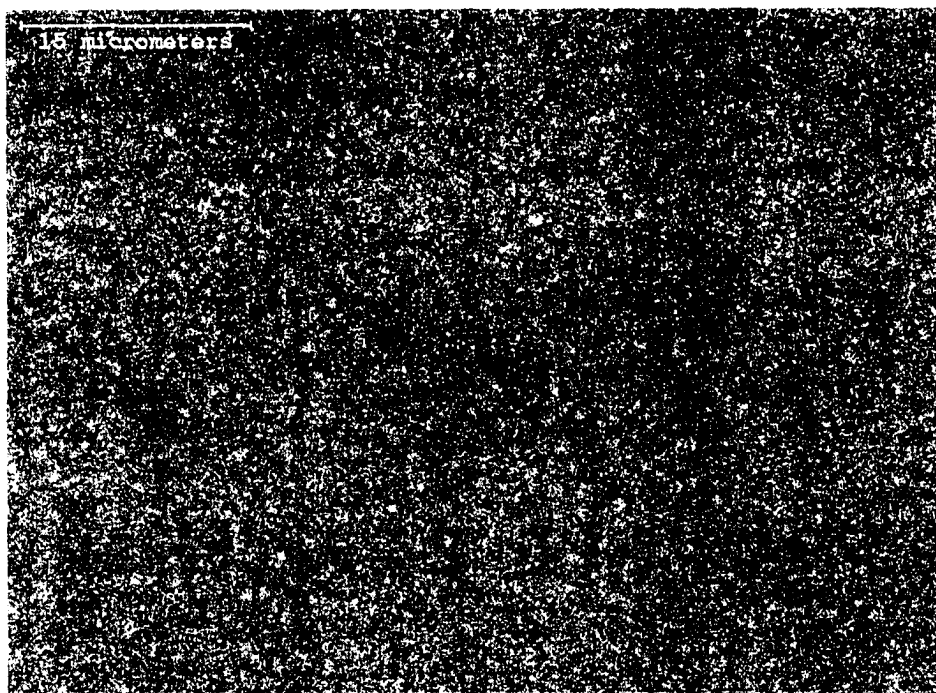


b. Magnification of circled part in a.

**Figure 4-8.** Plan view SEM SE images of CoFe film plated from a bath with 0 g/L ammonium citrate and pH 2.4 at  $i = 15\text{mA}/\text{cm}^2$ ;  $t_{\text{on}} = 6\text{ms}$ ;  $t_{\text{off}} = 4\text{ms}$ ; agitation of 600rpm.



a



b

**Figure 4-9.** Plan view SEM SE images of CoFe film plated from a bath with 5 g/L ammonium citrate and pH 4.4 at  $i = 15\text{mA}/\text{cm}^2$ ;  $t_{\text{on}} = 6\text{ms}$ ;  $t_{\text{on}} + t_{\text{off}} = 10\text{ms}$ ; agitation of 600rpm.

Plan view images of representative CoFe films plated from a conventional low pH bath (Table 3-1) and citrate-added bath (Table 3-2) are illustrated in Figures 4-8 and 4-9, respectively. It can be seen that the film deposited from the conventional low pH bath is porous, while the film plated from citrate-added bath is much more uniform.

#### *4.5.1.2 Cross-section views*

The cross-section views of the above CoFe films are illustrated in Figures 4-10 and 4-11, respectively. Similar to the plan views, the cross-section of the film deposited from the conventional low pH bath looks porous, while the cross-section of the film plated from citrate-added bath is denser.

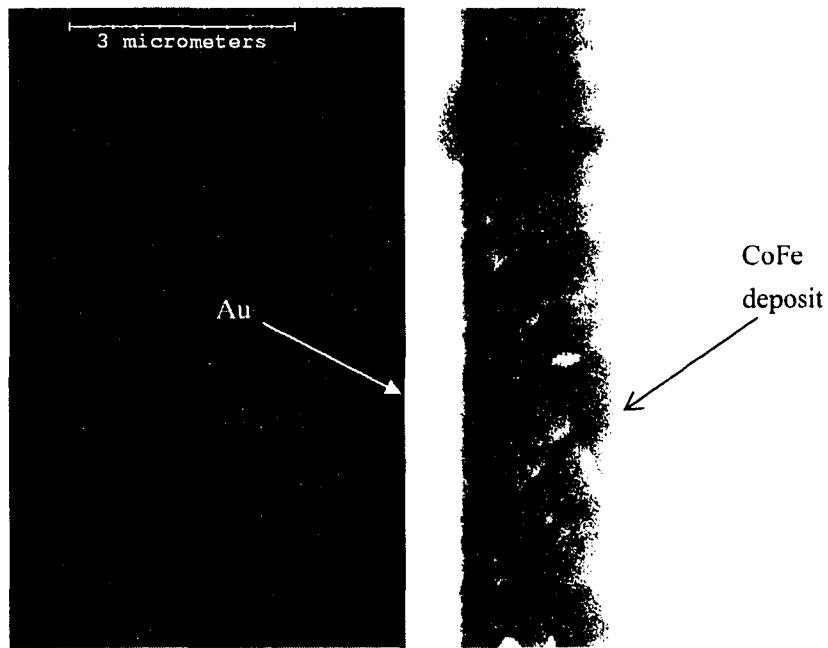


**Figure 4-10.** Cross-section SEM SE image of CoFe film plated from a bath with 0 g/L ammonium citrate and pH 2.4 at  $i = 15\text{mA}/\text{cm}^2$ ;  $t_{\text{ON}} = 6\text{ms}$ ;  $t_{\text{ON}} + t_{\text{OFF}} = 10\text{ms}$ ; agitation of 600rpm.

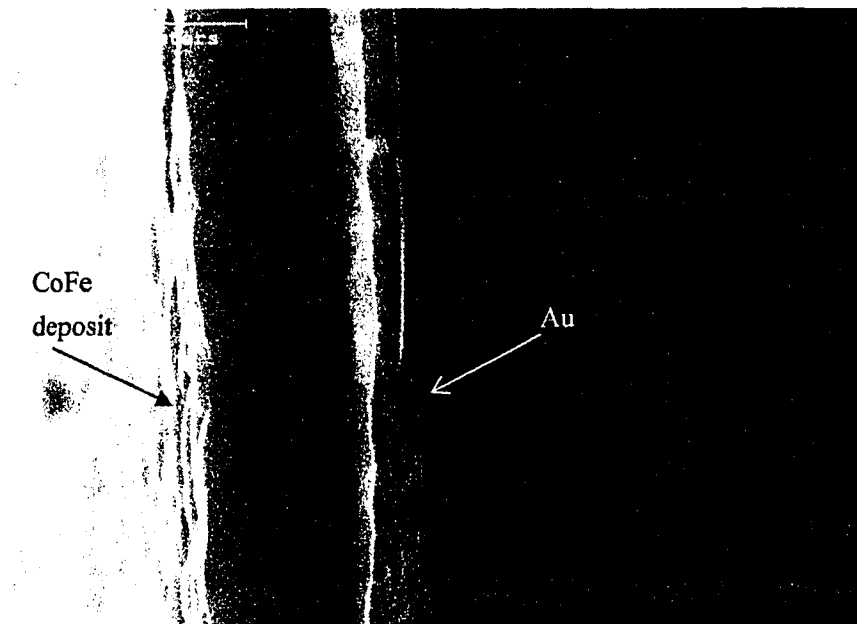


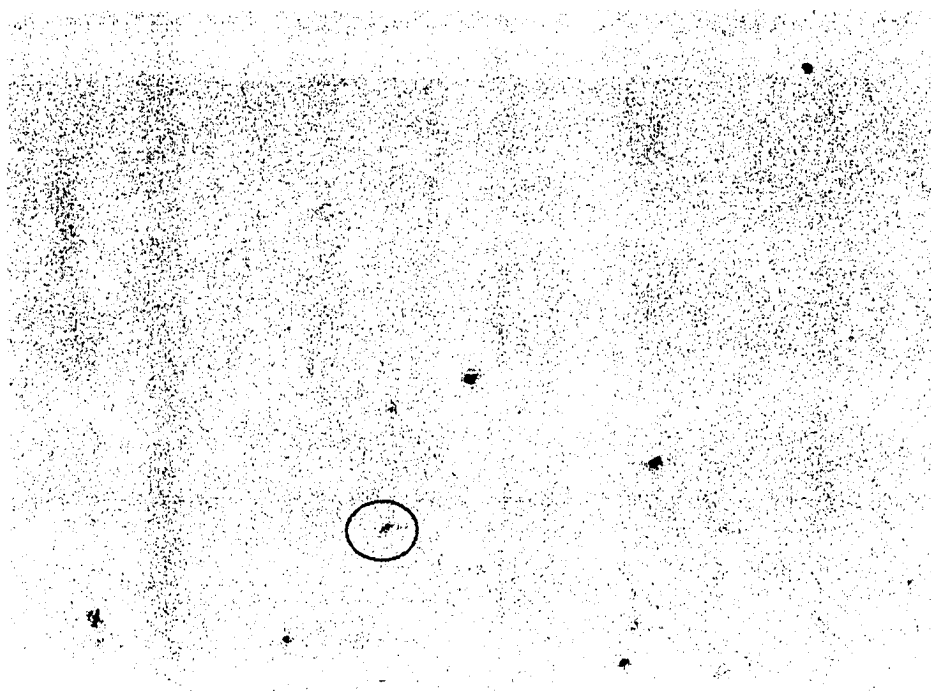
**Figure 4-11.** Cross-section SEM SE image of CoFe film plated from a bath with 5 g/L ammonium citrate and pH 4.4 at  $i = 15\text{mA}/\text{cm}^2$ ;  $t_{\text{ON}} = 6\text{ms}$ ;  $t_{\text{ON}} + t_{\text{OFF}} = 10\text{ms}$ ; agitation of 600rpm.

The morphology studies demonstrate that the CoFe film plated from citrate-added bath is more uniform and denser than that deposited from conventional low pH bath.

## 4.5.2 Morphologies of CoFeNi films

### 4.5.2.1 Plan views

Plan view images of representative CoFeNi films plated from a conventional low pH bath (Table 3-3) and citrate-added bath (Table 3-4) are shown in Figures 4-12 and 4-13, respectively. Similar to CoFe films, the CoFeNi film deposited from the conventional low pH bath are porous. The high magnification figure (Figure 4-12b) illustrates the microstructure of the holes. However, the CoFeNi film plated from citrate-added bath is much smoother and more uniform (Figure 4-13).

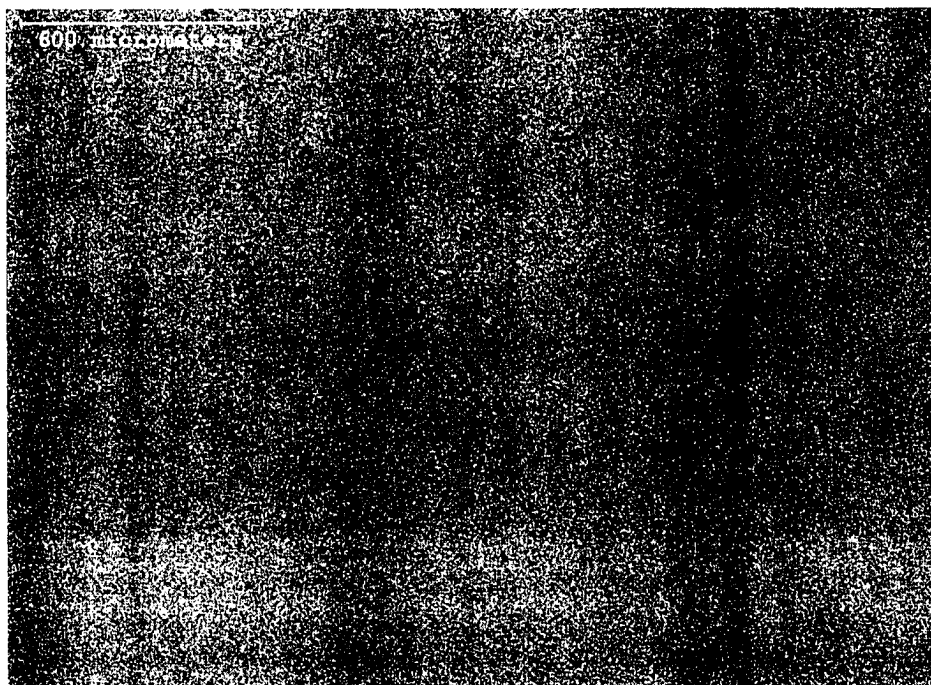


a



b. Magnification of circled part in a.

**Figure 4-12.** Plan view SEM SE images of CoFeNi film plated from a bath with 0 g/L ammonium citrate and pH 2.7 at  $i = 6\text{mA/cm}^2$ ;  $t_{\text{on}} = 0.3\text{ms}$ ;  $t_{\text{on}} + t_{\text{off}} = 10\text{ms}$ ; agitation of 600rpm.



a



b

**Figure 4-13.** Plan view SEM SE images of CoFeNi film plated from a bath with 50 g/L ammonium citrate and pH 5.3 at  $i = 6\text{mA/cm}^2$ ;  $t_{\text{on}} = 0.3\text{ms}$ ;  $t_{\text{on}} + t_{\text{off}} = 10\text{ms}$ ; agitation of 600rpm.

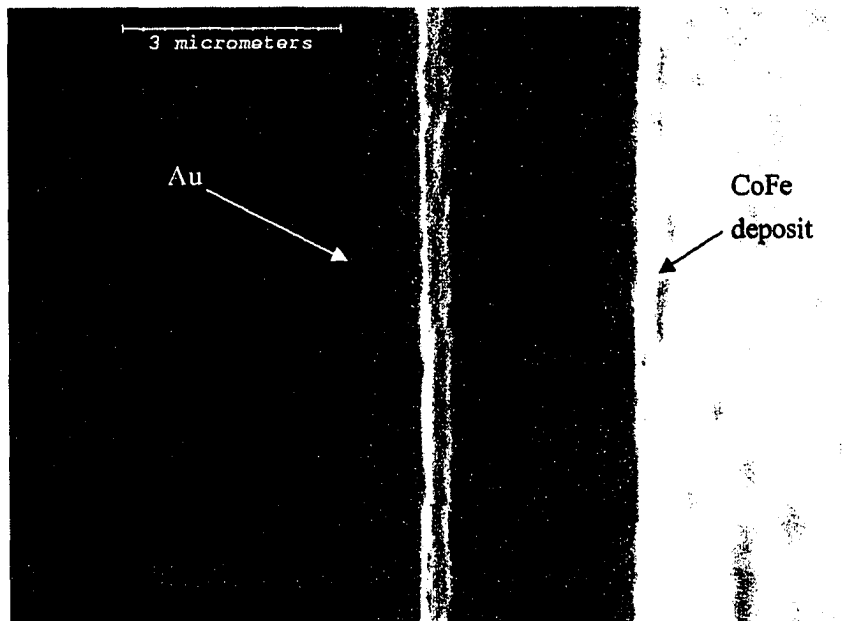


**Figure 4-14.** Cross-section SEM SE image of CoFeNi film plated from a bath with 0 g/L ammonium citrate and pH 2.7 at  $i = 6\text{mA/cm}^2$ ;  $t_{\text{on}} = 0.3\text{ms}$ ;  $t_{\text{on}} + t_{\text{off}} = 10\text{ms}$ ; agitation of 600rpm.

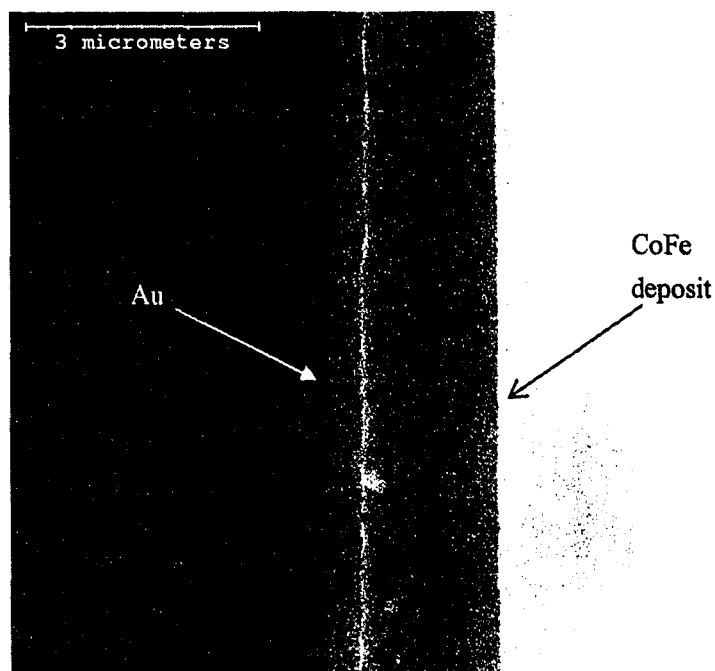


**Figure 4-15.** Cross-section SEM SE image of CoFeNi film plated from a bath with 50 g/L ammonium citrate and pH 5.3 at  $i = 6\text{mA/cm}^2$ ;  $t_{\text{on}} = 0.3\text{ms}$ ;  $t_{\text{off}} = 9.7\text{ms}$ ; agitation of 600rpm.

#### 4.5.2.2 Cross-section view

Cross-section views of the corresponding CoFeNi films are illustrated in Figures 4-14 and 4-15, respectively. The cross-section of the film deposited from the conventional bath is porous and corresponds to the plan view image (Figure 4-12b). The cross-section of the film plated from citrate-added bath is much denser.

The morphology analysis demonstrates that the CoFeNi film plated from the citrate-added bath is more uniform and denser than that deposited from the conventional low pH bath.

## 4.6 Summary

The calculated stability diagrams demonstrate that the stability of conventional CoFe and CoFeNi alloy plating baths open to air is dominated by the precipitation of  $\text{Fe}(\text{OH})_3$

at a pH above 3.1. Thermodynamically, citrate additives (ammonium citrate or potassium citrate) can effectively stabilize the single metal, CoFe and CoFeNi alloy plating baths, preventing the precipitation of metal hydroxides at higher pH levels. The employment of ammonium citrate creates an additional stable region of  $\text{Co}(\text{NH}_3)_6^{3+}$ , because of the complexing effect of  $\text{NH}_3$  on  $\text{Co}^{3+}$  ion.

The calculated stability diagrams also show that citrate has the strongest complexing power for Fe ions, followed by  $\text{Ni}^{2+}$  ions, and the weakest complexing effect for  $\text{Co}^{2+}$  ions.

The main complexing reactions in CoFe and CoFeNi alloy plating baths with citrate addition have been discussed.

Bath stability tests verify that the conventional CoFe and CoFeNi plating baths are not stable; ammonium citrate can significantly improve the stability of both CoFe and CoFeNi plating baths.

The morphology studies demonstrate that CoFe and CoFeNi films plated from the citrate-added baths are more uniform and denser than those deposited from the conventional low pH baths. Therefore, the introduction of ammonium citrate into the CoFe and CoFeNi plating baths can effectively stabilize the plating bath, elongate the bath life and improve the film morphology.

## Chapter 5 Electrodeposition of CoFe and CoFeNi thin films

Due to the advantages of simplicity, cost-effectiveness and controllable patterning, electrodeposition processes have major significance in the fabrication of thin-film recording heads. The introduction of electrodeposited permalloy ( $\text{Ni}_{80}\text{Fe}_{20}$ ) as the core material of thin film inductive heads by IBM in 1979 made thin-film recording heads technologically and economically viable. Write-head cores are currently fabricated by electrodeposition processes. [Chiu96] The need for recording heads to write on high-coercivity media has raised new requirements for the write-head material that cannot be met by  $\text{Ni}_{80}\text{Fe}_{20}$ . [Andricacos98] CoFe and CoFeNi alloys have been the most studied soft magnetic materials over the past several decades, because of their superior properties over FeNi alloys as write head core materials in magnetic storage technologies.

In this chapter, the fundamentals of electrodeposition are briefly introduced based on the literature [Gileadi93] [Bockris67] [Brenner 63] [Sun98], and the electrodeposition of CoFe and CoFeNi alloy films from citrate-added baths is studied.

### 5.1 Fundamentals of electrodeposition

Electrodeposition, also referred to as electroplating, is an electrochemical process by which metal is deposited on a conductive substrate (i.e., cathode) by passing a current through the bath (see Figure 2.10). The plating bath, also known as the electrolyte, is a liquid solution containing the desired metal ions or suspended particles to be deposited. The anode is connected to the positive terminal of the current supply. Usually it is a foil, net, or wire made of a noble metal such as platinum, or sometimes the metal to be deposited (assuming that the metal will dissolve into the electrolyte). The cathode, the substrate to be plated, is submerged into the plating bath. The cathode should be

electrically conductive and connected to the negative terminal of current supply. As the current is applied, positive metal ions in the solution are attracted to the negatively charged cathode and deposited on it.

Electroplating is governed by *Faraday's Laws*. The mass of metal deposited on cathode is proportional to the amount of current passed through the cell. When 96,485 coulombs of electrical charge passes through an electrolytic solution, one *equivalent* of substance is produced on an electrode. The gram equivalent weight (GEW) is the number of grams of substance per equivalent. The GEW of a chemical in an oxidation-reduction reaction is equal to its atomic or molecular weight divided by its valence change (number of electrons gained or lost) in the reaction. The weights of different substances produced at an electrode by the same amount of current are proportional to their GEW:

Weight produced at an electrode = (Current in amps)\*(time in sec)\*(GEW of substance deposited) / 96,485 grams

Of course, 100% plating efficiency is assumed in the above calculation.

## 5.1.1 Electrodeposition of single metal

### 5.1.1.1 Electrode reactions

A cathode reaction for metal deposition can be expressed as:

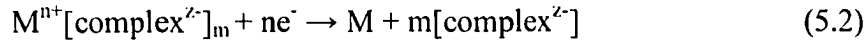


where  $n$  is the number of electrons that a metal ion needs to be reduced to a neutral atom, and  $M^{n+}$  is a simple aquo ion such as hydrated  $Co^{2+}$ ,  $Fe^{2+}$ , or  $Ni^{2+}$ . For conventional CoFeNi plating baths, without the addition of complexing agents, the deposition of metals from simple aquo ions involves (refer to Appendix 1, electrode potential vs. SHE):



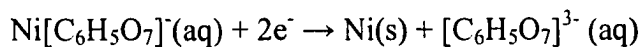
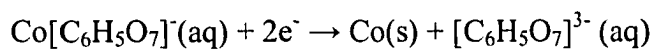
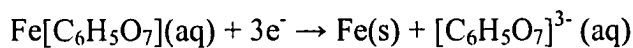
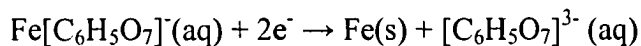


If the metal ion  $\text{M}^{n+}$  is complexed, the reduction of metal from a complexed metal ion can be expressed as:



where  $[\text{complex}^{z-}]$  represents the functional ion of a complexing agent, such as citrate ion  $[\text{C}_6\text{H}_5\text{O}_7]^{3-}$  or cyanide ion  $\text{CN}^-$ ;  $\text{M}^{n+}[\text{complex}^{z-}]_m$  is a complexed metal ion, such as  $\text{Co}[\text{C}_6\text{H}_5\text{O}_7]^-$ ,  $\text{Fe}[\text{C}_6\text{H}_5\text{O}_7]^-$  or  $\text{Ni}[\text{C}_6\text{H}_5\text{O}_7]^-$ . According to the existing theory, the deposition of metal from a complexed metal ion is a process whereby the metal is deposited by direct discharge from the complex ion, without first dissociating the complex ion to give a metal ion [Gileadi 93] [Tan 93]. The metal ion is stripped from its distorted sheath as the complex ion passes through the electrical double layer to the metal/solution interface, is neutralized by accepting electrons and then deposited on the cathode.

For the citrate-added baths, reduction reactions of metals from citrate-complexed ions include:



The most common secondary reaction at the cathode is hydrogen reduction, especially in acidic electrolytes:

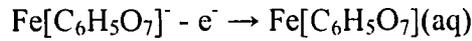


In this research, an inert anode (Pt foil) is employed. The anode reaction involves

oxygen evolution:



The metal ions may also be oxidized at the anode, such as:



If metallic cobalt is employed as the anode as in some of the literature [Liu00-2] [Liu03], the preferred anode reaction will be the dissolution of cobalt:



From the Nernst equation, the actual potential of an electrode can be calculated:

$$\varepsilon = \varepsilon^0 - \frac{RT}{nF} \ln \frac{\Pi a(\text{Red})}{\Pi a(\text{Ox})} \quad (5.3)$$

$$\text{or } \varepsilon = \varepsilon^0 + \frac{RT}{nF} \ln \frac{\Pi a(\text{Ox})}{\Pi a(\text{Red})} \quad (5.3\text{a})$$

where  $R$  is the universal gas constant ( $8.314 \text{ J mol}^{-1} \text{ K}^{-1}$ ),  $T$  is the absolute temperature (in K),  $n$  is the number of moles of electrons involved in the electrode reaction as written, and  $F$  is the Faraday constant ( $96,485 \text{ C mol}^{-1}$ ). The notation  $\Pi a(\text{RED})$  represents the product of the chemical activities of all species which appear on the reduced side of the electrode reaction, and the notation  $\Pi a(\text{OX})$  represents the product of the chemical activities of all species which appear on the oxidized side of the electrode reaction. For pure solid substances, such as Fe(s), Co(s) and Ni(s), or pure liquid substances, like  $\text{H}_2\text{O}(\text{l})$ , their activities are constant, so in the Nernst equation as elsewhere in chemical thermodynamics their values are considered to be 1. As a reasonable estimate, the activities of gases are usually taken as their partial pressures and the activities of solutes such as metal ions are usually taken as their molar concentrations.

For the electrodeposition of Fe(s) from 0.053M FeSO<sub>4</sub>·7H<sub>2</sub>O solution at T = 293K,

the actual electrode potential  $\epsilon_{Fe^{2+}/Fe}$  can be calculated:

$$\epsilon_{Fe^{2+}/Fe} = \epsilon_{Fe^{2+}/Fe}^0 - \frac{RT}{2F} \ln \frac{1}{C_{Fe^{2+}}}$$

$$\epsilon_{Fe^{2+}/Fe} = (-0.41 - \frac{8.314 \times 293}{2 \times 96485} \ln \frac{1}{0.053}) \text{ V} = -0.447 \text{ V}$$

Table 5-1 lists the calculated potentials for single metal electrodes at 293K (20°C) at different metal ion concentrations. Since the stability constants for the complexing reactions between the citrate ions and the metal ions are not available, the potentials for single metal electrodes involving metal-citrate complexing ions have not been calculated.

**Table 5-1.** Calculated potentials of single metal electrodes at 293K for different metal ion concentrations.

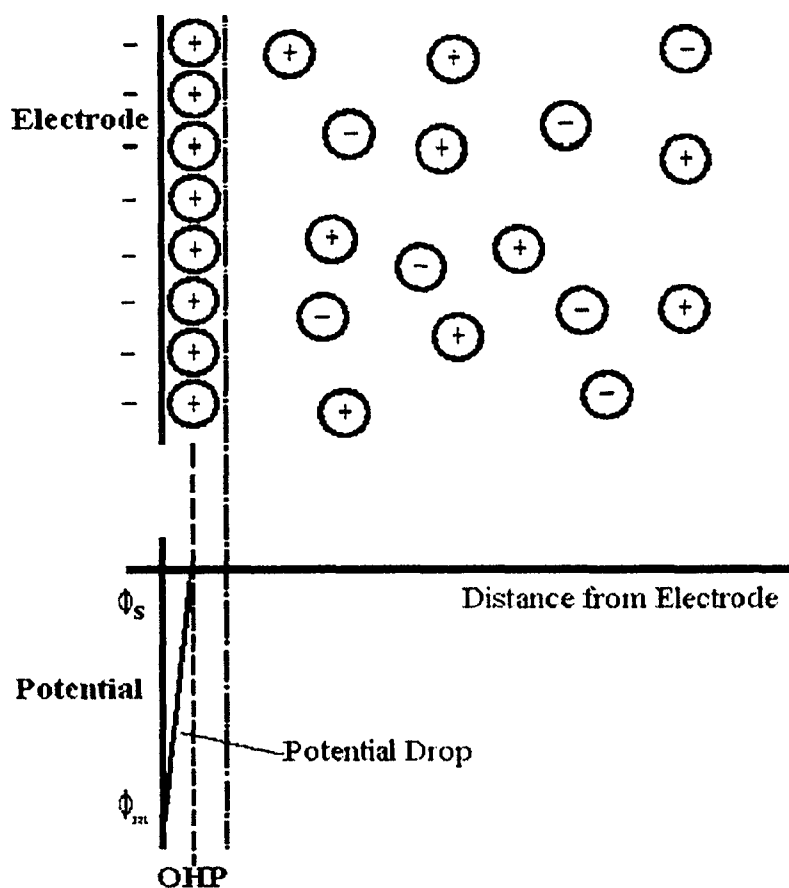
Cathode Reaction (Reduction)	Standard Potential $\epsilon^0$ (V)	Metal ion conc. (M)	Calculated Potential $\epsilon$ (V)
$Fe^{2+}(aq) + 2e^- \rightarrow Fe(s)$	-0.41	0.053	-0.447
		0.015	-0.463
$Co^{2+}(aq) + 2e^- \rightarrow Co(s)$	-0.28	0.120	-0.307
		0.050	-0.318
$Ni^{2+}(aq) + 2e^- \rightarrow Ni(s)$	-0.23	0.30	-0.245
		0.20	-0.250
$2H^+(aq) + 2e^- \rightarrow H_2(g)$	0.00	pH = 2.5	-0.145
		pH = 5.3	-0.308

Theoretically, the more positive the reduction potential, the easier the metal (or element) can be reduced (deposited). From Table 5-1, it can be seen that the employment of a relatively high pH level (pH = 5.3) will decrease the potential of the H<sup>+</sup>/H<sub>2</sub> electrode. Therefore, the evolution of H<sub>2</sub> gas can be more effectively suppressed at higher pH levels.

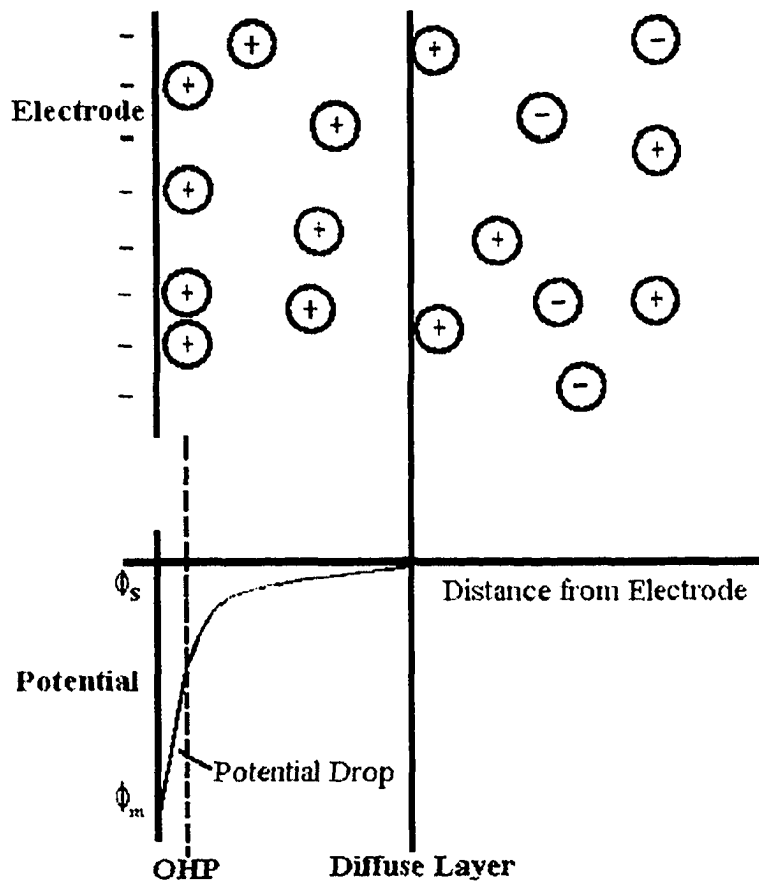
The adoption of higher metal ion concentrations will increase the reduction potential of the metal electrode and benefit the metal reduction.

### 5.1.1.2 The electrical double layer

In the discussion of electrode reactions, it is important to understand the nature of the electrode/electrolyte interface. A charged ion species in solution tends to be attracted to or repelled from the electrode-solution interface. This results in a separation of charge and the formation of a layer of solution with a different composition from the bulk solution, which is known as the electrical double layer. As a result of the charge separation, the electrical double layer has an apparent capacitance (known as the double layer capacitance). There are several theoretical descriptions of the structure of electrical double layer.



a. The Helmholtz model.



b. The Stern model.

**Figure 5-1.** Models of the electrical double layer. [Cartage04]

The first model to use the term 'electrical double layer' was presented by Helmholtz in the 1850's. [Cartage04] In his model, the interactions between the ions in solution and the electrode surface were assumed to be electrostatic in nature, and resulted from the fact that the electrode holds a charge density which arises from either an excess or deficiency of electrons at the electrode surface. The charge held on the electrode is balanced by an ion layer with opposite charge attracted to the electrode surface. The overall result is two electrical layers (the double layer) and a potential drop which is confined to this region (named the outer Helmholtz Plane, OHP) in the solution. The OHP position is assumed to be within the radius of an ion, or the solvation sphere around an ion, from the electrode surface. The Helmholtz electrical double layer model is shown

in Figure 5-1a.

The Helmholtz model does not account for many factors, such as diffusion/mixing in the solution, the possibility of adsorption onto the electrode surface and the interaction between solvent dipole moments and the electrode. A later model presented by Stern addresses some of these limitations (Figure 5-1b). The electrostatic interactions are in competition with Brownian motion, so the attracted ions are assumed to be able to move in solution. The potential drop occurs over the region called the diffuse layer, which is  $\sim 100 \times 10^{-10}$  m from the electrode surface. Many modifications and improvements have been made to these early models using numerical modeling approaches to simulate the ion redistribution around the electrode.

### 5.1.1.3 Overpotential

Overpotential is the deviation of an electrode potential from its equilibrium value as a current flows across the electrode/solution interface, i.e., overpotential  $\eta = \epsilon_{\text{applied}} - \epsilon^0$ . It represents the extra energy needed to drive the electrode reaction to proceed at a required rate (or its equivalent current density). There are three major types of overpotentials: activation overpotential, concentration overpotential, and ohmic overpotential. [Electrochem04]

Ohmic overpotential is simply associated with the ohmic loss which results from the IR drop in an electrochemical cell, where I and R represent current and resistance, respectively.

Activation overpotential is the overpotential associated with the charge-transfer reaction elementary step in the overall electrode reaction. It is positive for anodic polarization ( $\eta > 0$ ) and negative for cathodic polarization ( $\eta < 0$ ). The kinetics for an activation-controlled process can be generally expressed by the Butler-Volmer equation:

$$i = i_0 \left[ \exp\left(\frac{\beta nF}{RT} \eta\right) - \exp\left(-\frac{(1-\beta)nF}{RT} \eta\right) \right] \quad (5.4)$$

$$\text{where } i_0 = nFk_0C \exp\left(\frac{\beta nF}{RT} \varepsilon^0\right) \quad (5.5)$$

In the above formulas,  $k_0$  is a constant;  $i_0$  is the exchange current density;  $C$  is the bulk concentration of the metal ion, and  $\varepsilon^0$  is the equilibrium potential of the electrode.  $\beta$  is the charge transfer barrier or symmetry coefficient for the anodic or cathodic reaction.  $\beta$  values are typically close to 0.5. To describe a multi-step process,  $\beta$  must be replaced by an experimental parameter,  $\alpha$ , which is called the transfer coefficient.

Equation (5.4) retains a form which states that the measured current density at a certain overpotential is the sum of the partial cathodic and anodic current densities. When  $\eta$  is very low, such as  $\eta < 10$  mV, a limiting form of current density can be expressed as:

$$i = i_0 \frac{nF}{RT} \eta \quad (5.6)$$

Equation (5.6) demonstrates that  $i$  depends linearly on  $\eta$ . Another limiting form can be obtained when  $\eta < -50$  mV and the first term in the Butler-Volmer equation becomes negligible compared with the second. In this region, the equation can be simplified as:

$$\log(-i) = \log i_0 - \frac{\beta nF}{2.3RT} \eta \quad (5.7)$$

This equation is known as the cathodic Tafel equation. Similarly, positive overpotentials greater than 50 mV will give the anodic Tafel equation. More generally, the Tafel equation can be expressed as:

$$\eta = a + b \log|i| \quad (5.7a)$$

Figure 5-2 illustrates a  $\log|i|$  vs.  $\eta$  curve for an electrochemical cell. The exchange current density  $i_0$  and transfer coefficients  $\alpha$  are obtained from the intercepts and slopes, respectively.

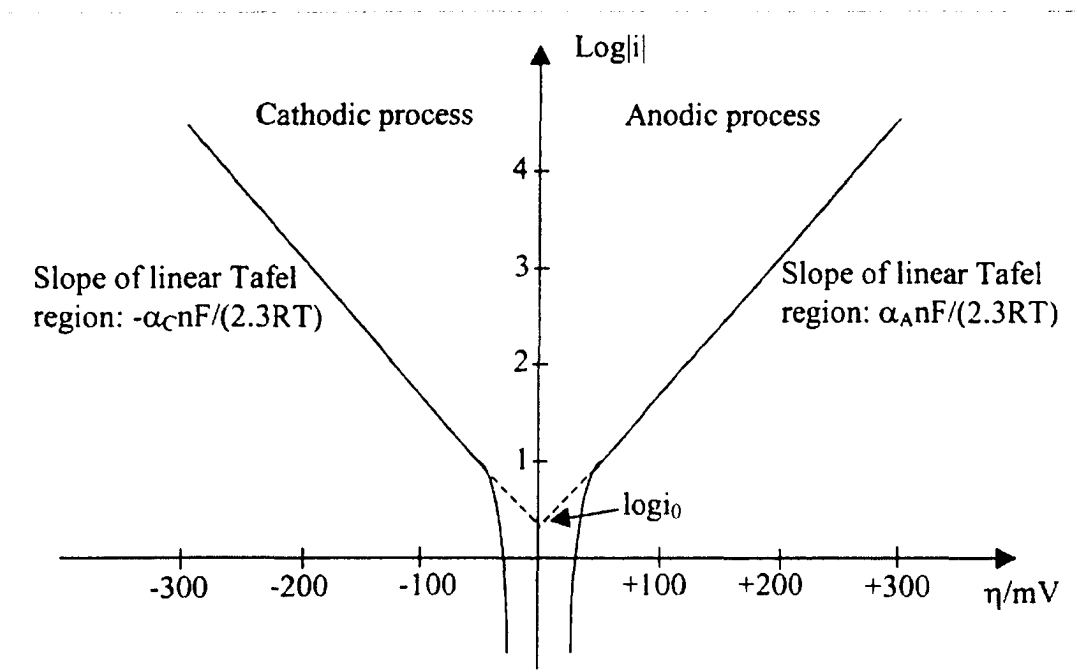


**Figure 5-2.**  $\log|i|$  versus  $\eta$  plot. [Gileadi 93]

Concentration overpotential is the overpotential associated with the mass transport of the reactants to the electrode surface from the bulk of the electrolyte and the reverse transport of the products. There are three different modes of mass transport, i.e., convection, migration and diffusion. Migration is the movement of charged species in response to an electric field. Convection is the physical movement of the solution in which the electroactive species is dissolved. It is the most efficient mode of mass transport. Diffusion is driven by a concentration gradient in the solution, and is the most common and important mode of mass transport. Diffusion of the electroactive species to the electrode surface is an elementary step in the overall electrode reaction. Concentration overpotential is also called "diffusion overpotential" or "mass-transport overpotential." Under the condition of mass transport control, the rate of electrode reaction is controlled by the diffusion of the electroactive species to the electrode surface. Due to diffusion delay, the concentration of the electroactive species near the cathode

surface is lower than that in the bulk solution. The concentration overpotential  $\eta_{\text{conc}}$  can be expressed as:

$$\eta_{\text{conc}} = 2.3(RT/nF)\log(1 - i/i_L) \quad (5.8)$$

where  $i_L$  is the limiting current density.

Theoretically, a fundamental limiting current density can be reached if the current density is increased to a large enough value, leading to no metal ions at the cathode surface. Metal ions are consumed at a faster rate than they can be supplied. However, before this point is reached, usually alternative electrode reactions such as the reduction of hydrogen at the cathode, that is, hydrogen overpotential, will take place. The limiting current density  $i_L$ , which is independent of potential can be expressed as:

$$i_L = nFDC^o/\delta \quad (5.9)$$

where  $D$  is the diffusion coefficient and  $C^o$  is the bulk concentration of metal ions.  $\delta$  is the Nernst diffusion layer thickness, which depends on the diffusion and convection conditions in the plating bath. To obtain a uniform deposited film with smooth morphology, the applied plating current density should be lower than about one half of  $i_L$ .

In quiescent solutions,  $\delta$  is time  $t$  dependent and can be given by

$$\delta(t) = (\pi Dt)^{1/2} \quad (5.10)$$

For a rotating-disc electrode,  $\delta$  can be estimated by

$$\delta = 1.61\nu^{1/6}D^{1/3}w^{-1/2} \quad (5.11)$$

where  $\nu$  is the kinematic viscosity (i.e., viscosity/density) of the solution and  $w$  is the angular rotation rate of the electrode in radians per second. The essence of mass transport relies on the quantity  $\delta$ . Decreasing  $\delta$  will increase  $i_L$ . Agitation will lower the value of  $\delta$ .

When the electrode process is dominated by mixed control, the activation and mass-transport processes occur in series and combine to determine the overall reaction rate. As current density represents the reaction rate, its reciprocal expresses the resistance for the process. If  $i$  represents the current density under mixed control,  $i_{ac}$  represents the

current density under activation control and  $i_L$  represents the limiting current density controlled by mass transport, the overall resistance  $1/i$  is the sum of the resistance of every step in series, that is:

$$1/i = 1/i_{ac} + 1/i_L \quad (5.12)$$

Therefore the smaller of the two current densities dominates the overall current density  $i$ . A qualitative description of the relationship between current density and potential is illustrated in Figure 5-3. [Gileadi 93]

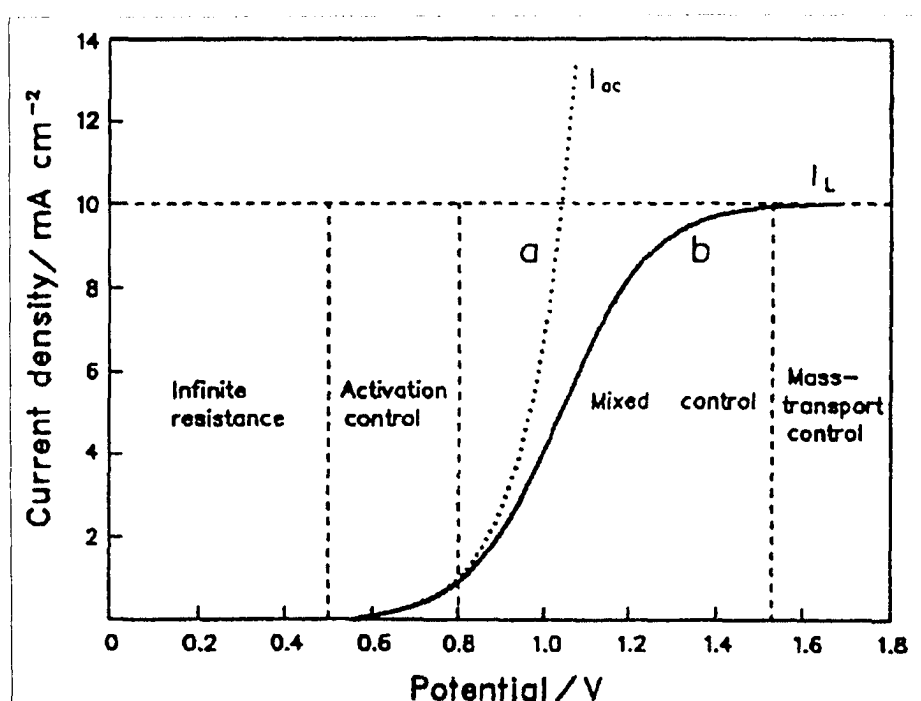


**Figure 5-3.** A qualitative description of the relationship between current density and potential. Curve a is the pure activation-controlled current  $i_{ac}$  and curve b is the actual current which will be measured, having a mass-transport-limited value  $i_L$ . [Gileadi 93]

#### 5.1.1.4 Underpotential deposition

Underpotential deposition (abbreviated as "UPD") is the electrodeposition of a metal on a foreign metal substrate at potentials less negative than the equilibrium potential of the deposition reaction. The discharge process in UPD is energetically unfavorable, and it

can occur only because of a strong interaction between the two metals, which makes the overall energetics favorable. Consequently, only one (rarely two) monolayer can be deposited this way, and this gives rise to a convenient way to produce well-controlled monolayer deposits. It is likely that the underpotential-deposited layer forms an epitaxial layer, i.e., taking on the crystal structure of the underlying substrate.

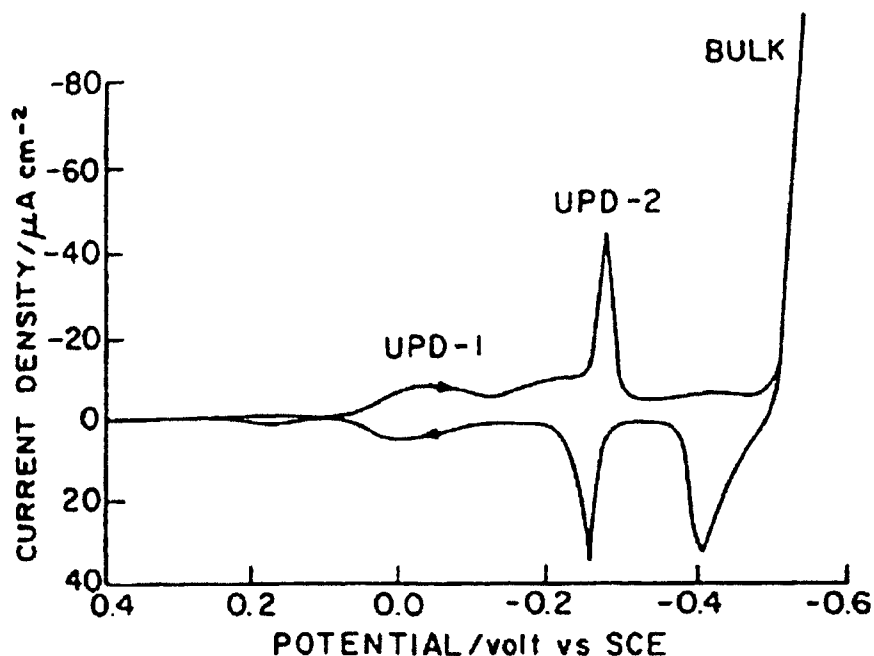


**Figure 5-4.** Underpotential deposition of lead on gold from a solution containing 0.001 M  $\text{Pb}(\text{ClO}_4)_2$  and 1.0 M  $\text{HClO}_4$ . Two underpotential deposition (UPD) and dissolution peaks were observed. [Gileadi93].

An example of underpotential deposition is the deposition of lead on gold from a  $\text{Pb}(\text{ClO}_4)_2/\text{HClO}_4$  solution. As shown in Figure 5-4, two UPD peaks (UPD-1 and UPD-2) correspond to the underpotential deposition of two different monolayers of lead on a gold substrate. [Gileadi93] The equilibrium potential for lead deposition refers to the free energy change for the reaction:



where  $\text{Pb}(-\text{Pb}_{\text{crystal}})$  means that the lead ion is reduced and incorporates into the lead

crystal lattice. This free energy change and corresponding equilibrium potential refer to the formation of Pb-Pb bonds.

In underpotential deposition:



where Pb-Au bonds have been formed. The reason that lead can be deposited on gold at a less negative potential than on lead is that Pb-Au bonds are more stable than Pb-Pb bonds. As might be expected, the UPD peaks occur at different potentials, e.g., UPD-1 and UPD-2, which demonstrates the underpotential deposition of lead on different gold crystal planes, with different atomic density and Pb-Au bonding strength. The bulk deposition of lead on gold, after the underpotential deposition of lead has finished, starts at a more negative potential than the equilibrium potential of lead deposition. The potential difference is referred to as the crystallization overpotential.

#### *5.1.1.5 Electrocrystallization*

There are two competing processes in electrocrystallization: the growth of existing crystals (grain growth) and the formation of new ones (nucleation). The elementary reactions and steps in electrocrystallization have been summarized by Bockris et al [Bockris67], as illustrated in Figure 5-5.

If the cathode is different to the metal to be deposited, the first step will be the formation of an atomic layer of this metal. Then the layer is thickened into a macroscopic deposit. Nucleation is achieved at an electrode surface by the application of a large overpotential. Once formed, the nuclei can grow rapidly at relatively low potentials, and under constant-current operation, the potential will decrease significantly after nucleation has occurred. The crystals grow by incorporating individual metal atoms into the formed crystal lattice. Of the possible sites for new atom incorporation in the formed crystal lattice, a kink where the atom can interact (bond) with three neighbors is the most

favorable position. Sometimes incorporation occurs at an edge site which has two neighbors. Adatoms contacting with only one neighbor atom may diffuse and migrate to more favorable sites or dissolve into the solution, although only a few will expand into new nuclei.

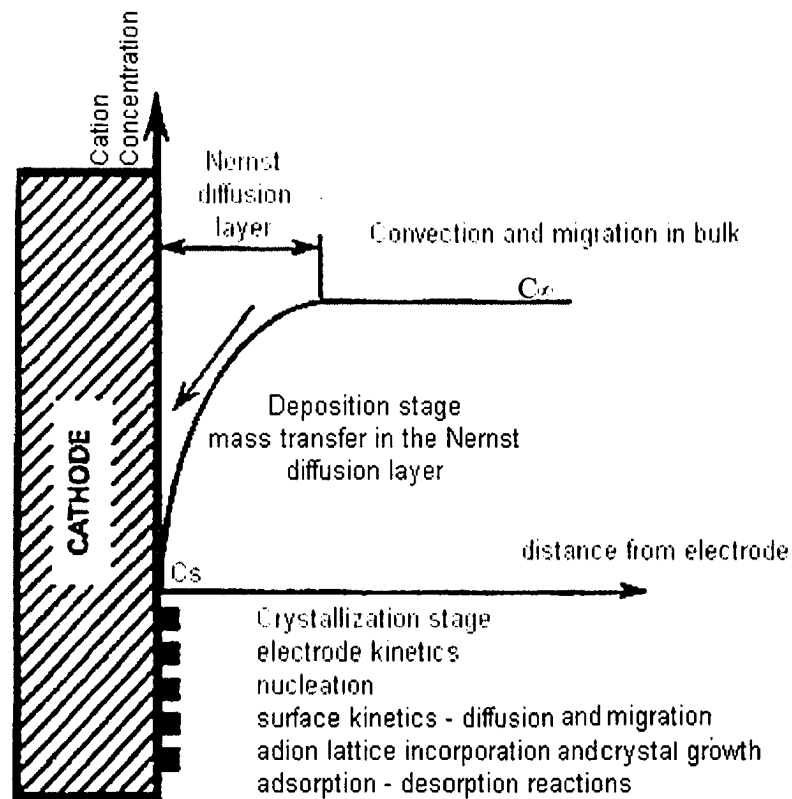


**Figure 5-5.** Elementary reactions and steps in electrocrystallization. [Bockris67]

The structure of the growing layer is determined largely by the relative rates of electron transfer to form an adatom, diffusion of the adatom across the surface to a position in the lattice, and the electrodeposition conditions, such as bath additives which may radically affect the electrocrystallization process. At low current densities, the diffusion and migration of an adatom on the surface is fast compared with electron transfer; therefore, the adatom is likely to fit into a favored site in the lattice to form a

perfect structure. At higher current densities, adatom diffusion is relatively slow compared with electron transfer and further nucleation is more favorable, so that the layer will be less ordered.

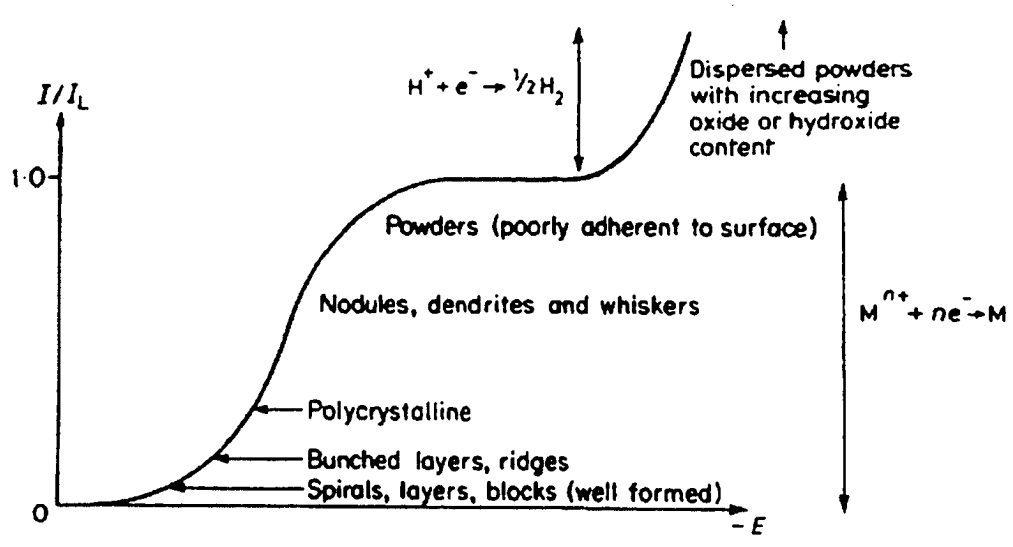


Figure 5-6. Microstructure dependence on current density. [Gileadi 93]

During the deposit thickening stage, a critical parameter is the current density. At low current densities, adatom diffusion is fast relative to electron transfer; hence, both the crystal lattice and structures such as screw dislocations can be well formed. At high current densities, it is difficult for adatoms to reach their equilibrium positions in the lattice, and nucleation of additional growth centers becomes the more favorable event. Therefore, the lattice formed will be less ordered, and macro irregular features, such as steps, ridges and polycrystalline block growth, become more probable. With further increase in current density, outward growth of the layer becomes more prominent, and problems resulting from mass transport control will occur, e.g., dendrites. Once this form of growth starts, it will predominate because of the enhanced rate of mass transport to the tip and the minimal IR drop to the tip as it is the closest point to the anode. A powdered texture usually results from an applied potential region of complete mass-transport

control. Figure 5.6 summarizes the way in which the structure depends on current density. [Gileadi93]

#### 5.1.1.6 Deposition rate and current efficiency

The average rate of metal deposition  $V_p$  is obtained by measuring the film thickness  $x$  during the plating time  $t$ :

$$V_p = x/t \quad (5.15)$$

Cathode current efficiency  $\Phi$  is the proportion of the total cathode current which is used in metal deposition. It is obvious that hydrogen evolution at the cathode lowers the current efficiency. The cathode current efficiency for metal deposition  $\Phi (\leq 1)$  can be estimated by assuming or measuring the deposit density  $\gamma$ . If the molar mass of plated metal is  $M_m$ , the applied current density is  $i$  and the surface area of deposited film is  $A$ , the number of moles of plated metal is:

$$(x \cdot A \cdot \gamma) / M_m = (\Phi \cdot i \cdot A \cdot t) / (nF) \quad (5.16)$$

Rearranging the above equation, will give a formula for the cathode current efficiency

$$\Phi = (x \cdot \gamma \cdot nF) / (i \cdot t \cdot M_m) \quad (5.16a)$$

### 5.1.2 Electrodeposition of metal alloys

A wide variety of binary and multi-element alloy coatings have been fabricated commercially using electrodeposition. The most common ones include noble metal alloys in the jewelry industry, zinc alloys for corrosion resistance, and iron group alloys as functional thin films.

Traditionally, alloy electrodeposition has been described as a simultaneous deposition of two or more components from the electrolyte. [Bockris67] [Bockris70] [Gileadi93] The components are reduced at the cathode surface and the alloy composition is determined by the relative ratios of the fluxes of the various components at cathode. The

galvanic potential between the cathode and the solution is the same for all the deposited components. Therefore, the various fluxes of the deposited components can be estimated from the current–potential curve of each component separately according to the current value at the applied potential (Figure 5-7). [Shacham00]

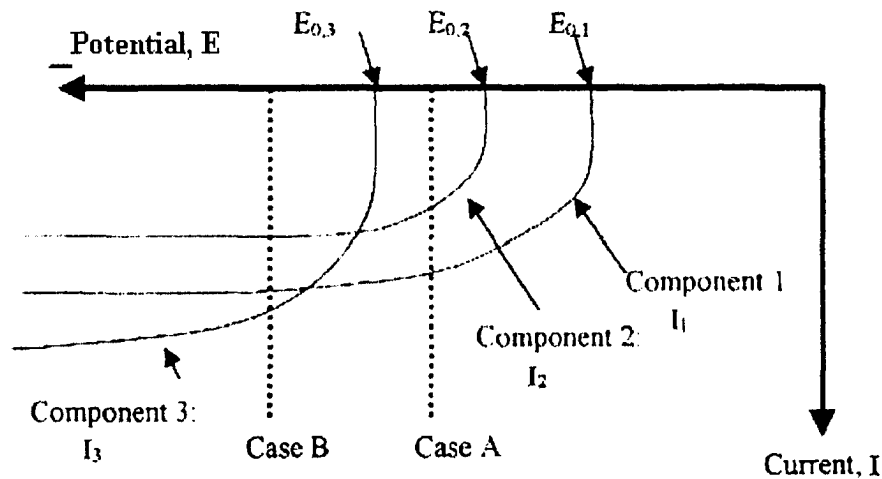


**Figure 5-7.** Current versus potential curves for deposition of three components: component 1 with the highest equilibrium potential; component 2 with lower  $E_0$  and lower mass transport limited current; and component 3 with lowest  $E_0$  and highest transport limited current. (Examples: Case A,  $I_1 > I_2$ ,  $I_3 = 0$ ; Case B,  $I_3 > I_1 > I_2$ ). [Shacham00]

Each of the components follows the conventional deposition process: (a) transport from the solution to the cathode surface and (b) deposition of the species at the cathode/solution interface. According to formula (5.9), the limiting current density of the  $x$ th component can be given by:

$$i_{Lx} = -D_x n F C_x^0 / \delta \quad (5.17)$$

where  $D_x$  is the diffusivity,  $n$  is the metal ion charge,  $C_x^0$  is the metal ion concentration in the solution and  $\delta$  is the diffusion layer thickness. The reaction can also be limited by the rate of the activation-controlled surface reaction. As the overpotential becomes more negative, the reverse or anodic current becomes less significant so that the total or net

current density approaches the condition of a purely cathodic current. For the high-field approximation, the Butler Volmer equation becomes:

$$i_x = i_{0,x} \exp(-a_x F \eta / RT) \quad (5.18)$$

where  $i_{0,x}$  is the surface exchange current and  $a_x$  is the activity. The total current is equal to the external current in electrodeposition.

The above theory is reasonable as long as all the components are deposited via a pure electrochemical process on the cathode, which typically occurs when the metals are in an ionic state in the solution and can be deposited independently. However, this is not always true, especially when co-depositing with refractory metals or with phosphorous or boron. In these cases, codeposition is a mixture of an electrochemical process on the cathode and a chemical reaction accompanying that process.

The composition of electrodeposited alloys depends on a number of factors and differs from that of the electrolyte. [Brenner 63] Brenner distinguishes codeposition behaviors as 'normal' or 'abnormal'. In the first category, the relative proportions of the metals in the electrodeposited alloy can be qualitatively determined on the basis of the equilibrium potentials of the corresponding metal electrodes, as mentioned above. Normal codeposition is further subdivided into 'regular' codeposition (diffusion controlled), 'irregular' codeposition (activation controlled) and 'equilibrium' codeposition. In abnormal codeposition, the deposit composition cannot be predicted from equilibrium considerations. This category of deposition includes 'anomalous' and 'induced' codeposition. In anomalous codeposition, the less noble component deposits preferentially and its relative concentration in the deposited alloy is higher than that in the electrolyte. Induced codeposition refers to the condition where a given element can be codeposited with other elements to form an alloy, but cannot be deposited in pure form, such as W and Mo.

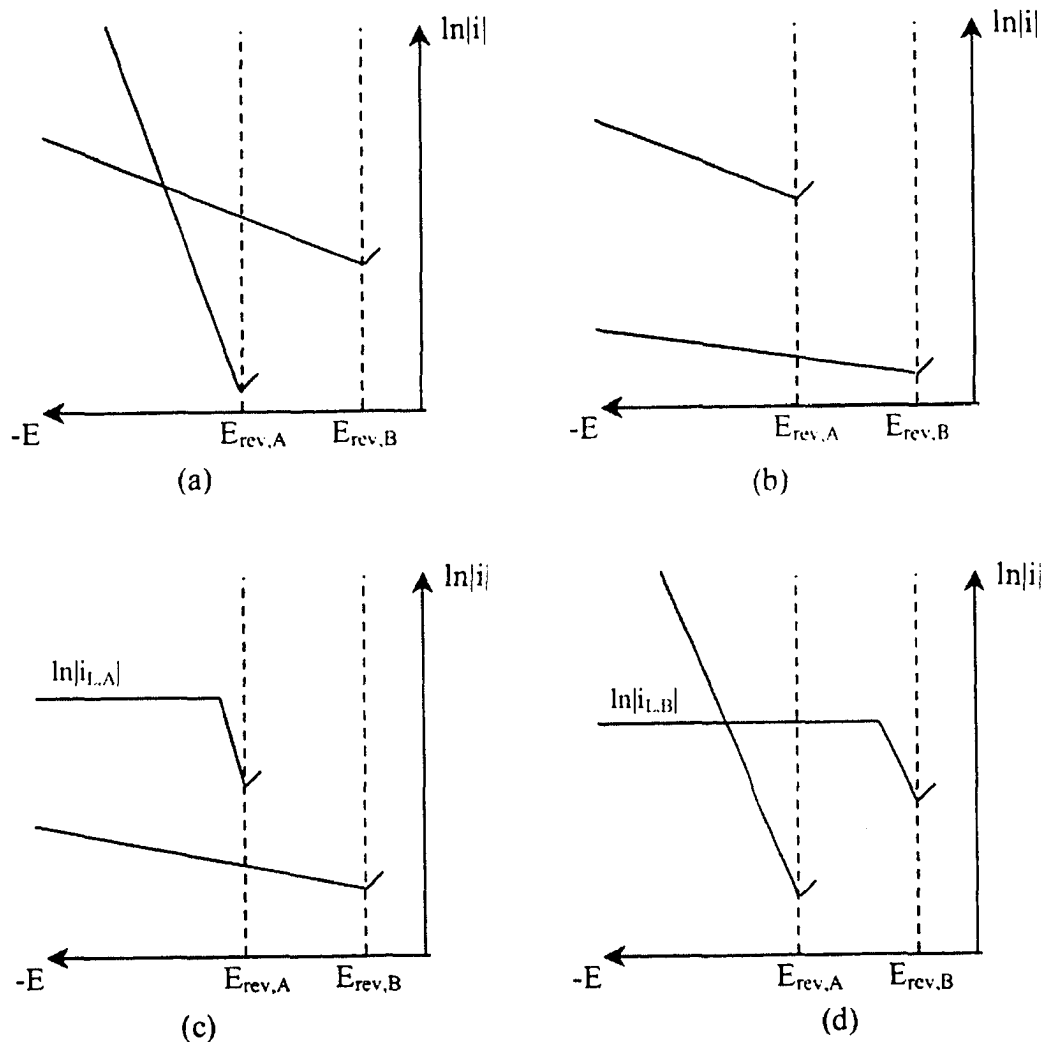


**Figure 5-8.** Evans diagrams representing the partial currents of components A and B in anomalous codeposition of a binary alloy AB. Figures (a) and (b): both partial reactions are charge transfer controlled. Figures (c) and (d): one of the partial reactions is mass transport controlled. [Landolt94]

An approach to explain alloy deposition is based on ‘mixed potential theory’, which states that the measured current in an electrochemical system is equal to the sum of the partial anodic and cathodic currents. [Landolt94] Under Tafel kinetic conditions, from formula (5.7), the logarithm of the ratio of cathodic partial current densities for species A and B can be given by:

$$\ln(i_A/i_B) = R_0 - (S_{c,A} - S_{c,B})E \quad (5.19)$$

$$\text{where } R_0 = \ln(i_{0,A}/i_{0,B}) + (S_{c,A}E_{\text{rev},A} - S_{c,B}E_{\text{rev},B}) \quad (5.20)$$

$S_{c,K}$  represents the inverse of the cathodic Tafel coefficient,  $i_{0,K}$  represents the exchange current density, and  $E_{\text{rev},K}$  represents the equilibrium potential of the corresponding metal electrode.

Formula (5.19) demonstrates that the composition of the deposited alloy is independent of applied potential  $E$ , if  $S_{c,A} = S_{c,B}$ . Formula (5.20) actually expresses the effect of the exchange current density ratio to deposit composition. A less noble metal A may deposit more readily than a more noble metal B ( $E_{\text{rev},B} > E_{\text{rev},A}$ ), if its exchange current density is larger ( $i_{0,A} > i_{0,B}$ ). Landolt discussed four possible situations where a less noble component A ( $E_{\text{rev},A} < E_{\text{rev},B}$ ) can deposit preferentially in a given potential range where  $\ln|i_A| > \ln|i_B|$  (see Figure 5-8). [Landolt94]

### 5.1.3 Pulsed current (PC) plating

Since the early 1970s, the application of pulsed current to the electrodeposition of pure metals and alloys has attracted considerable attention from both researchers and producers. Common waveforms employed in PC plating are illustrated in Figure 5-9 [Puiippe86]. Compared with direct current (DC) plating, one main characteristic of PC plating is the introduction of a  $t_{\text{off}}$  (or  $T_{\text{OFF}}$ ) time, which allows the recovery or partial recovery of initial status around cathode/electrolyte interface during electroplating. Therefore, PC plating can deposit films with more uniform composition and properties.

Due to the introduction of  $t_{\text{off}}$ , the applied current density  $i_{\text{pulse}}$  (i.e., peak current density) in PC plating is larger than that in DC plating at the same average plating current density. Hence, hydrogen evolution can be suppressed so that higher current efficiency and lower deposit porosity can be achieved. PC plating can be used to deposit alloys with compositions and microstructures not obtainable by DC plating.

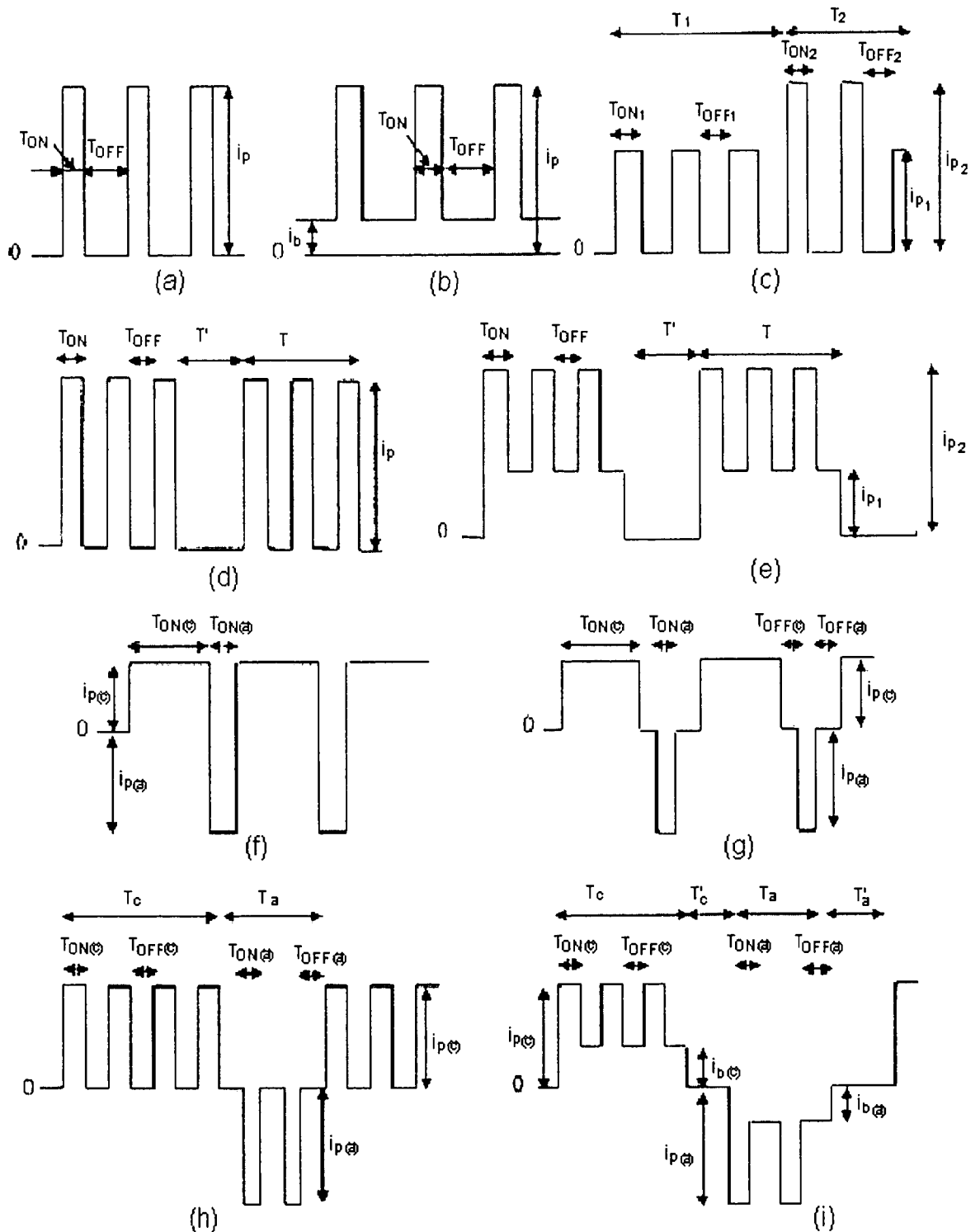


**Figure 5-9.** Schematic representation and suggested nomenclature for some square-wave-modulated current systems, and definition of related parameters. (a) Pulse, (b) superimposed pulse, (c) duplex pulse, (d) pulsed pulse, (e) pulse-on-pulse, (f) pulse reverse, (g) pulse reverse (with OFF time), (h) pulsed pulse reverse and (i) Pulse-on-pulse reverse. [Puipe86]

For mass transport in PC plating, there is a pulse-limiting current density  $i_{LP}$ , at which the concentration of electroactive species at the cathode surface reaches zero at the end of a pulse. It is similar to the limiting current density  $i_L$  in DC electrodeposition. Obviously, the value of  $i_{LP}$  depends on the choice of pulse parameters, such as  $t_{off}$  time.

An approximate model describing the mass transport processes in constant-current pulse deposition was presented by Ibl. [Ibl80] In his model, the diffusion layer is treated to consist of a pulsating part  $\delta_p$  and a stationary part  $\delta_s$ , as illustrated in Figure 5-10.

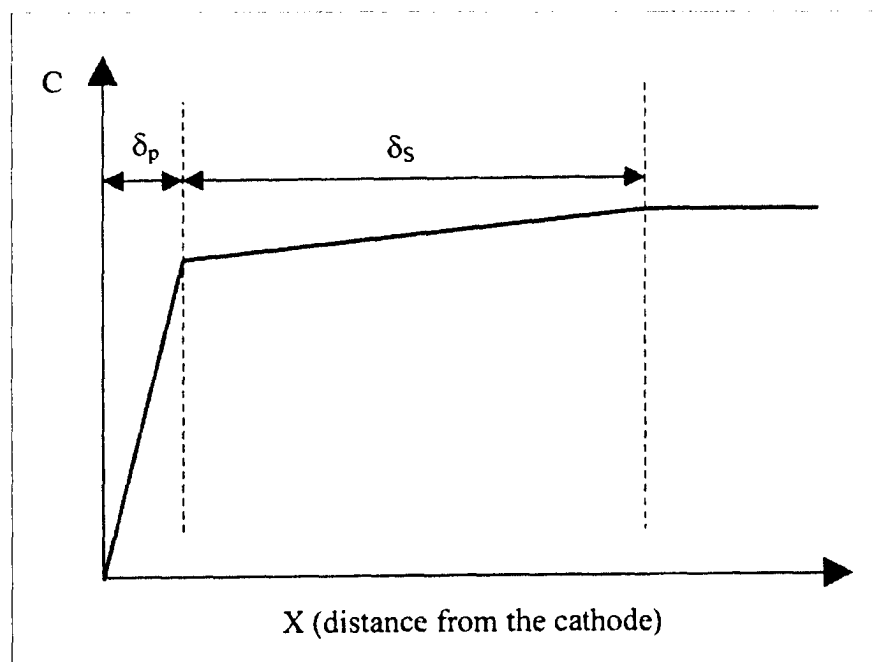


**Figure 5-10.** Concentration profiles of the two diffusion layers in PC plating at the end of a pulse.  $\delta_p$  is the thickness of the pulsating diffusion layer, and  $\delta_s$  is the thickness of the stationary diffusion layer. [Ibl80]

Assuming linear concentration profiles in each part, the thickness of the pulsating diffusion layer  $\delta_p$  can be expressed as:

$$\delta_p = \sqrt{\frac{4}{\pi} D t_{on} (1 - \gamma)} \quad (5.21)$$

The pulse-limiting current density  $i_{LP}$  can be given by:

$$i_{L,P} = i_L \left[ \sqrt{\frac{4 D t_{on}}{\pi \delta^2} (1 - \gamma)^{1.5} + \gamma} \right]^{-1} \quad (5.22)$$

where  $\gamma$  is the duty cycle defined as:

$$\gamma = \frac{t_{on}}{t_{on} + t_{off}} \quad (5.23)$$

$t_{on}$  and  $t_{off}$  are the pulse time (on time) and off time in a cycle, respectively. The average current density applied in PC plating can be given as

$$i_{average} = \gamma i_{pulse} \quad (5.24)$$

### *Periodic reverse-current (PRC) plating*

The main difference between PRC plating and common PC plating is the employment of a reverse (anodic) pulse in the current cycle for PRC plating. It has been claimed that PRC plating can improve deposit thickness uniformity and reduce internal stress by periodic inversion of current direction, which leads to partial dissolution of deposit. [Puippe86] The advantages of PRC plating include: polarization effects are at least partially reduced; bath impurities which have been discharged on the deposit surface may be dislodged; and electro-polishing conditions may be established. However, the periodic reverse current may also result in a lower current efficiency, if the forward-to-reverse current ratio is not kept at a reasonably high level.

## **5.2 Electrodeposition of CoFe and CoFeNi films from citrate-added baths**

To fabricate high-performance recording heads, thin films with optimal soft magnetic properties, especially high saturation flux density  $B_s$ , are preferred. These properties can only be achieved by controlling film chemical composition, phase formation (mixture of bcc and fcc phases), grain sizes (nanocrystalline) and microstructure with a suitable electroplating bath and process.

It is well known that CoFe and CoFeNi alloys with compositions around  $\text{Fe}_{60}\text{Co}_{40}$  have a high saturation flux density  $B_s$ , which can be as high as 2.4 Tesla. [Bozorth51] They do not possess a low coercivity  $H_c$ , however. Therefore, it is a challenge to deposit high  $B_s$  (>2 Tesla) CoFe or CoFeNi films with optimal soft magnetic properties by electroplating processes.

### 5.2.1 Electroplating of CoFe alloys

Yu and coworkers [Yu02] sputtered  $\text{Co}_{65}\text{Fe}_{35}$  alloys with a high saturation magnetization  $M_s$  of 2.35 Tesla, but with a coercivity  $H_c$  of more than 60 Oe. In this research, CoFe thin films with a composition around  $\text{Co}_{65}\text{Fe}_{35}$  are plated from the citrate-added baths. Plating bath composition and several operating parameters are varied, including citrate dosage, cobalt concentration, iron concentration, current density,  $t_{on}$ , agitation and plating temperature. The composition of the citrate-added bath for CoFe electrodeposition, used in all plating experiments except where specified, is listed in Table 3-2, where complexing agent ammonium citrate is introduced as the bath stabilizer.

#### 5.2.1.1 Effect of ammonium citrate

The effect of ammonium citrate dosage on the composition of plated CoFe films is shown in Figure 5-11. It is interesting to note that there is a linear relationship between the film composition (in at%) and ammonium citrate dosage. The Fe percentage in deposited film increases, while the Co percentage decreases, with increasing ammonium citrate dosage. Therefore, ammonium citrate affects the plating activity of both iron ion and cobalt ion species.

The effect of ammonium citrate dosage on plating rate is illustrated in Figure 5-12. Ammonium citrate dosage has a minor effect on plating rate up to a concentration of  $\sim 10\text{g/L}$ ; however, the plating rate decreases rapidly as the ammonium citrate dosage

further increases.

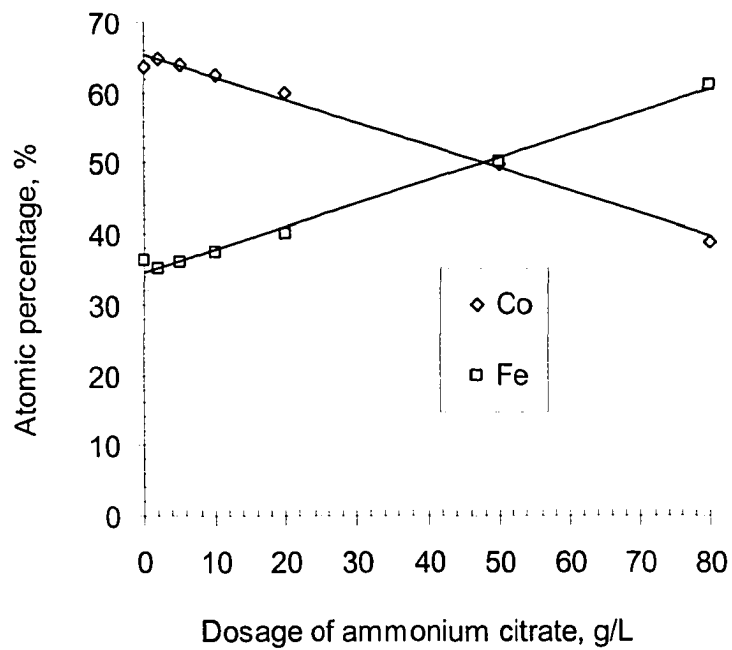


**Figure 5-11.** Effect of ammonium citrate dosage on the composition of CoFe films plated at  $i = 15\text{mA/cm}^2$ ;  $t_{\text{ON}} = 6\text{ms}$ ;  $t_{\text{OFF}} = 4\text{ms}$ ; agitation of 600rpm.

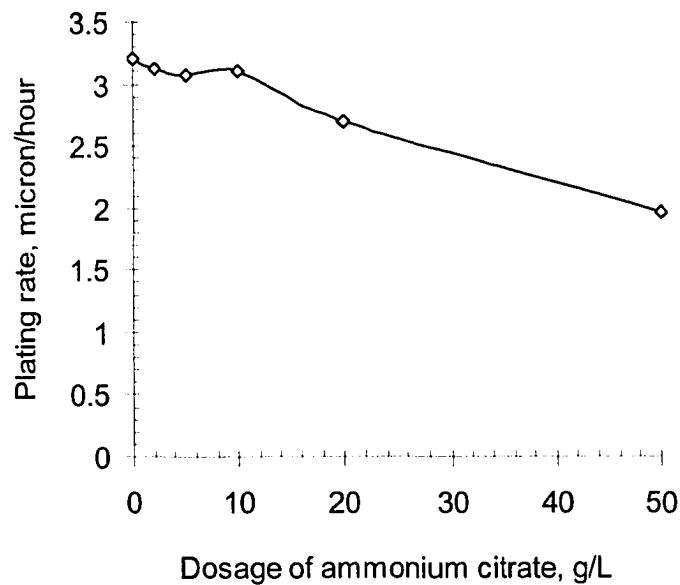


**Figure 5-12.** Effect of ammonium citrate dosage on the plating rate for depositing CoFe films at  $i = 15\text{mA/cm}^2$ ;  $t_{\text{ON}} = 6\text{ms}$ ;  $t_{\text{OFF}} = 4\text{ms}$ ; agitation of 600rpm.

### 5.2.1.2 Effect of cobalt concentration

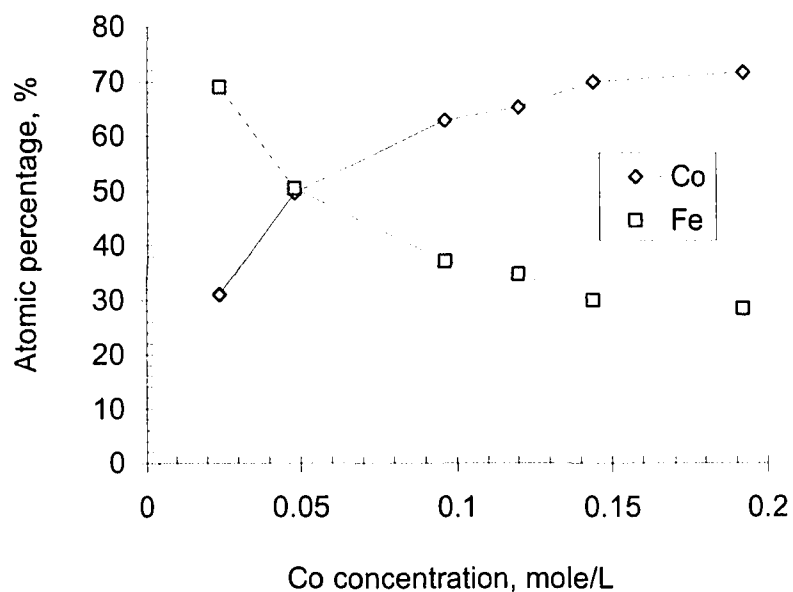


**Figure 5-13.** Effect of cobalt concentration on the composition of CoFe films plated at  $i = 15\text{mA/cm}^2$ ;  $t_{\text{on}} = 6\text{ms}$ ;  $t_{\text{on}} + t_{\text{off}} = 10\text{ms}$ ; agitation of 600rpm.

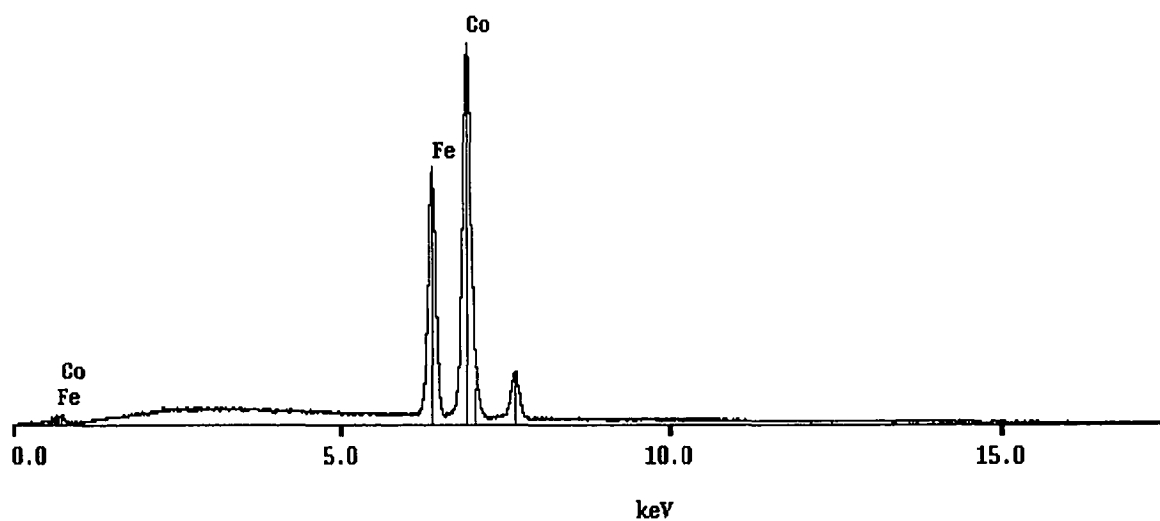


**Figure 5-14.** EDS spectrum from a deposited film with a composition corresponding to  $\text{Co}_{65}\text{Fe}_{35}$  plated at  $i = 15\text{mA/cm}^2$ ;  $t_{\text{on}} = 6\text{ms}$ ;  $t_{\text{off}} = 4\text{ms}$ .

Figure 5-13 shows the effect of cobalt concentration in the electrolyte on the composition of deposited CoFe films. The Co content in plated CoFe film increases,

while the Fe content decreases, as cobalt concentration in the plating bath goes up (Figure 5-13). This reflects the kinetics of electrodeposition, i.e., a higher metal ion concentration is beneficial for deposition of that metal.

At a Co concentration of 0.12M, the deposited film has a composition around  $\text{Co}_{65}\text{Fe}_{35}$  (refer to the EDS spectrum shown in Figure 5-14).

### 5.2.1.3 Effect of iron concentration

As illustrated in Figure 5-15, the Fe percentage in deposited CoFe films increases, while the Co percentage decreases with increasing iron concentration in electrolyte, which is expected from the kinetics of electroplating.

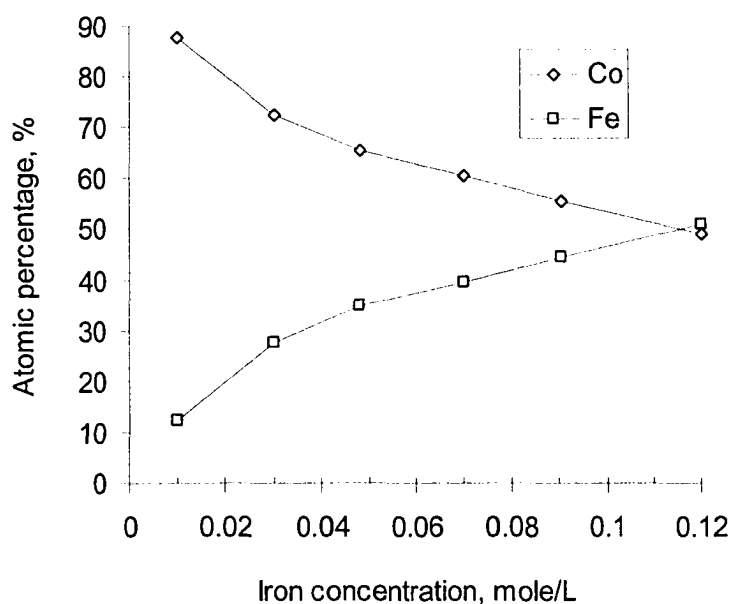


**Figure 5-15.** Effect of iron concentration on the composition of CoFe films plated at  $i = 15\text{mA/cm}^2$ ;  $t_{\text{on}} = 6\text{ms}$ ;  $t_{\text{on}} + t_{\text{off}} = 10\text{ms}$ ; agitation of 600rpm.

### 5.2.1.4 Effect of Co/Fe concentration ratio

The effect of Co/Fe concentration ratio was studied as a means to further understand the CoFe alloy plating process from the citrate-added bath. Table 5-2 illustrates the effect

of Co/Fe concentration ratio in the electrolyte on the Co/Fe content ratio in deposited CoFe films. The Co/Fe content ratio in the deposit increases with increasing Co/Fe concentration ratio. When the Co/Fe concentration ratio in electrolyte equals to 1, the cobalt and iron percentages in deposited film are close to 50 at%, i.e., the Co/Fe content ratio in deposited film is also close to 1 (i.e., 0.98 in Table 5-2). As the Co/Fe concentration ratio in the solution increases, it becomes larger than the Co/Fe content ratio in the deposit, which means Fe is more preferentially deposited than Co. However, from the standard electrode potentials listed in Appendix 1, the  $\text{Co}^{2+}/\text{Co}$  electrode has a more positive potential than the  $\text{Fe}^{2+}/\text{Fe}$  electrode, so Co should be plated out more easily. Therefore, Fe is anomalously deposited from the citrate-added CoFe plating bath. This is similar to the abnormal deposition of Fe observed by other researchers when traditional CoFe plating baths (no citrate addition and a lower pH of 2.0-3.0) are employed. [Zech99]

**Table 5-2.** Effect of Co/Fe concentration ratio in electrolyte on the Co/Fe content ratio in deposit. The Fe concentration is fixed at 0.048M.

Co/Fe conc. ratio in electrolyte	Co content (at%)	Fe content (at%)	Co/Fe content ratio in deposit
0.5	31.0	69.0	0.45
1	49.6	50.4	0.98
1.33	55.7	44.3	1.26
1.71	60.7	39.3	1.54
2	62.9	37.1	1.70
2.5	65.3	34.7	1.88
3	70	30	2.33
4	71.6	28.4	2.52
12*	87.6	12.4	7.06

\* The Fe concentration is 0.01M.

For films deposited from baths with the same Co/Fe concentration ratio, but with different metal concentrations as listed in Table 5-3, the film compositions are quite close. Therefore, the film composition is determined mainly by the Co/Fe concentration ratio in plating bath under the employed conditions. This implies that the diffusion of cobalt and iron ions to cathode/solution interface from the bulk is quick enough compared with the metal deposition rate, i.e., the metal ion concentration ratio around the cathode surface is consistent with the bulk concentration ratio under the utilized metal ion concentrations. Therefore, the CoFe plating process is activation controlled, not mass-transport controlled, under the applied conditions.

**Table 5-3.** CoFe films deposited from baths with the same Co/Fe concentration ratio but different metal concentrations.

Co/Fe conc. Ratio	Fe conc. (M)	Co content (at%)	Fe content (at%)
1	0.12	49.0	51.0
1	0.048	49.6	50.4
4	0.048	70.5	29.5
4	0.048	71.6	28.4
4	0.03	72.4	27.6

#### 5.2.1.5 Effect of current density

Current density is always an important factor for electrodeposition. It can affect the microstructure and properties of deposited films. Figure 5-16 illustrates the effect of current density on deposit composition. At current densities of 10 and 12 mA/cm<sup>2</sup>, the film composition is around Co<sub>70</sub>Fe<sub>30</sub>. At current densities higher than 15 mA/cm<sup>2</sup>, the film composition is about Co<sub>64</sub>Fe<sub>36</sub>. Therefore, high current density is beneficial for Fe deposition.

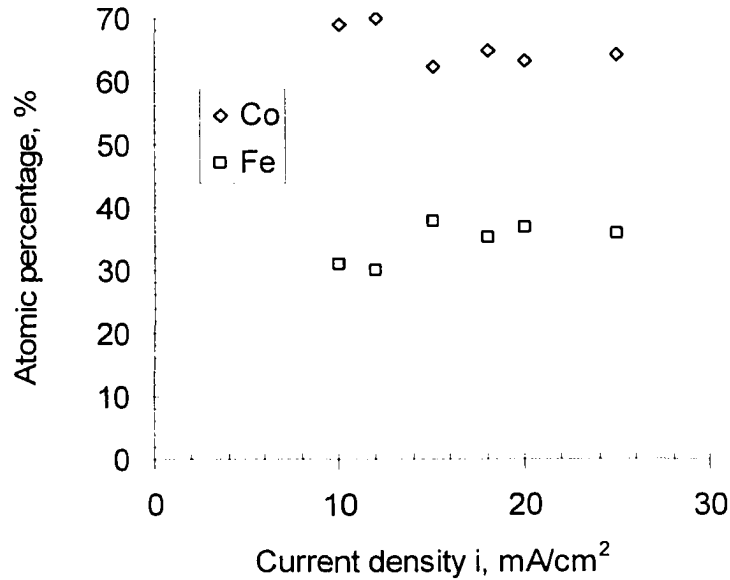


**Figure 5-16.** Effect of current density on the composition of CoFe films plated at  $t_{on} = 6\text{ms}$ ;  $t_{on} + t_{off} = 10\text{ms}$ ; agitation of 600rpm.

#### 5.2.1.6 Effect of $t_{on}$

The on time  $t_{on}$ , adopted in PC plating, controls the deposition time in a cycle and affects the pulse current density  $i_{pulse}$  at a given average current density  $i_{average}$ :

$$i_{pulse} = \frac{t_{on} + t_{off}}{t_{on}} i_{average} \quad (5.25)$$

The on time also affects the diffusion of electroactive species at a given frequency (i.e., fixed cycle time). A low  $t_{on}$  will allow for better diffusion of metal ions, which helps to maintain the initial ion concentration around the cathode.

As shown in Figure 5-17, the Co content in deposited film decreases slightly from 68 at% to 64 at%, and Fe content increases slightly from 32 at% to 36 at% as  $t_{on}$  increases from 1ms to 6ms. With reference to the test result of current density  $i$ , it can be deduced that the diffusion rate of iron ions is faster relative to that of cobalt ions. The film composition is around  $\text{Co}_{65}\text{Fe}_{35}$  as  $t_{on}$  further increases. Generally,  $t_{on}$  has a slight effect on film composition under the employed conditions.

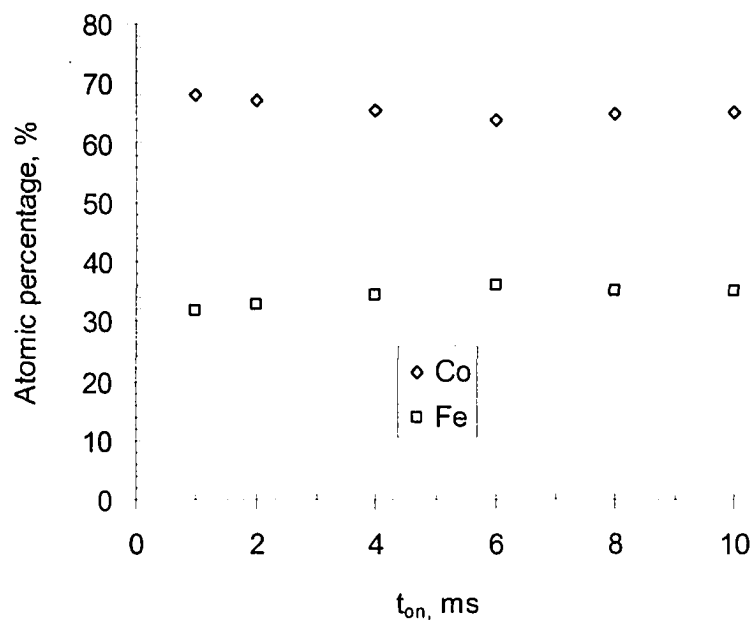


**Figure 5-17.** Effect of  $t_{on}$  on the composition of CoFe films plated at  $i = 15\text{mA}/\text{cm}^2$ ;  $t_{on} + t_{off} = 10\text{ms}$ ; agitation of 600rpm.

#### 5.2.1.7 Effect of agitation

Agitation will result in convection of the electrolyte, accelerate the mass transport of metal ions to the cathode, affect the metal ion ratio near the cathode surface and make the concentrations of metal ions around the cathode surface closer to their bulk concentrations.

As illustrated in Figure 5-18, with no agitation, the composition of deposited film is  $\text{Co}_{69}\text{Fe}_{31}$ . With the introduction of agitation at 100 to 1000 rpm, the film composition changes to around  $\text{Co}_{64}\text{Fe}_{36}$ . Therefore, the introduction of agitation benefits iron deposition, which means the mass transport of the iron ion species to the cathode is more favorably improved by agitation. In general, the agitation speed has little effect on film composition. This implies that the metal ion concentrations employed and metal ion transport are sufficient for obtaining stable film composition under the applied conditions.

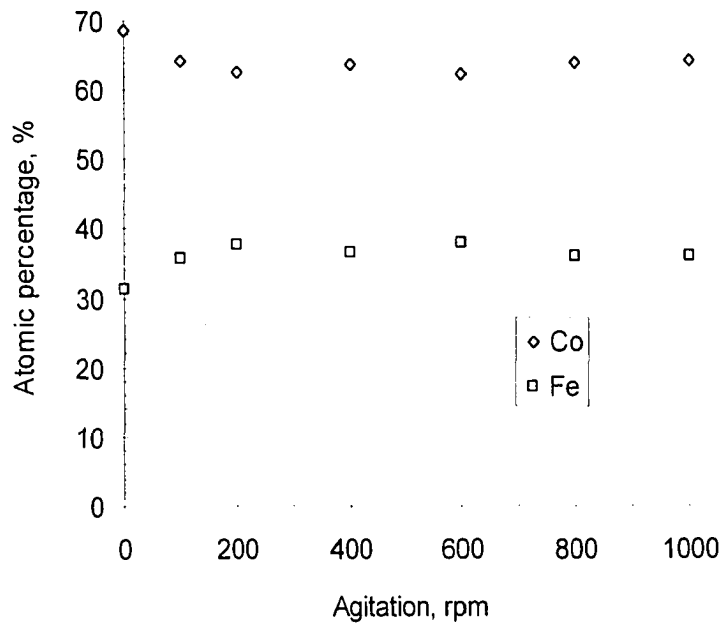


**Figure 5-18.** Effect of agitation on the composition of CoFe films plated at  $i = 15\text{mA/cm}^2$ ;  $t_{\text{on}} = 6\text{ms}$ ;  $t_{\text{on}} + t_{\text{off}} = 10\text{ms}$ .

#### 5.2.1.8 Effect of plating temperature

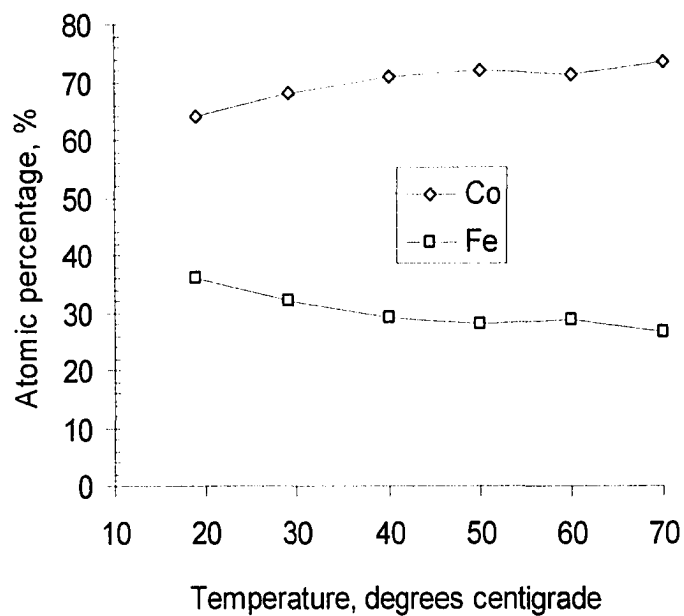
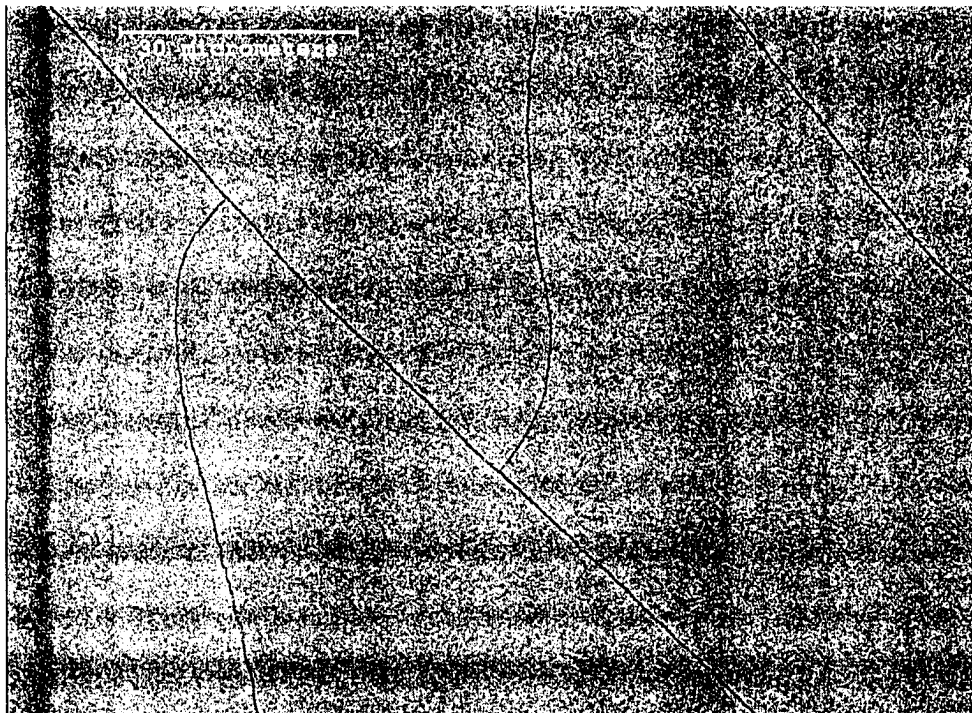
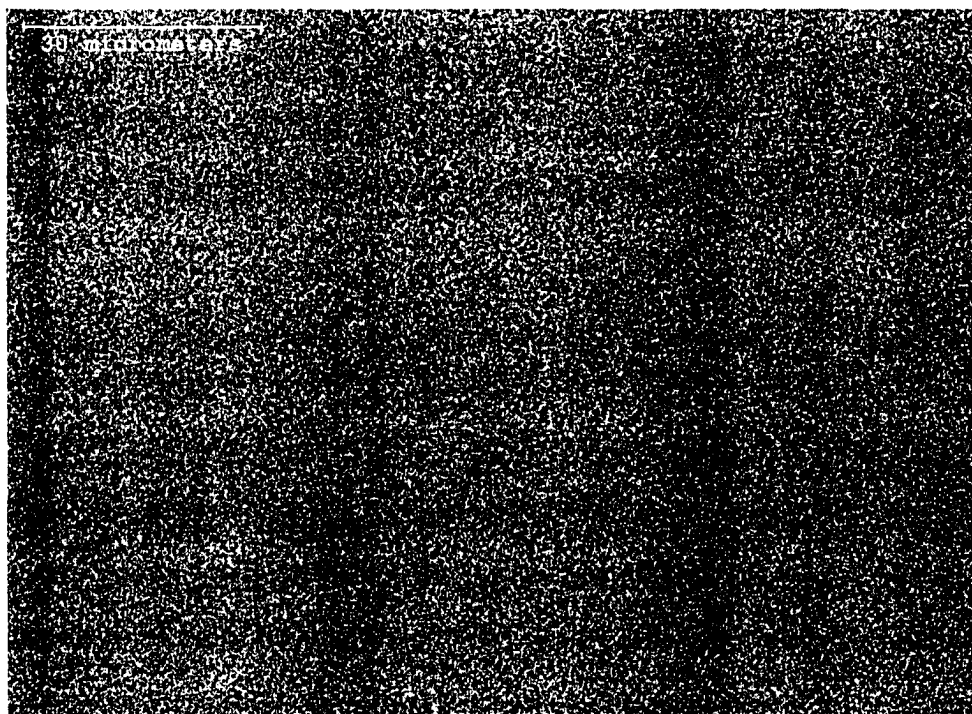


**Figure 5-19.** Effect of plating temperature on the composition of CoFe films plated at  $i = 15\text{mA/cm}^2$ ;  $t_{\text{on}} = 6\text{ms}$ ;  $t_{\text{on}} + t_{\text{off}} = 10\text{ms}$ ; agitation of 600rpm.



a. Plating temperature of 18°C



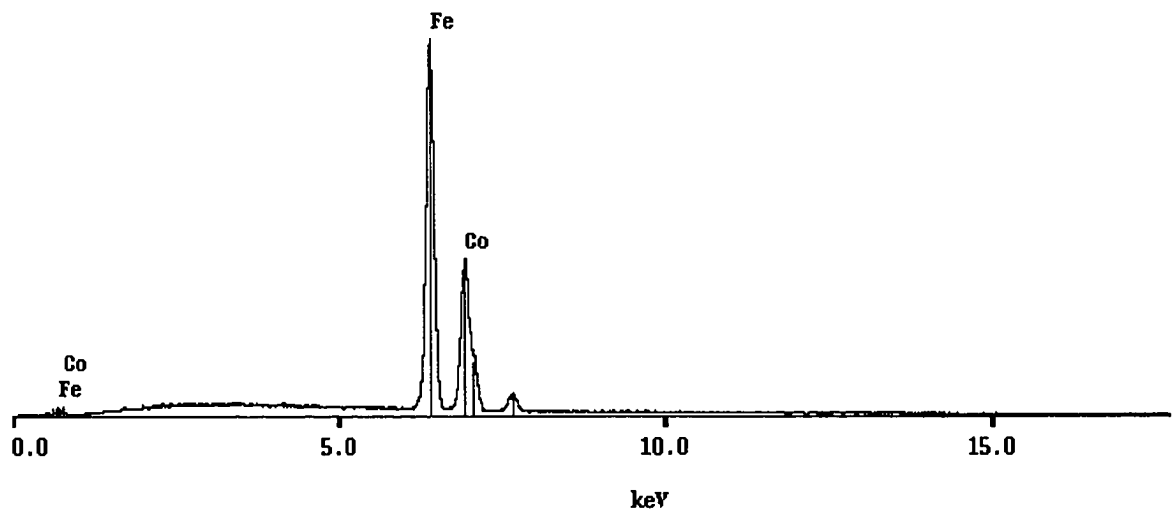
b. Plating temperature of 40°C

**Figure 5-20.** Plan view SEM SE images of CoFe films plated at different temperatures at  $i = 15\text{mA/cm}^2$ ;  $t_{\text{on}} = 6\text{ms}$ ;  $t_{\text{on}} + t_{\text{off}} = 10\text{ms}$ ; agitation of 600rpm.

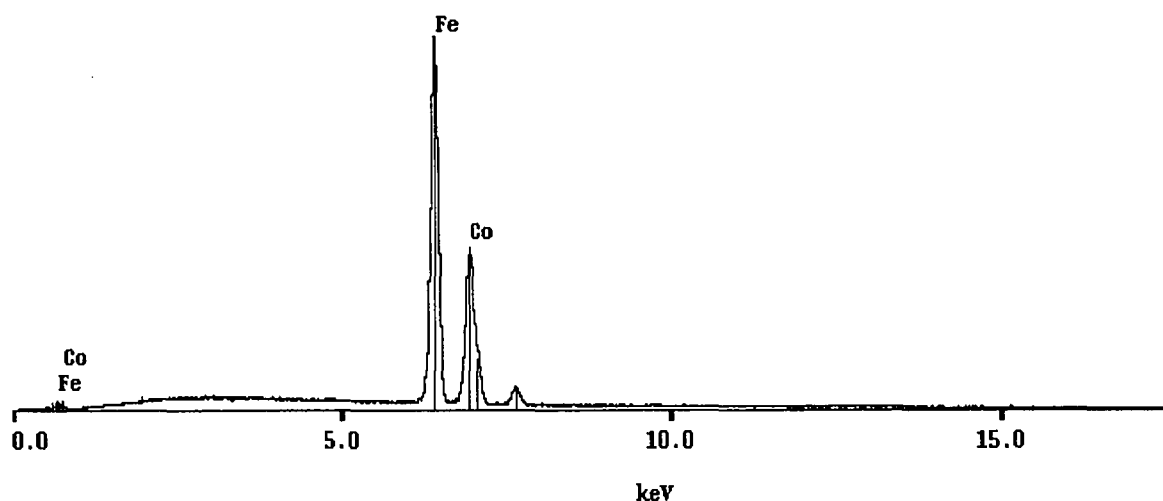
The effect of plating temperature on film composition is illustrated in Figure 5-19. Generally, the cobalt content in the deposited film increases as the plating temperature goes up. For iron content in the plated film, the situation is reversed. Therefore, higher temperatures are more beneficial for cobalt deposition in contrast to iron.

Increased plating temperature should accelerate the mass transport of metal ions to the cathode and help overcome the energy barrier for metal deposition. In this case, the effect is more pronounced for cobalt. Increased plating temperature can also help reduce stress and cracking in deposited films (see Figure 5-20).

To compare with the CoFe films with high iron content ( $\text{Co}_{35}\text{Fe}_{65}$ ) plated by Osaka et al [Osaka03-1], films with a composition around  $\text{Co}_{33}\text{Fe}_{67}$  were also plated from a conventional low pH bath (refer to Table 3-1). A representative EDS spectrum is shown in Figure 5-21a. At the same times, films with a composition around  $\text{Co}_{34}\text{Fe}_{66}$  were plated from a citrate-added bath (Table 5-4). A representative EDS spectrum is illustrated in Figure 5-21b.



a.  $\text{Co}_{33}\text{Fe}_{67}$  film plated from conventional low pH bath



b.  $\text{Co}_{34}\text{Fe}_{66}$  film plated from citrate-added bath

**Figure 5-21.** EDS spectra from deposited CoFe films with high iron contents.

**Table 5-4.** Composition of citrate-added bath for electroplating  $\text{Co}_{34}\text{Fe}_{66}$  films.

Chemical	Concentration	Chemical	Concentration
$\text{CoSO}_4 \cdot 7\text{H}_2\text{O}$	0.048 M	$\text{H}_3\text{BO}_3$	0.4 M
$\text{FeSO}_4 \cdot 7\text{H}_2\text{O}$	0.096 M	Sodium lauryl sulfate	0.01 g/L
Bath pH= 4.5 (natural)		Ammonium citrate	5 g/L

From the above study, in general, bath composition has a more pronounced effect on the composition of deposited CoFe films than plating conditions.

### 5.2.2 Electroplating of CoFeNi alloys

CoFeNi films with a composition of  $\text{Co}_{65}\text{Fe}_{23}\text{Ni}_{12}$  have been reported as having ideal soft magnetic properties by Osaka and coworkers. [Osaka98-1] [Osaka98-2] It is known that the  $\text{Co}_{65}\text{Fe}_{35}$  alloy has a very high saturation magnetization  $M_s$  of 2.35 Tesla [Yu02], so that the effect appears to be related to partial substitution of iron with nickel. The electroplating of CoFeNi thin films from the citrate-added bath (see Table 3-4), as a function of bath composition and operation parameters, has been investigated.

### 5.2.2.1 Effect of ammonium citrate

The effect of ammonium citrate dosage on the composition of deposited CoFeNi films is shown in Figure 5-22. Generally, ammonium citrate has the most prominent effect on deposit Fe content, followed by Ni content, and only a minor effect on Co content. The results agree with the calculated stability diagrams (see Figures 4-5d, 4-6b and 4-6c), which demonstrate that citrate has the most powerful complexing effect on Fe ions, then  $\text{Ni}^{2+}$ , and finally  $\text{Co}^{2+}$ . At low citrate dosage, the Fe content in the deposited films is lowered, while as the citrate dosage is increased, the Fe content goes up. This is because at low citrate dosage, only Fe ions are complexed; as citrate dosage increases, the Ni and Co ions will also be complexed. Metals are more difficult to plate out from the complexed metal ions, due to higher activation energies and lower diffusivities to the cathode.

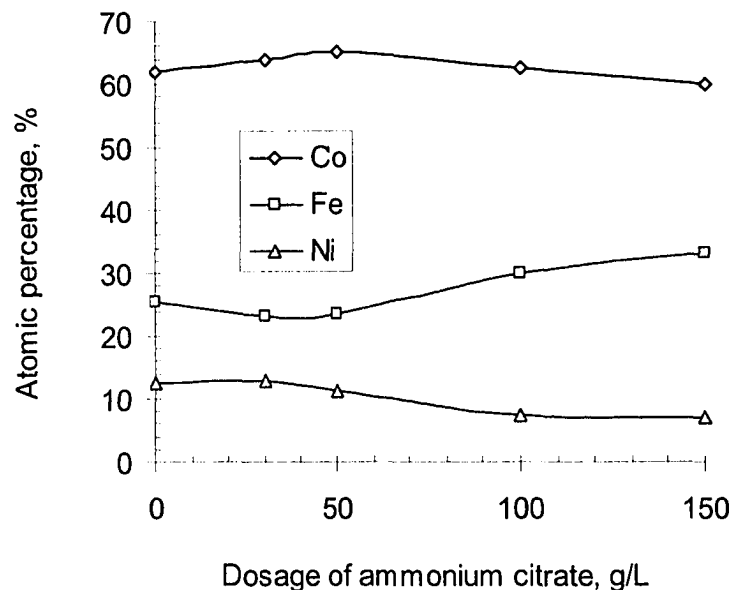


**Figure 5-22.** Effect of ammonium citrate dosage on the electroplating of CoFeNi films at  $i = 6\text{mA/cm}^2$ ;  $t_{\text{on}} = 0.3\text{ms}$ ;  $t_{\text{off}} = 9.7\text{ms}$ ; agitation of 600rpm.

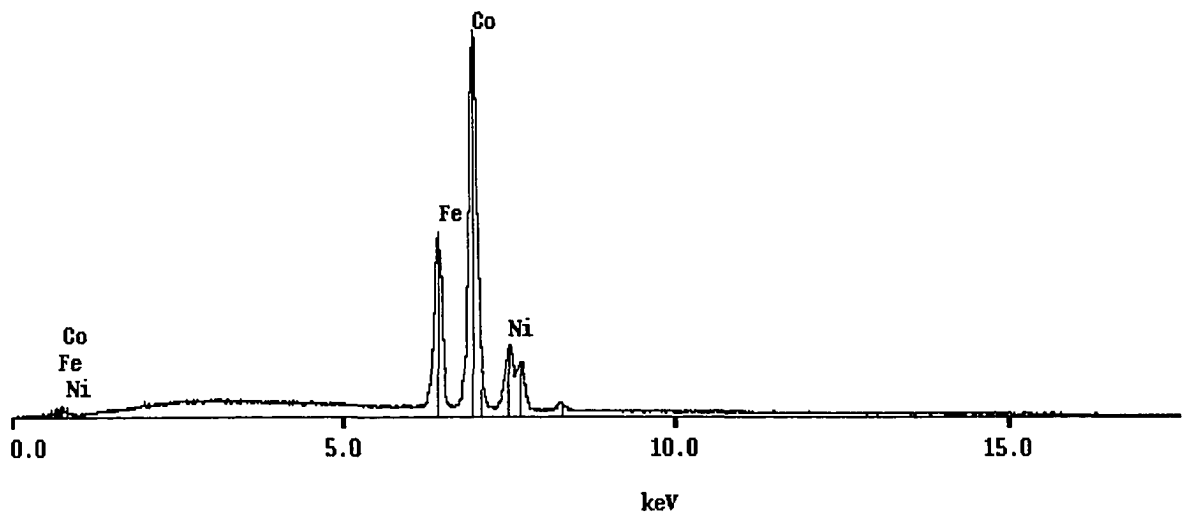


**Figure 5-23.** EDS spectrum of  $\text{Co}_{66}\text{Fe}_{23}\text{Ni}_{11}$  film plated from citrate-added bath.

At an ammonium citrate dosage of 50g/L (0.206 M), a film with a composition around  $\text{Co}_{66}\text{Fe}_{23}\text{Ni}_{11}$  has been plated out (refer to the EDS spectrum in Figure 5-23). This film is very close in composition to the film with optimal soft magnetic properties, which has a composition of  $\text{Co}_{65}\text{Fe}_{23}\text{Ni}_{12}$  with a high saturation flux density  $B_s$  of 2.1 Tesla and

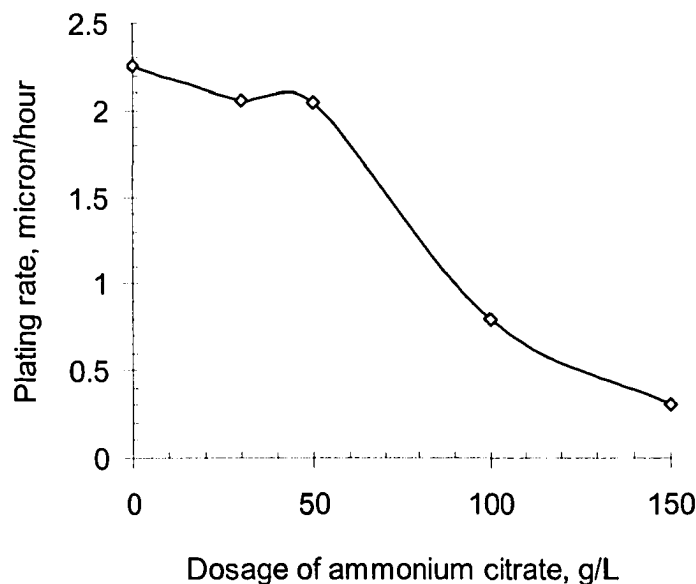


**Figure 5-24.** Effect of ammonium citrate dosage on the plating rate for depositing CoFeNi films at  $i = 6\text{mA}/\text{cm}^2$ ;  $t_{\text{ON}} = 0.3\text{ms}$ ;  $t_{\text{OFF}} = 9.7\text{ms}$ ; agitation of 600rpm.

a low coercivity  $H_c$  of 1.20 Oe, claimed by Osaka and coworkers. [Osaka98-1]  
[Osaka98-2]

The effect of ammonium citrate dosage on plating rate is shown in Figure 5-24. The ammonium citrate dosage has a minor effect on plating rate up to a concentration of 50g/L, after which the plating rate drops rapidly.

#### 5.2.2.2 Effect of cobalt concentration

The effect of cobalt concentration in the plating bath on deposit composition is illustrated in Figure 5-25. Cobalt content in the deposit increases rapidly, while Fe and Ni contents decrease as the cobalt concentration increases. This corresponds to the kinetics of plating process.

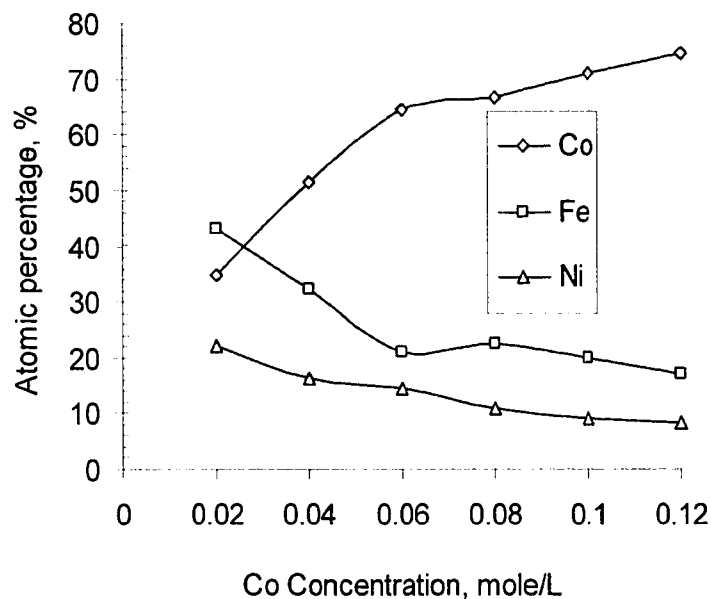


**Figure 5-25.** Effect of cobalt concentration on the composition of CoFeNi films plated at  $i = 6\text{mA/cm}^2$ ;  $t_{\text{on}} = 0.3\text{ms}$ ;  $t_{\text{on}} + t_{\text{off}} = 10\text{ms}$ ; agitation of 600rpm.

#### 5.2.2.3 Effect of iron concentration

Iron concentration tests (Figure 5-26) demonstrate that iron content in deposited films

increases, while cobalt content decreases, with increasing iron concentration in the plating bath. It is interesting that Ni content is almost constant as the iron concentration is varied, which may be due to the much lower concentration of iron relative to nickel in the plating bath.

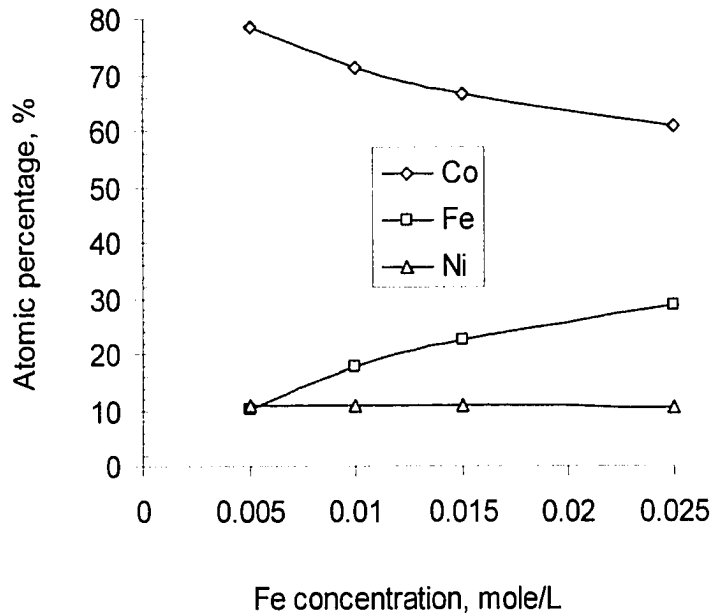


**Figure 5-26.** Effect of iron concentration on the composition of CoFeNi films plated at  $i = 6\text{mA/cm}^2$ ;  $t_{\text{on}} = 0.3\text{ms}$ ;  $t_{\text{on}} + t_{\text{off}} = 10\text{ms}$ ; agitation of 600rpm.

#### 5.2.2.4 Effect of nickel concentration

The effect of nickel concentration on CoFeNi alloy deposition is shown in Figure 5-27. The Ni content in the deposit increases, while Co and Fe contents oscillate, as nickel concentration in the plating bath goes up.

#### 5.2.2.5 Effect of current density

Tests on the effect of current density (Figure 5-28) demonstrate that, at low current densities, the composition of deposited CoFeNi films varies as the current density increases. At current densities higher than  $6\text{mA/cm}^2$ , the metal contents in deposited

films are almost constant.

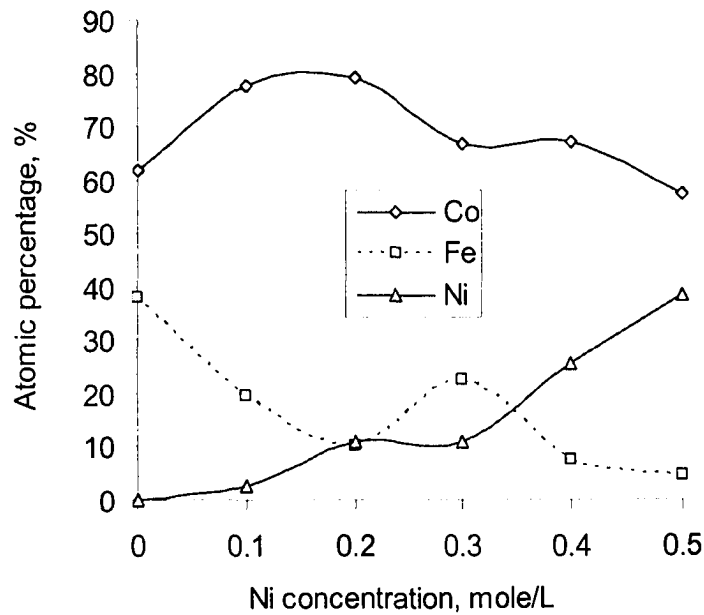


**Figure 5-27.** Effect of nickel concentration on the composition of CoFeNi films plated at  $i = 6\text{mA/cm}^2$ ;  $t_{\text{on}} = 0.3\text{ms}$ ;  $t_{\text{on}} + t_{\text{off}} = 10\text{ms}$ ; agitation of 600rpm.

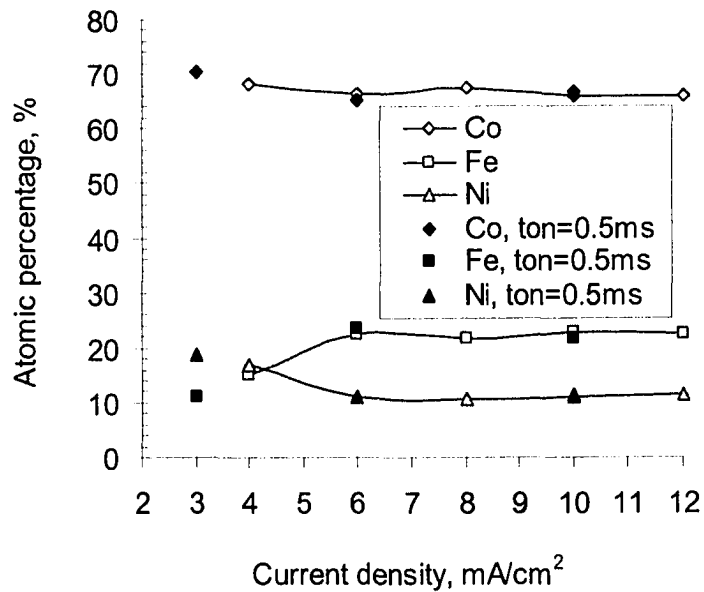


**Figure 5-28.** Effect of current density on the composition of CoFeNi films plated at  $t_{\text{on}} = 0.3\text{ms}$ ;  $t_{\text{on}} + t_{\text{off}} = 10\text{ms}$ ; agitation of 600rpm.

### 5.2.2.6 Effect of $t_{on}$

To obtain uniform composition through the thickness of deposited films, i.e., to avoid metal content gradients, pulsed current plating is usually employed for maintaining initial metal ion concentrations around the cathode. Figure 5-29 shows the effect of on-time  $t_{on}$  of the duty cycle on the plating of CoFeNi alloys. The metal contents in deposits have very little fluctuation with  $t_{on}$  variation. The deposited films have a composition around  $Co_{67}Fe_{22}Ni_{11}$ .

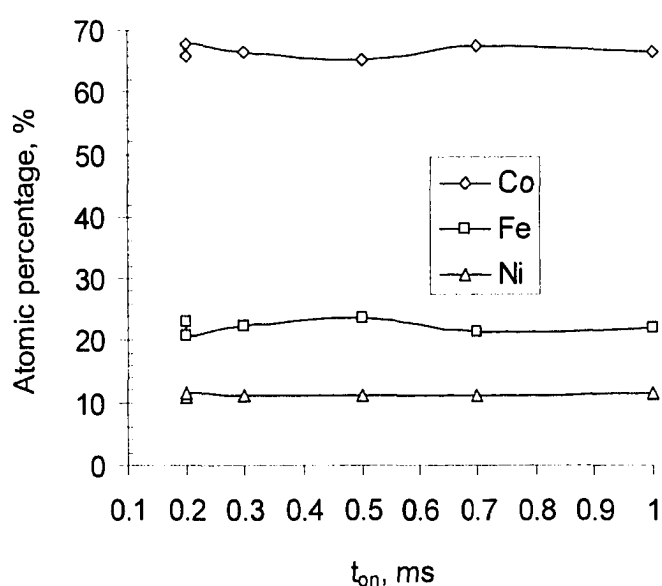


**Figure 5-29.** Effect of  $t_{on}$  on the composition of CoFeNi films plated at  $i = 6\text{mA/cm}^2$ ;  $t_{on} + t_{off} = 10\text{ms}$ ; agitation of 600rpm.

### 5.2.2.7 Effect of agitation

The introduction of agitation changes the composition of plated CoFeNi films (Figure 5-30). This is because agitation accelerates the mass transport of metal ions to the cathode and affects the metal ion ratio near the cathode surface. The Fe and Ni contents are more affected, with little change in Co content.

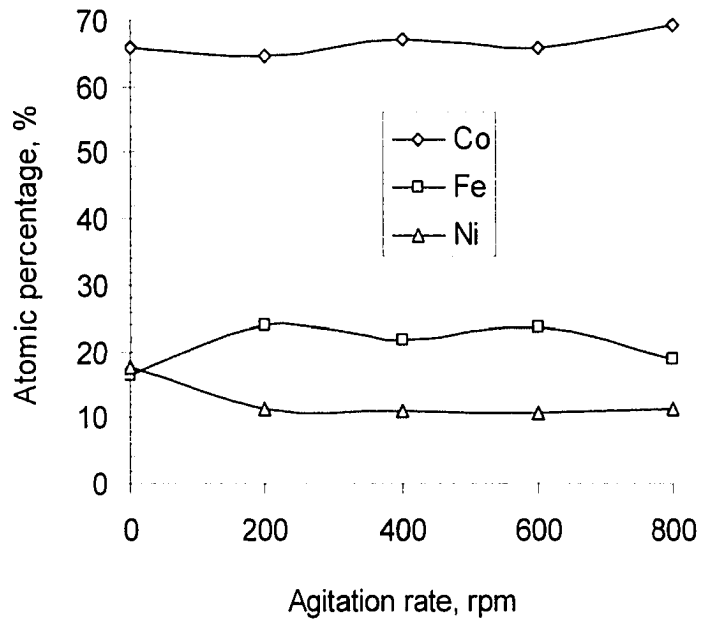


**Figure 5-30.** Effect of agitation on the composition of CoFeNi films plated at  $i = 6\text{mA/cm}^2$ ;  $t_{\text{on}} = 0.3\text{ms}$ ;  $t_{\text{on}} + t_{\text{off}} = 10\text{ms}$ .

#### 5.2.2.8 Effect of plating temperature

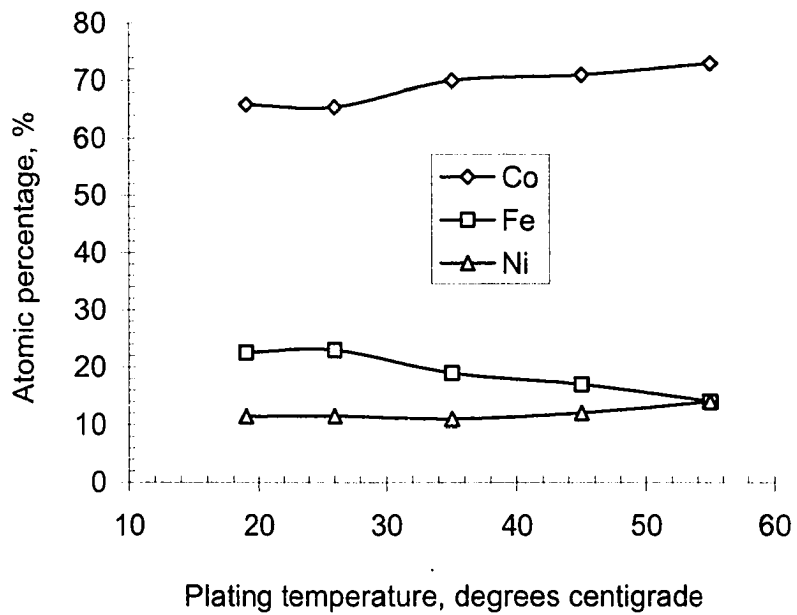
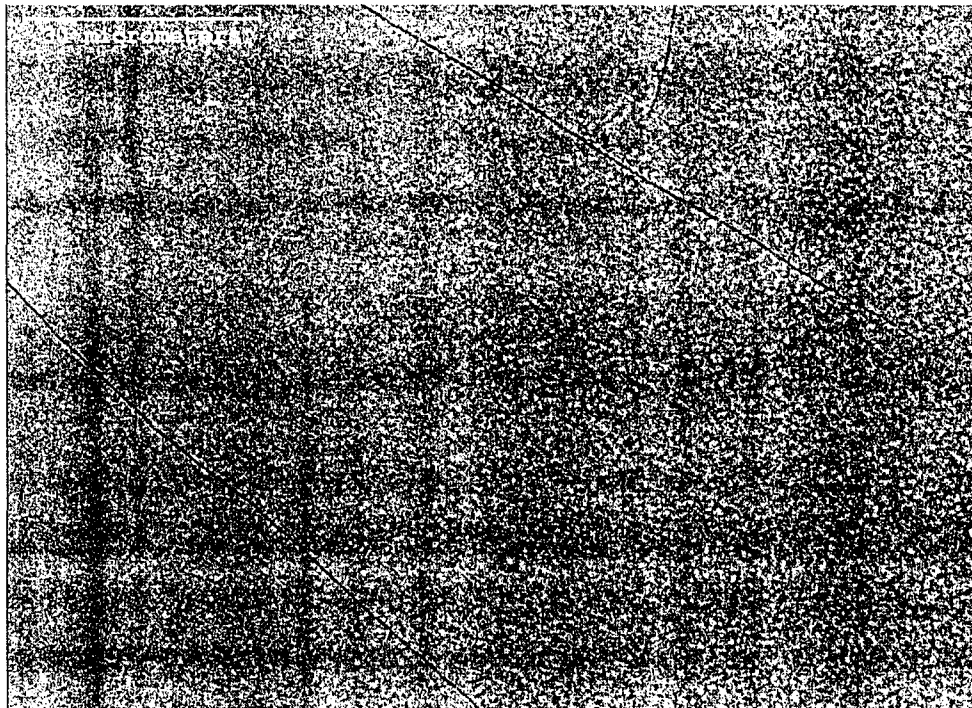


**Figure 5-31.** Effect of plating temperature on the composition of CoFeNi films plated at  $i = 12\text{mA/cm}^2$ ;  $t_{\text{on}} = 0.3\text{ms}$ ;  $t_{\text{on}} + t_{\text{off}} = 10\text{ms}$ ; agitation of 600rpm.

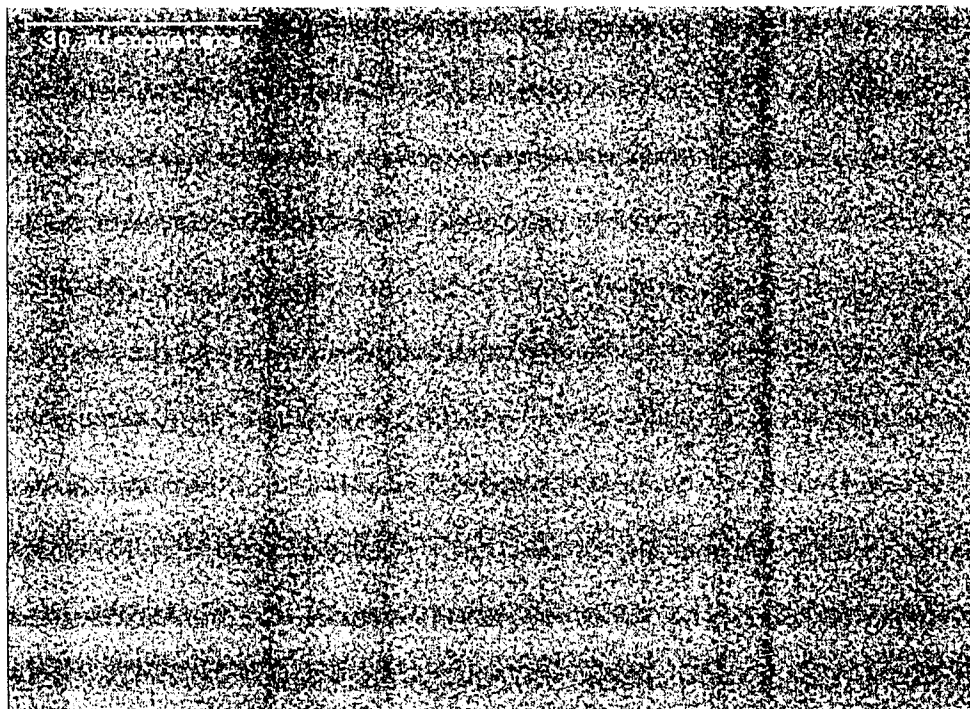
The effect of plating temperature on the composition of deposited CoFeNi films is illustrated in Figure 5-31. Similar to the CoFe alloy plating system, the cobalt content in deposited films increases, while the iron content decreases, as the plating temperature increases. Increasing the plating temperature also slightly facilitates the deposition of nickel.

Higher plating temperatures can help reduce the residual stress in deposited films. Figures 5-32a and 5-32b illustrate plan view images of films plated at 19°C and 45°C, respectively. It can be seen that the film deposited at higher temperature (45°C) is more uniform and has much less cracking.

Generally, the effects of plating conditions on CoFeNi film composition are not as prominent as that of bath composition.



a. CoFeNi film plated at 19°C



b. CoFeNi film plated at 45°C

**Figure 5-32.** Plan view SEM SE images of CoFeNi films plated at different temperatures at  $i = 12\text{mA/cm}^2$ ;  $t_{\text{on}} = 0.3\text{ms}$ ;  $t_{\text{on}} + t_{\text{off}} = 10\text{ms}$ ; agitation of 600rpm.

#### 5.2.2.9 Anomalous phenomenon in CoFeNi alloy plating

Checking the plating bath composition (Table 3-4), it can be seen that the metal contents in deposited CoFeNi films are not proportional to the metal concentrations in the plating bath. By referring to Figures 5-22 and 5-25 to 5-32, Ni is the most difficult metal to plate out. However, from the standard electrode potentials listed in Appendix 1,  $\text{Ni}^{2+}/\text{Ni}$  has the most positive potential among the three metal electrodes; it should be the metal plated out first. Therefore, Ni was anomalously deposited from the citrate-added bath. The anomalous deposition of Ni in alloy plating was also reported previously by several researchers. [Vaes00] [Golodnitsky00] [Zhuang03]

Table 5-5 illustrates the effect of Co/Fe concentration ratio in the electrolyte on the

composition of deposited CoFeNi films. The Co/Fe content ratio in deposits increases with the Co/Fe concentration ratio in plating bath, but at a proportion lower than 1. For example, at a Co/Fe concentration ratio of 1.33, the Co/Fe content ratio in the deposit is about 0.80. Therefore, iron has been preferentially deposited compared with cobalt. This is similar to the anomalous deposition of Fe observed in CoFe alloy plating. The larger the Co/Fe concentration ratio in plating bath, the larger the difference compared with the Co/Fe content ratio in deposit.

**Table 5-5.** Effect of Co/Fe concentration ratio in the electrolyte on the composition of deposited CoFeNi films.\*

Co/Fe conc. ratio in electrolyte	Co, at%	Fe, at%	Ni, at%	Co/Fe content ratio in deposit
1.33	34.7	43.1	22.2	0.80
2.67	51.5	32.3	16.2	1.59
4	64.4	21.2	14.4	3.04
5.33	66.5	22.5	11.0	2.96
6.67	71.1	19.8	9.1	3.59
8	74.7	17.0	8.3	4.38

\* The plating current density was  $6\text{mA/cm}^2$ ; Fe and Ni concentrations are fixed at 0.015M and 0.30M, respectively.

**Table 5-6.** CoFeNi films deposited at the same Co/Fe concentration ratio in the plating bath but different metal concentrations (Ni concentration is fixed at 0.30M).

Co/Fe conc. ratio	Fe conc. (M)	Co (at%)	Fe (at%)	Ni (at%)
4	0.015	64	21	15
4	0.020	61	29	10

For CoFeNi films deposited from baths with the same Co/Fe concentration ratio, but

different metal concentrations (Table 5-6), the compositions are not similar. This is in contrast to the CoFe alloy plating system (Table 5-3).

To compare with the magnetic properties of films with the composition of  $\text{Co}_{65}\text{Fe}_{23}\text{Ni}_{12}$  deposited by Osaka et al [Osaka98-1] [Osaka98-2], films with a composition around  $\text{Co}_{64}\text{Fe}_{24}\text{Ni}_{11}$  were also plated out from a conventional low pH bath (refer to Table 3-3). An EDS spectrum is shown in Figure 5-33.

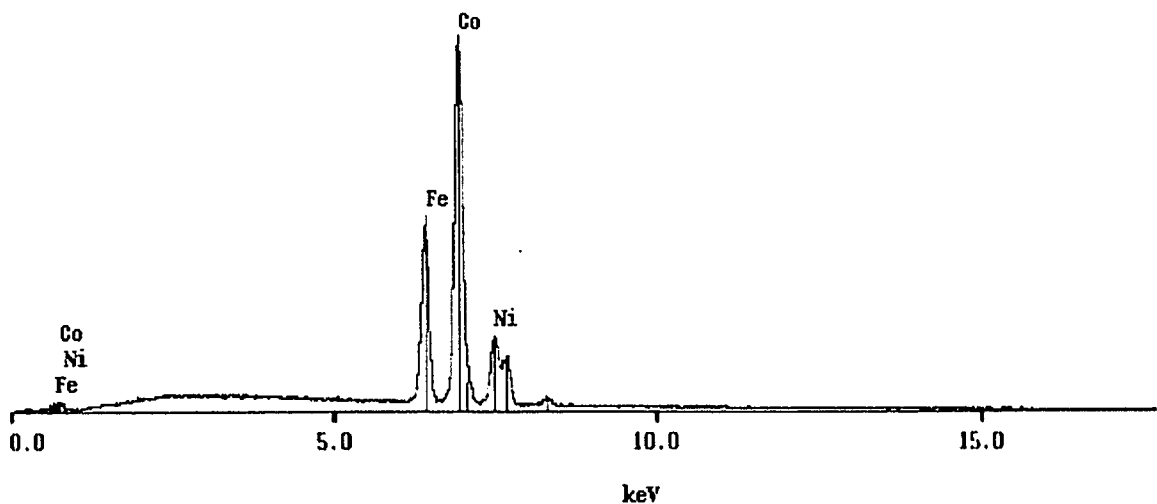
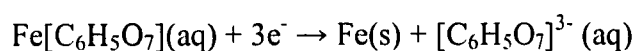
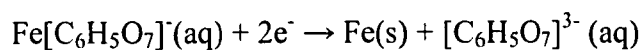


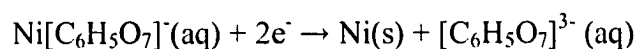
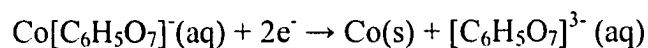
**Figure 5-33.** EDS spectrum of  $\text{Co}_{64}\text{Fe}_{24}\text{Ni}_{11}$  film deposited from a conventional bath.

### 5.3 Summary

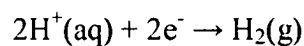
The fundamentals of electrodeposition are briefly discussed in this chapter. In terms of the existing theory, for the deposition of metal from a complexed metal ion, the metal is deposited by direct discharge from the complex ion, without first dissociation of the complex ion to give a metal ion.

For the citrate-added baths, the reduction reactions for metals from citrate-complexed ions include:





The secondary reaction at cathode involves hydrogen evolution, especially in acidic electrolytes:



Generally, for both CoFe and CoFeNi alloy plating, the metal content in deposited films increases with increasing metal concentration in the electrolyte, which reflects the kinetics of electrodeposition. The effects of electroplating conditions on the composition of deposited films are not as prominent as that of bath composition. Ammonium citrate has a minor effect on plating rate at low dosages, while the plating rate drops rapidly at high dosages. The cobalt content in deposited films increases, while the iron content decreases, at higher plating temperatures. Higher plating temperatures help to reduce the residual stress in deposited films, which are more uniform and have less cracking.

For CoFe plating, the metal contents in deposited films are linearly dependent on ammonium citrate dosage. For CoFeNi deposition, ammonium citrate has the most prominent effect on Fe content, followed by Ni content, and only a minor effect on Co content.

For CoFe plating, films deposited from baths with the same Co/Fe concentration ratio, but with different metal concentrations, have almost the same composition. The situation is different for CoFeNi plating.

Anomalous behaviors for Fe and Ni depositions were also observed during the electrodeposition of CoFe and CoFeNi films from the citrate-added baths.

## Chapter 6 Electrochemical Study of the Electrodeposition and Corrosion Properties of CoFe and CoFeNi Films

Cyclic voltammetry (CV) and linear sweep voltammetry (actually the negative sweep in the CV scan) are popular techniques for initial studies of new electrochemical systems and are very useful for obtaining information about electrode reactions and processes. Using linear sweep voltammetry, Zhuang and Podlaha [Zhuang00] investigated the polarization behavior for the deposition of Co, Fe and Ni single metals and CoFeNi alloys from sulphate baths with pH around 3.0. Hu and Bai [Hu02] and Afshar et al [Afshar02] conducted cyclic voltammetry studies of the codepositon of iron group alloys. In order to investigate the electrochemical mechanisms for the electrodeposition of CoFe and CoFeNi films from citrate-added baths and citrate-free baths, linear sweep voltammetry and cyclic voltammetry studies of the deposition of Co, Fe and Ni single metals and CoFe and CoFeNi alloys from the electrolytes of interest have been conducted in this study.

The corrosion resistance of soft magnetic films is also an important property to be considered for the manufacture of magnetic devices. Osaka and coworkers [Osaka99-4] [Osaka98-1] studied the corrosion behavior of electroplated CoFeNi films with different crystalline structures and various sulfur contents. The corrosion properties of CoFeNi films depended highly on the sulfur content and also on the microstructure of the film. A film with a low S content (deposited from SCA-free bath) had high corrosion resistance, and a bcc film was less resistant to corrosion than fcc and fcc-bcc films. Saito et al [Saito99] observed that films plated at a high current density ( $15 \text{ mA/cm}^2$ ), from a bath without saccharin, had a sufficient anodic pitting-corrosion potential ( $-65 \text{ mV}$ ). Films plated at a low current density ( $5 \text{ mA/cm}^2$ ) from saccharin-free baths had pitting-corrosion potentials of less than  $-300 \text{ mV}$ ; the corrosion resistance was improved

after annealing above 100°C. Films plated from baths containing saccharin also had pitting-corrosion potentials of less than -300 mV. However, their corrosion resistance was not improved after annealing at 250°C. Saito et al believe that the degeneration of the corrosion resistance is attributed to defects that increase the fcc (111) lattice constant. One of the most important characteristics of a highly corrosion-resistant CoNiFe film is a fine crystal structure with very few defects. Tanaka et al [Tanaka93] also conducted similar investigations on the corrosion resistance of CoFeNi alloys for thin film inductive heads.

## **6.1 Linear sweep voltammetry and cyclic voltammetry studies**

All electrochemical experiments were conducted in a three-electrode cell without agitation. The working electrode was a sectioned Si wafer coated with a Ti (25nm)/Au (250nm) blanket metallization, with an exposed area of 0.5 to 1.0 cm<sup>2</sup> defined with lacquer. The working electrode was essentially the same as the cathode used in electrodeposition. A Pt foil was employed as the counter electrode, and a Corning saturated calomel electrode (SCE) was used as the reference electrode. The polarization curves obtained from linear sweep voltammetry and cyclic voltammograms obtained from cyclic voltammetry were all measured at a sweep rate of 1mV/s.

### **6.1.1 Polarization curves for single metal depositions**

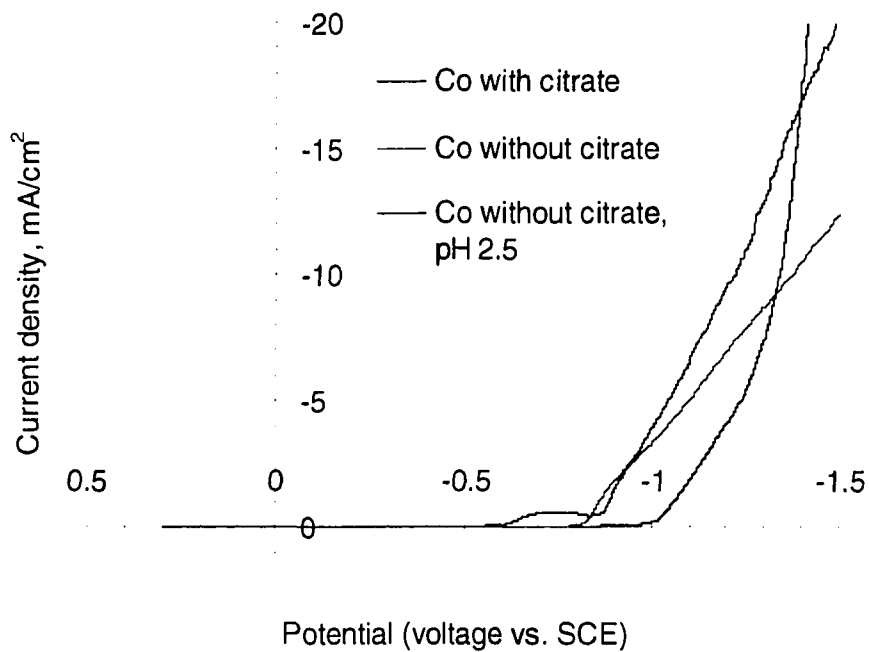
The polarization curves for the deposition of Co, Fe and Ni single metals from different baths are shown in Figures 6-1a, b and c, respectively. The compositions of the employed baths are listed in Table 6-1.

For single Co depositions (Figure 6-1a), Co was first deposited from the citrate-free bath with natural pH (purple line) at about -0.83V. Then the cathodic current density (deposition current density) increased sharply, due to the deposition of Co, with a

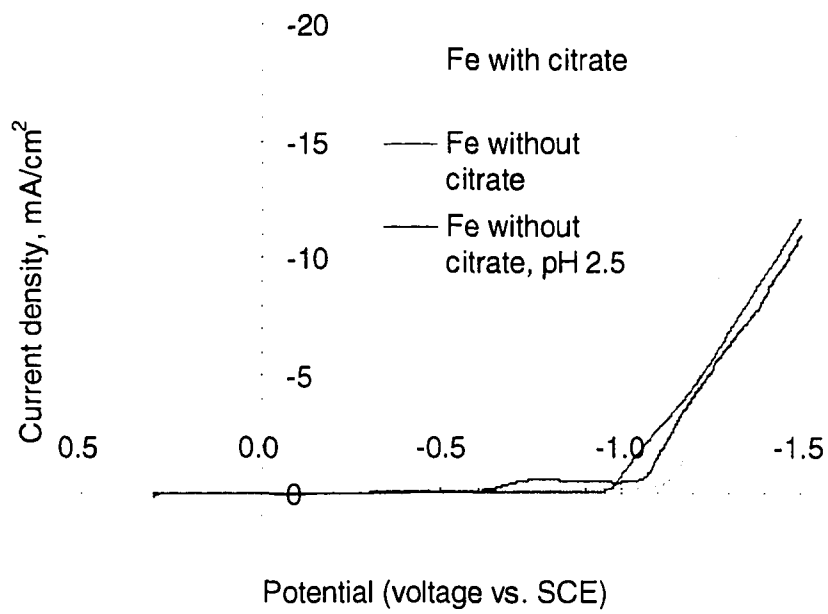
negative shift in applied potential. The deposition of Co from the citrate-free bath with a low pH of 2.5 (blue line) commenced at about -0.86V. Previous to Co deposition, hydrogen reduction was observed. The minor plateau before Co deposition represents the reduction of hydrogen under mass transport limiting conditions. The deposition of Co from the citrate-added bath (dark line) started at a potential of around -1.0V. Therefore, the addition of ammonium citrate delayed the occurrence of Co deposition to a more negative potential. This reflects the complexing of citrate ions with  $\text{Co}^{2+}$ , as the deposition of metal from complexed metal ions needs a higher activation energy, which corresponds to a more negative potential. After Co deposition was initiated, and the potential was scanned in negative direction, the cathodic current density for Co deposition from the citrate-added bath increased faster than those from the citrate-free baths under the employed experimental conditions.

**Table 6-1.** Compositions of baths employed in single metal depositions.

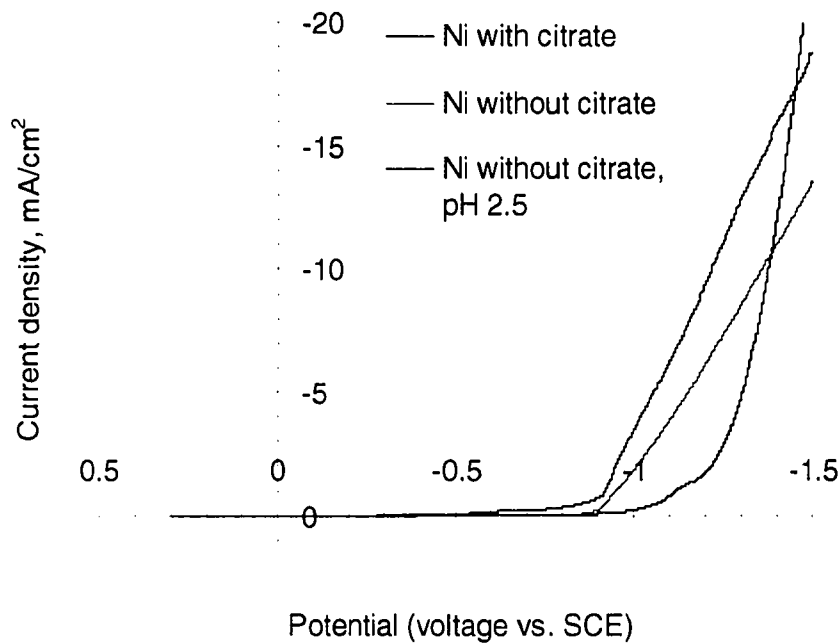
Bath	$\text{CoSO}_4$	$\text{FeSO}_4$	$\text{NiSO}_4$	Ammonium citrate	$\text{H}_3\text{BO}_3$	pH
Co bath	0.08M			0g/L	0.4M	4.5 (Natural)
	0.08M			0g/L	0.4M	2.5
	0.08M			50g/L	0.4M	6.2 (Natural)
Fe bath		0.08M		0g/L	0.4M	4.0 (Natural)
		0.08M		0g/L	0.4M	2.5
		0.08M		50g/L	0.4M	6.0 (Natural)
Ni bath			0.08M	0g/L	0.4M	4.5 (Natural)
			0.08M	0g/L	0.4M	2.5
			0.08M	50g/L	0.4M	6.2 (Natural)



a. Co deposition.



b. Fe deposition.



c. Ni deposition.

**Figure 6-1.** Polarization curves for Co, Fe and Ni single metal depositions.

The deposition of Fe (Figure 6-1b) was similar to the above Co depositions. Iron deposition commenced at about -0.97V, -1.07V and -1.15V from the citrate-free bath with natural pH (purple line), the citrate-free bath with a low pH of 2.5 (blue line) and the citrate-added bath (dark line), respectively. Apparently, the addition of citrate also delayed Fe deposition. For the deposition of Fe from the citrate-free bath with a low pH of 2.5, hydrogen reduction was observed previous to Fe deposition. The stage before Fe deposition represented the reduction of hydrogen under mass transport control. After deposition started, as the potential was shifted to more negative values, the cathodic current density for Fe deposition from the citrate-added bath increased faster than those from the citrate-free bath with pH 2.5 and citrate-free bath with natural pH.

For Ni reductions (Figure 6-1c), deposition started at about -0.89V, -0.91V and -1.11V from the citrate-free bath with natural pH, the citrate-free bath with a low pH of 2.5 and

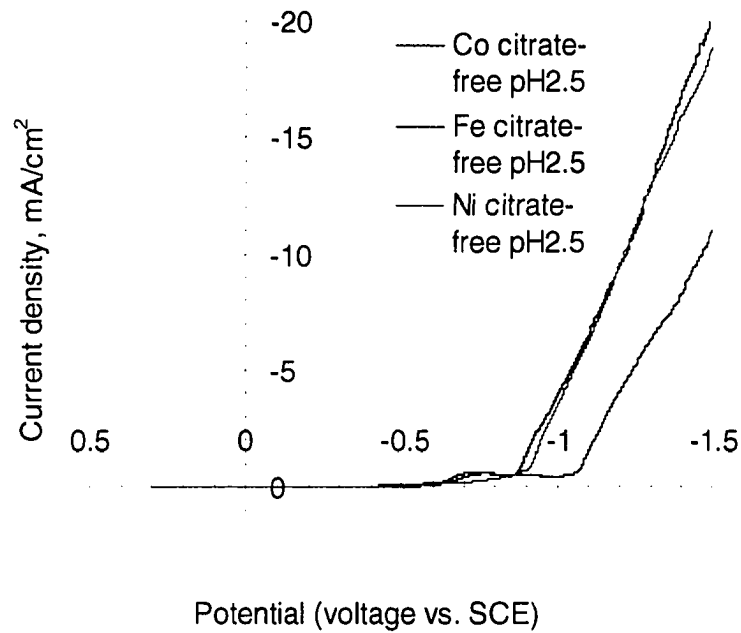
the citrate-added bath, respectively. Hence, the occurrence of Ni deposition was delayed by citrate addition. The hydrogen reduction from the citrate-free bath with a pH of 2.5 was not as obvious as that observed in Co and Fe depositions. The current density of the citrate-added bath increased slowly before -1.1V. This may be attributed to the charging of electrode double-layer. After -1.1V, the cathodic current density for Ni deposition from the citrate-added bath generally increased faster with a more negative shift in potential than those from the citrate-free bath with pH 2.5 and the citrate-free bath with natural pH.

In general, the addition of ammonium citrate delayed the occurrence of deposition of Co, Fe and Ni single metals to more negative potentials, which reflects the complexing effect of citrate ions on the metal ions. For the citrate-free baths, the bath with higher pH (natural pH) was more beneficial for metal deposition, which may be attributed to the lower  $H^+$  concentration leading to less competitive reduction of hydrogen. However, as stated in Chapter 4, the citrate-free baths with higher pH are less stable.

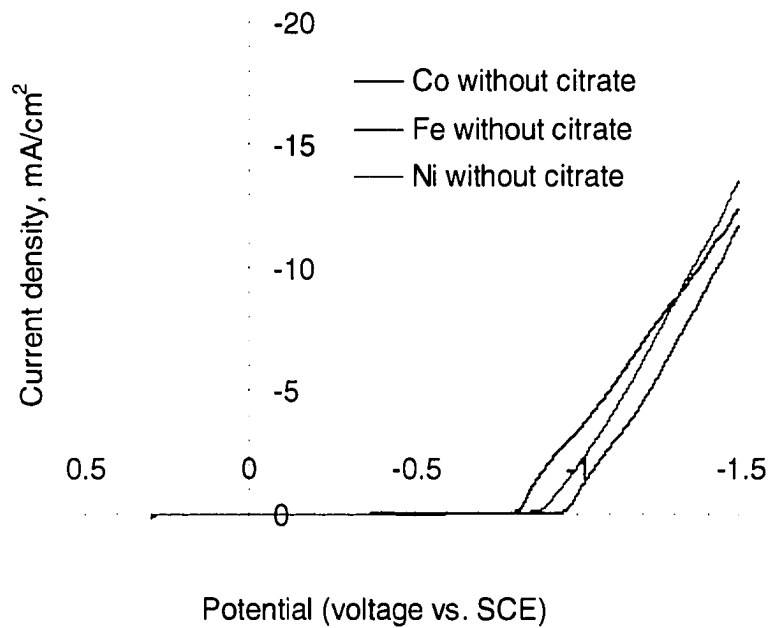
To compare the deposition of Co, Fe and Ni single metals under similar conditions, the above polarization curves are rearranged and summarized in Figures 6-2a, b and c.

For the single metal depositions from citrate-free baths with a low pH of 2.5 (Figure 6-2a), the starting potential for Co deposition (-0.86V) was less negative than those for Ni deposition (-0.91V) and Fe deposition (-1.07V). According to the standard potentials of the metal electrodes (see Appendix 1), the Ni electrode has the least negative potential, and should be deposited first. The shift of Ni deposition to more negative potentials was affected by complicated factors. One factor may be related to the selection of the cathode material. Au-Ni bonding or the formation of Au-Ni bonds may be less favoured, which results in a more negative overpotential for the deposition of the first Ni layer. Zhuang and Podlaha also obtained a more negative starting potential for Ni deposition than that for Co deposition from baths with pH 3.0 using a Cu cylinder as the cathode. [Zhuang00]

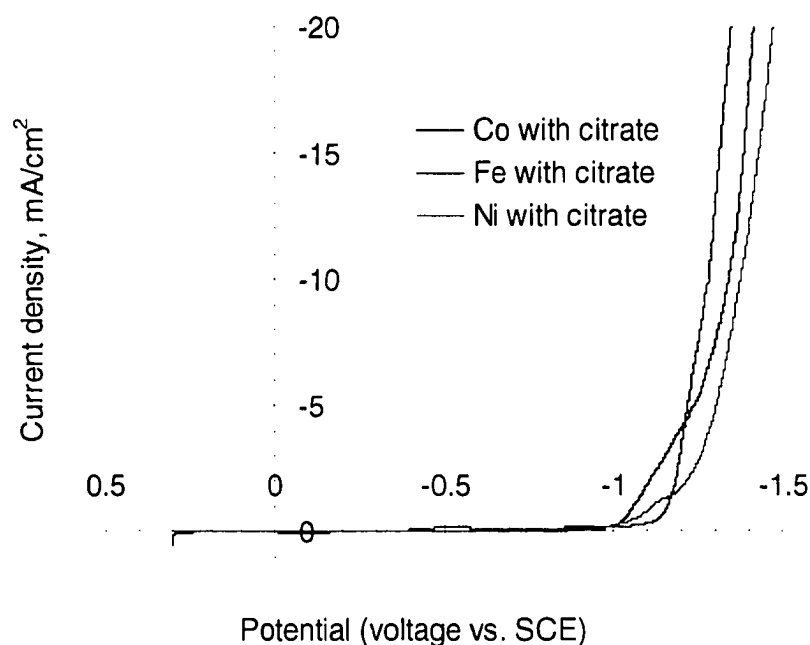
After the depositions started, the deposition behavior for Ni was very close to that for Co.



a. Polarization curves for depositions of Co, Fe and Ni single metals from citrate-free baths with pH 2.5.



b. Polarization curves for depositions of Co, Fe and Ni single metals from citrate-free baths with natural pH.



c. Polarization curves for depositions of Co, Fe and Ni single metals from citrate-added baths.

**Figure 6-2.** Comparisons of polarization curves for Co, Fe and Ni single metal depositions.

The depositions of Co, Fe and Ni single metals from citrate-free baths with natural pH are illustrated in Figure 6-2b. The deposition of Co, Ni and Fe started at about -0.83V, -0.89V and -0.97V, respectively. The deposition of Ni still commenced at a more negative potential than the deposition of Co, just like the situation in low pH baths.

For the depositions of Co, Fe and Ni single metals from citrate-added baths (Figure 6-2c), the deposition of Co, Ni and Fe started at about -1.0V, -1.1V and -1.15V, respectively. After the depositions started, as the potential was shifted to more negative values, the cathodic current density for Fe deposition increased more steeply than the current densities for Co and Ni depositions.

Generally, the deposition of Ni started at a more negative potential than the deposition of Co, and the deposition of Fe commenced at the most negative potential

under the experimental conditions.

## 6.1.2 Polarization curves for CoFe and CoFeNi alloy depositions

### 6.1.2.1 Polarization curves for the deposition of CoFe alloys with high Co content

The polarization curves for the deposition of CoFe alloys with high Co content (compositions around  $Co_{65}Fe_{35}$ ) from different baths are shown in Figure 6-3. The compositions of the employed solutions are listed in Table 6-2.

**Table 6-2.** Compositions of baths employed in the deposition of CoFe alloys with high Co content.

Bath	CoSO <sub>4</sub>	FeSO <sub>4</sub>	Ammonium citrate	H <sub>3</sub> BO <sub>3</sub>	pH
Citrate-free	0.12M	0.048M	0g/L	0.4M	3.9 (Natural)
Citrate-added	0.12M	0.048M	5 g/L (0.0206M)	0.4M	4.4 (Natural)

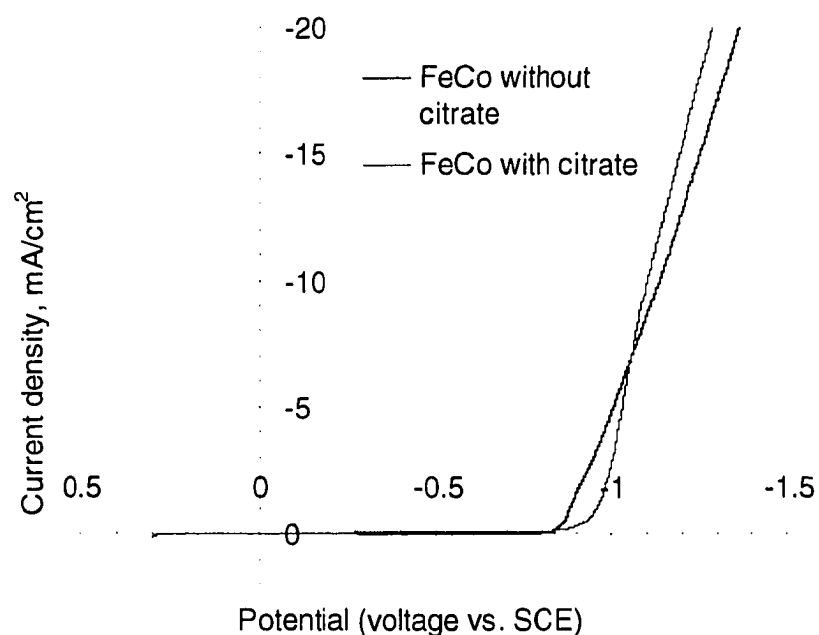


**Figure 6-3.** Polarization curves for the deposition of CoFe alloys with high Co content.

The deposition of CoFe alloys with high Co content from the citrate-free bath (dark line) and the citrate-added bath (purple line) commenced at about -0.84V and -0.93V, respectively. Therefore, similar to the deposition of single Co and Fe metals, the addition of ammonium citrate delayed the occurrence of CoFe alloy deposition to a more negative potential. After CoFe deposition was initiated, as the potential was scanned in negative direction, the cathodic current density for CoFe deposition from the citrate-added bath increased faster than that from the citrate-free bath under the employed experimental conditions.

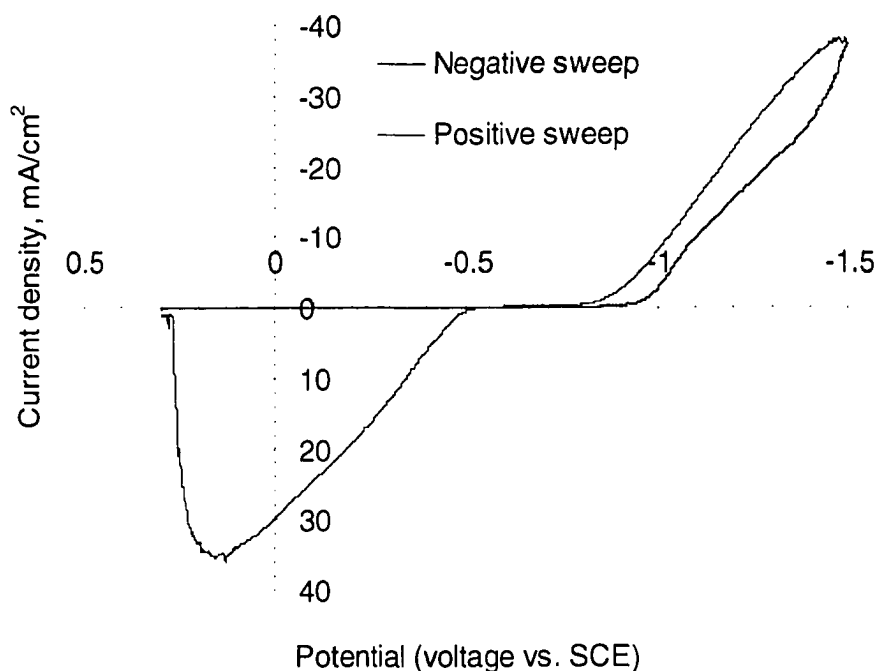


**Figure 6-4.** Cyclic voltammogram for the deposition of CoFe alloy with high Co content from the citrate-added bath.

The cyclic voltammogram for the deposition of CoFe alloy with high Co content from the citrate-added bath is illustrated in Figure 6-4. For the negative sweep (blue line), from a potential of 0.3V to 0V, the anodic current (density) was nearly zero, indicating no oxidation/dissolution of the Au substrate. When the potential was in the range of 0V to

about -0.92V, a minor cathodic current density ( $< 0.5\text{mA/cm}^2$ ) was detected, corresponding to the charging of the electrode double-layer. As the potential shifted to a value more negative than -0.92V, the cathodic current (density) increased quickly with a negative shift in potential due to the codeposition of the CoFe alloy. During the reverse, positive sweep (purple line), the cathodic deposition of the CoFe alloy continued. The cathodic current density (corresponding to the deposition rate), during the positive sweep from -1.5V to about -0.8V, was obviously higher than that for the negative sweep at the same potential. This could be attributed to the significant effect of CoFe nucleation on the negative sweep. The anodic current (density), due to the dissolution of deposited CoFe alloy, started at a potential around -0.50V during the positive sweep.

#### 6.1.2.2 Polarization curves for the deposition of CoFe alloys with high Fe content

The polarization curves for the deposition of CoFe alloys with high Fe content (around  $\text{Co}_{35}\text{Fe}_{65}$ ) from different baths are illustrated in Figure 6-5. The compositions of the employed solutions are shown in Table 6-3.

**Table 6-3.** Compositions of baths employed in the deposition of CoFe alloys with high Fe content.

Bath	$\text{CoSO}_4$	$\text{FeSO}_4$	Ammonium citrate	$\text{H}_3\text{BO}_3$	pH
Citrate-free	0.048M	0.050M	0g/L	0.4M	4.0 (Natural)
Citrate-free	0.048M	0.050M	0g/L	0.4M	2.4
Citrate-added	0.048M	0.096M	5g/L (0.0206M)	0.4M	4.5 (Natural)

The deposition of CoFe alloys with high Fe content from the citrate-free bath with natural pH (dark line), the citrate-free bath with a low pH of 2.4 (blue line) and the citrate-added bath (purple line) commenced at about -0.87V, -0.95V, and -1.0V, respectively. Hence, the addition of citrate delayed the occurrence of the deposition of

CoFe alloys with high Fe content to a more negative potential. Similar to the depositions of single Co and Fe metals (see Figures 6-1a and b), the reduction of hydrogen was detected in the citrate-free bath with a low pH of 2.4.

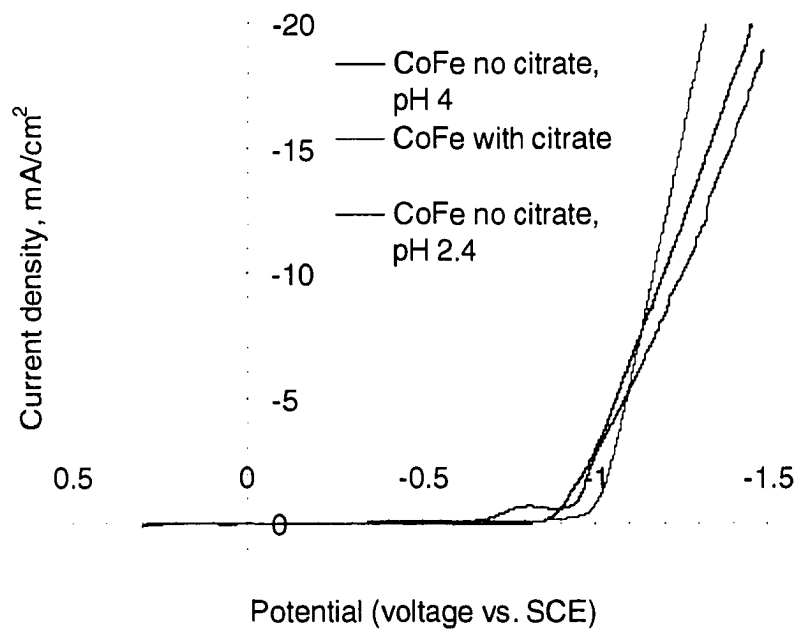


**Figure 6-5.** Polarization curves for the deposition of CoFe alloys with high Fe content.

The cyclic voltammogram for the deposition of CoFe alloy with high Fe content from the citrate-added bath is shown in Figure 6-6. The plot looks similar to the cyclic voltammogram in Figure 6-4. On the negative sweep (blue line), the cathodic current (density) increased sharply after -1.0V, with a negative shift in potential, due to the deposition of CoFe alloy. During the positive sweep (purple line), the cathodic deposition of CoFe alloy continued, while the cathodic current density during the positive sweep from -1.5V to about -0.88V was apparently higher than that for the negative sweep at same potential. This can be attributed to the significant effect of CoFe nucleation on the negative sweep. Anodic current (density) due to the dissolution of the deposited CoFe

alloy commenced at about -0.59V on the positive sweep.

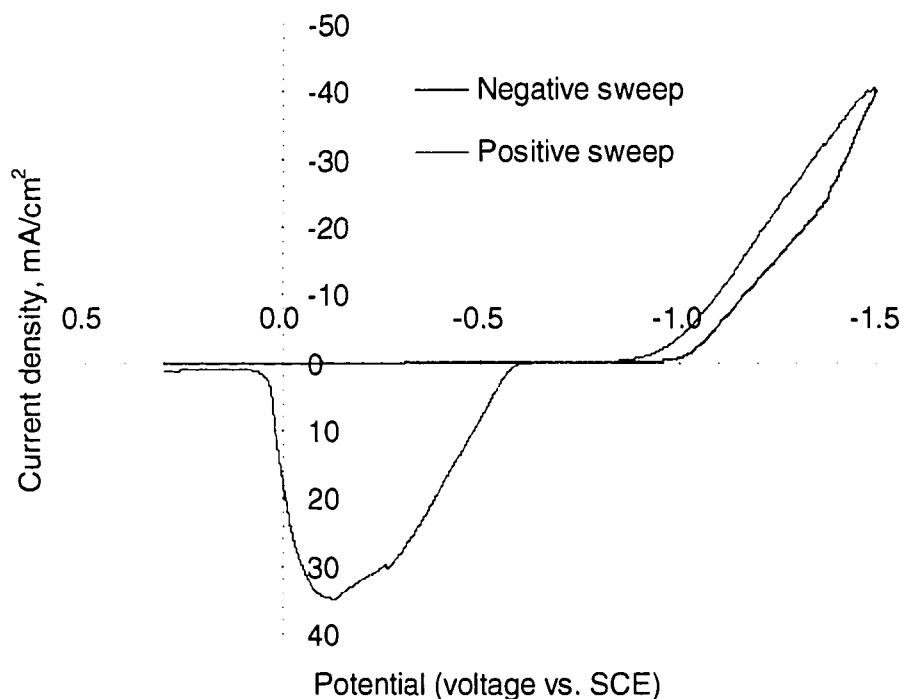


**Figure 6-6.** Cyclic voltammogram for the deposition of CoFe alloy with high Fe content from the citrate-added bath.

### 6.1.2.3 Polarization curves for the deposition of CoFeNi alloys

The polarization curves for CoFeNi alloy deposition from different baths are shown in Figure 6-7. The compositions of the employed solutions are listed in Table 6-4.

**Table 6-4.** Compositions of baths employed in the deposition of CoFeNi alloys.\*

Bath	CoSO <sub>4</sub>	FeSO <sub>4</sub>	NiSO <sub>4</sub>	Ammonium citrate	NH <sub>4</sub> Cl	pH
Citrate-free	0.063M	0.012M	0.20M	0g/L	0.28M	4.1 (Natural)
Citrate-free	0.063M	0.012M	0.20M	0g/L	0.28M	2.8
Citrate-added	0.08M	0.015M	0.30M	50g/L	0 M	5.2 (Natural)

\*0.4M H<sub>3</sub>BO<sub>3</sub> in all baths.

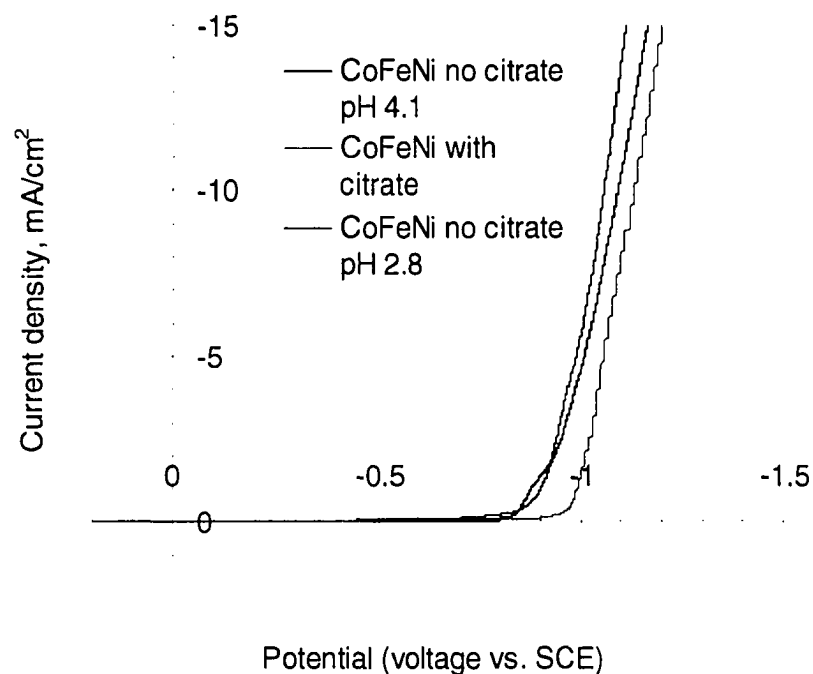


**Figure 6-7.** Polarization curves for the deposition of CoFeNi alloys from different baths.

The deposition of CoFeNi alloys from citrate-free baths, with natural pH (dark line) and a low pH of 2.8 (blue line), commenced at almost an identical potential around -0.84V, and the deposition of CoFeNi alloy from the citrate-added bath (purple line) started at about -0.97V. Apparently, the addition of citrate delayed the occurrence of CoFeNi alloy deposition to a more negative potential. The reduction of hydrogen from the low pH bath was not as obvious as that observed for CoFe alloy deposition (Figure 6-5).

The cyclic voltammogram for the deposition of CoFeNi alloy from the citrate-added bath is illustrated in Figure 6-8. The cathodic current (density) increased quickly after -0.97V during the negative sweep (blue line), due to the deposition of the CoFeNi alloy. During the positive sweep (purple line), the cathodic deposition of CoFeNi alloy continued. The cathodic current density, during the positive sweep from -1.5V to about -0.8V, was obviously higher than that for the negative sweep for same potential. This is

attributed to the significant effect of CoFeNi nucleation on the negative sweep. Anodic current (density) due to the dissolution of the deposited CoFeNi alloy started at about -0.48V during the positive sweep. Since the cathodic charge for CoFeNi alloy deposition is much larger than the anodic charge for CoFeNi alloy dissolution, the CoFeNi alloy can be effectively deposited from the citrate-added bath using the cyclic voltammetry method. This is different from the cyclic voltammograms for the depositions of CoFe alloys (Figures 6-4 and 6-6), which have large anodic charges.

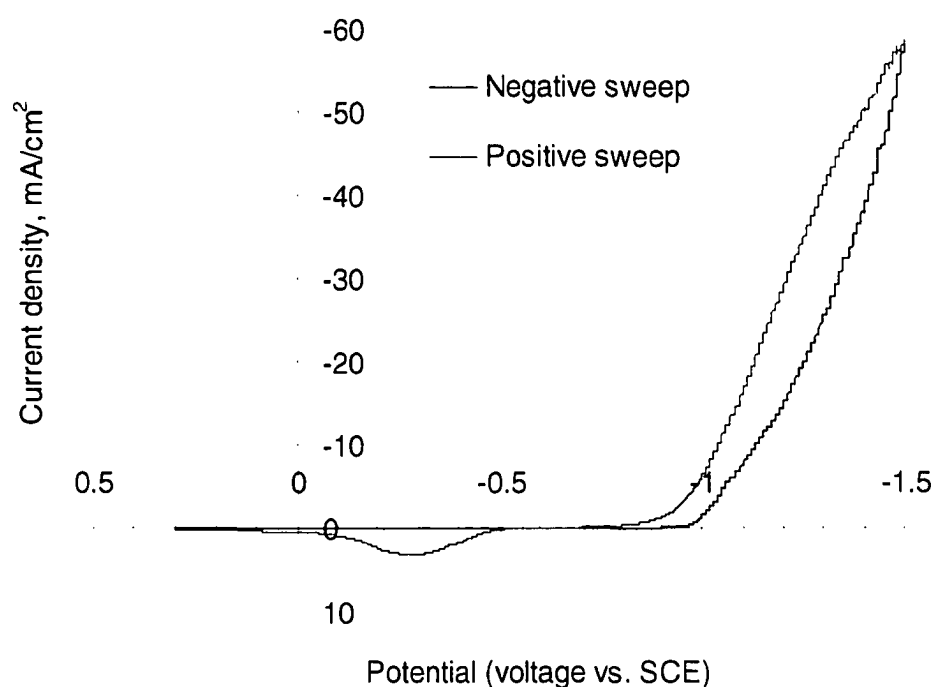


**Figure 6-8.** Cyclic voltammogram for the deposition of CoFeNi alloy from citrate-added bath.

## 6.2 Corrosion properties of electroplated CoFe and CoFeNi films

To understand the effect of citrate addition in plating baths on the corrosion behavior of deposited films, the corrosion properties of CoFe and CoFeNi films plated from citrate-added baths and citrate-free baths were investigated. The corrosion properties of electroplated CoFe and CoFeNi films were determined by anodic polarization in 2.5 wt%

NaCl solution (same solution as used in references [Osaka99-4] [Saito99]) using a 1mV/s potentiodynamic scan. All potentials were referred to the saturated calomel electrode (SCE). A Pt foil was employed as the counter electrode.

The anodic polarization curves for CoFe films with high Co content (composition around  $\text{Co}_{65}\text{Fe}_{35}$ ), electroplated from the citrate-added bath and the citrate-free bath with natural pH (see Table 6.2 - additional 0.01 g/L sodium lauryl sulfate was added), are illustrated in Figure 6-9. The curves are similar to the typical polarization curve for a metal or alloy that displays an active-passive transition as shown in Figure 6-10 [Bradford01]. For a normal metal or alloy, which does not passivate, the polarization curve only has the straightforward “active” form. Therefore, the anodic current density increases quickly with a potential shift in the anodic direction. For the anodic polarization curve of the CoFe film plated from citrate-added bath (blue line), within relatively low potentials (<0mV), the anodic current density increased almost linearly as the potential was scanned in anodic direction, as for normal metals and alloys. This range can be recognized as the “active” region. With increasing potential, the anodic current density suddenly decreased to a significantly lower value, which indicates the passivation of the CoFe alloy, i.e., the formation of a passive layer. As the potential was increased to about 680mV, the anodic current density began to rise again, which indicates the occurrence of pitting corrosion (as indicated by an arrow in the figure). For a metal or alloy, a high pitting corrosion potential and low anodic current density represent excellent corrosion resistance. The CoFe film plated from the citrate-free bath (purple line), had a polarization curve similar to that for the CoFe film plated from the citrate-added bath, and also displayed the passivation phenomenon. Its pitting corrosion potential is around 610mV, which is less anodic than that for the CoFe film plated from the citrate-added bath. Generally, the corrosion resistance of the two CoFe films is similar.

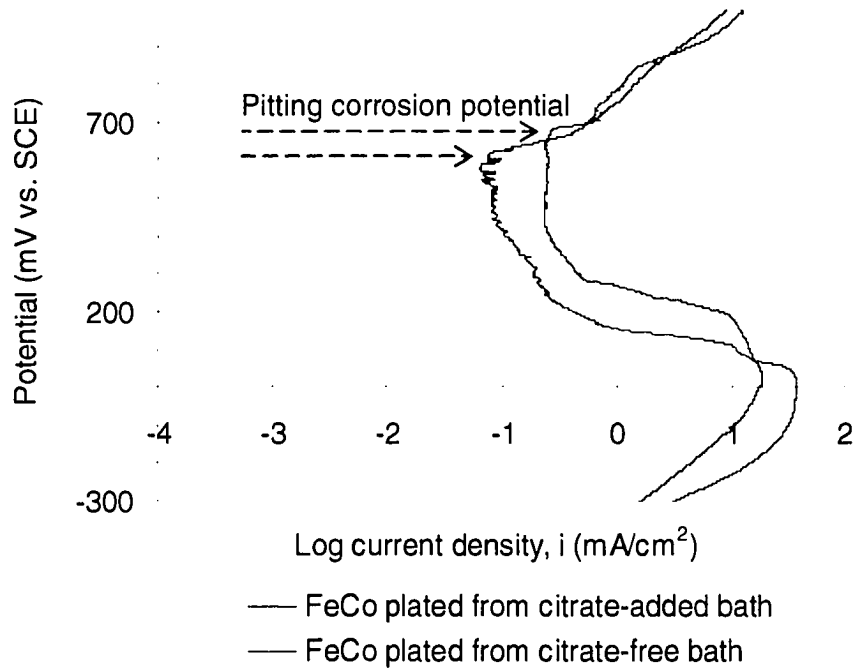


**Figure 6-9.** Anodic polarization curves for CoFe films with high Co content, plated at  $i = 15\text{mA}/\text{cm}^2$ ;  $t_{\text{ON}} = 6\text{ms}$ ;  $t_{\text{ON}} + t_{\text{OFF}} = 10\text{ms}$ ; agitation of 600rpm.

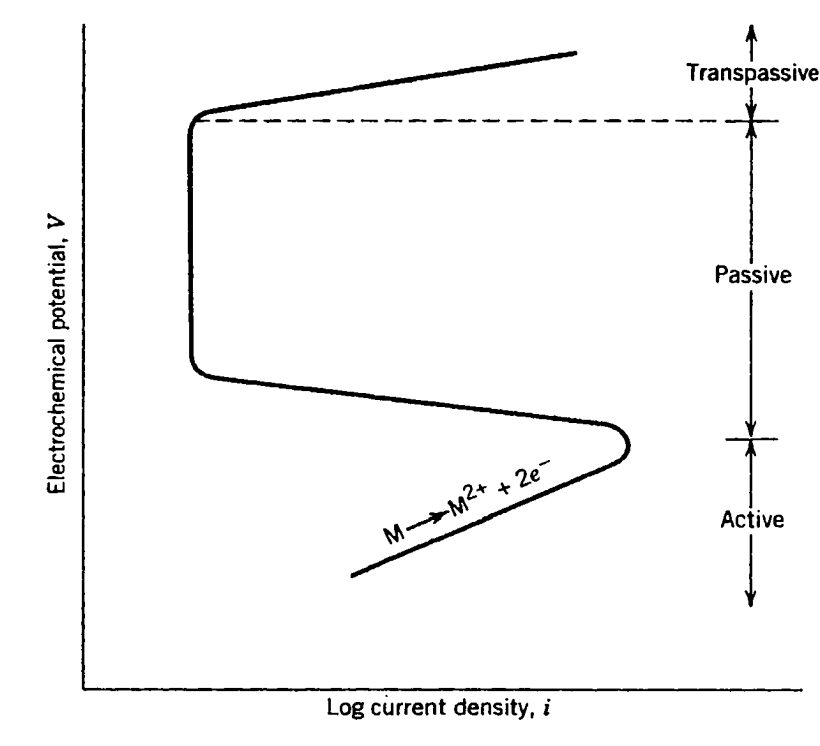


**Figure 6-10.** Schematic polarization curve for a metal or alloy that displays an active-passive transition. [Bradford01]

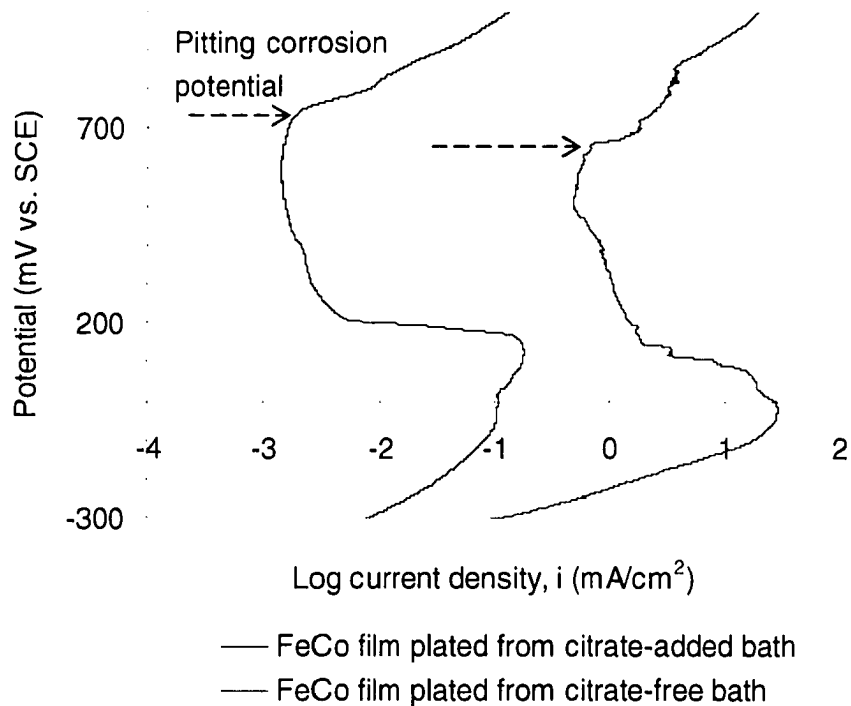


**Figure 6-11.** Anodic polarization curves for CoFe films with high Fe content plated at  $i = 15\text{mA/cm}^2$ ;  $t_{\text{on}} = 6\text{ms}$ ;  $t_{\text{on}} + t_{\text{off}} = 10\text{ms}$ ; agitation of 600rpm.

The anodic polarization curves for CoFe films with high Fe content (composition around  $\text{Co}_{35}\text{Fe}_{65}$ ), deposited from the citrate-added bath and the citrate-free bath with a pH of 2.4 (see Table 6.3 - additional 0.01 g/L sodium lauryl sulfate was added), are shown in Figure 6-11. They both exhibit the passivation phenomenon. The CoFe film plated from the citrate-added bath (blue line) has a higher pitting potential (around 730mV) than the CoFe film plated from the citrate-free bath (around 670mV, purple line), and a much lower anodic current density. This means the CoFe film plated from the citrate-added bath is more resistant to corrosion than the CoFe film plated from the citrate-free bath with low pH.

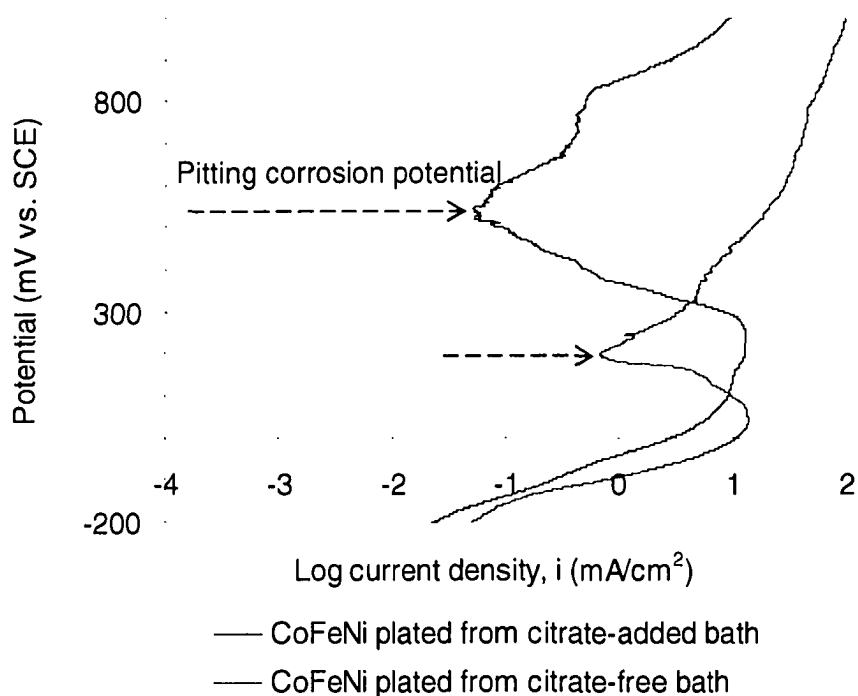


**Figure 6-12.** Anodic polarization curves for CoFeNi films plated at  $i = 6\text{mA/cm}^2$ ;  $t_{\text{on}} = 0.3\text{ms}$ ;  $t_{\text{on}} + t_{\text{off}} = 10\text{ms}$ ; agitation 600rpm.

The anodic polarization curves for CoFeNi films plated from the citrate-added bath and the citrate-free bath with a pH of 2.8 (see Table 6.4 - additional 0.01 g/L sodium lauryl sulfate was added) are illustrated in Figure 6-12. Unlike the CoFe films, they both exhibit an abrupt shift for the passive-transpassive transition. The CoFeNi film plated from the citrate-added bath (blue line) has a much higher pitting potential (around 550mV) than the CoFeNi film plated from the citrate-free bath (only around 190mV, purple line), and a lower anodic current density in the transpassive region. Therefore, the CoFeNi film plated from the citrate-added bath is more resistant to corrosion than the CoFeNi film plated from the citrate-free bath with low pH.

In general, for all the CoFe and CoFeNi films investigated, passivation phenomena were observed during anodic polarizations. CoFe and CoFeNi films plated from citrate-added baths exhibited better corrosion resistance. This may be attributed to the

denser deposits achieved by plating with citrate-added baths of relatively high pH levels.

### **6.3 Summary**

The addition of ammonium citrate delayed the occurrence of deposition of Co, Fe and Ni single metals to more negative potentials, which reflects the complexing effects of citrate ions on the metal ions. For the citrate-free baths, the bath with the higher pH (natural pH) was more beneficial for metal deposition.

For the deposition of Co, Fe and Ni single metals, the deposition of Ni started at a more negative potential than the deposition of Co, and the deposition of Fe commenced at the most negative potential under the experimental conditions studied.

Similar to the deposition of single metals, the addition of ammonium citrate also delayed the occurrence of the deposition of CoFe and CoFeNi alloys to more negative potentials.

During CV sweeps, the cathodic charge for CoFeNi alloy deposition from the citrate-added bath was much larger than the anodic charge for CoFeNi alloy dissolution. Therefore, CoFeNi alloys can be effectively deposited from the citrate-added bath using the cyclic voltammetry method. The situation is different for the cyclic voltammograms for the deposition of CoFe alloys, which have large anodic charges.

Generally, the CoFe and CoFeNi films plated from citrate-added baths exhibited better corrosion resistance. This may be attributed to the denser deposits achieved by plating with citrate-added baths of relatively high pH levels. For all the CoFe and CoFeNi films studied, passivation phenomena were observed during anodic polarization.

## **Chapter 7 Phase formation in electroplated CoFe and CoFeNi thin films**

The magnetic properties of electroplated CoFe and CoFeNi films are determined by their chemical composition, phase formation, microstructure and plating conditions. According to the studies of many researchers [Osaka98-1] [Osaka98-2] [Tabakovic02] [Liu03], to obtain optimal soft magnetic properties, the co-deposition of fcc and bcc phases in electroplated CoFe and CoFeNi films is necessary. The competition of crystallization between different phases will lead to finer grain sizes, which result in lower coercivity  $H_c$  [Herzer90], i.e., softer magnetic properties. In this study, thin film XRD and TEM methods were employed to analyze the phase formation and grain sizes in electroplated CoFe and CoFeNi deposits.

### **7.1 Thin film X-ray diffraction**

According to several studies [Tabakovic02] [Liu03], for electrodeposited CoFe and CoFeNi alloys, the major XRD peaks for fcc and bcc phases are fcc (111) at around  $2\theta = 44.1^\circ$  and bcc (110) at around  $2\theta = 45.2^\circ$ .

#### **7.1.1 Thin film XRD study of electrodeposited CoFe films**

The effects of film composition (Fe content) and electrolyte composition on the phase formation in deposited CoFe films have been studied using thin film XRD.

##### *7.1.1.1 Effect of Fe content on phase formation in deposited CoFe films*

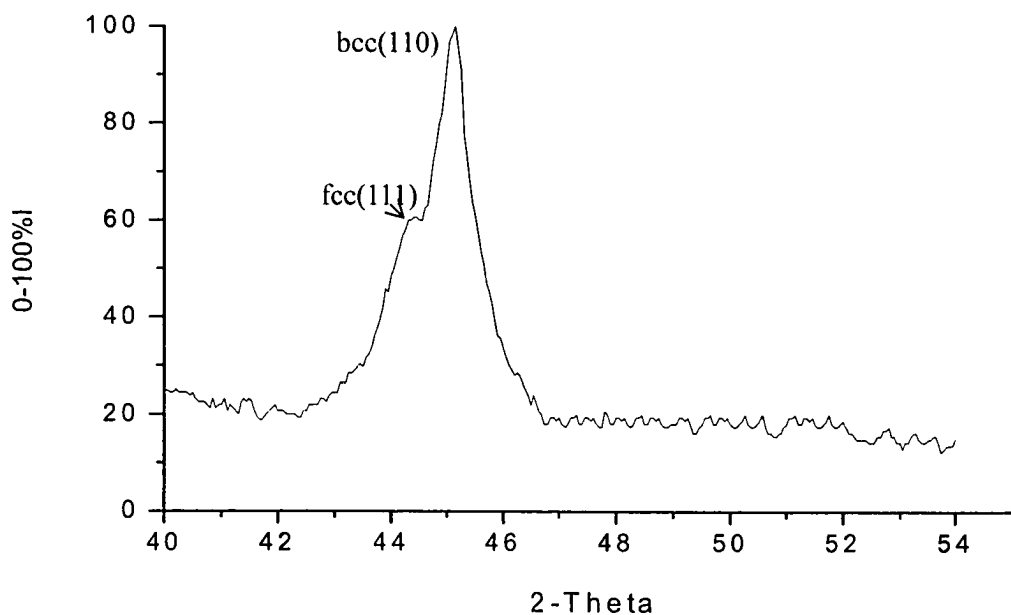
The thin film XRD spectra of CoFe films with different Fe contents (from 29-69 at%), electroplated from citrate-added baths (refer to Table 7-1) at  $i = 15 \text{ mA/cm}^2$ ,  $t_{\text{on}} = 6 \text{ ms}$ ,  $t_{\text{on}} + t_{\text{off}} = 10 \text{ ms}$  and agitation of 600rpm, are shown in Figures 7-1a-d. Under the employed

conditions, the fcc(111)/bcc(110) intensity ratio (corresponding to the fcc/bcc phase ratio) increases with Fe content increase in the deposited film. When the Fe content is 69at% (Figure 7-1d), only the pure fcc phase is detected. Therefore, Fe content affects the phase formation in deposited CoFe films. The thin film XRD spectra demonstrate that fcc and bcc phases can be co-deposited in electroplated CoFe films at specific Fe contents.

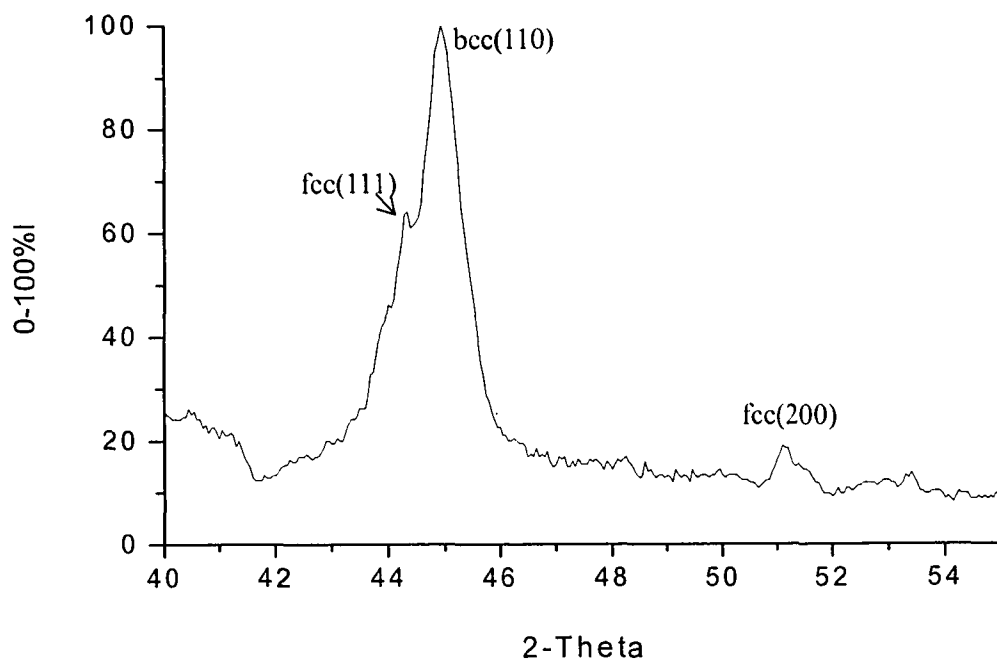
**Table 7-1.** Composition of electrolyte for plating a  $\text{Co}_{71}\text{Fe}_{29}$  thin film whose XRD spectrum is shown in Figure 7-1a.

Chemical	Concentration	Chemical	Concentration
$\text{CoSO}_4 \cdot 7\text{H}_2\text{O}$	0.120 M	$\text{H}_3\text{BO}_3$	0.4 M
$\text{FeSO}_4 \cdot 7\text{H}_2\text{O}$	0.030 M*	Sodium lauryl sulfate	0.01 g/L
Natural pH~4.4		Ammonium citrate	5 g/L

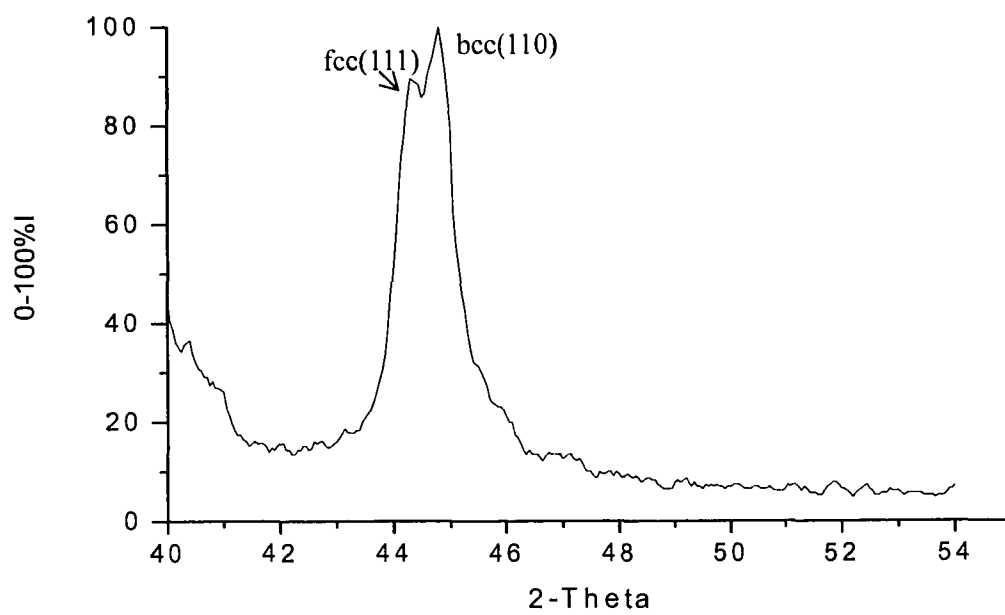
\* Fe concentration in bath was varied to deposit CoFe films with different Fe contents.



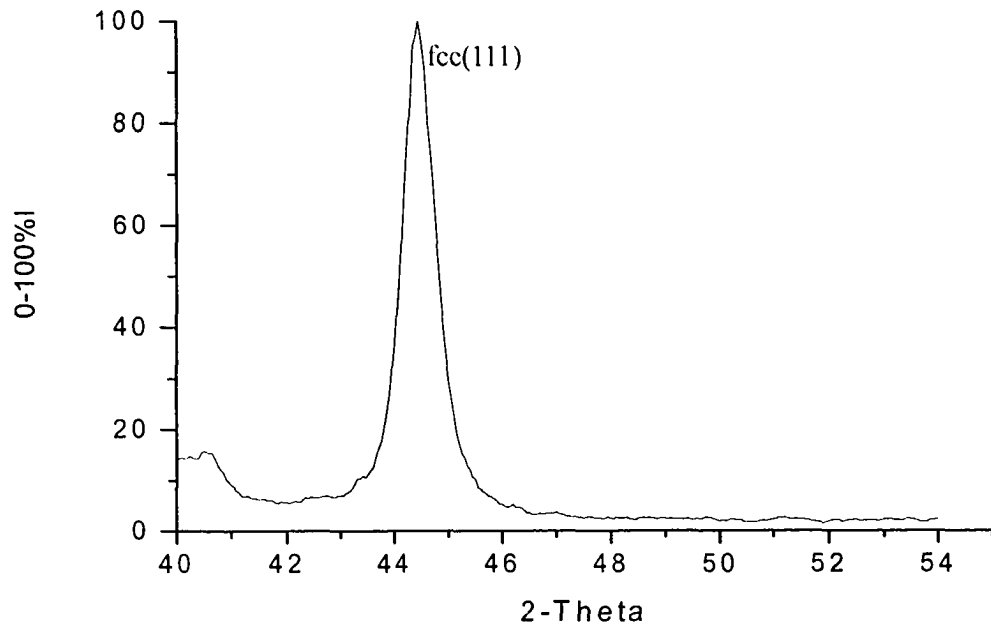
a.  $\text{Co}_{71}\text{Fe}_{29}$  film plated from bath with composition listed in Table 7-1.



b. Film composition  $\text{Co}_{65}\text{Fe}_{35}$ .



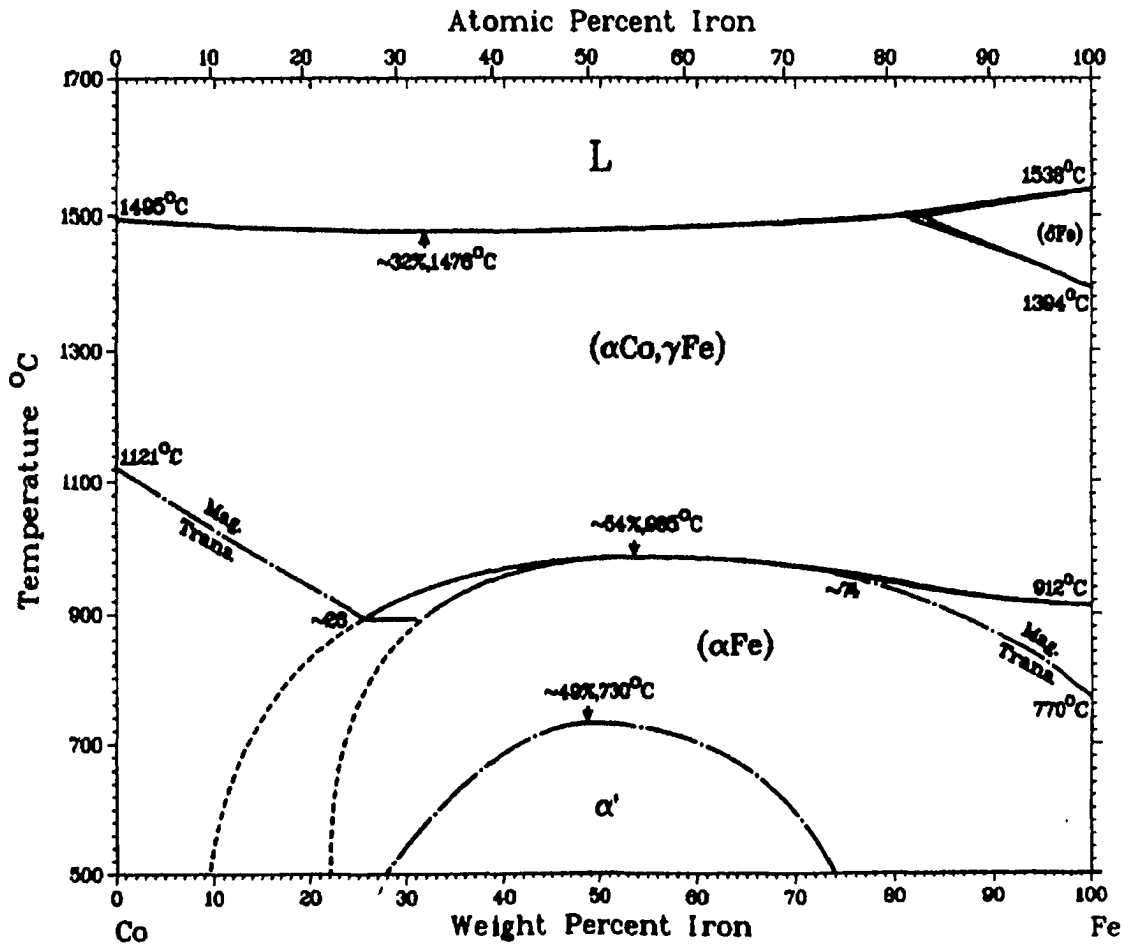
c. Film composition  $\text{Co}_{50}\text{Fe}_{50}$ .



d. Film composition  $\text{Co}_{31}\text{Fe}_{69}$ .

**Figure 7-1.** Thin film XRD spectra of CoFe films with different Fe contents electroplated at  $i = 15\text{mA/cm}^2$ ,  $t_{\text{on}} = 6\text{ms}$ ,  $t_{\text{on}} + t_{\text{off}} = 10\text{ms}$  and agitation of 600rpm.

The phase diagram for the Co-Fe system is illustrated in Figure 7-2 [Baker92]. At room temperature, the  $\alpha'$  phase (CsCl type structure) is stable for Co-Fe alloys with Fe contents from 29-69 at%. The XRD results obtained here demonstrate that the bcc ( $\alpha(\text{Fe})$ ) and fcc ( $\gamma(\text{Fe})/\alpha(\text{Co})$ ) phases or the fcc ( $\gamma(\text{Fe})$ ) phase alone are formed in the electrodeposited CoFe films containing 29 to 69 at% of Fe. Therefore, phase formation in the electroplated CoFe films is controlled by kinetic conditions, i.e., phase formation deviates from equilibrium conditions. This result is not surprising, as the deposition rates under the current conditions utilized here do not provide sufficient time for ordering of the Co and Fe atoms on specific lattice positions to form the ordered  $\alpha'$  phase. Other researchers have also electrodeposited CoFe films with only bcc and/or fcc phases, and without the  $\alpha'$  phase. [Liu00-1] [Myung01]



Phase	Composition, wt% Fe	Pearson symbol	Space group
(αCo, γFe)	0 to 100	<i>cF4</i>	<i>Fm<math>\bar{3}m</math></i>
α'	~28 to ~74	<i>cP2</i>	<i>Pm<math>\bar{3}m</math></i>
(αFe)	~22 to 100	<i>cI2</i>	<i>Im<math>\bar{3}m</math></i>
(δFe)	82 to 100	<i>cI2</i>	<i>Im<math>\bar{3}m</math></i>
<b>Metastable phase</b>			
η	0.5 to 5.7	<i>hP4</i>	<i>P6<math>_3</math>/mmc</i>

Figure 7-2. Phase diagram for the Co-Fe system. [Baker92]

### 7.1.1.2 Effect of electrolyte composition on phase formation in deposited CoFe films

The XRD spectrum for a CoFe film with a composition around  $\text{Co}_{71}\text{Fe}_{29}$ , electroplated from a citrate-added bath (bath composition is listed in Table 7-2), is shown in Figure 7-3. This film has almost the same composition as the CoFe film (see Figure 7-1a) deposited from a bath whose composition is listed in Table 7-1. The main difference between these two baths is the metal concentrations; however, they have the same Co/Fe concentration ratio of 4:1. Figure 7-1a has a bcc(110)/fcc(111) intensity ratio higher than 1, while Figure 7-3 has a bcc(110)/fcc(111) intensity ratio lower than 1 and a small fcc(200) peak. Therefore, the metal concentration in plating bath, i.e., the bath composition, affects the phase formation of deposited CoFe films.

**Table 7-2.** Composition of electrolyte for plating a  $\text{Co}_{71}\text{Fe}_{29}$  thin film whose XRD spectrum is shown in Figure 7-3.

Chemical	Concentration	Chemical	Concentration
$\text{CoSO}_4 \cdot 7\text{H}_2\text{O}$	0.192 M	$\text{H}_3\text{BO}_3$	0.4 M
$\text{FeSO}_4 \cdot 7\text{H}_2\text{O}$	0.048 M	Sodium lauryl sulfate	0.01 g/L
Natural pH~4.3		Ammonium citrate	5 g/L

Figure 7-4 shows the XRD spectrum for a CoFe film with a composition around  $\text{Co}_{62}\text{Fe}_{38}$ , electroplated from a bath containing 50g/L ammonium citrate (refer to Table 3-4 - with no  $\text{NiSO}_4$  addition). The plating conditions were  $i = 6\text{mA}/\text{cm}^2$ ,  $t_{\text{on}} = 0.3\text{ms}$ ,  $t_{\text{on}} + t_{\text{off}} = 10\text{ms}$  and agitation of 600rpm. This spectrum is very different from the spectrum for the  $\text{Co}_{65}\text{Fe}_{35}$  film shown in Figure 7-1b (the sample in Figure 7-4 has significantly more fcc phase), even though the two CoFe films have similar compositions. Therefore, differences in bath composition (such as different citrate dosage) and operation parameters affect the phase formation in deposited CoFe films.

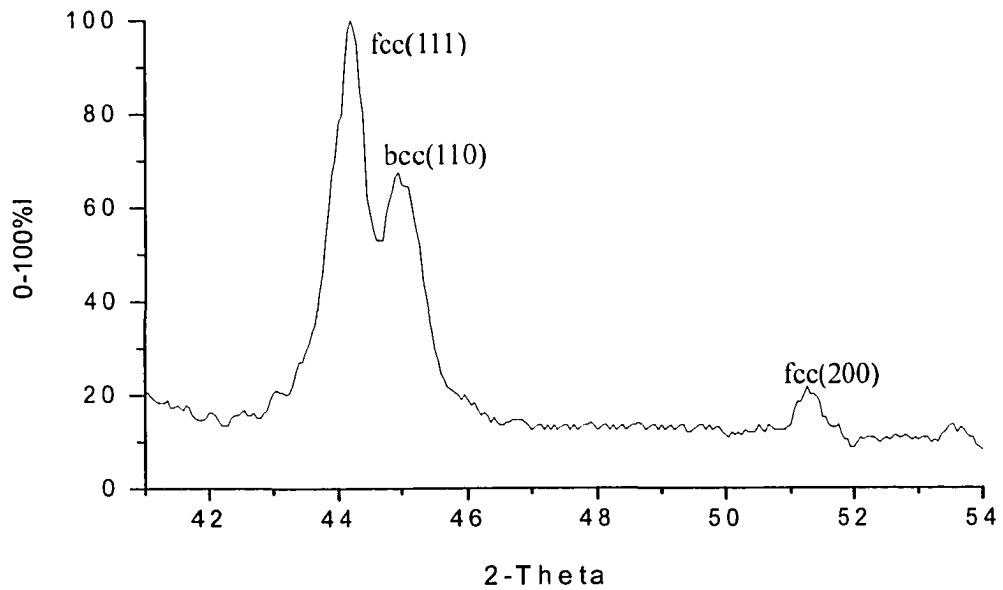


**Figure 7-3.** Thin film XRD spectrum of  $\text{Co}_{71}\text{Fe}_{29}$  film plated at  $i = 15\text{mA}/\text{cm}^2$ ,  $t_{\text{on}} = 6\text{ms}$ ,  $t_{\text{on}} + t_{\text{off}} = 10\text{ms}$  and agitation of 600rpm. Bath composition is listed in Table 7-2.

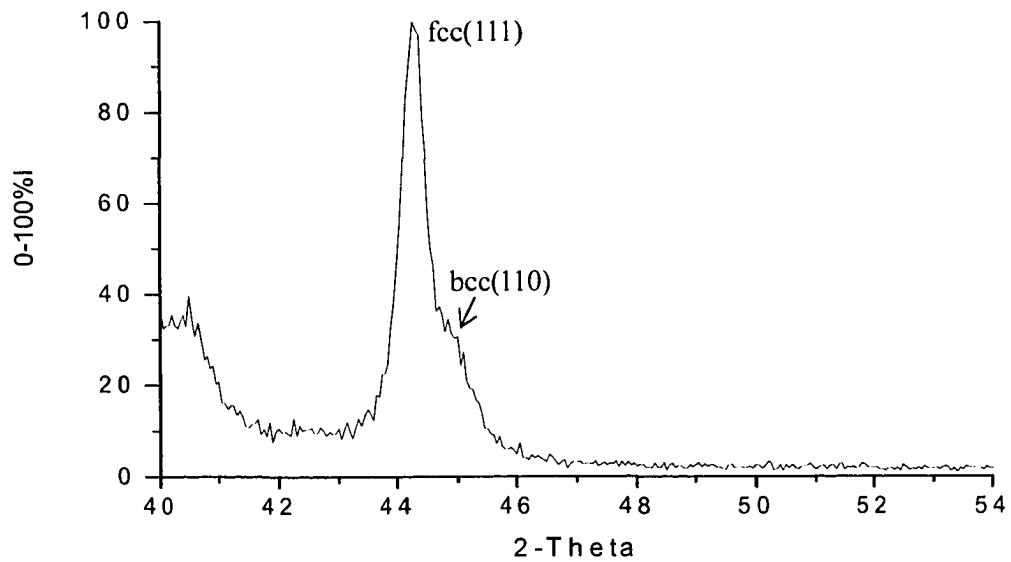


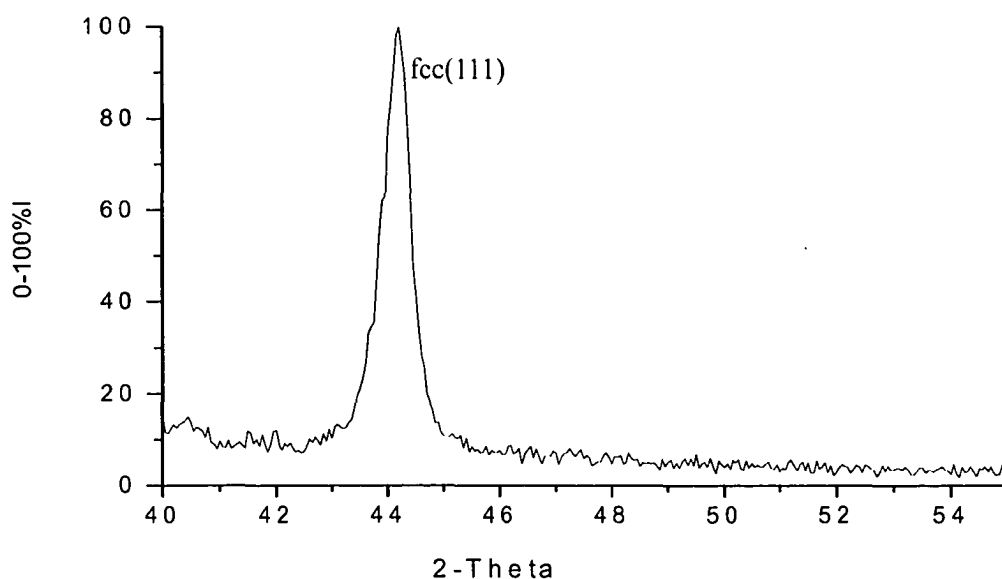
**Figure 7-4.** Thin film XRD spectrum of CoFe film plated at ammonium citrate dosage of 50g/L,  $i = 6\text{mA}/\text{cm}^2$ ,  $t_{\text{on}} = 0.3\text{ms}$ ,  $t_{\text{on}} + t_{\text{off}} = 10\text{ms}$  and agitation of 600rpm. Film composition is  $\text{Co}_{62}\text{Fe}_{38}$ .

### 7.1.2 Thin film XRD study of electrodeposited CoFeNi films

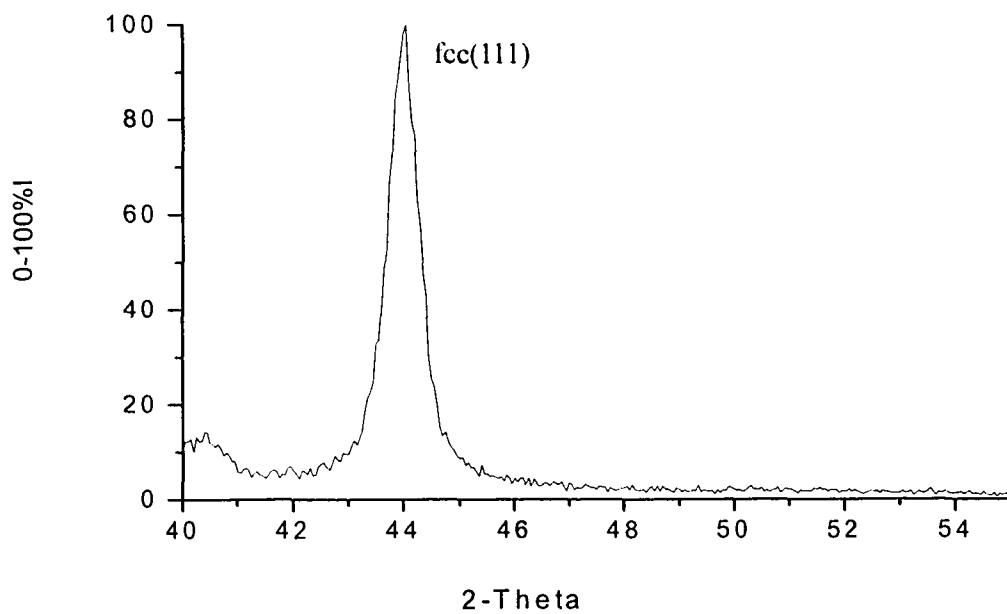
In this study, the effects of film composition (Fe content) and electrolyte composition on phase formation in CoFeNi films, electroplated from citrate-added baths and citrate-free baths, have been investigated.

#### 7.1.2.1 Phase formation in CoFeNi films deposited from citrate-added baths

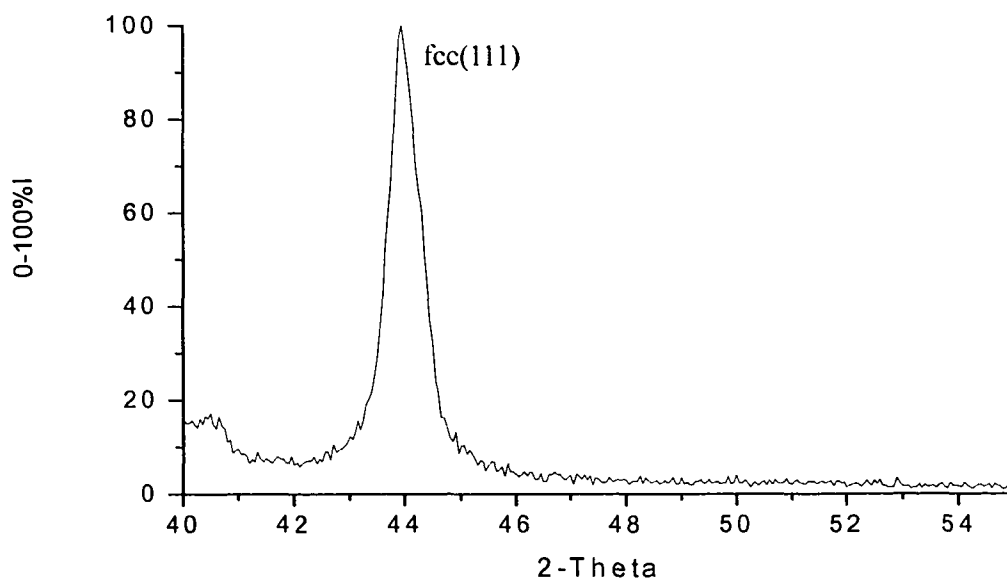
The thin film XRD spectra of representative CoFeNi films with Ni content of 9-11at%, electroplated from citrate-added baths containing 50g/L ammonium citrate (refer to Table 3-4 with varied Fe concentration) at  $i = 6\text{mA/cm}^2$ ,  $t_{\text{on}} = 0.3\text{ms}$ ,  $t_{\text{off}} = 9.7\text{ms}$ , and agitation of 600rpm, are illustrated in Figures 7-5a to f. Under the employed conditions, only the fcc phase is formed in deposited films as the Fe content is low (<20 at%). Fcc and bcc phases are co-deposited in films with Fe contents higher than 21 at%. The bcc(110)/fcc(111) intensity ratio (corresponding roughly to the bcc/fcc phase ratio) increases as the Fe content increases in deposited films. This is consistent with the literature. [Osaka00-1] [Liu03] Hence, the phase formation in CoFeNi films plated



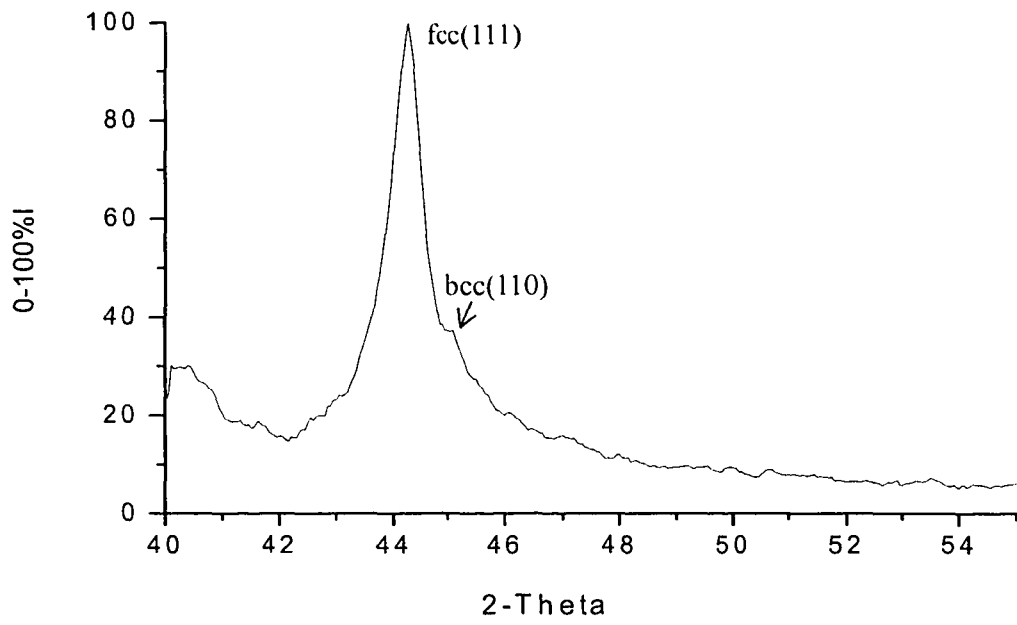
a. Film composition is  $\text{Co}_{79}\text{Fe}_{10}\text{Ni}_{11}$ .



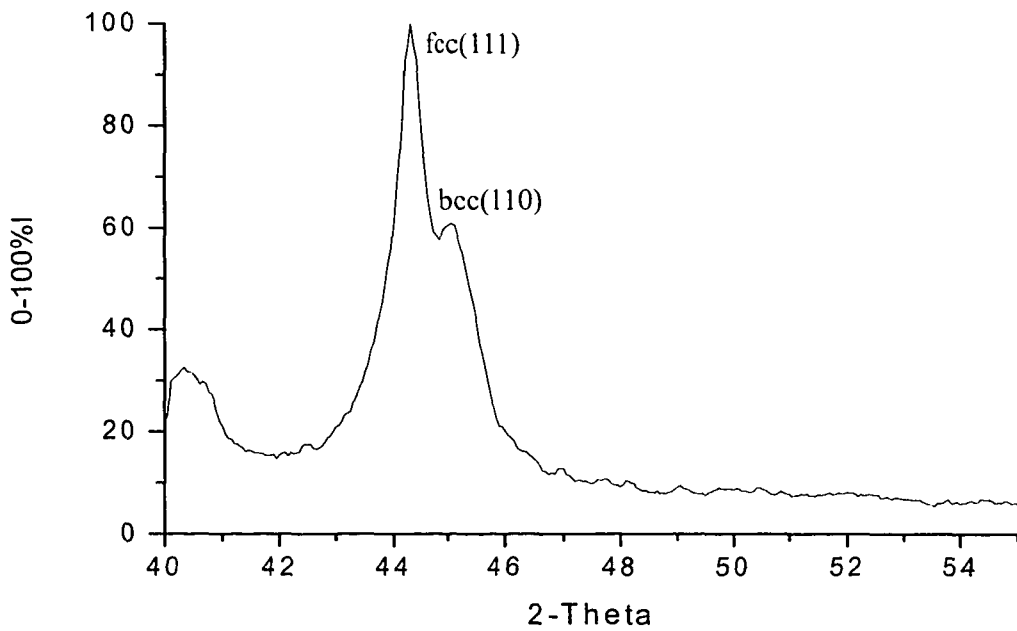
b. Film composition is  $\text{Co}_{71}\text{Fe}_{18}\text{Ni}_{11}$ .



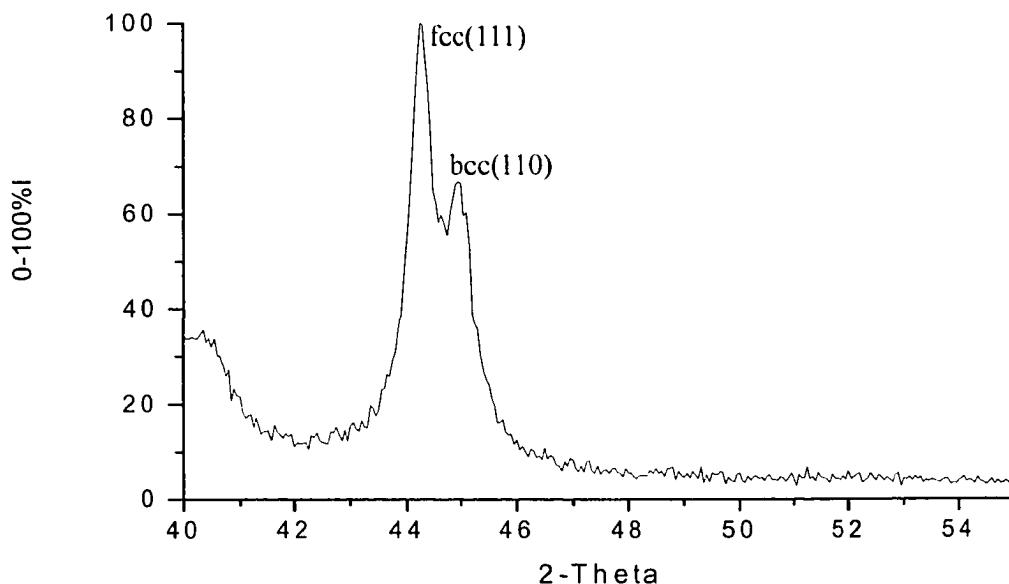
c. Film composition is  $\text{Co}_{71}\text{Fe}_{20}\text{Ni}_9$ .



d. Film composition is  $\text{Co}_{68}\text{Fe}_{21}\text{Ni}_{11}$ .



e. Film composition is  $\text{Co}_{65}\text{Fe}_{24}\text{Ni}_{11}$ .



f. Film composition is  $\text{Co}_{61}\text{Fe}_{28}\text{Ni}_{11}$ .

**Figure 7-5.** Thin film XRD spectra of representative CoFeNi films plated from citrate-added baths, with ammonium citrate dosage 50g/L, at  $i = 6\text{mA}/\text{cm}^2$ ,  $t_{\text{on}} = 0.3\text{ms}$ ,  $t_{\text{on}} + t_{\text{off}} = 10\text{ms}$  and agitation of 600rpm.

from citrate-added baths is affected by Fe content. The effect of Fe content in CoFeNi films is opposite to the effect in CoFe films where the amount of fcc increases with increasing Fe content.

Figure 7-6 illustrates the XRD spectrum for a CoFeNi film with a composition of  $\text{Co}_{61}\text{Fe}_{28}\text{Ni}_{11}$  electroplated from a citrate-added bath, with 5g/L ammonium citrate (bath composition is listed in Table 7-3), at  $i = 12\text{mA}/\text{cm}^2$ ,  $t_{\text{on}} = 9\text{ms}$ ,  $t_{\text{off}} = 6\text{ms}$  and agitation of 600rpm. Only the bcc phase was detected in this film. The film shown in Figure 7-5f, with the same composition of  $\text{Co}_{61}\text{Fe}_{28}\text{Ni}_{11}$ , contains both fcc and bcc phases and was deposited from a bath with 50g/L ammonium citrate at  $i = 6\text{mA}/\text{cm}^2$ ,  $t_{\text{on}} = 0.3\text{ms}$ ,  $t_{\text{on}} + t_{\text{off}} = 10\text{ms}$  and agitation of 600rpm. Therefore, changing the bath composition (different citrate dosage) and operating parameters will affect phase formation in electroplated CoFeNi films.

The above study demonstrates that fcc and bcc phases can be co-deposited by controlling the plating bath composition and/or the plating conditions.

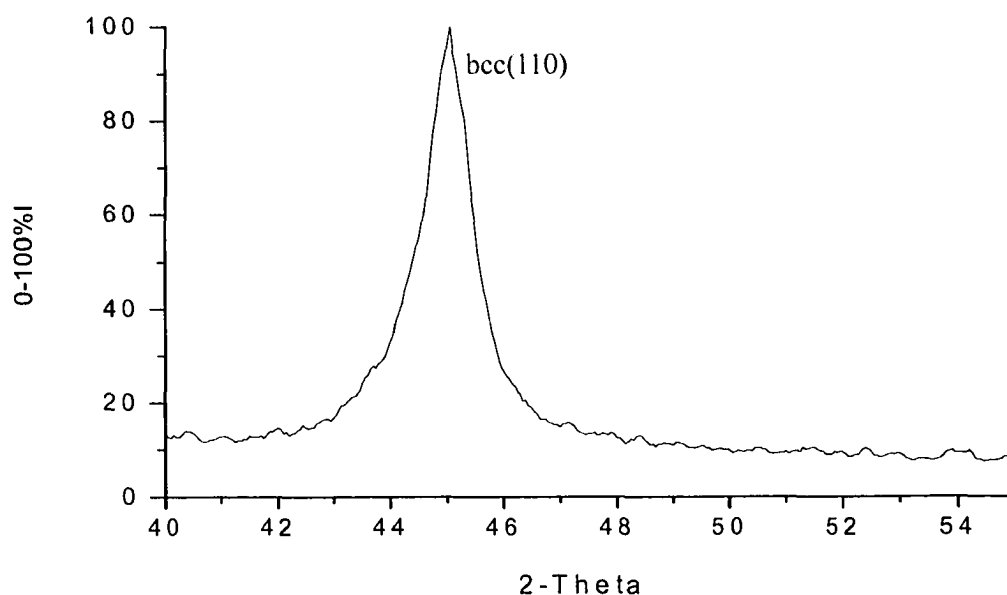


**Figure 7-6.** Thin film XRD spectrum of CoFeNi film plated from citrate-added bath, with ammonium citrate dosage 5 g/L, at  $i = 12\text{mA}/\text{cm}^2$ ,  $t_{\text{on}} = 9\text{ms}$  and  $t_{\text{off}} = 6\text{ms}$ . Film composition is  $\text{Co}_{61}\text{Fe}_{28}\text{Ni}_{11}$ .

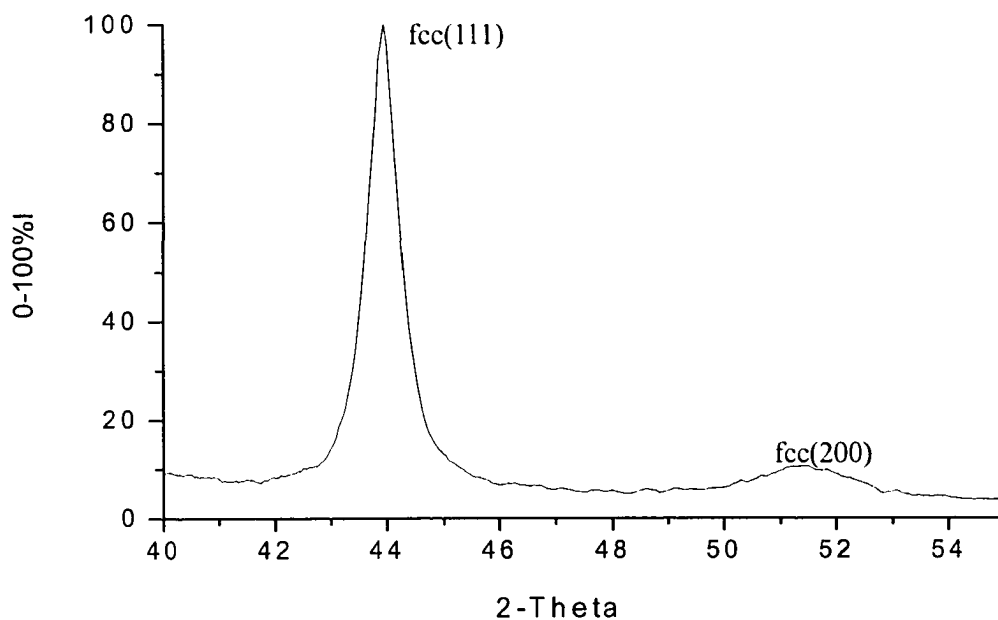
**Table 7-3.** Composition of electrolyte for plating  $\text{Co}_{61}\text{Fe}_{28}\text{Ni}_{11}$  thin film whose XRD spectrum is shown in Figure 7-6.

Chemical	Concentration	Chemical	Concentration
$\text{CoSO}_4 \cdot 7\text{H}_2\text{O}$	0.120 M	$\text{H}_3\text{BO}_3$	0.4 M
$\text{FeSO}_4 \cdot 7\text{H}_2\text{O}$	0.034 M	Sodium lauryl sulfate	0.01 g/L
$\text{NiSO}_4 \cdot 6\text{H}_2\text{O}$	0.3 M	Ammonium citrate	5 g/L
Bath pH 4.2 (natural)			

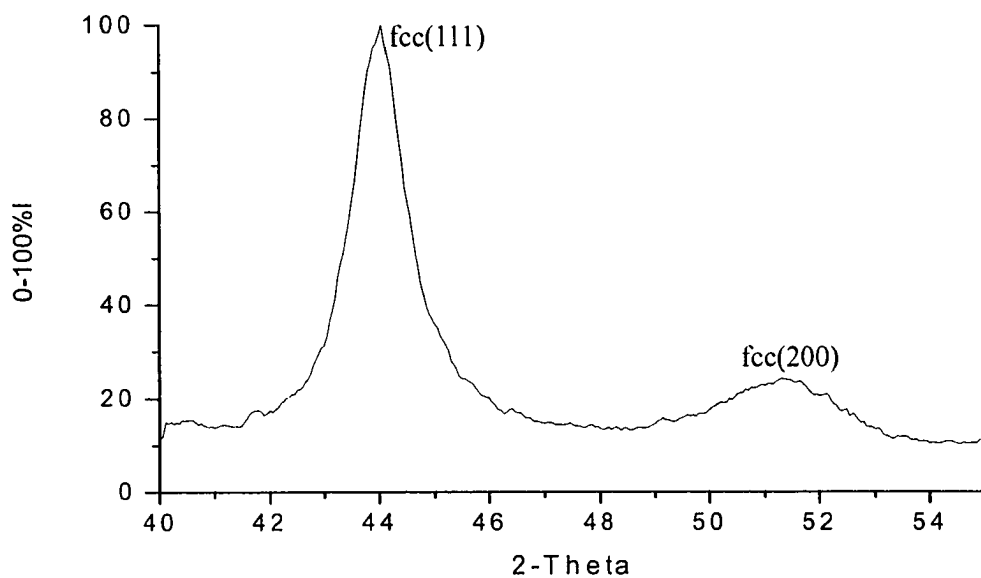
#### 7.1.2.2 Phase formation in CoFeNi films deposited from citrate-free baths

The thin film XRD spectra of CoFeNi films with ~12at% Ni and different Fe contents, electroplated from citrate-free baths (refer to Table 3-3 with varied Fe concentration)

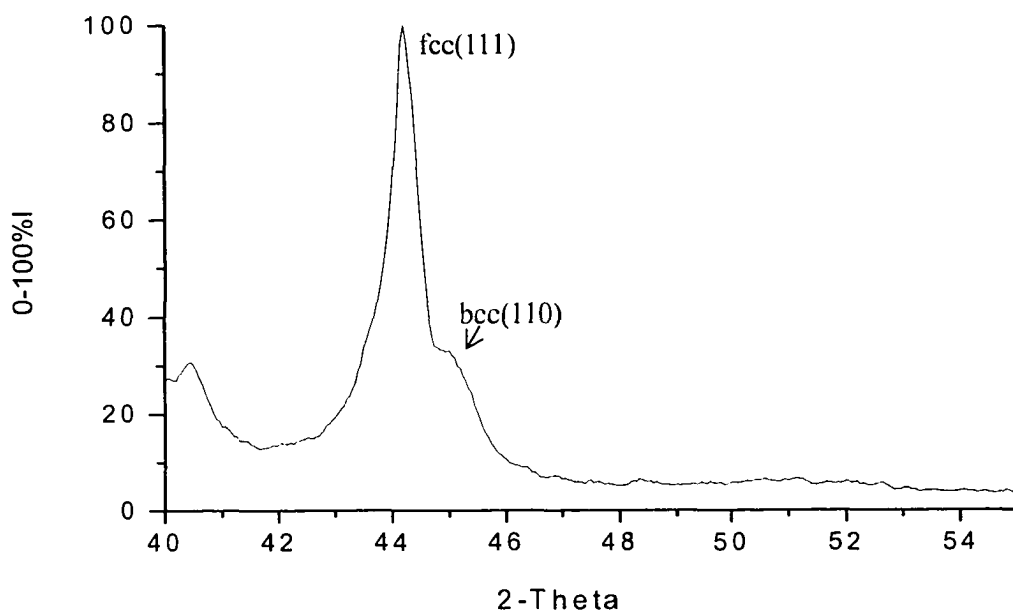
under different conditions, are illustrated in Figure 7-7.



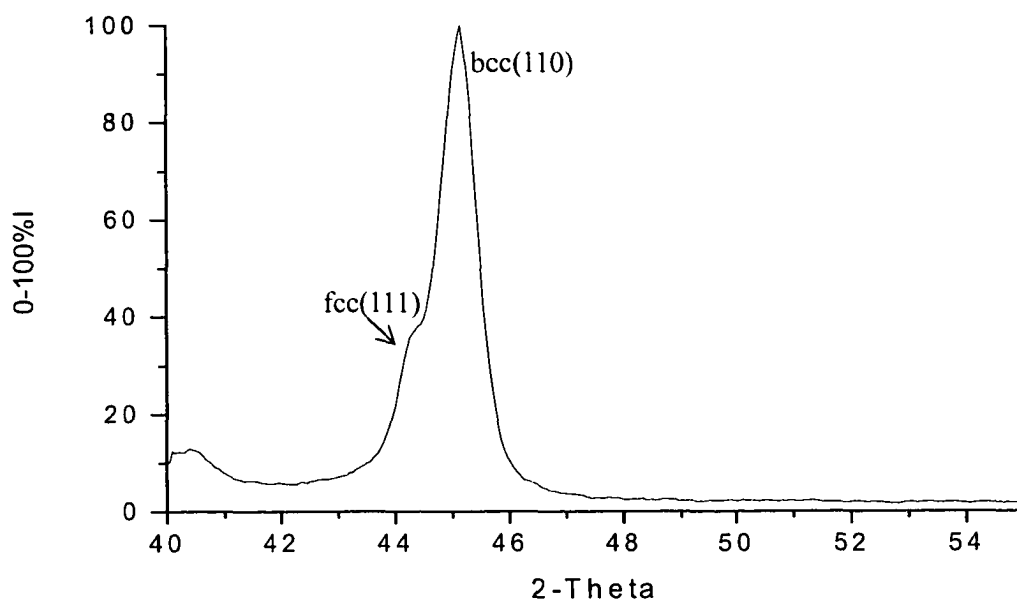
a. CoFeNi film plated from citrate-free bath with natural pH at  $i = 6\text{mA/cm}^2$ ,  $t_{\text{on}} = 0.3\text{ms}$ ,  $t_{\text{on}} + t_{\text{off}} = 10\text{ms}$  and agitation of 600rpm. Film composition is  $\text{Co}_{66}\text{Fe}_{21}\text{Ni}_{13}$ .



b. CoFeNi film plated from citrate-free bath with  $\text{pH} = 2.7$  at  $i = 6\text{mA/cm}^2$ ,  $t_{\text{on}} = 0.3\text{ms}$ ,  $t_{\text{on}} + t_{\text{off}} = 10\text{ms}$  and agitation of 600rpm. Film composition is  $\text{Co}_{64}\text{Fe}_{24}\text{Ni}_{12}$ .



c. CoFeNi film plated from citrate-free bath with pH=2.7 at  $i = 10\text{mA/cm}^2$ ,  $t_{\text{on}}=0.3\text{ms}$ ,  $t_{\text{on}} + t_{\text{off}}=10\text{ms}$  and agitation of 600rpm. Film composition  $\text{Co}_{61}\text{Fe}_{27}\text{Ni}_{12}$ .

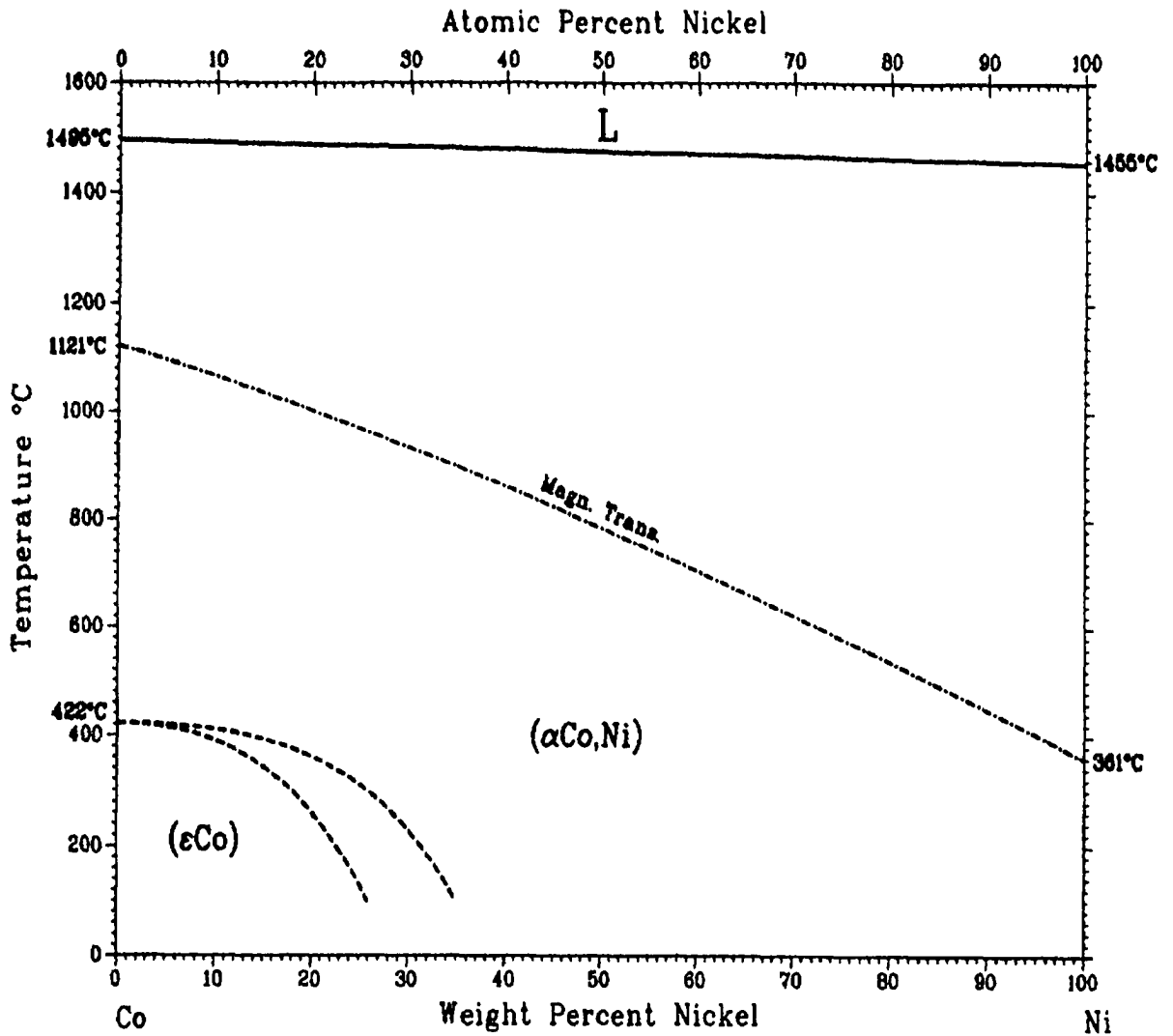


d. CoFeNi film plated from citrate-free bath with pH=2.7 at  $i = 18\text{mA/cm}^2$ ,  $t_{\text{on}}=1\text{ms}$ ,  $t_{\text{on}} + t_{\text{off}} = 10\text{ms}$  and agitation of 600rpm. Film composition is  $\text{Co}_{60}\text{Fe}_{29}\text{Ni}_{11}$ .

**Figure 7-7.** Thin film XRD spectra of CoFeNi films with different Fe contents electroplated from citrate-free baths under different conditions.

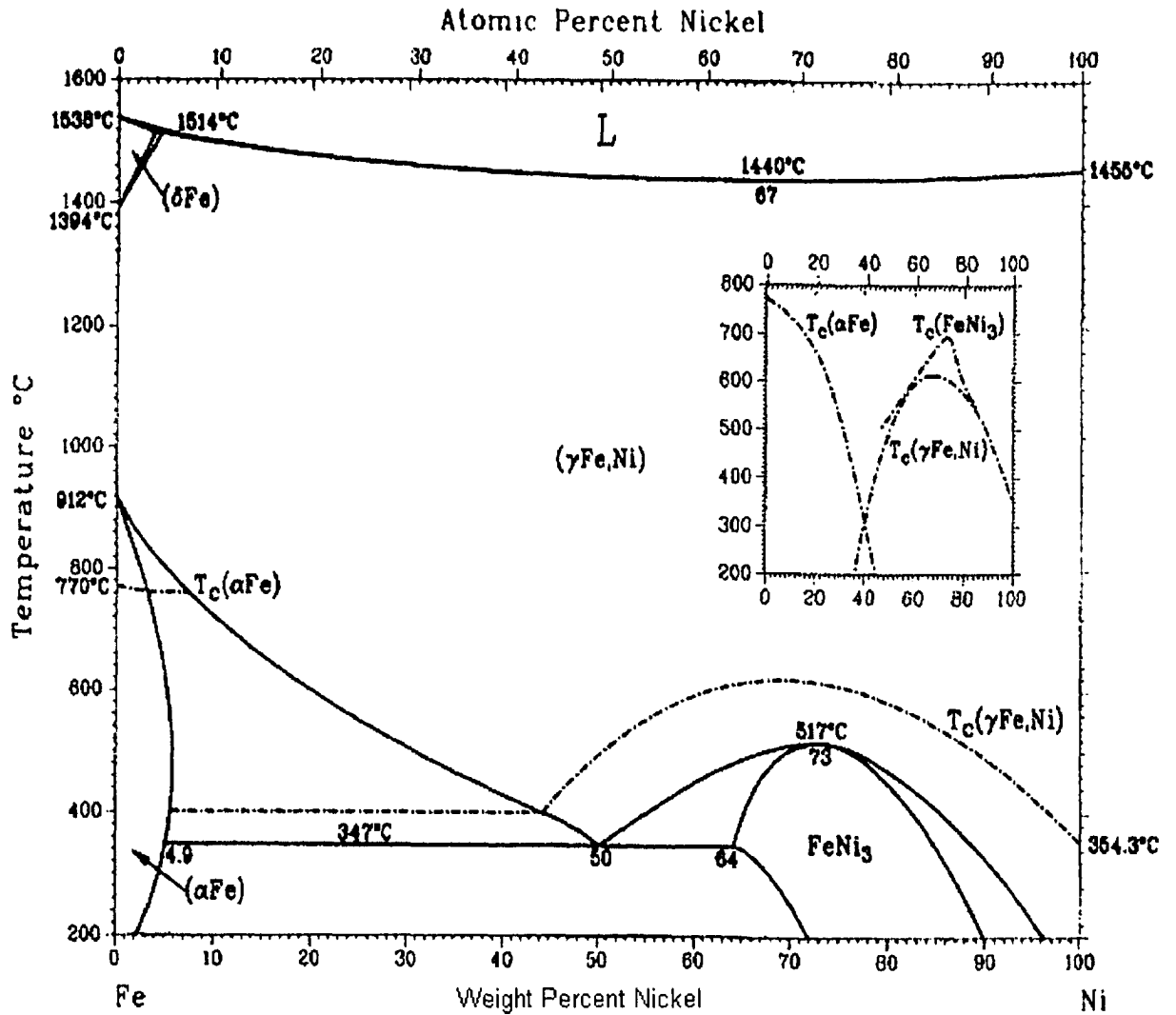
As other CoFeNi films plated from citrate-added baths, the fcc phase is dominant in deposited films at low Fe contents (up to 27at%), while the bcc phase forms and is dominant at higher Fe content (29at%). This is consistent with the literature. [Osaka00-1] [Liu03] Hence, the phase formation in deposited CoFeNi films, plated from citrate-free baths, is affected by Fe content. Comparison of Figures 7-5f, 7-6 and 7-7d shows that the XRD spectra are different even though the films have very similar compositions. Bath composition and operation parameters affect phase formation in deposited films.

The thin film XRD study demonstrates that the fcc ( $\alpha(\text{Co})/\gamma(\text{Fe})$ ) and bcc ( $\alpha(\text{Fe})$ ) phases can be co-deposited in CoFeNi films, with compositions around  $\text{Co}_{65}\text{Fe}_{23}\text{Ni}_{12}$  at room temperature, by controlling the plating bath composition and/or the plating conditions. This is not consistent with the binary phase diagrams for the Co-Fe, Co-Ni and Fe-Ni systems (Figures 7-2, 7-8a and 7-8b). According to these phase diagrams, the  $\alpha'$  phase (CsCl type structure),  $\epsilon(\text{Co})$  phase (hcp),  $\alpha(\text{Fe})$  phase (bcc) and  $\text{FeNi}_3$  phase are stable for films with compositions around  $\text{Co}_{65}\text{Fe}_{23}\text{Ni}_{12}$  at room temperature. Therefore, phase formation in the electroplated CoFeNi films, as for the electroplated CoFe films, is controlled by kinetic conditions. The conditions for phase formation in CoFeNi alloy during electrodeposition deviate from equilibrium. The effect of Fe content on phase formation in electrodeposited CoFeNi films is opposite to that in electrodeposited CoFe films. This may be attributed to the introduction of Ni and employment of different plating parameters.



Phase	Composition, wt% Ni	Pearson symbol	Space group
(αCo,Ni)	0 to 100	<i>cF4</i>	<i>Fm<math>\bar{3}m</math></i>
(εCo)	0 to 35	<i>hP2</i>	<i>P6<math>_3</math>/mmc</i>

a. Phase diagram for the Co-Ni system. [Baker92]



Phase	Composition, wt % Ni	Pearson symbol	Space group
( $\delta$ Fe)	0 to 3.7	<i>cI2</i>	<i>Im<math>\bar{3}m</math></i>
( $\gamma$ Fe, Ni)	0 to 100	<i>cF4</i>	<i>Fm<math>\bar{3}m</math></i>
( $\alpha$ Fe)	0 to 5.8	<i>cI2</i>	<i>Im<math>\bar{3}m</math></i>
Fe <sub>3</sub> Ni(a)	26	<i>cP4</i>	<i>Pm<math>\bar{3}m</math></i>
FeNi(a)	51	<i>tP2</i>	<i>P4/mmm</i>
FeNi <sub>3</sub>	64 to ~90	<i>cP4</i>	<i>Pm<math>\bar{3}m</math></i>

(a) Metastable

Figure 7-8. b. Phase diagram for the Fe-Ni system. [Baker92]

To summarize and to compare the phase formation behavior for deposited CoFe and CoFeNi films in this study with the literature, the ternary Co-Fe-Ni alloy diagram presented in reference [Osaka99-4] is illustrated in Figure 7-9, and the XRD results for CoFe and CoFeNi films electrodeposited in this work are superimposed on the diagram. For CoFeNi films, only the fcc phase is formed at low Fe contents, e.g., Fe content <20 at% for CoFeNi films plated from citrate-added baths. Mixed fcc and bcc phases are co-deposited in films with medium Fe contents, e.g., 21 at% ≤ Fe content ≤ 28 at% for CoFeNi films plated from citrate-added baths. Only the bcc phase is formed for high levels of Fe content, e.g., Fe content >28 at% for CoFeNi films plated from citrate-added baths. This trend is consistent with the literature. [Osaka99-4] [Osaka00-1] [Liu03] The bcc phase can be formed at lower Fe contents for CoFeNi films plated from citrate-added baths (≥ 21 at% Fe) than for CoFeNi films plated from citrate-free baths (≥ 27 at% Fe). It is seen that the deposited CoFe films are different from CoFeNi films.

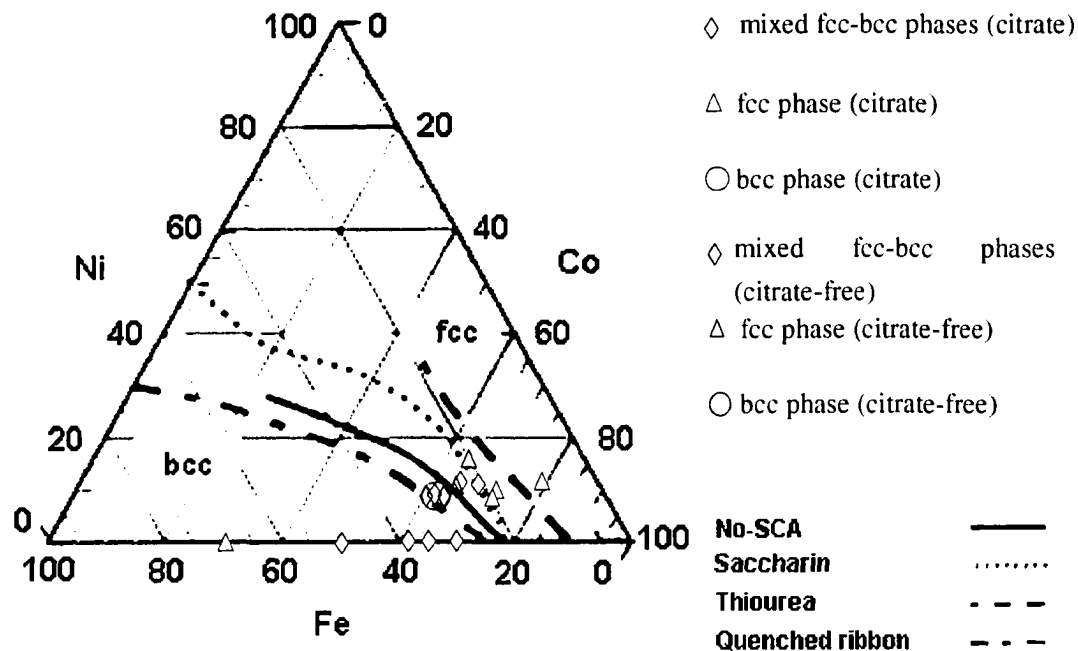


**Figure 7-9.** Ternary Co-Fe-Ni alloy diagram for phase formation as presented in reference [Osaka99-4]. Data from this work are superimposed on the diagram.

## 7.2 TEM analysis

Transmission electron microscopy (TEM) is a characterization method widely used in materials science and engineering for the study of microstructure and crystallization of materials. In this research, TEM is employed to study the grain sizes and phase formation in electroplated CoFe and CoFeNi films.

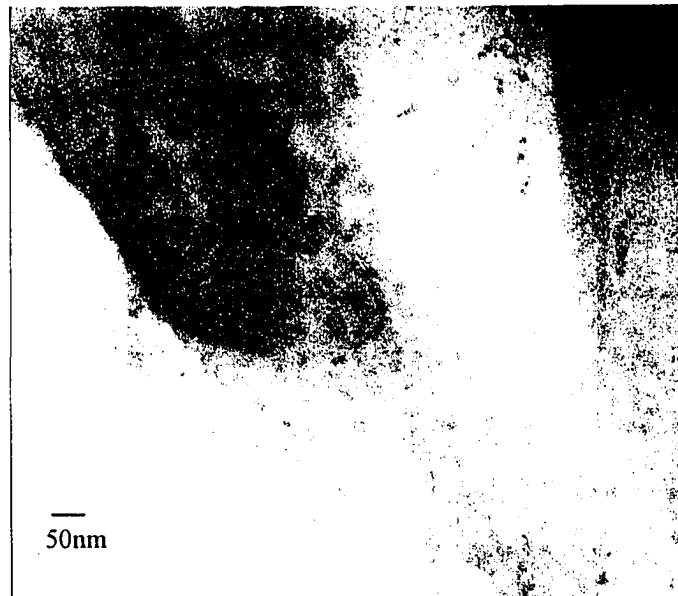
### 7.2.1 TEM analysis of electroplated CoFe films

Bright field and dark field images of a CoFe film with composition  $\text{Co}_{65}\text{Fe}_{35}$ , plated from a citrate-added bath (refer to Table 3-2) at  $i = 15 \text{ mA/cm}^2$ ,  $t_{\text{on}} = 6 \text{ ms}$ ,  $t_{\text{off}} = 4 \text{ ms}$  and agitation of 600rpm, are shown in Figures 7-10a and b, respectively. The average grain sizes in the CoFe deposit are around 10-20 nm, which is very fine and beneficial for achieving optimal soft magnetic properties. Due to the very small grain sizes of the deposited CoFe crystals and the thin nature of the TEM specimens, the electron diffraction pattern is very weak. The strongest reflections are those from the fcc (111) and bcc (110) planes, which agrees with the thin film x-ray diffraction results. The dark field image (Figure 7-10b) was formed from part of the fcc (111) and bcc (110) diffraction rings. All diffracted planes which can be identified from the original pattern are listed in Table 7-4. The calculated d-spacings are derived from the thin film XRD spectrum (Figure 7-1b). The lattice constants  $a$  for the bcc and fcc phases are determined from the bcc(110) and fcc(111) peaks, respectively, using the Bragg equation and the cubic d-spacing formula:

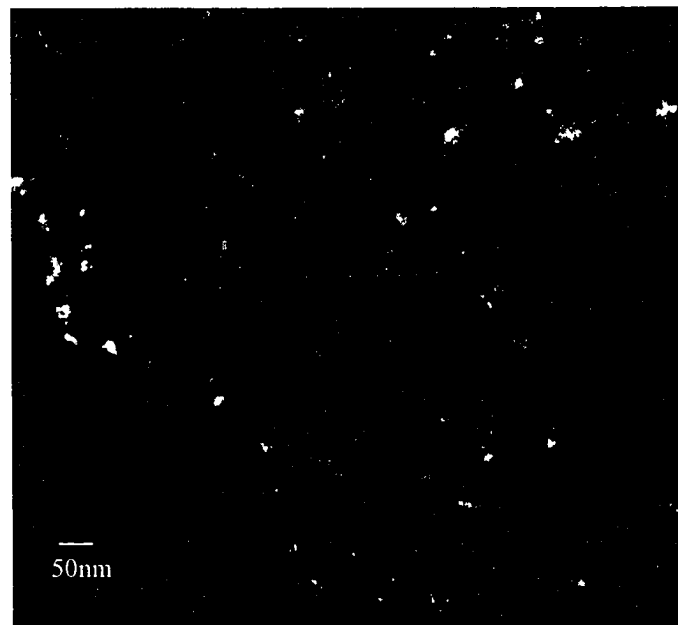
$$\lambda = 2d \sin \theta \quad (7-1)$$

$$1/d^2 = (h^2 + k^2 + l^2)/a^2 \quad (7-2)$$

From the obtained lattice constant  $a$ , the d-spacing of the (hkl) planes can be calculated from the above cubic d-spacing formula.



a. Bright field image



b. Dark field image

**Figure 7-10.** TEM bright field image and dark field image of a CoFe film plated from a bath with ammonium citrate dosage of 5g/L, at  $i = 15 \text{ mA/cm}^2$ ,  $t_{\text{on}} = 6 \text{ ms}$ ,  $t_{\text{off}} = 4 \text{ ms}$  and agitation of 600rpm. Film composition is  $\text{Co}_{65}\text{Fe}_{35}$ .

The lattice constants  $a$  for the bcc and fcc phases determined from the XRD spectrum are 0.28440 nm and 0.35472 nm, respectively. The lattice constant  $a$  for bcc phase is a bit

smaller than that for bcc Fe, which is 0.28664 nm. This may be attributed to the smaller radius of Co atom. The lattice constant  $a$  for the fcc phase is close to that for fcc Co, which is 0.35447 nm. [Liu03]

**Table 7-4.** Diffraction planes identified from electron diffraction pattern.

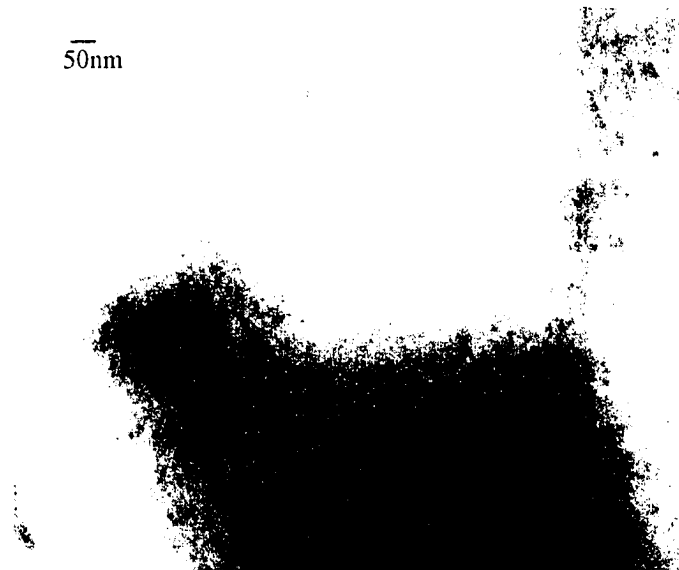
<b>bcc planes</b>	<b>d-spacing measured, nm</b>	<b>d-spacing calculated, nm</b>	<b>fcc planes</b>	<b>d-spacing measured, nm</b>	<b>d-spacing calculated, nm</b>
(110)	0.1985	0.2011	(111)	0.2030	0.2048
(200)	0.1381	0.1422	(220)	0.1250	0.1254
(211)	0.1144	0.1161	(222)	0.0994	0.1024
(220)	0.0994	0.1006	(400)	0.0885	0.0887
(222)	0.0820	0.0821			
(321)	0.0754	0.0760			

The electron diffraction analysis further verifies the co-existence of fcc and bcc phases in  $\text{Co}_{65}\text{Fe}_{35}$  films plated from the citrate-added bath.

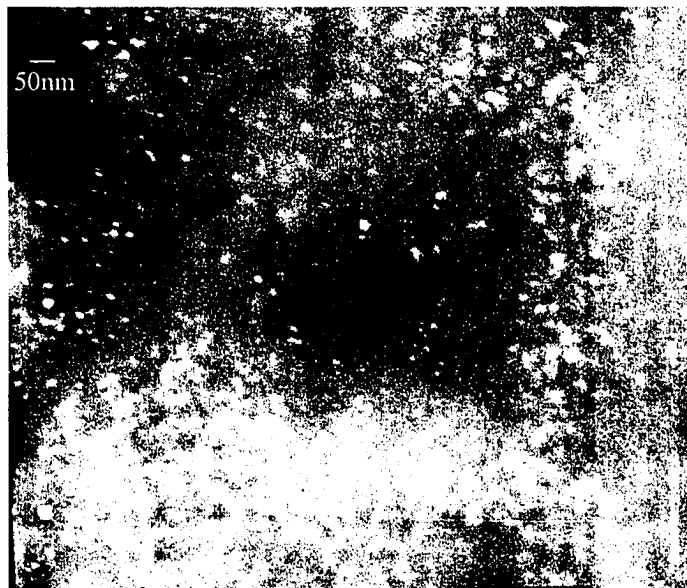
### 7.2.2 TEM analysis of electroplated CoFeNi films

Bright field and dark field images as well as an electron diffraction pattern for a CoFeNi film with composition  $\text{Co}_{66}\text{Fe}_{23}\text{Ni}_{11}$ , plated from a citrate-added bath (refer to Table 3-4) at  $i = 6 \text{ mA/cm}^2$ ,  $t_{\text{on}} = 0.3 \text{ ms}$ ,  $t_{\text{off}} = 9.7 \text{ ms}$  and agitation of 600rpm, are shown in Figures 7-11a, b and c, respectively. The bright field and dark field images (Figure 7-11a and b) show that the average diameter of crystal grains in this CoFeNi film is 10-20 nm, which is close to the grain sizes in the CoFeNi film with the best soft magnetic properties obtained by Osaka et al. [Osaka98-1] [Osaka98-2] The electron diffraction pattern (Figure 7-11c) confirms the co-existence of fcc and bcc phases. The diffraction rings from bcc planes are wider and more diffuse, which means that the bcc phase has a finer

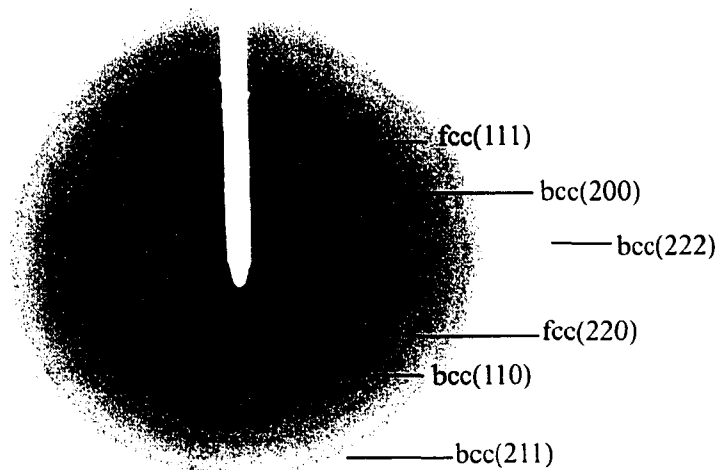
grain size and is near amorphous in structure. The dark field image was formed from part of the fcc (111) and bcc (110) diffraction rings.



a. Bright field image



b. Dark field image



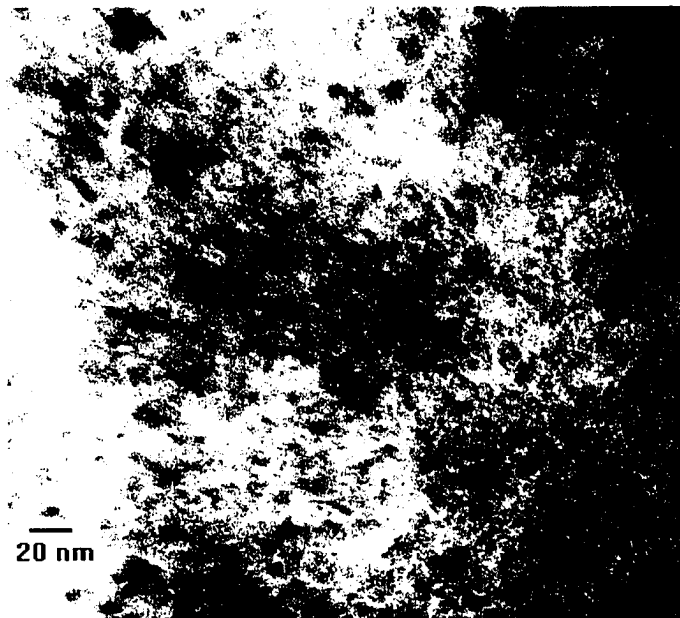
### c. Electron diffraction pattern

**Figure 7-11.** TEM bright field image, dark field image and electron diffraction pattern of a CoFeNi film plated, from a solution with an ammonium citrate dosage of 50g/L, at  $i = 6 \text{ mA/cm}^2$ ,  $t_{\text{on}} = 0.3 \text{ ms}$ ,  $t_{\text{on}} + t_{\text{off}} = 10 \text{ ms}$  and agitation of 600rpm. Film composition is  $\text{Co}_{66}\text{Fe}_{23}\text{Ni}_{11}$ .

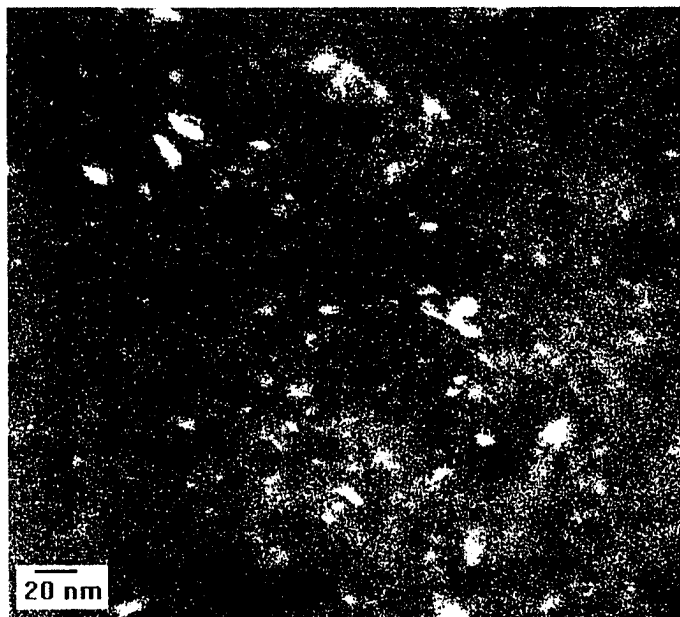
The lattice constants  $a$  for the bcc and fcc phases determined from the XRD spectrum are 0.28355 nm and 0.35472 nm, respectively. The lattice constant  $a$  for bcc phase is a bit smaller than that for bcc Fe, which is 0.28664 nm. The lattice constant  $a$  for the fcc phase is a bit larger than those for fcc Co and fcc Ni, which are 0.35447 nm and 0.35238 nm, respectively. [Liu03] This is consistent with the larger radius of Fe atom relative to Co and Ni atoms.

Figure 7-12 illustrates the bright field image, dark field image and electron diffraction pattern for a CoFeNi film with composition  $\text{Co}_{72}\text{Fe}_{21}\text{Ni}_7$  plated from a citrate-added bath with 100g/L ammonium citrate dosage. The bright field and dark field images (Figure 7-12a and b) show that, similar to the above  $\text{Co}_{66}\text{Fe}_{23}\text{Ni}_{11}$  film, the crystal grains in the  $\text{Co}_{72}\text{Fe}_{21}\text{Ni}_7$  film are also 10-20 nm in diameter. The electron diffraction pattern (Figure

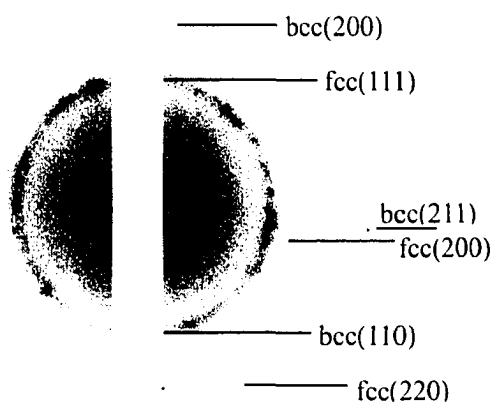
7-12c) demonstrates the co-deposition of fcc and bcc phases in this film. Only the fcc (111) and bcc (110) planes diffract strongly. This agrees with the thin film x-ray diffraction results. The dark field image was formed from part of the fcc (111) and bcc (110) diffraction rings (Figure 7-12c).



a. Bright field image



b. Dark field image



c. Electron diffraction pattern

**Figure 7-12.** TEM bright field image, dark field image and electron diffraction pattern of a CoFeNi film plated, from a solution with an ammonium citrate dosage of 100g/L, at  $i = 10 \text{ mA/cm}^2$ ,  $t_{\text{on}} = 0.3 \text{ ms}$ ,  $t_{\text{on}} + t_{\text{off}} = 10 \text{ ms}$  and agitation of 600rpm. Film composition is  $\text{Co}_{72}\text{Fe}_{21}\text{Ni}_7$ .

The lattice constants  $a$  for the bcc and fcc phases determined from the XRD spectrum are 0.28320 nm and 0.35358 nm, respectively. The lattice constant  $a$  for the bcc phase is a bit smaller than that for bcc Fe; and the lattice constant  $a$  for the fcc phase is a bit smaller than that for fcc Co, but larger than that of fcc Ni. [Liu03]

Generally, the lattice constants  $a$  for the bcc and fcc phases in the  $\text{Co}_{65}\text{Fe}_{35}$  film are close to those for the  $\text{Co}_{66}\text{Fe}_{23}\text{Ni}_{11}$  and  $\text{Co}_{72}\text{Fe}_{21}\text{Ni}_7$  films even though these films have different compositions. The lattice constants  $a$  for the bcc and fcc phases in the electroplated CoFe and CoFeNi films are close to those of bcc Fe and fcc Co, respectively.

### 7.3 Summary

For CoFe films electroplated from citrate-added baths under the employed conditions, the fcc/bcc phase ratio increases with increasing Fe content in the deposited films. Iron

content affects phase formation in deposited CoFe films. The thin film XRD study demonstrates that fcc and bcc phases can be co-deposited in electroplated CoFe films with specific Fe contents. Bath composition (e.g., ammonium citrate dosage) and operating parameters affect phase formation in deposited CoFe films.

For CoFeNi films, electroplated from citrate-added baths under the employed conditions, only the fcc phase is formed in deposited films with Fe contents <20 at%. Fcc and bcc phases are co-deposited in films with Fe contents higher than 21 at%. The bcc(110)/fcc(111) diffraction intensity ratio increases with increasing Fe content in deposited films, which is opposite to the trend for electroplated CoFe films. Hence, phase formation in CoFeNi films plated from citrate-added baths is affected by Fe content. For CoFeNi films electroplated from citrate-free baths, phase formation is also affected by Fe content. Bath composition and operation parameters affect the phase formation in deposited films. Both fcc and bcc phases can be co-deposited by controlling the bath composition and/or the plating conditions.

TEM analysis demonstrated that the average grain size in Co<sub>65</sub>Fe<sub>35</sub> films plated from citrate-added baths was 10-20 nm, which is quite fine and beneficial for achieving optimal soft magnetic properties. Electron diffraction confirmed the co-existence of fcc and bcc phases in CoFe deposits. The fcc (111) and bcc (110) planes diffracted strongly, which also agrees with the thin film x-ray diffraction results.

TEM analysis of CoFeNi films plated from citrate-added baths showed that the average grain size of CoFeNi films was 10-20 nm, which is close to the grain sizes for CoFeNi films with best soft magnetic properties obtained by Osaka and coworkers. Electron diffraction patterns demonstrated the co-existence of fcc and bcc phases in CoFeNi films plated from citrate-added baths. Diffraction was strongest from the fcc (111) and bcc (110) planes, which agrees with the thin film x-ray diffraction results.

Generally, the lattice constants  $a$  for bcc and fcc phases in CoFe and CoFeNi films

are close despite their different compositions. The lattice constants  $a$  for bcc and fcc phases in the studied CoFe and CoFeNi films are close to those for bcc Fe and fcc Co, respectively.

## Chapter 8 Magnetic Properties of Electroplated CoFe and CoFeNi Thin Films

It is known that many CoFe and CoFeNi alloys, with compositions near  $\text{Fe}_{60}\text{Co}_{40}$ , have high saturation magnetic flux densities  $B_s$  (as high as 2.4 Tesla). Bozorth [Bozorth51] reported the composition- $B_s$  diagram for bulk CoFeNi ternary alloys (see Figure 2-8) in 1951. However, these alloys usually do not possess low coercivity  $H_c$ , i.e., soft magnetic properties. Therefore, it has been a challenge to fabricate high  $B_s$  (>2 Tesla) CoFe or CoFeNi films with optimal soft magnetic properties by electrodeposition. In this study, the magnetic properties of CoFe and CoFeNi films plated from citrate-added baths and citrate-free baths have been investigated.

### 8.1 Magnetic properties of electroplated CoFe thin films

Since the soft magnetic properties of deposited films are of concern, the effects of ammonium citrate dosage, Fe content in film, plating current density and plating temperature on film coercivity  $H_c$  have been studied.

The effect of ammonium citrate dosage in the plating bath (refer to Table 3-2) on the coercivities  $H_c$  of deposited CoFe films is shown in Figure 8-1. The error for  $H_c$  measurement was  $\pm 1$  Oe. For the CoFe film plated from a citrate-free bath with natural pH, the coercivity  $H_c$  was as high as 22 Oe. The film coercivity  $H_c$  dropped abruptly to around 10 Oe at low ammonium citrate dosages (2 to 20 g/L). This may be attributed to the low stress in CoFe films plated from citrate-added baths, which results in a low coercivity  $H_c$ . [Tabakovic02] The deposition of metal atoms may be delayed from citrate-complexed ions, which leads to more time for the adatoms to fit into favored sites in the lattice to form a structure with fewer defects and lower stress. The coercivity  $H_c$  increases quickly, however, for higher ammonium citrate dosages (>50 g/L). Therefore, a

low ammonium citrate dosage (<20 g/L) is beneficial for the coercivity  $H_c$  of deposited CoFe films, and a high ammonium citrate dosage is not favored for plating CoFe films with optimal soft magnetic properties. The typical ammonium citrate dosage employed in CoFe alloy plating was 5g/L (refer to Chapter 5).

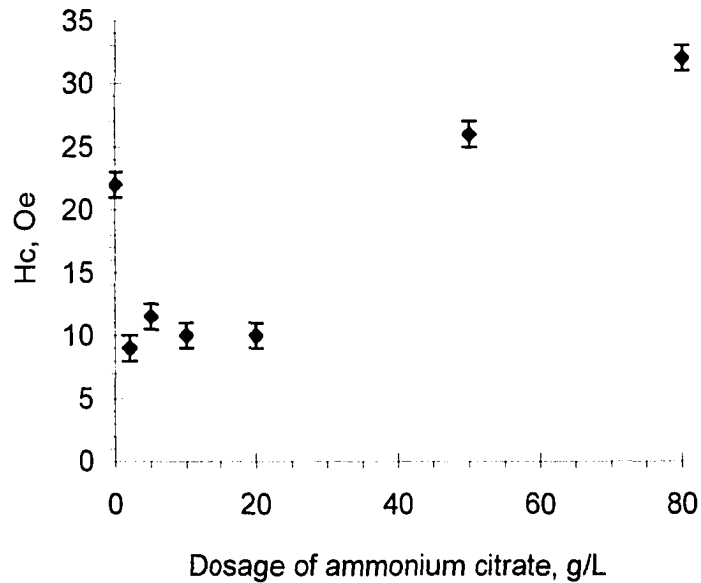
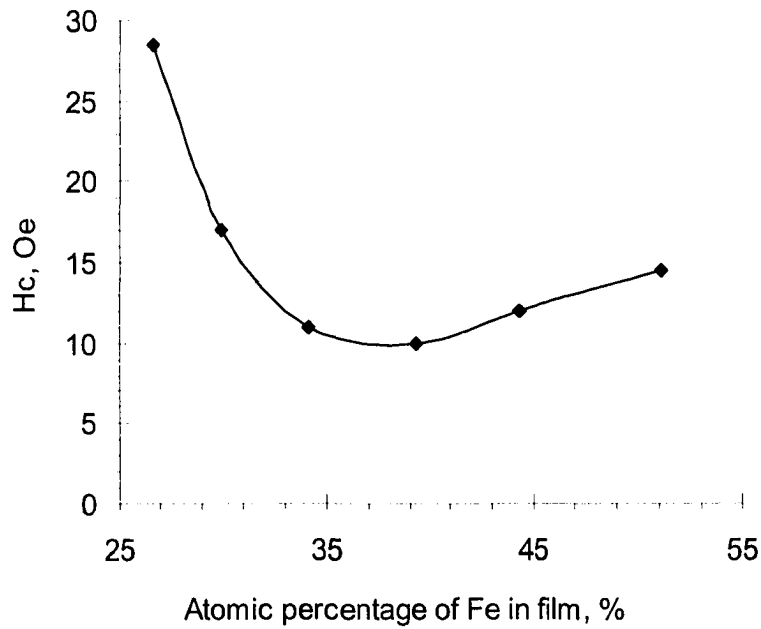


**Figure 8-1.** Effect of ammonium citrate dosage on the coercivity  $H_c$  of CoFe films plated at  $i = 15\text{mA/cm}^2$ ;  $t_{\text{on}} = 6\text{ms}$ ;  $t_{\text{on}} + t_{\text{off}} = 10\text{ms}$ ; agitation 600 rpm.

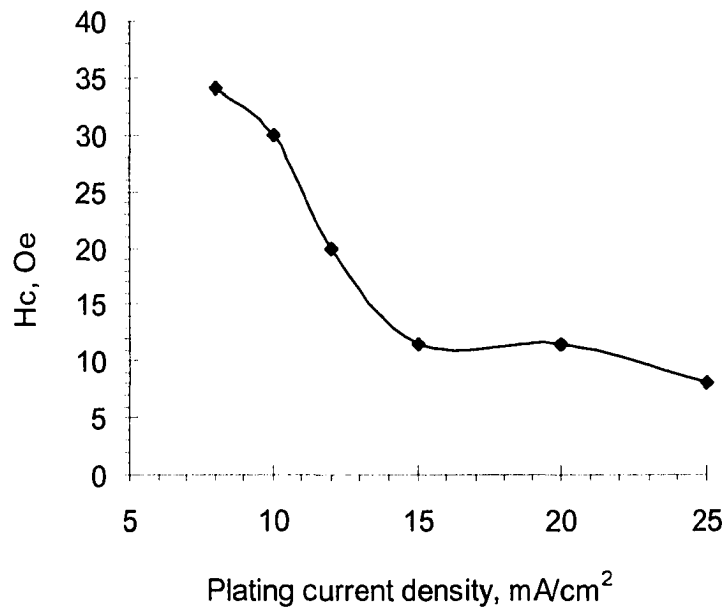
The effect of Fe content in deposited CoFe films on coercivity  $H_c$  is illustrated in Figure 8-2. At low Fe content, the coercivity  $H_c$  of deposited film decreases as Fe content increases reaching a minimum at about 40 at% Fe, with  $H_c$  values less than 15 Oe for the composition range of ~30-50 at% Fe. This composition range corresponds to that where both the bcc and fcc phases co-exist. Above 50 at% Fe, only the fcc phase is present.

Figure 8-3 shows the effect of plating current density on the coercivity  $H_c$  of deposited CoFe films. Generally, the coercivity  $H_c$  of deposited films decreases as the current density goes up. When the current density is higher than  $15\text{mA/cm}^2$ , the coercivity  $H_c$  of deposited film can be lower than 12 Oe, which is good. A higher current

density is more beneficial for achieving low  $H_c$ . This may be attributed to the finer grain sizes in films plated at higher current densities, which results in a lower coercivity  $H_c$ .



**Figure 8-2.** Effect of Fe content on the coercivity  $H_c$  of CoFe films plated at  $i = 15\text{mA/cm}^2$ ;  $t_{\text{on}} = 6\text{ms}$ ;  $t_{\text{on}} + t_{\text{off}} = 10\text{ms}$ ; agitation 600 rpm.



**Figure 8-3.** Effect of plating current density on the coercivity  $H_c$  of CoFe films plated at  $t_{\text{on}} = 6\text{ms}$ ;  $t_{\text{on}} + t_{\text{off}} = 10\text{ms}$ ; agitation 600 rpm.

The effect of plating temperature on the coercivity  $H_c$  of deposited CoFe films is shown in Figure 8-4. There is an excellent linear relationship between plating temperature and the coercivity  $H_c$  of deposited films for the employed experimental conditions. A high plating temperature is not beneficial for depositing CoFe films with low  $H_c$ , i.e., good soft magnetic properties.

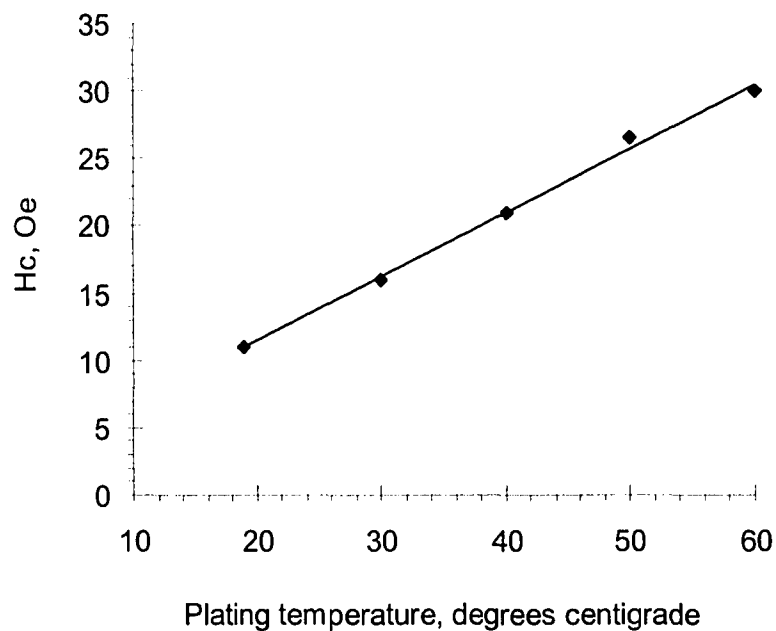


**Figure 8-4.** Effect of plating temperature on the coercivity  $H_c$  of CoFe films plated at  $i = 15\text{mA/cm}^2$ ;  $t_{\text{on}} = 6\text{ms}$ ;  $t_{\text{on}} + t_{\text{off}} = 10\text{ms}$ ; agitation 600 rpm.

The in-plane hysteresis loops of representative CoFe films plated from the citrate-added baths and citrate-free baths are illustrated in Figures 8-5 to 8-8.

For the film with a composition of  $\text{Co}_{65}\text{Fe}_{35}$ , deposited from a citrate-added bath (see Table 3-2 and Figure 8-5), a coercivity of 8 Oe and a saturation magnetization  $M_s$  of 1.96 Tesla were obtained, which are similar to the magnetic properties of  $\text{Co}_{90}\text{Fe}_{10}$  films plated by Liao et al [Liao87] [Liao88]. Their films have a coercivity  $H_c$  of about 9 Oe and a saturation flux density  $B_s$  of 1.9 Tesla. The coercivity for the deposited  $\text{Co}_{65}\text{Fe}_{35}$

film is lower than the coercivity for  $\text{Co}_{35}\text{Fe}_{65}$  films plated by Osaka and coworkers [Osaka03-1] [Imai02], which is about 15 Oe, but the saturation magnetization is also lower for the  $\text{Co}_{65}\text{Fe}_{35}$  film deposited in this work.

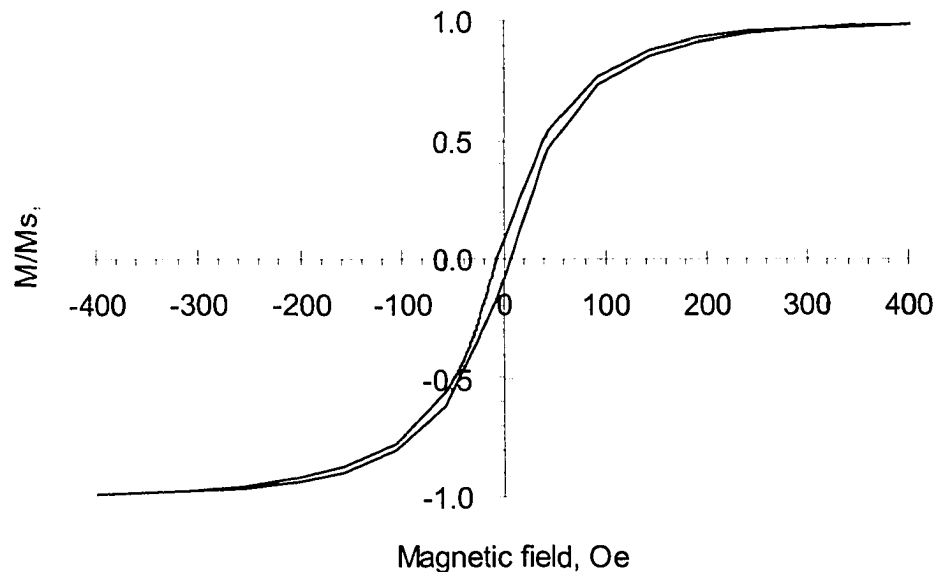


**Figure 8-5.** In-plane hysteresis loop for CoFe film deposited from citrate-added bath (film composition  $\text{Co}_{65}\text{Fe}_{35}$ ) at  $i = 15\text{mA}/\text{cm}^2$ ;  $t_{\text{on}} = 2\text{ms}$ ;  $t_{\text{on}} + t_{\text{off}} = 10\text{ms}$ ; agitation 600 rpm.

The hysteresis loop for the CoFe film (film composition  $\text{Co}_{64}\text{Fe}_{36}$ ) deposited from a citrate-free bath with natural pH (see Table 3-2, 0 g/L citrate) is shown in Figure 8-6. The film has a coercivity of 22 Oe, and a saturation magnetization  $M_s$  of 1.83 Tesla, which means the soft magnetic properties are somewhat worse than those for the above  $\text{Co}_{65}\text{Fe}_{35}$  film deposited from citrate-added bath.

Figure 8-7 illustrates the hysteresis loop of the CoFe film (composition  $\text{Co}_{34}\text{Fe}_{66}$ ) deposited from a citrate-added bath (refer to Table 5-4). The film demonstrates good soft magnetic properties with a coercivity of 17 Oe and a saturation magnetization  $M_s$  of 2.04 Tesla.

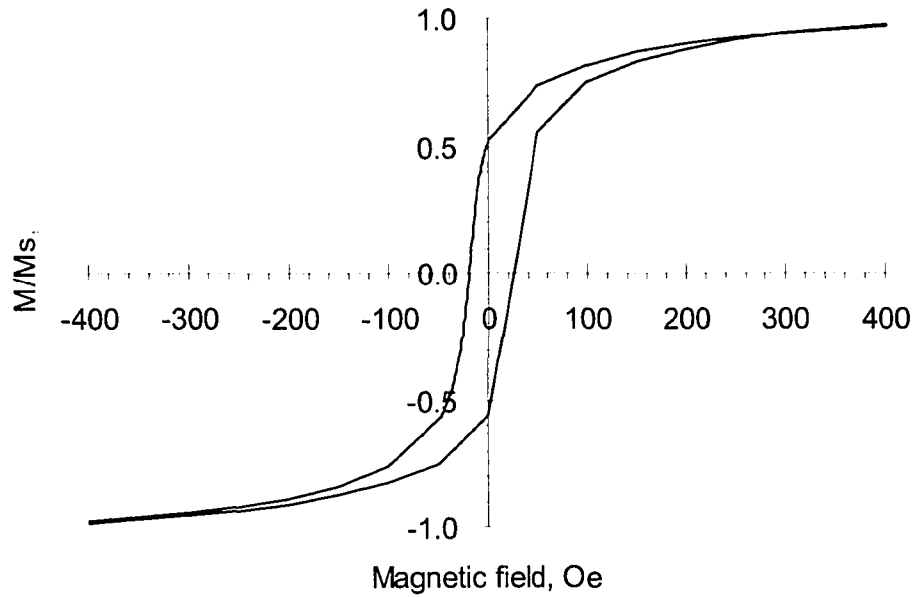


**Figure 8-6.** In-plane hysteresis loop for CoFe film deposited from citrate-free bath with natural pH (film composition  $\text{Co}_{64}\text{Fe}_{36}$ ) at  $i = 15\text{mA}/\text{cm}^2$ ;  $t_{\text{on}} = 2\text{ms}$ ;  $t_{\text{on}} + t_{\text{off}} = 10\text{ms}$ ; agitation 600 rpm.

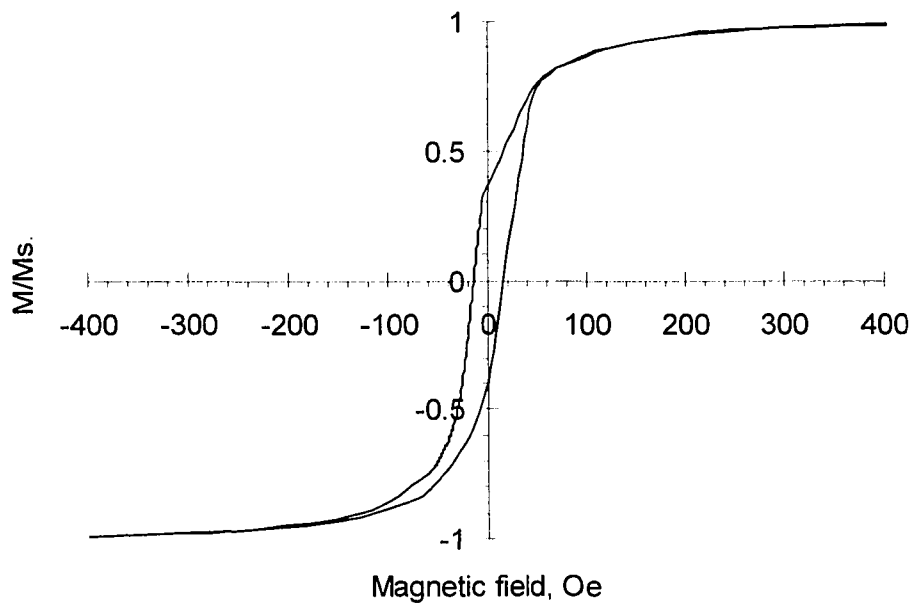


**Figure 8-7.** In-plane hysteresis loop for CoFe film deposited from citrate-added bath (film composition  $\text{Co}_{34}\text{Fe}_{66}$ ) at  $i = 15\text{mA}/\text{cm}^2$ ;  $t_{\text{on}} = 2\text{ms}$ ;  $t_{\text{on}} + t_{\text{off}} = 10\text{ms}$ ; agitation 600 rpm.

The hysteresis loop for the CoFe film (composition  $\text{Co}_{33}\text{Fe}_{67}$ ) deposited from a citrate-free bath with a low pH of 2.4 (refer to Table 3-1) is shown in Figure 8-8. This film has a coercivity of 26 Oe and a saturation magnetization  $M_s$  of 1.91 Tesla, i.e., worse soft magnetic properties than those for the  $\text{Co}_{34}\text{Fe}_{66}$  film deposited from a citrate-added bath.

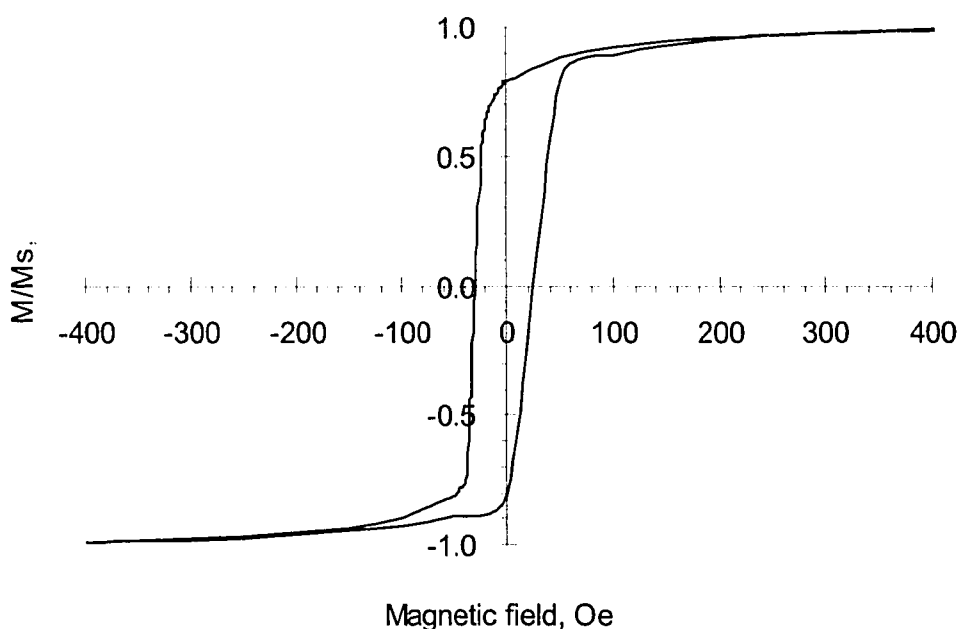


**Figure 8-8.** In-plane hysteresis loop for CoFe film deposited from citrate-free bath with a pH of 2.4 (film composition  $\text{Co}_{33}\text{Fe}_{67}$ ) at  $i = 15\text{mA}/\text{cm}^2$ ;  $t_{\text{ON}} = 2\text{ms}$ ;  $t_{\text{ON}} + t_{\text{OFF}} = 10\text{ms}$ ; agitation 600 rpm.

In general, the CoFe films plated from citrate-added baths exhibited better soft magnetic properties than those deposited from citrate-free baths under the employed experimental conditions, which means the addition of citrate into the plating baths will not sacrifice the magnetic properties of the deposited films. The magnetic properties of the representative CoFe films are further summarized in Table 8-1. The CoFe films plated from citrate-added baths can have coercivities  $H_c$  of 8 to 17 Oe, which is

acceptable, and saturation magnetizations  $M_s$  of 1.96 to 2.04 Tesla, which is quite good. The saturation magnetizations  $M_s$  are lower than those for  $\text{Co}_{35}\text{Fe}_{65}$  films plated by Osaka and coworkers, who claimed values as high as 2.4 Tesla. [Osaka03-1] [Imai02]

**Table 8-1.** Magnetic properties of representative CoFe films plated from citrate-free baths and citrate-added baths.

Plating bath	Film composition	Coercivity $H_c$ (Oe)	Saturation flux density $B_s$ (Tesla)
Citrate-added bath	$\text{Co}_{65}\text{Fe}_{35}$	8	1.96
Citrate-free bath (natural pH)	$\text{Co}_{64}\text{Fe}_{36}$	22	1.83
Citrate-added bath	$\text{Co}_{34}\text{Fe}_{66}$	17	2.04
Citrate-free bath (pH 2.4)	$\text{Co}_{33}\text{Fe}_{67}$	26	1.91

## 8.2 Magnetic properties of electroplated CoFeNi thin films

The effects of ammonium citrate dosage, Fe content in deposited film, plating current density and plating temperature on the coercivity  $H_c$  of electroplated CoFeNi films have been studied.

The effect of ammonium citrate dosage in the electrolyte (refer to Table 3-4 and Chapter 5) on the coercivity  $H_c$  of deposited CoFeNi films is shown in Figure 8-9. The coercivity  $H_c$  is high for the film plated from bath with 0 g/L ammonium citrate and natural pH. The coercivity  $H_c$  of deposited film decreases for low citrate dosage (30 g/L), but increases as the ammonium citrate dosage goes up if the ammonium citrate dosage exceeds 30 g/L. Therefore, a high ammonium citrate dosage is not favored for depositing CoFeNi films with low coercivity  $H_c$ .

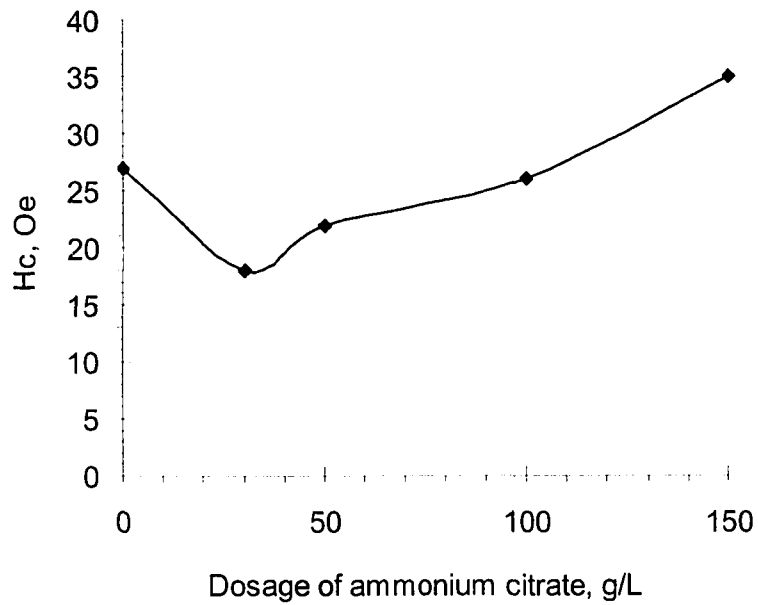


**Figure 8-9.** Effect of ammonium citrate dosage on the coercivity  $H_c$  of CoFeNi films plated at  $i = 6\text{mA/cm}^2$ ;  $t_{\text{on}} = 0.3\text{ms}$ ;  $t_{\text{on}} + t_{\text{off}} = 10\text{ms}$ ; agitation 600 rpm.

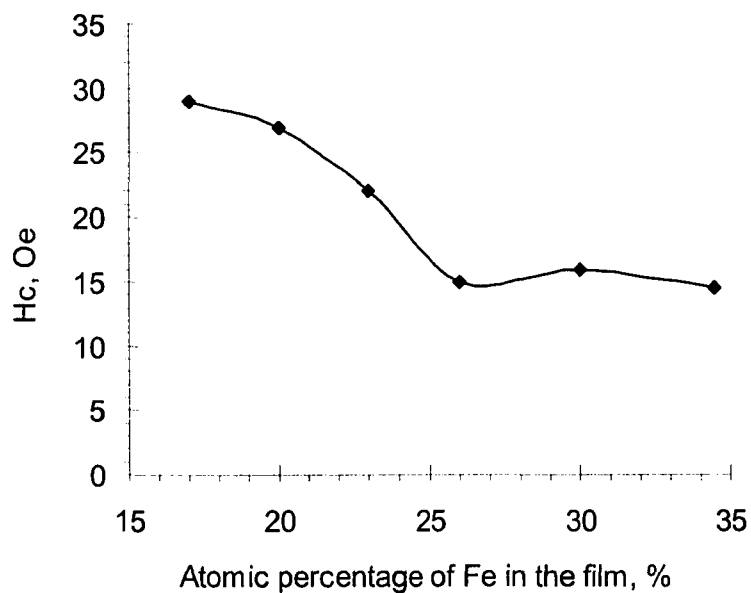


**Figure 8-10.** Effect of Fe content on the coercivity  $H_c$  of CoFeNi films plated at  $i = 6\text{mA/cm}^2$ ;  $t_{\text{on}} = 0.3\text{ms}$ ;  $t_{\text{on}} + t_{\text{off}} = 10\text{ms}$ ; agitation 600 rpm.

Figure 8-10 illustrates the effect of Fe content in deposited CoFeNi films on coercivity  $H_c$ . The coercivity  $H_c$  of deposited films decreases with increasing Fe content, leveling out at  $\sim 15$  Oe for Fe compositions between 25 and 35 at%. From the XRD spectra in Figures 7-5a to f, it is clear that only the fcc phase is formed in deposited films for Fe contents lower than 20 at%. Mixed fcc-bcc phases are deposited in films with Fe contents higher than 21 at%. Therefore, films with single fcc phase have a higher coercivity, while mixed fcc-bcc phases are beneficial for soft magnetic properties. This is consistent with the literature. [Osaka98-1] [Osaka99-1] [Liu00-1] [Liu00-2] [Liu01-1] [Liu01-2] [Liu02] [Liu03]

The effect of plating current density on the coercivity  $H_c$  of deposited CoFeNi films is shown in Figure 8-11. At low current density ( $3 \text{ mA/cm}^2$ ), the coercivity  $H_c$  of deposited films is under 20 Oe. As the current density increases, the coercivity initially increases, peaks out at about 23 Oe ( $6-7 \text{ mA/cm}^2$ ), and then decreases continually to a value of about 15 Oe at a current density of  $18 \text{ mA/cm}^2$ .

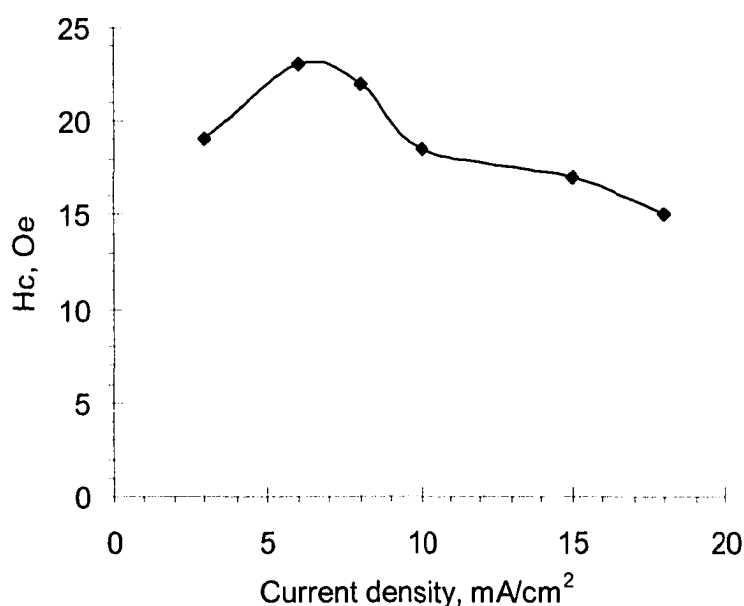


**Figure 8-11.** Effect of plating current density on the coercivity  $H_c$  of CoFeNi films plated at  $t_{\text{on}} = 0.3\text{ms}$ ;  $t_{\text{on}} + t_{\text{off}} = 10\text{ms}$ ; agitation 600 rpm.

The effect of plating temperature on the coercivity  $H_c$  of deposited CoFeNi films is illustrated in Figure 8-12. Generally, the coercivity  $H_c$  of deposited film decreases with increasing plating temperature under the employed experimental conditions. The lowest value obtained was  $\sim 16$  Oe at  $55^\circ\text{C}$ . This behavior is opposite to that for plated CoFe films.

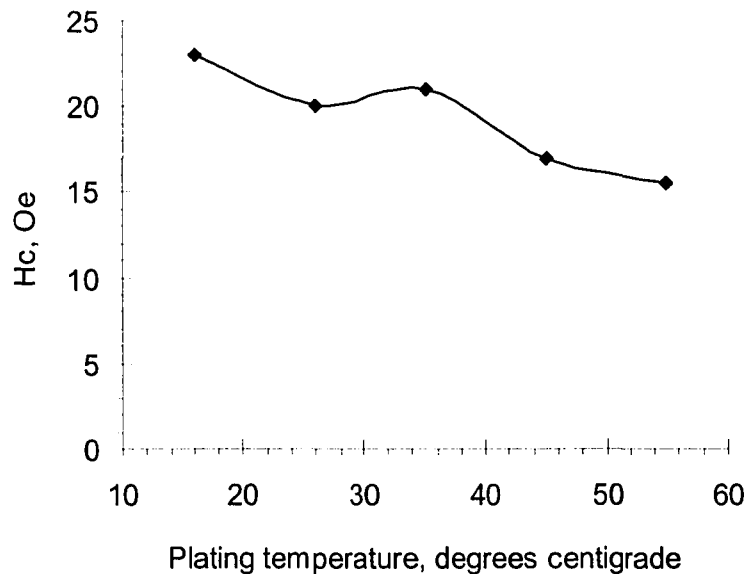


**Figure 8-12.** Effect of plating temperature on the coercivity  $H_c$  of CoFeNi films plated at  $i = 6\text{mA}/\text{cm}^2$ ;  $t_{\text{ON}} = 0.3\text{ms}$ ;  $t_{\text{ON}} + t_{\text{OFF}} = 10\text{ms}$ ; agitation 600 rpm.

The hysteresis loop for a CoFeNi film with composition  $\text{Co}_{64}\text{Fe}_{26}\text{Ni}_{10}$  deposited from the citrate-added bath (refer to Table 3-4) is illustrated in Figure 8-13. This film has a coercivity of 15 Oe and a saturation magnetization  $M_s$  of 2.10 Tesla. Its saturation magnetization is almost the same as the  $\text{Co}_{65}\text{Fe}_{23}\text{Ni}_{12}$  films with optimal soft magnetic properties claimed by Osaka and coworkers [Osaka98-1] [Osaka98-2], while its coercivity  $H_c$  is higher, but still acceptable.

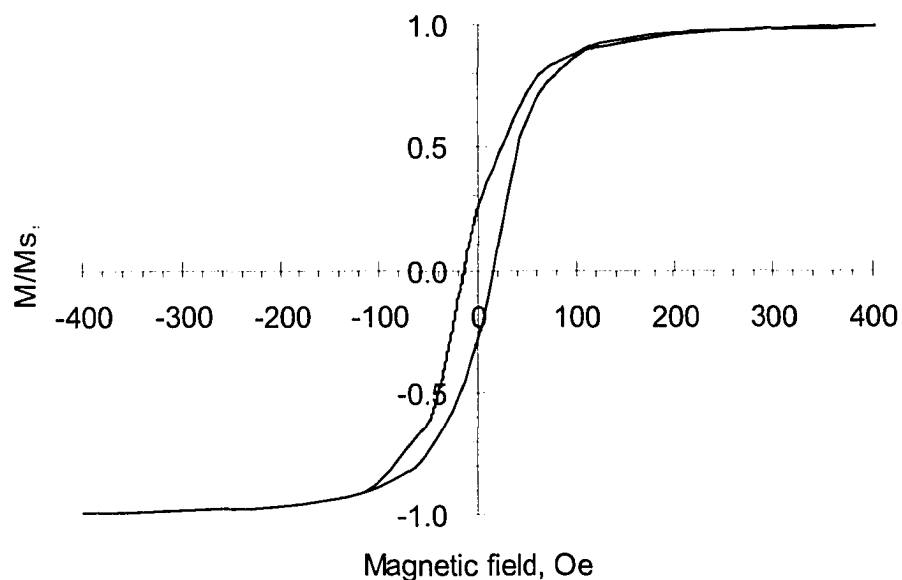


**Figure 8-13.** In-plane hysteresis loop for CoFeNi film deposited from citrate-added bath (film composition  $\text{Co}_{64}\text{Fe}_{26}\text{Ni}_{10}$ ) at  $i = 6\text{mA/cm}^2$ ;  $t_{\text{on}} = 0.3\text{ms}$ ;  $t_{\text{on}} + t_{\text{off}} = 10\text{ms}$ ; agitation 600 rpm.

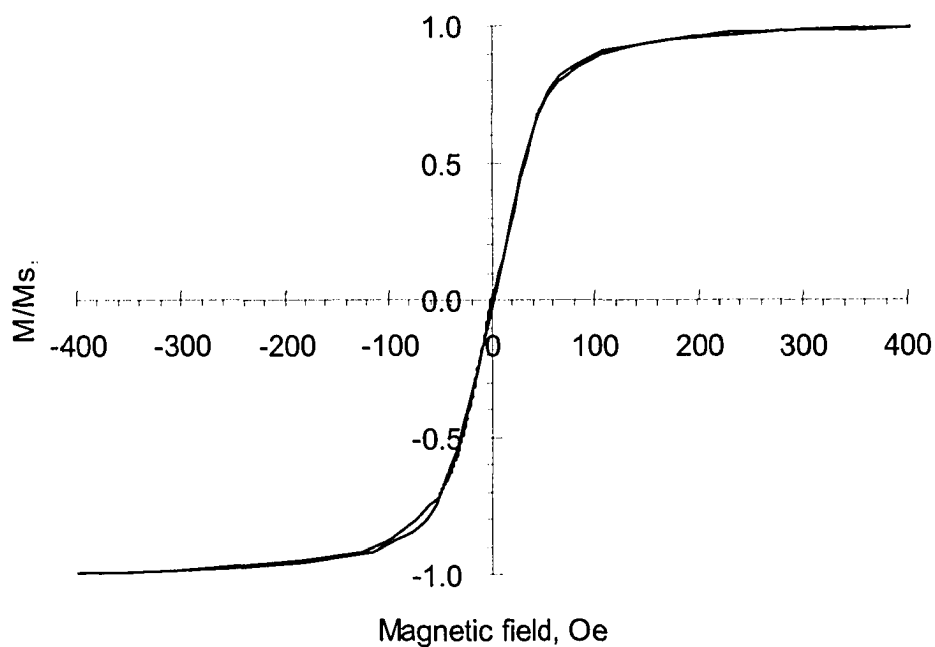


**Figure 8-14.** In-plane hysteresis loop for CoFeNi film deposited from citrate-free bath with pH 2.7 (film composition  $\text{Co}_{64}\text{Fe}_{24}\text{Ni}_{12}$ ) at  $i = 6\text{mA/cm}^2$ ;  $t_{\text{on}} = 0.3\text{ms}$ ;  $t_{\text{on}} + t_{\text{off}} = 10\text{ms}$ ; agitation 600 rpm.

The hysteresis loop for the CoFeNi film (composition  $\text{Co}_{64}\text{Fe}_{24}\text{Ni}_{12}$ ) deposited from a citrate-free bath (refer to Table 3-3) with a low pH of 2.7 is shown in Figure 8-14. This film has a coercivity of 1.5 Oe and a saturation magnetization  $M_s$  of 2.01 Tesla. It is similar to the film with optimal soft magnetic properties claimed by Osaka and coworkers, which had a composition of  $\text{Co}_{65}\text{Fe}_{23}\text{Ni}_{12}$  with a low coercivity  $H_c$  of 1.20 Oe and a high saturation flux density  $B_s$  of 2.1 Tesla. [Osaka98-1] [Osaka98-2]

**Table 8-2.** Magnetic properties of representative CoFeNi films plated from traditional low pH bath and citrate-added bath.

Plating bath	Film composition	Coercivity $H_c$ (Oe)	Saturation flux density $B_s$ (Tesla)
Low pH bath (pH 2.7)	$\text{Co}_{64}\text{Fe}_{24}\text{Ni}_{12}$	1.5	2.01
	$\text{Co}_{65}\text{Fe}_{24}\text{Ni}_{11}$	5.5	1.91
	$\text{Co}_{60}\text{Fe}_{29}\text{Ni}_{11}$	18	1.84
Citrate-added bath (pH 5.3)	$\text{Co}_{64}\text{Fe}_{26}\text{Ni}_{10}$	15	2.10
	$\text{Co}_{61}\text{Fe}_{29}\text{Ni}_{10}$	16	1.98

The magnetic properties of representative CoFeNi films plated from conventional low pH bath and the citrate-added bath are listed in Table 8-2. In general, the most important magnetic property, saturation magnetization  $M_s$ , for CoFeNi films plated from citrate-added baths is close to that for CoFeNi films deposited from citrate-free baths. While CoFeNi films plated from citrate-added baths have coercivities  $H_c$  over 15 Oe, which is acceptable and better than the coercivity for CoFeNi films obtained from a saccharin-containing bath (~40 Oe) [Osaka00-1] and the coercivity for CoFe films obtained with vacuum techniques (20-60 Oe) for recording head fabrication [Liao88] [Yu02], improvement is still needed. Some researchers believe that CoFe-based films

with coercivity around 40–90 Oe are feasible for possible applications in recording heads, as the magnetic field generated by a writer coil usually exceeds 200 Oe. [Vas'ko02]

The soft magnetic properties for electrodeposited films are determined by many factors; they can be affected by bath composition, organic additives and operation parameters in complicated ways. Currently, it is only known that fine grain sizes (10-20 nm) and fcc-bcc mixed phase formation are beneficial for achieving optimal soft magnetic properties. [Herzer90] [Hoffmann93] [Osaka98-1] [Osaka99-1] [Liu00-1] [Liu00-2] [Liu01-1] [Liu01-2] [Liu02] [Liu03] [Andricacos98] [Andricacos96] [Chen03] From Table 2-2, it is seen that the saturation polarizations  $I_s$  for pure Fe, Co and Ni are 2.15, 1.76 and 0.60 Tesla, respectively, while the saturation polarization  $I_s$  of CoFe films can be as high as 2.4 Tesla. [Bozorth51] [Osaka03-1] The variety of CoFeNi thin film compositions for which optimal soft magnetic properties have been achieved by different research groups suggests that the exploration of new film compositions for optimal properties is possible. [Osaka98-1] [Osaka99-1] [Liu00-1] [Liu01-1] [Liu01-2] [Liu02] Additional systematic studies on the fabrication of CoFe and CoFeNi films with optimal soft magnetic properties by electrodeposition from citrate-added baths, and the correlation between the soft magnetic properties and the composition and microstructure of deposited films, are needed.

### 8.3 Summary

For CoFe films electroplated from citrate-added baths, ammonium citrate has a minor effect on the coercivity  $H_c$  of deposited films at low dosage (less than 20 g/L ammonium citrate). The coercivity  $H_c$  increases quickly, however, as the citrate dosage is increased further. The coercivity  $H_c$  of deposited films decreases as the current density goes up.

Generally, CoFe films electroplated from citrate added baths exhibited better soft magnetic properties than those deposited from citrate-free baths under the employed

experimental conditions, i.e., the addition of citrate into the plating baths will not sacrifice the magnetic properties of deposited films. The CoFe films plated from citrate-added baths have coercivities  $H_c$  of 8 to 17 Oe, and saturation magnetizations  $M_s$  of 1.96 to 2.04 Tesla, which means good soft magnetic properties.

For CoFeNi films electroplated from citrate-added baths, a high ammonium citrate dosage is not favored for plating CoFeNi films with low coercivity  $H_c$ . The coercivity  $H_c$  of deposited films was lower when a high current density was applied.

The saturation magnetization  $M_s$  for CoFeNi films plated from citrate-added baths was close to that for CoFeNi films deposited from citrate-free baths. They both were close to or over 2 Tesla, which is excellent. CoFeNi films plated from citrate-added baths have coercivities  $H_c$  over 15 Oe, which need to be improved, but are still acceptable and better than the coercivities for CoFeNi films obtained from a saccharin-containing bath and CoFe films obtained with vacuum techniques for recording head fabrication. More systematic studies on the electrodeposition of CoFe and CoFeNi films with ideal soft magnetic properties from citrate-added baths are necessary.

# Chapter 9 Conclusions and Recommendations for Future Work

## 9.1 Main conclusions

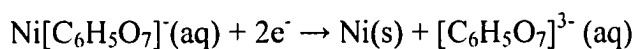
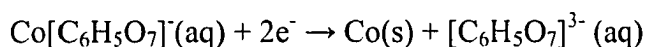
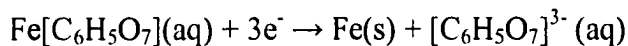
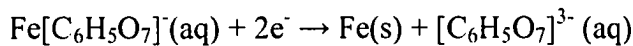
CoFe and CoFeNi alloys have been the most studied soft magnetic materials over the past several decades due to their superior properties over FeNi alloys as write head core materials in hard-disk-drives. [Osaka00-1] With increasing storage density, the need for recording heads to write on high-coercivity media has raised new requirements for the write-head material that cannot be met by permalloy ( $\text{Ni}_{80}\text{Fe}_{20}$ ). [Andricacos98] Therefore, new soft magnetic materials with higher saturation flux density  $B_s$  ( $\gg 1$  Tesla), such as CoFe alloys, CoFeNi alloys and other CoFe-based alloys, have been developed.

With the advantages of simplicity, cost-effectiveness and controllable patterning, electroplating processes are being employed in the fabrication of thin-film recording heads. A stable bath is desired for commercial fabrication of metal or alloy thin films by electrodeposition. For conventional CoFe or CoFeNi alloy plating baths, low pH levels (typically 2.0-3.0) are employed to stabilize the plating bath. In these cases, acids (most often sulfuric acid  $\text{H}_2\text{SO}_4$  or hydrochloric acid  $\text{HCl}$ ) act as the bath stabilizers. However, even at low pH, these plating baths still suffer from stability problems. Precipitation occurs rapidly with time [Liu03], which is a critical issue for commercial production. Furthermore, the low pH employed in conventional baths leads to significant hydrogen evolution on the cathode surface, which results in voids in deposited films and low current density efficiency. The voids included in the deposit will degenerate film uniformity and magnetic properties. Therefore, the development of stable baths with relatively high pH levels is crucial and of practical significance for commercial

fabrication of CoFe and CoFeNi thin films with optimal soft magnetic properties. In this study, stable baths with relatively high pH levels (natural pH) have been developed for CoFe or CoFeNi alloy plating by introducing ammonium citrate as a complexing agent and bath stabilizer. The main conclusions obtained are summarized here.

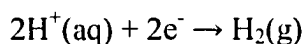
The calculated stability diagrams demonstrate that the stability of conventional CoFe and CoFeNi alloy plating baths, open to air, is dominated by the precipitation of  $\text{Fe}(\text{OH})_3$  at a pH above 3.1. Thermodynamically, citrate can effectively stabilize single metal, CoFe and CoFeNi alloy plating baths, preventing the precipitation of metal hydroxides at higher pH levels. The calculated stability diagrams also show that citrate has the strongest complexing power for Fe ions, followed by  $\text{Ni}^{2+}$  ions, with the weakest complexing effect for  $\text{Co}^{2+}$  ions. Bath stability tests verify that the conventional CoFe and CoFeNi plating baths are not stable; citrate can significantly improve the stability of both CoFe and CoFeNi plating baths. The morphology studies demonstrate that CoFe and CoFeNi films plated from the citrate-added baths are denser and more uniform than those deposited from conventional low pH baths. Therefore, the introduction of citrate can effectively stabilize the CoFe or CoFeNi plating baths, elongate the bath life and improve film uniformity.

In terms of the existing theory, for the deposition of a metal from a complexed metal ion, the metal is deposited by direct discharge from the complex ion, without initial dissociation of the complex ion to give a metal ion. For the citrate-added baths, the reduction reactions for the metals from citrate-complexed ions include:



The secondary reaction at the cathode involves hydrogen evolution, especially in

acidic electrolytes:



Generally, for both CoFe and CoFeNi alloy plating, the metal content in deposited films increases with the metal concentration in the electrolyte, which reflects the kinetics of electrodeposition. The effects of electroplating conditions on the composition of deposited films are not as prominent as that of bath composition. Ammonium citrate has a minor effect on plating rate at low dosages, while plating rate drops rapidly at high dosages. Higher plating temperatures help to reduce the residual stress in deposited films, which are more uniform and have less cracking.

For CoFe plating, ammonium citrate has a linear effect on the metal content in deposited films under the employed experimental conditions. As with CoFeNi deposition, ammonium citrate has the most prominent effect on Fe content, followed by Ni content, and only a minor effect on Co content. For CoFe plating, films deposited from baths with the same Co/Fe concentration ratio, but with different metal concentrations, have almost the same composition. The situation is different for CoFeNi plating. The anomalous behavior of Fe and Ni during deposition has also been observed during the electrodeposition of CoFe and CoFeNi films from the citrate-added baths. CoFe and CoFeNi films with compositions close to those of films claimed with optimal soft magnetic properties in references [Osaka03-1] [Yu02] [Osaka98-1] [Osaka98-2] have been deposited from the citrate-added baths and citrate-free baths in this research.

Linear sweep voltammetry and cyclic voltammetry studies, of Co, Fe and Ni single metal deposition and CoFe and CoFeNi alloy deposition from the electrolytes of interest, have been conducted to investigate the electrochemical mechanisms for CoFe and CoFeNi film deposition from citrate-added baths and citrate-free baths. The addition of citrate delayed the occurrence of Co, Fe and Ni single metal deposition to more negative potentials, which reflects the complexing effects of citrate ions on the metal ions. For the

citrate-free baths, the bath with the higher pH (natural pH) was more beneficial for metal deposition. For the deposition of Co, Fe and Ni single metals, the deposition of Ni started at a more negative potential than that for Co, and the deposition of Fe commenced at the most negative potential under the experimental conditions studied. Similar to the deposition of single metals, the addition of citrate also delayed the occurrence of the deposition of CoFe and CoFeNi alloys to more negative potentials. During CV sweeps, the cathodic charge for CoFeNi alloy deposition from the citrate-added bath was much larger than the anodic charge for CoFeNi alloy dissolution. Therefore, CoFeNi alloys can be effectively deposited from the citrate-added bath using the cyclic voltammetry method. The situation is different for the cyclic voltammograms for the depositions of CoFe alloys, which have large anodic charges.

Generally, the CoFe and CoFeNi films plated from citrate-added baths exhibited better corrosion resistance than those deposited from citrate-free baths. This may be attributed to the denser deposits achieved by plating with citrate-added baths at relatively high pH levels. Passivation phenomena were observed during anodic polarization for all the CoFe and CoFeNi films studied.

The thin film XRD study demonstrated that fcc and bcc phases can be co-deposited in electroplated CoFe films with specific Fe contents. Bath composition (e.g., citrate dosage) and operating parameters affect phase formation in deposited CoFe films. TEM analysis demonstrated that the average grain sizes in  $\text{Co}_{65}\text{Fe}_{35}$  films plated from the citrate-added bath are 10-20 nm, which is beneficial for achieving optimal soft magnetic properties. Electron diffraction also confirmed the co-existence of fcc and bcc phases in CoFe deposits. The fcc (111) and bcc (110) planes diffracted strongly, which agrees with the thin film x-ray diffraction results.

The phase formation in deposited CoFeNi films plated from citrate-added baths and citrate-free baths is affected by Fe content. Both electrolyte composition and operating

parameters affect the phase formation in deposited films. Fcc and bcc phases can be co-deposited by controlling the plating bath composition and/or the plating conditions. TEM analysis of CoFeNi films plated from citrate-added baths showed that the average grain size of CoFeNi films was 10-20 nm, which is close to the grain sizes for CoFeNi films with the best soft magnetic properties obtained by Osaka and coworkers. Electron diffraction patterns further demonstrated the co-existence of fcc and bcc phases in CoFeNi films plated from citrate-added baths. Diffraction was strongest from the fcc (111) and bcc (110) planes, which agrees with the thin film x-ray diffraction results.

Generally, the CoFe films electroplated from citrate added baths exhibited better soft magnetic properties than those deposited from citrate-free baths under the employed experimental conditions, i.e., the addition of citrate into the plating baths did not sacrifice the magnetic properties of deposited films. The CoFe films plated from citrate-added baths have coercivities  $H_c$  of 8 to 17 Oe, and saturation magnetizations  $M_s$  of 1.96 to 2.04 Tesla, which means good soft magnetic properties.

The saturation magnetizations  $M_s$  for CoFeNi films plated from citrate-added baths were close to those for CoFeNi films deposited from the citrate-free baths. Both were close to or over 2 Tesla, which is excellent. CoFeNi films plated from the citrate-added baths have coercivities  $H_c$  over 15 Oe, which needs to be improved, but is still acceptable and better than the coercivities for CoFeNi films obtained from a saccharin-containing bath and for CoFe films obtained with vacuum techniques for recording head fabrication.

In summary, stable electrolytes with the introduction of ammonium citrate as a complexing agent and bath stabilizer and relatively high pH levels (natural pH) have been developed for the electrodeposition of CoFe or CoFeNi alloys in this study. Citrate can effectively improve the stability of CoFe and CoFeNi plating baths. Denser and more uniform deposits can be plated out from the citrate-added baths because of the higher pH

levels. CoFe and CoFeNi thin films with preferred composition, mixed fcc-bcc phases, and 10-20nm grain sizes, which are necessary for achieving ideal soft magnetic properties, have been electroplated out from the citrate-added baths. So far, the saturation magnetizations of CoFe and CoFeNi films plated from citrate-added baths can exceed 2 Tesla, which is excellent. The coercivities of the deposited CoFe and CoFeNi films are acceptable but a bit high, necessitating further study.

## 9.2 Recommendations for future work

The first object of future studies, of course, is to plate out CoFe and CoFeNi thin films with optimal soft magnetic properties, especially low coercivity  $H_c$  ( $<2.0$  Oe), from the citrate-added baths. This may be realized by exploring the following possible approaches:

Coercivity  $H_c$  decreases with decreasing grain size, so CoFe and CoFeNi films with finer grain sizes (less than 10 nm) should be deposited and studied. This may be achieved by employing higher current densities, low  $t_{on}$  time ratio in a plating cycle, and suitable bath compositions.

The annealing of deposited films in a magnetic field may also be investigated to reduce the coercivity  $H_c$  and improve magnetic properties. [Vas'ko02] [Osaka03-1]

The introduction of an additional element such as boron into the CoFe or CoFeNi films may also be considered. Boron is known to reduce the coercivity of CoFeNi films. [Chesnutt93]

Films with suitable chemical composition, phase formation and microstructures may be plated out by controlling bath composition, such as pH and metal ion concentration, and plating parameters, such as current density, PC plating pattern, plating temperature and applied magnetic fields. [Liu00-1] [Liu01-1] The correlation between the composition and microstructure of CoFe and CoNiFe thin films, plated from citrate-added baths, and their magnetic properties also needs to be investigated systematically, which should demonstrate directions for future study.

Systematic and in-depth study of the electrochemical and chemical reactions controlling the bath stability and electrodeposition is necessary for understanding the mechanism dominating the CoFe and CoNiFe plating systems. IR or UV spectroscopy may be employed to study the complexing reactions between citrate and metal ions, and calculations with quantum chemistry methods (such as CNDO, MINDO, and ab initio methods) can be applied to derive stable structures of citrate-metal complexing ions. X-ray photoelectron spectroscopy (XPS) can be applied to investigate the valence change of metal ions. Electrochemical analyses, such as cyclic voltammetry, can be employed to systematically study the electrochemical behavior of electrolytes and metal or alloy deposition.

## Appendix 1

### Standard electrode potentials

In a half-reaction, the standard electrode potential (abbreviated as  $E^\circ$  or  $\varepsilon^\circ$ ) is the electrode potential measured between any electrode under standard conditions, i.e., 298K, 1 mol/L concentration (strictly, activity) and 1 atm pressure, and a reference electrode such as the standard hydrogen electrode (SHE). Standard electrode potentials may also be calculated from the chemical and electrochemical reactions of interest. The following table lists the standard potentials of common electrodes.

Standard electrode potentials (vs SHE) at 25°C in aqueous solution. [The04]

Cathode (Reduction) Half-Reaction	Standard Potential $E^\circ$ (volts)	Best reducing agents
$\text{Li}^+(\text{aq}) + \text{e}^- \rightarrow \text{Li}(\text{s})$	-3.04	
$\text{K}^+(\text{aq}) + \text{e}^- \rightarrow \text{K}(\text{s})$	-2.92	
$\text{Ca}^{2+}(\text{aq}) + 2\text{e}^- \rightarrow \text{Ca}(\text{s})$	-2.76	
$\text{Na}^+(\text{aq}) + \text{e}^- \rightarrow \text{Na}(\text{s})$	-2.71	
$\text{Mg}^{2+}(\text{aq}) + 2\text{e}^- \rightarrow \text{Mg}(\text{s})$	-2.38	
$\text{Al}^{3+}(\text{aq}) + 3\text{e}^- \rightarrow \text{Al}(\text{s})$	-1.66	
$\text{Zn}^{2+}(\text{aq}) + 2\text{e}^- \rightarrow \text{Zn}(\text{s})$	-0.76	
$\text{Cr}^{3+}(\text{aq}) + 3\text{e}^- \rightarrow \text{Cr}(\text{s})$	-0.74	
$\text{Fe}^{2+}(\text{aq}) + 2\text{e}^- \rightarrow \text{Fe}(\text{s})$	-0.41	
$\text{Cd}^{2+}(\text{aq}) + 2\text{e}^- \rightarrow \text{Cd}(\text{s})$	-0.40	
$\text{Ni}^{2+}(\text{aq}) + 2\text{e}^- \rightarrow \text{Ni}(\text{s})$	-0.23	
$\text{Sn}^{2+}(\text{aq}) + 2\text{e}^- \rightarrow \text{Sn}(\text{s})$	-0.14	
$\text{Pb}^{2+}(\text{aq}) + 2\text{e}^- \rightarrow \text{Pb}(\text{s})$	-0.13	

Oxidizing power increases ↓	$\text{Fe}^{3+}(\text{aq}) + 3\text{e}^{-} \rightarrow \text{Fe}(\text{s})$	-0.04	↑ Reducing power increases
	$2\text{H}^{+}(\text{aq}) + 2\text{e}^{-} \rightarrow \text{H}_2(\text{g})$	0.00	
	$\text{Sn}^{4+}(\text{aq}) + 2\text{e}^{-} \rightarrow \text{Sn}^{2+}(\text{aq})$	0.15	
	$\text{Cu}^{2+}(\text{aq}) + \text{e}^{-} \rightarrow \text{Cu}^{+}(\text{aq})$	0.16	
	$\text{ClO}_4^{-}(\text{aq}) + \text{H}_2\text{O}(\text{l}) + 2\text{e}^{-} \rightarrow \text{ClO}_3^{-}(\text{aq}) + 2\text{OH}^{-}(\text{aq})$	0.17	
	$\text{AgCl}(\text{s}) + \text{e}^{-} \rightarrow \text{Ag}(\text{s}) + \text{Cl}^{-}(\text{aq})$	0.22	
	$\text{Cu}^{2+}(\text{aq}) + 2\text{e}^{-} \rightarrow \text{Cu}(\text{s})$	0.34	
	$\text{ClO}_3^{-}(\text{aq}) + \text{H}_2\text{O}(\text{l}) + 2\text{e}^{-} \rightarrow \text{ClO}_2^{-}(\text{aq}) + 2\text{OH}^{-}(\text{aq})$	0.35	
	$\text{IO}^{-}(\text{aq}) + \text{H}_2\text{O}(\text{l}) + 2\text{e}^{-} \rightarrow \text{I}^{-}(\text{aq}) + 2\text{OH}^{-}(\text{aq})$	0.49	
	$\text{Cu}^{+}(\text{aq}) + \text{e}^{-} \rightarrow \text{Cu}(\text{s})$	0.52	
	$\text{I}_2(\text{s}) + 2\text{e}^{-} \rightarrow 2\text{I}^{-}(\text{aq})$	0.54	
	$\text{ClO}_2^{-}(\text{aq}) + \text{H}_2\text{O}(\text{l}) + 2\text{e}^{-} \rightarrow \text{ClO}^{-}(\text{aq}) + 2\text{OH}^{-}(\text{aq})$	0.59	
	$\text{Fe}^{3+}(\text{aq}) + \text{e}^{-} \rightarrow \text{Fe}^{2+}(\text{aq})$	0.77	
	$\text{Hg}_2^{2+}(\text{aq}) + 2\text{e}^{-} \rightarrow 2\text{Hg}(\text{l})$	0.80	
	$\text{Ag}^{+}(\text{aq}) + \text{e}^{-} \rightarrow \text{Ag}(\text{s})$	0.80	
	$\text{Hg}^{2+}(\text{aq}) + 2\text{e}^{-} \rightarrow \text{Hg}(\text{l})$	0.85	
	$\text{ClO}^{-}(\text{aq}) + \text{H}_2\text{O}(\text{l}) + 2\text{e}^{-} \rightarrow \text{Cl}^{-}(\text{aq}) + 2\text{OH}^{-}(\text{aq})$	0.90	
	$2\text{Hg}^{2+}(\text{aq}) + 2\text{e}^{-} \rightarrow \text{Hg}_2^{2+}(\text{aq})$	0.90	
	$\text{NO}_3^{-}(\text{aq}) + 4\text{H}^{+}(\text{aq}) + 3\text{e}^{-} \rightarrow \text{NO}(\text{g}) + 2\text{H}_2\text{O}(\text{l})$	0.96	
	$\text{Br}_2(\text{l}) + 2\text{e}^{-} \rightarrow 2\text{Br}^{-}(\text{aq})$	1.07	
$\text{O}_2(\text{g}) + 4\text{H}^{+}(\text{aq}) + 4\text{e}^{-} \rightarrow 2\text{H}_2\text{O}(\text{l})$	1.23		
$\text{Cr}_2\text{O}_7^{2-}(\text{aq}) + 14\text{H}^{+}(\text{aq}) + 6\text{e}^{-} \rightarrow 2\text{Cr}^{3+}(\text{aq}) + 7\text{H}_2\text{O}(\text{l})$	1.33		
$\text{Cl}_2(\text{g}) + 2\text{e}^{-} \rightarrow 2\text{Cl}^{-}(\text{aq})$	1.36		

Best oxidizing agents	$\text{Ce}^{4+}(\text{aq}) + \text{e}^{-} \rightarrow \text{Ce}^{3+}(\text{aq})$	1.44
	$\text{MnO}_4^{-}(\text{aq}) + 8\text{H}^{+}(\text{aq}) + 5\text{e}^{-} \rightarrow \text{Mn}^{2+}(\text{aq}) + 4\text{H}_2\text{O}(\text{l})$	1.49
	$\text{H}_2\text{O}_2(\text{aq}) + 2\text{H}^{+}(\text{aq}) + 2\text{e}^{-} \rightarrow 2\text{H}_2\text{O}(\text{l})$	1.78
	$\text{Co}^{3+}(\text{aq}) + \text{e}^{-} \rightarrow \text{Co}^{2+}(\text{aq})$	1.82
	$\text{S}_2\text{O}_8^{2-}(\text{aq}) + 2\text{e}^{-} \rightarrow 2\text{SO}_4^{2-}(\text{aq})$	2.01
	$\text{O}_3(\text{g}) + 2\text{H}^{+}(\text{aq}) + 2\text{e}^{-} \rightarrow \text{O}_2(\text{g}) + \text{H}_2\text{O}(\text{l})$	2.07
	$\text{F}_2(\text{g}) + 2\text{e}^{-} \rightarrow 2\text{F}^{-}(\text{aq})$	2.87

## Appendix 2

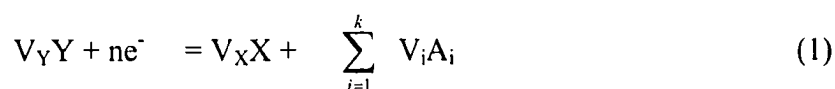
### Construction of stability diagrams

In a plating system, for each reduction-oxidation subsystem, the following steps should be followed [OLI03]:

- First, all independent equilibrium equations involving species of interest are constructed.
- Equilibrium lines are calculated for the chemical reactions.
- Equilibrium lines are calculated for the electrochemical reactions.
- Finally, the predominant species and corresponding areas are determined.

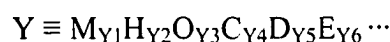
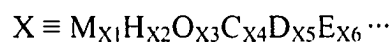
#### *Construction of equilibrium equations*

Each pair of species X and Y in a particular reduction-oxidation subsystem can be related with an equilibrium equation:



$$n = 0, 1, 2, 3, \dots; V_X = 1, 2, 3, \dots; V_Y = 1, 2, 3, \dots; V_i = 0, \pm 1, \pm 2, \pm 3, \dots$$

where X, Y have the general formula:



M is the element associated with the reduction-oxidation system.

$A_i$  is the basis species containing H, O, C, D, E, etc., but not M. For example,

(a)  $H^+$  is the basis species that contains H;

(b)  $H_2O$  is the basis species that contains O;

(c) The basis species containing C, D, E, etc. are the ones with the minimum possible number of hydrogen and oxygen atoms in addition to C, D, E, ...

The following illustrates two examples:

For a system composed of Cu, NH<sub>3</sub> and H<sub>2</sub>O:

$$X \equiv \text{Cu}_{x_1} \text{H}_{x_2} \text{O}_{x_3} \text{N}^{-3}_{x_4}$$

Therefore X could be Cu, CuO, Cu<sub>2</sub>O, Cu(OH)<sub>2</sub>, Cu(NH<sub>3</sub>)<sub>4</sub>, ...

Basis species: H<sup>+</sup>, OH<sup>-</sup>, O<sup>2-</sup>, H<sub>2</sub>O, NH<sub>3</sub>(aq), ...

For a system composed of Fe, H<sub>2</sub>O and sulfur-bearing species:

$$X \equiv \text{Fe}_{x_1} \text{H}_{x_2} \text{O}_{x_3} \text{S}^{-2}_{x_4} \text{S}^0_{x_5} \text{S}^{+6}_{x_6}$$

X could be Fe, FeO, Fe(OH)<sub>2</sub>, Fe(OH)<sub>3</sub>, FeSO<sub>4</sub>, FeS, ...

Basis species: H<sup>+</sup>, OH<sup>-</sup>, H<sub>2</sub>O, S<sup>2-</sup>, S<sup>0</sup> (solid), SO<sub>4</sub><sup>2-</sup>, ...

In cases where both the metal and ligands are subject to redox equilibria, one determines which basis species are stable in which area of the stability diagram; then only the stable species in the basis are retained and the unstable ones are deleted; the deleted species are not considered for constructing the equilibrium equations.

#### *Construction of equilibrium lines for chemical reactions*

The driving force A of a chemical reaction between X and Y expressed in equation (1) is given below:

$$A = -\Delta G_{\text{Reaction}} = - (V_X \bar{G}_X + \sum_{i=1}^k V_i \bar{G}_{A_i} - V_Y \bar{G}_Y) \quad (2)$$

$\bar{G}_i$  is the partial molar Gibbs free energy:

$$\bar{G}_i = \bar{G}_i^0 + RT \ln a_i \quad (3)$$

and  $a_i$  is the activity of component i. Substitution of formula (3) into equation (2), and rearrangement gives:

$$A = -(V_X \bar{G}_X^0 + \sum_{i=1}^k V_i \bar{G}_{.A_i}^0 - V_Y \bar{G}_Y^0) - RT(V_X \ln a_X + \sum_{i=1}^k V_i \ln a_{.A_i} - V_Y \ln a_Y) \quad (4)$$

where  $(V_X \bar{G}_X^0 + \sum_{i=1}^k V_i \bar{G}_{.A_i}^0 - V_Y \bar{G}_Y^0) = \Delta G_{\text{Reaction}}^0 = -RT \ln K$ . Therefore

$$A = RT \ln K - RT(V_X \ln a_X + \sum_{i=1}^k V_i \ln a_{.A_i} - V_Y \ln a_Y) \quad (5)$$

For each reaction, from equation (5), a discrete function of the independent variable is constructed:

$$A = f(\text{var})$$

The root of  $f(\text{var}_0) = 0$  is determined. (at equilibrium  $A = 0$ )

According to the negativity of  $A$ , the species which is stable at  $\text{var} < \text{var}_0$  or  $\text{var} > \text{var}_0$  is determined. From the chemical reactions, the boundary lines parallel to the axis of equilibrium potential are determined, that is, those reactions do not depend on electrochemical potential.

For the electrochemical pair of species  $X$  and  $Y$ :

$$A = -\Delta G_{\text{Reaction}} = nF\varepsilon \quad (6)$$

$$(V_X \bar{G}_X^0 + \sum_{i=1}^k V_i \bar{G}_{.A_i}^0 - V_Y \bar{G}_Y^0) = \Delta G_{\text{Reaction}}^0 = -nF\varepsilon^0 \quad (7)$$

From formulas (4), (6) and (7), the equilibrium potential can be obtained

$$\varepsilon = \varepsilon^0 - \frac{RT}{nF}(V_X \ln a_X + \sum_{i=1}^k V_i \ln a_{.A_i} - V_Y \ln a_Y) \quad (8)$$

$$\text{or } \varepsilon = \varepsilon^0 + \frac{RT}{nF}(V_Y \ln a_Y - V_X \ln a_X - \sum_{i=1}^k V_i \ln a_{.A_i})$$

For the electrochemical reaction of interest, from equation (8), a discrete function of the independent variable is constructed:

$$E = g(\text{var})$$

Finally, the function  $E = g(\text{var})$  is approximated using splines. Usually, the pH is selected as the independent variable.

#### *Determination of predominance areas*

For each species:

Firstly, the boundaries are determined:

- a) Upper boundaries: equilibria with species in higher oxidation states;
- b) Lower boundaries: equilibria with species in lower oxidation states;
- e) Right-hand side boundaries: Other species which are more stable at higher values of the independent variable (such as higher pH);
- d) Left-hand side boundaries: Other species which are more stable at lower values of the independent variables (such as lower pH);

Intersections between boundaries are determined and finally, active boundaries are determined.

## References

- [Afshar02] A. Afshar, A. G. Dolati, and M. Ghorbani, *Materials Chemistry and Physics*, **77** (2), 352 (2002).
- [Anderson87] N. C. Anderson, and R. B. Chesnutt, *US Patent* 4,661, 216 (1987).
- [Andricacos89] P.C. Andricacos, C. Arana, J. Tabib, J. Dukovic, and L. T. Romankiw, *Journal of the Electrochemical Society*, **136** (5), 1336 (1989).
- [Andricacos96] P. C. Andricacos, J. W. Chang, W. J. Horkans, J. D. Olsen, B. Petek, and L. T. Romankiw, *U.S. Patent* no. 5,582,927 (1996).
- [Andricacos98] P. C. Andricacos and N. Robertson, *IBM J. Res. Develop. (Electrochemical Microfabrication)*, **42** (5), 671 (1998).
- [Angstrom04] Angstrom Sciences,  
<http://www.angstromsciences.com/technology/sputtering.htm> (2004).
- [Bai03-1] A. Bai and C.-C. Hu, *Electrochemistry Communications*, **5** (1), 78 (2003).
- [Bai03-2] A. Bai, C.-C. Hu, and T.-C. Wen, *Electrochimica Acta*, **48** (17), 2425 (2003).
- [Baker97] B.C. Baker and A.C. West, *Journal of the Electrochemical Society*, **144** (1), 169 (1997).
- [Baker92] H. Baker (Editor), *ASM Handbook, Volume3 Alloy Phase Diagrams*, ASM International, Materials Park, Ohio (1992).
- [Bertazzoli93] R. Bertazzoli and D. Pletcher, *Electrochimica Acta*, **38** (5), 671 (1993).
- [Biallozor84] S. Biallozor and M. Lieder, *Surface Technology*, **21** (1), 1 (1984).
- [Bieliński79] J. Bieliński and J. Przyłuski, *Surface Technology*, **9** (1), 53 (1979).
- [Birmingham04] University of Birmingham, the Applied Alloy Chemistry Group,  
[http://www.aacg.bham.ac.uk/magnetic\\_materials/](http://www.aacg.bham.ac.uk/magnetic_materials/) (2004).
- [Bockris67] J. O. M. Bockris and G. A. Razumney, *Fundamental Aspects of Electrocrystallization*, Plenum Press, New York, 27 (1967).

- [Bockris70] J. O. M. Bockris and A. K. H. Reddy, *Modern Electrochemistry*, Plenum Press, New York (1970).
- [Bozorth51] R. M. Bozorth, In: *Ferromagnetism V*, D. Van Nostrand Company, New York, 160 (1951).
- [Bradford01] S. A. Bradford, *Corrosion Control* (2<sup>nd</sup> Edition), CASTI Publishing Inc., Edmonton, Canada (2001).
- [Brenner 63] A. Brenner, *Electrodeposition of Alloys*, Academic Press, New York, (1963).
- [Cartage04] <http://www.cartage.org.lb/en/themes/Sciences/Chemistry/Electrochemis/Electrochemical/ElectricalDouble/ElectricalDouble.htm> (2004).
- [Chang90] J. W. Chang, P. C. Andricacos, B. Petek, and L. T. Romankiw, *Proceedings of the Symposium on Magnetic Materials, Processes, and Devices*, PV 90-8, The Electrochemical Society, Pennington, NJ, 361 (1990).
- [Chang92] J.W. Chang, P.C. Andricacos, B. Petek, and L.T. Romankiw, *Proceedings of the Second International Symposium on Magnetic Materials, Processes, and Devices*, **PV 92-10**, The Electrochemical Society, Pennington, NJ, 275 (1992).
- [Chapman79] V. B. Chapman, A. S. Marwaha, and A. J. Collins, *Thin Solid Films*, **58** (2), 247 (1979).
- [Chapman81] V. B. Chapman, A. S. Marwaha, and A. J. Collins, *Thin Solid Films*, **76** (1), 77 (1981).
- [Chemical04] Chemical Education, Purdue University, <http://chemed.chem.purdue.edu/genchem/topicreview/bp/ch20/electro.html#table> (2004).
- [Chen00] Y. Chen, C. Qian, C. Hung, and M. Miller, *Journal of Applied Physics*, **87** (9), 5864 (2000).
- [Chen03] C. Chen, K. Lin, and J. W. Chang, *US Patent Application 20030044303* (2003).

- [Chen99] Y. Chen, S. Hossain, C. Qian, M. Miller, and H. Tong, *Journal of Applied Physics*, **85**(8), 4562 (1999).
- [Chesnutt93] R. Chesnutt, *Journal of Applied Physics*, **73** (10), 6223 (1993).
- [Chiu96] A. Chiu, I. Croll, D. E. Heim, R. E. Jones, Jr., P. Kasiraj, K. B. Klaassen, C. D. Mee, and R. G. Simmons, *IBM J. Res. Develop.*, **40**, 283 (1996).
- [Collins81] A. J. Collins, C. J. Prior, and R. C. J. Hicks, *Thin Solid Films*, **86** (2-3), 165 (1981).
- [Electrochem04] <http://electrochem.cwru.edu/ed/dict.htm> (2004).
- [Electronic04] Electronic Engineering, University of Surrey, <http://www.ee.surrey.ac.uk/Workshop/advice/coils/terms.html#strength> (2004).
- [Gangasingh91] D. Gangasingh and J.B. Talbot, *Journal of the Electrochemical Society*, **138** (12), 3605 (1991).
- [Gao95] L. J. Gao, G. W. Anderson, P. R. Norton, Z-H. Lu, J. P. McCaffrey, and M. J. Graham, *Journal of Applied Physics*, **78** (9), 5795 (1995).
- [Gao97] L. J. Gao, P. Ma, K. M. Novogradecz, and P. R. Norton, *Journal of Applied Physics*, **81** (11), 7595 (1997).
- [Gileadi93] E. Gileadi, Chapter 1-15, in '*Electrode Kinetics for Chemists, Chemical Engineers, and Material Scientists*', VCH Publishers Inc., 1 (1993).
- [Golodnitsky00] D. Golodnitsky, N. V. Gudin and G. A. Volyanuk, *Journal of the Electrochemical Society*, **147**, 4156 (2000).
- [Grande93-1] W.C. Grande and J.B. Talbot, *Journal of the Electrochemical Society*, **140** (3), 669 (1993).
- [Grande93-2] W.C. Grande and J.B. Talbot, *Journal of the Electrochemical Society*, **140** (3), 675 (1993).
- [Harris99] T. M. Harris, J. L. Wilson and M. Bleakley, *Journal of The Electrochemical Society*, **146** (4), 1461 (1999).

- [Herzer90] G. Herzer, *IEEE Trans. Magn.*, **26**, 1397 (1990).
- [Hironaka90] K. Hironaka and S. Uedaira, *IEEE Trans. Magn.* **26**, 2421 (1990).
- [Hoffmann93] H. Hoffmann and T. Fujii, *J. Magn. Magn. Mater.*, **128** (3), 395 (1993).
- [Hoshiand86] Y. Hoshiand and M.Naoe, *IEEE Trans. Magn.*, **MAG-22**(5), 632 (1986).
- [Howard86] J. K. Howard, *J. Vac. Sci. Technol. A*, **4** (1), 1 (1986).
- [Hu94] H.L.Hu, L. Vo, T. Nguyen, N. Robertson, M. Re, and C. Jahnes, *IEEE Trans. Magn.*, **30**(6), 3870 (1994).
- [Hu02] C.-C. Hu and A. Bai, *Journal of The Electrochemical Society*, **149** (11), C615 (2002).
- [Huang02] Q. Huang, D. P. Young, J. Y. Chan, J. Jiang, and E. J. Podlaha, *Journal of The Electrochemical Society*, **149** (6), C349 (2002).
- [Huang04] Q. Huang and E. J. Podlaha, *Journal of The Electrochemical Society*, **151** (2), C119 (2004).
- [Ibl80] N. Ibl, *Surface Technology*, **10**, 81 (1980).
- [Ikeda02] S. Ikeda, I. Tagawa, Y. Uehara, T. Kubomiya, J. Kane, M. Kakehi, and A. Chikazawa, *IEEE Trans. Magn.*, **38**, 2219 (2002).
- [Ikeda02-1] S. Ikeda, I. Tagawa, T. Kubomiya, J. Kane, Y. Uehara, and T. Koshikawa, in *Digests of the 26th Annual Conference on Magnetism in Japan*, The Magnetism Society of Japan, p. 259 (2002), In Japanese.
- [Imai02] K. Imai, T. Yokoshima, D. Shiga, K. Takashima, and T. Osaka, in *Digests of the 26th Annual Conference on Magnetism in Japan*, The Magnetism Society of Japan, p. 258(2002), In Japanese.
- [Ishiwata91] N. Ishiwata, C. Wakabayashi, and H. Urai, *Journal of Applied Physics*, **69**, 5616 (1991.)
- [Jiang02] H. Jiang, Y. Chen, L. Chen, and Y. Huai, *Journal of Applied Physics*, **91**(10), 6821 (2002).

- [Jones95] R. E. Jones, Jr. J. Williams, L. Spector, C. Lin, S. Wang, S. Pichai, and B. M. Clemens, *IEEE Trans. Magn.*, **31** (6), 3817 (1995).
- [Kakuno97] E. M. Kakuno, D. H. Mosca, I. Mazzaro, N. Mattoso, W. H. Schreiner, M. A. B. Gomes, and M. P. Cantao, *J. Electrochem. Soc.*, **144**, 3222 (1997).
- [Kieling97] V. C. Kieling, *Surface and Coatings Technology*, **96** (2-3), 135 (1997).
- [Kijima89] K. Kijima and N. Honda, *IEEE Translation Journal on Magnetics in Japan*, **4**, 473 (1989).
- [Kim03] D. Kim, D. Y. Park, B. Y. Yoo, P. T. A. Sumodjo, and N. V. Myung, *Electrochimica Acta*, **48** (7), 819 (2003).
- [Kim95] D. Kim, K. Aoki and O. Takano, *Journal of the Electrochemical Society*, **142** (11), 3763 (1995).
- [Klemmer00] T. J. Klemmer, K. A. Ellis, L. H. Chen, B. van Dover, and S. Jin, *Journal of Applied Physics*, **87** (2), 830 (2000).
- [Krause97] T. Krause, L. Arulnayagam, and M. Pritzker *J. Electrochem. Soc.* **144**, 960 (1997).
- [Krusch86] K. Krusch, *IEEE Trans. Magn.*, **22** (5), 626 (1986).
- [Lallemand02] F. Lallemand, L. Ricq, P. Berçot, and J. Pagetti, *Electrochimica Acta*, **47** (26), 4149 (2002).
- [Lallemand04-1] F. Lallemand, L. Ricq, M. Wery, P. Berçot, and J. Pagetti, *Surface and Coatings Technology*, **179** (2-3), 314 (2004).
- [Lallemand04-2] F. Lallemand, L. Ricq, M. Wery, P. Berçot, and J. Pagetti, *Applied Surface Science*, **228** (1-4), 326 (2004).
- [Landolt94] D. Landolt, *Electrochimica Acta*, **39**, 1075 (1994).
- [Lehman80] E. B. Lehman and A. Riesenkauf, *Surface Technology*, **11** (5), 349 (1980).
- [Leith99] S. D. Leith, S. Ramli, and D. T. Schwartz, *Journal of The Electrochemical Society*, **146** (4), 1431 (1999).

- [Liao87] S. H. Liao, *IEEE Trans. Magn.* **MAG-23**, 2981 (1987).
- [Liao88] S. H. Liao and C. H. Tolman, *U.S. Patent* 4,756,816 (1988).
- [Liao92-1] S. H. Liao, *U.S. Patent* 5,168,410 (1992).
- [Liao92-2] S. H. Liao, G. E. Roberts, and E. C. Darr, *International Magnetics Conference*, St. Louis, MO, Paper GC-04, 1992.
- [Lieder85] M. Lieder and S. Biallozor, *Surface Technology*, **26** (1), 23 (1985).
- [Liu00-1] X. Liu, P. Evans, and G. Zangari, *IEEE Transactions on Magnetism*, **36** (5), 3479-3481 (2000).
- [Liu00-2] X. Liu, G. Zangari, and L. Shen, "Electrodeposition of Soft, High Moment Co-Fe-Ni Thin Films", *Journal of Applied Physics*, **87** (9), 5410 (2000).
- [Liu01-1] X. Liu, P. Evans, and G. Zangari, *J. Magn. Magn. Mater.*, **226-230**, Part 2, 2073 (2001).
- [Liu01-2] X. Liu and G. Zangari, *IEEE Transactions on Magnetism*, **37** (4), 1764 (2001).
- [Liu02] X. Liu, F. Huang, G. Zangari, and M. L. Weaver, *IEEE Transactions on Magnetism*, **38** (5), 2231 (2002).
- [Liu03] X. Liu, G. Zangari, and M. Shamsuzzoha, *Journal of The Electrochemical Society*, **150** (3), C159 (2003).
- [Magnetics 04] The Magnetics Society of Japan,  
<http://www.wdc-jp.com/msj/english/paper/unit.html> (2004).
- [Matlosz93] M. Matlosz, *J. Electrochem. Soc.*, **140** (8), 2272 (1993).
- [MEMS04] MEMS and Nanotechnology Clearinghouse  
<http://www.memsnets.org/mems/beginner/deposition.html> (2004).
- [Mizutani00] S. Mizutani, T. Yokoshima, H.-S. Nam, T. Nakanishi, T. Osaka and Y. Yamazaki, *IEEE Transactions on Magnetism*, **36** (5), 2539 (2000).
- [Myung01] N. V. Myung and K. Nobe, *Journal of The Electrochemical Society*, **148** (3), C136 (2001).

- [Myung03] N. V. Myung, D. -Y. Park, B. -Y. Yoo, and P. T. A. Sumodjo, *Journal of Magnetism and Magnetic Materials*, **265** (2), 189 (2003).
- [Nakanishi01] T. Nakanishi, M. Ozaki, H. Nam, T. Yokoshima, and T. Osaka, *Journal of The Electrochemical Society*, **148** (9), C627 (2001).
- [Nam01] H. Nam, T. Yokoshima, T. Nakanishi, T. Osaka, Y. Yamazaki, and D. Lee, *Thin Solid Films*, **384**, 288 (2001).
- [Nonaka00] Y. Nonaka, H. Honjo, T. Toba, S. Saito, T. Ishi, M. Saito, N. Ishiwata, and K. Ohashi, *IEEE Transactions on Magnetism*, **36** (5), 2514 (2000).
- [Ohashi98] K. Ohashi, Y. Yasue, M. Saito, K. Yamada, T. Osaka, M. Takai, and K. Hayashi, *IEEE Transactions on Magnetism*, **34** (4), 1462 (1998).
- [Ohashi99] K. Ohashi, N. Morita, T. Tsuda, and Y. Nonaka, *IEEE Transactions on Magnetism*, **35** (5), 2538 (1999).
- [Ohnuma99] S. Ohnuma, N. Kobayashi, T. Masumoto, S. Mitani, and H. Fujimori, *Journal of Applied Physics*, **85**, 4574 (1999).
- [Ohnuma02] S. Ohnuma, N. Kobayashi, H. Fujimori, T. Masumoto, X. Y. Xiong, and K. Hono, in *Digests of the 26th Annual Conference on Magnetism in Japan*, The Magnetism Society of Japan, p. 335 (2002), In Japanese.
- [OLI03] OLI systems, *A guide to using the Corrosion Analyzer*, Chapter 4 (2003).
- [Omata90-1] Y. Omata, *IEEE Transl. J. Magn. Jpn.* **5**, 17 (1990).
- [Omata90-2] Y. Omata, S. Mitani, T. Kai, A. Taniguchi and S. Nakagawa, *IEEE Transl. J. Magn. Jpn.* **5**, 956 (1990).
- [Osaka00-1] T. Osaka, *Electrochimica Acta*, **45** (20), 3311 (2000).
- [Osaka00-2] T. Osaka and T. Yokoshima, *Journal of the Magnetism Society of Japan*, **24** (11), 1333 (2000).
- [Osaka00-3] T. Osaka, M. Takai, and H. Tachibana, *US Patent* 6,063,512 (2000).
- [Osaka01] T. Osaka, *Electrochimica Acta*, **47** (1-2), 23 (2001).

- [Osaka03-1] T. Osaka, T. Yokoshima, D. Shiga, K. Imai, and K. Takashima, *Electrochemical and Solis-State Letters*, **6**(4), C53 (2003).
- [Osaka03-2] T. Osaka, N. Takano, and T. Yokoshima, *Surface and Coatings Technology*, **169-170**, 1 (2003).
- [Osaka91] T. Osaka, T. Homma, N. Masubuchi, K. Saito, M. Yoshino, and T. Namikawa, *IEEE Transl. J. Magn. Jpn.* **6**, 85 (1991).
- [Osaka92] T. Osaka, T. Homma, K. Saito, A. Takekoshi, Y. Yamazaki, and T. Namikawa, *Proceedings of the Second International Symposium on Magnetic Materials, Processes, and Devices*, PV 92-10, The Electrochemical Society, Pennington, NJ, p. 267 (1992).
- [Osaka94] T. Osaka, T. Homma, K. Kageyama, and Y. Matsunae, *Denki Kagaku* (presently *Electrochemistry*), **62**, 987(1994).
- [Osaka98-1] T. Osaka, M. Takai, K. Hayashi, K. Ohashi, M. Saito, and K. Yamada, *Nature*, **392**, 796 (1998).
- [Osaka98-2] T. Osaka, M. Takai, K. Hayashi, Y. Sogawa, K. Ohashi, and Y. Yasue, *IEEE Transactions on Magnetics*, **34** (4), 1432 (1998).
- [Osaka99-1] T. Osaka, *Electrochimica Acta*, **44** (21-22), 3885 (1999).
- [Osaka99-2] T. Osaka, T. Momma, and T. Yokoshima, *Electrochemistry*, **67** (9), 894 (1999).
- [Osaka99-3] T. Osaka, T. Sawaguchi, F. Mizutani, T. Yokoshima, M. Takai, and Y. Okinaka, *Journal of The Electrochemical Society*, **146** (9), 3295 (1999).
- [Osaka99-4] T. Osaka, M. Takai, Y. Sogawa, T. Momma, K. Ohashi, M. Saito, and K. Yamada, *Journal of The Electrochemical Society*, **146** (6), 2092 (1999).
- [Phan91] N. H. Phan, M. Schwartz, and K. Nobe, *J. Appl. Electrochem.*, **21** (8), 672 (1991).
- [Phan94] N. H. Phan, M. Schwartz, and K. Nobe, *Electrochimica Acta*, **39** (3), 449 (1994).

- [Puiippe86] J. C. Puiippe and F. Leaman, *Theory and Practice of Pulse Plating*, American Electroplaters and Surface Finishers Society (1986).
- [Qiu93] G. Qiu, E. Haftek, and J. A. Barnard, *Journal of Applied Physics*, **73** (10), 6573 (1993).
- [Ramasubramanian96] M. Ramasubramanian, S.N. Popova, B.N. Popov, R.E. White, and K.-M. Yin, *Journal of the Electrochemical Society*, **143** (7), 2164 (1996).
- [Ricq01] L. Ricq, F. Lallemand, M. P. Gigandet, and J. Pagetti, *Surface and Coatings Technology*, **138** (2-3), 278 (2001).
- [Robertson97] N. Robertson, H.L. Hu, and C. Tsang, *IEEE Trans. Mag.*, **33**(5), 2818 (1997).
- [Romankiw75] L. T. Romankiw and P. Simon, *IEEE Trans. Mag.*, **MAG-11**, 50 (1975).
- [Romankiw78] L. Romankiw, M. Blakeslee, and R. Acosta, *IEEE Trans. Mag.*, **MAG-14** (5), 424 (1978).
- [Romankiw90] L. T. Romankiw, and J. D. Olsen, *Proceedings of the Symposium on Magnetic Materials, Processes, and Devices*, PV 90-8, The Electrochemical Society, Pennington, NJ, p. 339 (1990).
- [Russak92] M. A. Russak, C. V. Jahnes, E. Klokhholm, J. Lee, M. E. Re, and B. C. Webb, *Journal of Magnetism and Magnetic Materials*, **104-107**(3), 1851 (1992).
- [Saito02] M. Saito, N. Ishiwata, and K. Ohashi, *Journal of The Electrochemical Society*, **149** (12), C642 (2002).
- [Saito99] M. Saito, K. Yamada, K. Ohashi, Y. Yasue, Y. Sogawa, and T. Osaka, *Journal of The Electrochemical Society*, **146** (8), 2845 (1999).
- [Sasaki00] K.Y. Sasaki and J.B. Talbot, *Journal of the Electrochemical Society*, **147** (1), 189 (2000).
- [Sasaki95] K. Y. Sasaki and J. B. Talbot, *J. Electrochem. Soc.*, **142** (3), 775 (1995).

- [Sasaki98] K. Y. Sasaki and J. B. Talbot, *Journal of the Electrochemical Society*, **145** (3), 981 (1998).
- [Shacham00] Y. Shacham-Diamand and Y. Sverdlov, *Microelectronic Engineering*, **50** (1-4), 525 (2000).
- [Shao03] I. Shao, P. M. Vereecken, C. L. Chien, R. C. Cammarata, and P. C. Searson, *Journal of The Electrochemical Society*, **150** (3), C184 (2003).
- [Shinoura93] O. Shinoura and A. Kamijima, *J. Surf. Finishing Soc. Jpn*, **44**, 1114 (1993).
- [Shinoura94] O. Shinoura, A. Kamijima, and Y. Narumiya, *IEEE Transl. J. Magn. Jpn.*, **9**, 118 (1994).
- [Shinoura95] O. Shinoura, *Denki Kagaku*, **63** (6), 473 (1995).
- [Shintaku02] K. Shintaku, K. Yamakawa, and K. Ouchi, in *Digests of the 26th Annual Conference on Magnetism in Japan*, The Magnetism Society of Japan, p. 337 (2002), In Japanese.
- [Sobue02] M. Sobue, T. Segawa, T. Yokoshima, T. Osaka, D. Kaneko, and A. Tanaka, *IEEE Trans. Magn.*, **38**, 2228 (2002).
- [Sogawa00] Y. Sogawa, A. Kawashima, T. Yokoshima, T. Nakanishi, H.-S. Nam, T. Osaka, and K. Ohashi, *Journal of the Magnetism Society of Japan*, **24** (4), 699 (2000).
- [Sun00] N. X. Sun and S. X. Wang, *IEEE Trans. Magn.*, **36**(5), 2506 (2000).
- [Sun02] N. X. Sun, S. X. Wang, T. J. Silva, and A. B. Kos, *IEEE Trans. Magn.*, **38**(1), 146 (2002).
- [Sun98] Wenzhen Sun, *Electroplating of gold-tin eutectic solder*, Thesis (M. Sc.), University of Alberta (1998).
- [Tabakovic00] I. Tabakovic, S. Riemer, V. Inturi, P. Jallen, and A. Thayer, *Journal of the Electrochemical Society*, **147** (1), 219 (2000).
- [Tabakovic02] I. Tabakovic, V. Inturi, and S. Riemer, *Journal of The Electrochemical Society*, **149** (1), C18 (2002).

- [Tagawa01] I. Tagawa, S. Ikeda, and Y. Uehara, *FUJITSU Sci. Tech. J.*, **37**(2), 164 (2001).
- [Takahashi90] M. Takahashi, H. Shoji, M. Abe, H. Komaba, and T. Wakiyama, *J. Magn. Soc. Jpn.*, **14**, 283 (1990).
- [Takai95] M. Takai, K. Kageyama, S. Takefusa, A. Nakamura, and T. Osaka, *IEICE Transactions on Electronics*, **E78-C** (11), 1530 (1995).
- [Takai97] M. Takai, K. Hayashi, M. Aoyagi, and T. Osaka, *Journal of the Electrochemical Society*, **144** (7), L203 (1997).
- [Takahashi90] M. Takahashi, H. Shoji, M. Abe, H. Komaba, and T. Wakiyama, *J. Magn. Soc. Jpn.*, **14**, 283 (1990).
- [Tan93] A. C. Tan, Chapter 8, 9 and 10, in ‘*Tin and Solder Plating in the Semiconductor Industry*’, Chapman & Hall, 197 (1993).
- [Tanaka93] S. Tanaka, F. Suzuki, K. Hosono, M. Oshiki, and A. Kakehi, *IEEE Trans. Magn.*, **29** (6), 3852 (1993).
- [Terada84] N. Terada, Y. Hoshi, M. Naoe, and S. Yamanaka, *IEEE Trans. Magn.*, **20**(5), 1451 (1984).
- [The04] TheFreeDictionary.com,  
<http://encyclopedia.thefreedictionary.com/Table%20of%20standard%20electrode%20potentials> (2004).
- [Thompson00] D. A. Thompson and J. S. Best, *IBM J. Res. Develop. (Directions in information technology)*, **44** (3), 311 (2000).
- [Vaes00] J. Vaes, J. Fransaer, and J. Celis, *Journal of the Electrochemical Society*, **147** (10), 3718 (2000).
- [Vas'ko02] V. A. Vas'ko, V. R. Inturi, S. C. Riemer, A. Morrone, D. Schouweiler, R. D. Knox, and M. T. Kief, *Journal of Applied Physics*, **91** (10), 6818 (2002).
- [Venkatasetty70] H.V. Venkatasetty, *Journal of the Electrochemical Society*, **117** (3), 403

(1970).

[Wang03] X. Wang, W. T. Zheng, L. J. Gao, L. Wei, W. Guo, Y. B. Bai, W. D. Fei, S. H. Meng, X. D. He, and J. C. Han, *Journal of Vacuum Science & Technology A: Vacuum, Surfaces, and Films*, **21** (4), 983 (2003).

[Wang00] S. X. Wang, N. X. Sun, M. Yamaguchi, and S. Yabukami, *Nature* **407**, 150 (2000).

[Wang90] S. Wang and M. H. Kryder, *Journal of Applied Physics*, **67** (9), 5134 (1990.)

[Wang99] H. Y. Wang, Y. J. He, Z. W. Ma, E. Y. Jiang, H. S. Huang, and W. H. Mao, *Journal of Applied Physics*, **85** (7), 3745 (1999).

[Waseda1] Waseda University,

<http://www.appchem.waseda.ac.jp/fm-eng/OSAKA-E.HTM> (2004).

[Waseda2] Waseda University,

<http://www.appchem.waseda.ac.jp/physical/research/rese06.htm#section1> (2004).

[Wolf57] J. W. Wolf, *Journal of Applied Physics*, Supplement to Vol. **33** (3), 1152 (1957).

[Yang89] M. M. Yang and J. A. Aboaf, *Journal of Applied Physics*, **66** (8), 3734 (1989).

[Yin95] K.-M. Yin, J.-H. Wei, J.-R. Fu, B.N. Popov, S.N. Popova, and R.E. White, *Journal of Applied Electrochemistry*, **25** (6), 543 (1995).

[Yin96-1] K.-M. Yin and S.-L. Jan, *Surface and Coatings Technology*, **79** (1-3), 252 (1996).

[Yin96-2] K. -M. Yin and B. -T. Lin, *Surface and Coatings Technology*, **78** (1-3), 205 (1996).

[Yin97] K.-M. Yin, *Journal of the Electrochemical Society*, **144** (5), 1560 (1997).

[Yokoshima00] T. Yokoshima, D. Kaneko, M. Akahori, H. Nam, and T. Osaka, *Journal of Electroanalytical Chemistry*, **491** (1-2), 197 (2000).

[Yokoshima99] T. Yokoshima, M. Kaseda, M. Yamada, T. Nakanishi, T. Momma, and T. Osaka, *IEEE Transactions on Magnetics*, **35** (5), 2499 (1999).

[Yu00] R.H. Yu, S. Basu, L. Ren, Y. Zhang, A. Parvizi-Majidi, K.M. Unruh, and J.Q. Xiao, *IEEE Trans. Mag.*, **36**(5), 3388 (2000).

[Yu02] W. Yu, J. A. Bain, Y. Peng, and D. E. Laughlin, *IEEE Trans. Magn.*, **38**(5), 3030 (2002).

[Zech99-1] N. Zech, E.J. Podlaha, and D. Landolt, *J. Electrochem. Soc.* **146** (8), 2886 (1999).

[Zech99-2] N. Zech, E. J. Podlaha, and D. Landolt, *J. Electrochem. Soc.* **146** (8), 2892 (1999).

[Zhuang00] Y. Zhuang and E. J. Podlaha, *Journal of The Electrochemical Society*, **147** (6), 2231 (2000).

[Zhuang03-1] Y. Zhuang and E. J. Podlaha, *Journal of The Electrochemical Society*, **150** (4), C219 (2003).

[Zhuang03-2] Y. Zhuang and E. J. Podlaha, *Journal of The Electrochemical Society*, **150** (4), C225 (2003).

# Curriculum Vitae

## Part I Personal Information

Family Name: **Zhang**

First Name: **Yahui**

Date of Birth: September 10, 1966

Gender: Male

Nationality: Chinese

## Part II Previous Academic Record

<i>Name of institution</i>	<i>From</i>	<i>To</i>	<i>Major</i>	<i>Degree</i>
1. Wuhan University of Technology, China.	Sept. 1983	Jul. 1987	Mineral Processing	Bachelor
2. Wuhan University of Technology, China.	Sept. 1987	Mar. 1990	Mineral Processing	Master
3. Central South University of Technology, China.	Sept. 1993	Oct. 1996	Mineral Processing	Ph. D.
4. University of Alberta, Canada.	Sept. 2001	Dec. 2004	Materials Engineering	Ph. D.

## Part III Previous Working Experience

<i>Name of institution</i>	<i>From</i>	<i>To</i>	<i>Occupation (Title)</i>
1. Beijing General Research Institute of Mining and Metallurgy, China.	Mar. 1990	Aug. 1993	Engineer
2. Beijing General Research Institute of Mining and Metallurgy, China.	Nov. 1996	Aug. 1999	Senior Engineer
3. University of Alberta, Canada.	Sept. 1999	Aug. 2001	Postdoctorate

#### Part IV Awards

<i>Name of award</i>	<i>Date</i>	<i>Name of institution</i>
1. Conference Support for Graduate Students	2003	Committee of GaAs MANTECH International Conference.
2. Second Prize for Scientific and Technological Development	1998	China National Nonferrous Metal Industry Corporation.
3. Pioneer Worker	1998	Beijing General Research Institute of Mining and Metallurgy, China.

#### Part V Publications and patents during Ph.D. study

##### *Papers:*

1. Yahui Zhang and Douglas G. Ivey, "Electroplating of Nanocrystalline CoFeNi Soft Magnetic Thin Films from a Stable Citrate-Based Bath", *Chemistry of Materials*, **16**(7), 1189-1194 (2004).
2. Yahui Zhang and Douglas G. Ivey, "Electroplating of Gold-Tin Alloys from a Sulfite-Citrate Bath", *Plating & Surface Finishing*, **91**(2), 28-33 (2004).
3. Yahui Zhang and Douglas G. Ivey, "Development of Stable Baths for Electroplating CoFe and CoFeNi Soft Magnetic Thin Films", *AESF SUR/FIN 2004 World Congress*, Chicago, USA, 821-834 (2004).
4. Yahui Zhang and Douglas G. Ivey, "Phase Formation in Gold-Tin Alloys Electroplated from a Non-cyanide Bath", *2003 International Conference on Compound Semiconductor Manufacturing Technology (GaAs MANTECH)*, Scottsdale, Arizona, USA, Paper#8.5, 136-139 (2003).

##### *Patents:*

1. Douglas G. Ivey and Yahui Zhang, "Solution for the Electroplating of Soft Magnetic Co-Fe-Ni Alloys", *Canadian Patent Application No. 2,461,107* (2004).
2. Douglas G. Ivey and Yahui Zhang, "Solution for the Electroplating of Soft Magnetic Co-Fe-Ni Alloys", *US Patent* (2004, under processing).